

# **Seismic Performance Evaluation of Concentrically Braced Frames**

Po-Chien Hsiao

A dissertation  
Submitted in partial fulfillment of the  
Requirements for the degree of

Doctor of Philosophy

University of Washington  
2012

Reading Committee:  
Charles W. Roeder, Chair  
Dawn E. Lehman, co-Chair  
Jeffrey W. Berman

Program Authorized To Offer Degree:  
Civil and Environmental Engineering



University of Washington

**Abstract**

**Seismic Performance Evaluation of Concentrically Braced Frames**

Po-Chien Hsiao

Chair of the Supervisory Committee:

Professor Charles W. Roeder

Department of Civil and Environmental Engineering

Concentrically braced frames (CBFs) are broadly used as lateral-load resisting systems in buildings throughout the US. In high seismic regions, special concentrically braced frames (SCBFs) where ductility under seismic loading is necessary. Their large elastic stiffness and strength efficiently sustains the seismic demands during smaller, more frequent earthquakes. During large, infrequent earthquakes, SCBFs exhibit highly nonlinear behavior due to brace buckling and yielding and the inelastic behavior induced by secondary deformation of the framing system. These response modes reduce the system demands relative to an elastic system without supplemental damping. In design the re reduced demands are estimated using a response modification coefficient, commonly termed the R factor.

The R factor values are important to the seismic performance of a building.

Procedures put forth in FEMAP695 developed to R factors through a formalized procedure with the objective of consistent level of collapse potential for all building types. The primary objective of the research was to evaluate the seismic performance of SCBFs.

To achieve this goal, an improved model including a proposed gusset plate connection model for SCBFs that permits accurate simulation of inelastic deformations of the brace, gusset plate connections, beams and columns and brace fracture was developed and validated using a large number of experiments. Response history analyses were conducted using the validated model. A series of different story-height SCBF buildings were designed and evaluated. The FEMAP695 method and an alternate procedure were applied to SCBFs and NCBFs. NCBFs are designed without ductile detailing. The evaluation using P695 method shows contrary results to the alternate evaluation procedure and the current knowledge in which short-story SCBF structures are more venerable than taller counterparts and NCBFs are more vulnerable than SCBFs.

# Table of Contents

<b>List of Figures.....</b>	<b>vii</b>
<b>List of Tables.....</b>	<b>xiii</b>
<b>Chapter 1 : Introduction and Research Objectives.....</b>	<b>1</b>
1.1 Introduction.....	1
1.2 Research Objectives .....	5
1.3 Overview of Document .....	7
<b>Chapter 2 : Overview of Previous Experimental and Analytical Investigations.....</b>	<b>9</b>
2.1 Introduction.....	9
2.2 Seismic Design Requirements of CBFs .....	10
2.2.1 Balance Design Procedure for SCBFs.....	14
2.3 Overview of Previous Experimental Investigations.....	16
2.3.1 Prior Experimental Program .....	20
2.3.2 Important Insight and Improved Designs of SCBFs .....	24
2.4 Overview of Previous Analytical Work and Modeling of SCBFs .....	25
2.4.1 Simulation of the Braces.....	26
2.4.1.1 Fiber-Type Finite Element Models.....	29
2.4.2 Simulation of the Gusset Plate Connections.....	30
2.4.3 Simulation of the Full Systems .....	31

## **Chapter 3 : Continuum Finite Element Analysis on**

### **Three-Story SCBF Systems.....35**

3.1	Introduction.....	35
3.2	TEST SPECIMENS .....	36
3.3.	Continuum Finite Element Model with Modifications .....	38
3.3.1	Modeling Approach of Brace Buckling.....	40
3.3.2	Modeling Composite Slab .....	42
3.4	Applications of the Extended Finite Element model .....	44
3.4.1	Clearance Design of Midspan Gusset Plate Connections.....	44
3.4.2	Design of Double Conner Gusset Connections.....	48
3.4.3	Design of In-plane Buckling Connections.....	49
3.5	Analytical Responses of the 3-story Braced Frames.....	51
3.5.1	Analytical Results of TCBF2-1 with OOP HSS Braces Buckling.....	52
3.5.2	Analytical Results of TCBF2-2 with OOP WF Braces Buckling .....	63
3.5.3	Analytical Results of TCBF2-3 with IP HSS Braces Buckling .....	71

### **Chapter 4 : Improved Analytical Model of SCBF Systems...77**

4.1	Introduction.....	77
4.2	Simulated SCBF Tests for Development of Analytical Models .....	78
4.3	The Improved Line-element Model of SCBFs .....	82
4.3.1	Braces, Beams and Columns.....	83
4.3.2	Gusset Plate connections .....	84
4.3.2	Beam-to-Column Connections.....	88
4.3.3	Processing Functions of Members.....	90

4.3.4 Model Setup of The Brace Frame Specimens.....	92
4.4 Comparative Approaches.....	96
4.5 Simulation results.....	97
4.5.1 Single-story Frames.....	98
4.5.2 Multi-story Frames.....	105
4.6 Error Evaluation.....	112

## **Chapter 5 : A Model to Simulate SCBFs Beyond Brace**

### **Fracture..... 115**

5.1 Introduction.....	115
5.2 Prior Brace Fracture Simulation Models.....	118
5.3 Experimental Data Set.....	124
5.4 Evaluation of Fracture Life of the Brace.....	131
5.4.1 Brace Axial Deformations.....	131
5.4.2 STRAIN-RANGE FRACTURE MODEL.....	133
5.5 Constitutive Model for Brace Fracture Simulation.....	141
5.6 Comparison of Prior and Proposed Fracture Models.....	144
5.7 Impact of Design Parameters of Predicted Fracture.....	148

## **Chapter 6 : Evaluation of the Collapse Potential & Response**

### **Modification Coefficient of SCBFs..... 151**

6.1 Introduction.....	151
6.2 Design of the Model Buildings.....	153
6.3 System Modeling.....	158
6.3.1 Effect of Gravity Frames.....	158

6.4	Collapse Assessment Using FEMA P695 Methodology .....	162
6.4.1	An Overview of FEMA P695 Methodology .....	162
6.4.2	Collapse Assessment of the SCBF Model Buildings .....	165
6.5	Multi-performance Level Evaluation Procedure .....	169
6.6	Deflection Amplification and Overstrength Factors .....	181
6.7	Comparison of the Proposed and FEMA P695 Procedures.....	185
 <b>Chapter 7 : Seismic Vulnerable of Older CBF Systems .....</b>		<b>187</b>
7.1	Introduction.....	187
7.2	Experimental Results of A NCBF .....	190
7.3	Nonlinear Line Element Models for CBF Systems .....	196
7.4	Nonlinear Dynamic Analysis of SCBF and NCBF Systems .....	202
7.4.1	Selection and Scaling of Ground Motions.....	204
7.4.2	Seismic Performance of CBFs .....	207
7.4.3	Comparison of P695 Evaluation of SCBF and NCBF Buildings .....	209
 <b>Chapter 8 : Summary, Conclusions and Recommendations</b>		
.....		<b>213</b>
8.1	Continuum Finite Element Simulations of SCBFs .....	214
8.2	Development of Discrete Line Element Models of SCBFs.....	215
8.2.1	Fracture Modeling of Braces in SCBFs.....	216
8.3	Evaluation of Seismic Performance of SCBFs .....	218
8.4	Seismic Vulnerability of Older CBF Systems .....	221
8.5	Recommendations for Future Research .....	223
 <b>Appendix A: Journal Paper of the FEA Study .....</b>		<b>225</b>



A.1 Journal Paper.....	225
<b>Appendix B: Journal Paper of the Improved Model of SCBFs</b>	
.....	<b>227</b>
B.1 Journal Paper .....	227
<b>Appendix C.: Processing Functions for Model Construction</b>	
<b>of each component member .....</b>	<b>229</b>
C.1 Bracing Members .....	229
C.2 Beam and Column Members.....	230
C.3 Source Code of Bracemake( ) .....	231
C.4 Source Code of BeamColumnMake( ).....	233
<b>Appendix D: Journal Paper and Tables of Analytical Results of</b>	
<b>the Fracture Model.....</b>	<b>237</b>
D.1 Journal Paper.....	237
D.2 Tables of Analytical Results.....	237
<b>Appendix E: New Material Model Object for Simulate Brace</b>	
<b>Fracture.....</b>	<b>241</b>
E.1 New Facture Material Model.....	241
E.2 Source Code of the Fracture Material Model.....	242
<b>Appendix F: Journal Paper and Tables of Analytical Results</b>	
<b>of the Performance Evaluations of SCBFs .....</b>	<b>253</b>

F.1 Journal Paper..... 253  
F.2 Tables of Analytical Results..... 253

**Appendix G: Journal Paper and Tables of Analytical Results  
of the Performance Evaluations of NCBFs.....255**

G.1 Journal Paper ..... 255  
G.2 Tables of Analytical Results ..... 255

**References .....257**

## List of Figures

<i>Figure 1.1 Typical SCBF System and Gusset Plate Connections .....</i>	<i>5</i>
<i>Figure 2.1 Typical Gusset Plate Connections with Current AISC Design Requirements.....</i>	<i>11</i>
<i>Figure 2.2 Illustrations of Gusset Plate Connections .....</i>	<i>12</i>
<i>Figure 2.3 Typical Test Specimens .....</i>	<i>22</i>
<i>Figure 2.4 Schematics of the three categories of brace hysteretic models.....</i>	<i>28</i>
<i>Figure 2.5 Comparison of Results of Detailed Analysis with Experiments .....</i>	<i>33</i>
<i>Figure 3.1 Typical TCBF2 Specimen Configuration.....</i>	<i>37</i>
<i>Figure 3.2 The Typical Applied Element Mesh, the Boundary Conditions and Mesh Sizes. ....</i>	<i>39</i>
<i>Figure 3.3 Mesh and the Applied Loads at Midspan of the Brace.....</i>	<i>41</i>
<i>Figure 3.4 Comparison of the Story Drift Distribution of TCBF1-1(HSS).....</i>	<i>42</i>
<i>Figure 3.5 The Photo and the Mesh of the Composite Slab with the Blockouts. ....</i>	<i>43</i>
<i>Figure 3.6 Photo of the Midspan Gusset Plate Connection with Edge Stiffeners in TCBF1-1.....</i>	<i>45</i>
<i>Figure 3.7 The EPS Responses of the Midspan Gussets with Clearances of <math>2t_p</math>, <math>4t_p</math> and <math>6t_p</math>.....</i>	<i>46</i>
<i>Figure 3.8 Photo of Gusset Plate Yielding and Stress Distribution of the Gusset of TCBF2-1 .....</i>	<i>48</i>
<i>Figure 3.9 Comparison of the Equivalent Stress Distribution With and Without the Stiffener .....</i>	<i>49</i>
<i>Figure 3.10 A Schematic of the In-Plane Buckling Connections for TCBF2-3. ....</i>	<i>51</i>

<i>Figure 3.11 Photo and the Crack Map of the 1st-story Slab After the Test. ....</i>	<i>53</i>
<i>Figure 3.12 Schematics of the FE model and comparisons of story drift distribution.....</i>	<i>54</i>
<i>Figure 3.13 Comparison of experimental and analytical hysteric responses of TCBF2-1.....</i>	<i>55</i>
<i>Figure 3.14 Individual story drifts versus the average story drifts of TCBF2-1.....</i>	<i>56</i>
<i>Figure 3.15 Comparison of the brace of TCBF2-1. ....</i>	<i>58</i>
<i>Figure 3.16 Comparison of the beams of TCBF2-1. ....</i>	<i>58</i>
<i>Figure 3.17 Comparison of the columns of TCBF2-1. ....</i>	<i>59</i>
<i>Figure 3.18 Comparison of the midspan gusset plates of TCBF2-1. ....</i>	<i>61</i>
<i>Figure 3.19 Comparison of the corner gusset plates of TCBF2-1. ....</i>	<i>62</i>
<i>Figure 3.20 Comparison of distortions of gusset plates of TCBF2-1.....</i>	<i>63</i>
<i>Figure 3.21 Comparison of hysteric responses of the TCBF2-2.....</i>	<i>65</i>
<i>Figure 3.22 Individual story drifts versus the average story drifts of TCBF2-2.....</i>	<i>67</i>
<i>Figure 3.23 Comparison of the brace of TCBF2-2. ....</i>	<i>69</i>
<i>Figure 3.24 Comparison of the midspan gusset plates of TCBF2-2. ....</i>	<i>70</i>
<i>Figure 3.25 Comparison of the corner gusset plates of TCBF2-2. ....</i>	<i>71</i>
<i>Figure 3.26 Comparison of hysteric responses of the TCBF2-3.....</i>	<i>73</i>
<i>Figure 3.27 Individual story drifts versus the average story drifts of TCBF2-3.....</i>	<i>74</i>
<i>Figure 3.28 Comparison of the connections of TCBF2-3 .....</i>	<i>75</i>

<i>Figure 3.29 Comparison of the 1st-, 2nd- and 3rd-story knife plates of TCBF2-3.</i>	76
<i>Figure 4.1 Fiber Discretization.</i>	84
<i>Figure 4.2 Proposed Connection Model.</i>	86
<i>Figure 4.3 Illustration of the Zero-length Rotational Spring Model.</i>	87
<i>Figure 4.4 Illustration of the Shear-tab Connection Model.</i>	90
<i>Figure 4.5 The Model Created by the Functions of BraceMake( ) and BeamColumnMake( ).</i>	91
<i>Figure 4.6 Illustration of the Typical Model Setup for the Single-story Specimens.</i>	93
<i>Figure 4.7 Illustration of the Typical Model Setup for the Two-story Specimens.</i>	94
<i>Figure 4.8 Illustration of the Typical Model Setup for the Three-story Specimens.</i>	95
<i>Figure 4.9 Illustrations of the Pinned, Rigid and Proposed Models.</i>	97
<i>Figure 4.10 Comparisons of OOP Deformation at Midspan of the Braces.</i>	104
<i>Figure 4.11 Analytical Moment-Rotation Hysteretic Responses.</i>	105
<i>Figure 5.1 The Global and Local Behavior Resulting in Brace Fracture.</i>	117
<i>Figure 5.2 Definition of Displacement Components <math>\Delta 1</math> and <math>\Delta 2</math>.</i>	120
<i>Figure 5.3 Comparison of Predicted and Experimental Measured Fracture Life.</i>	121
<i>Figure 5.4 Simplified deformed shapes of out-of-plane deformations for single bracing.</i>	122
<i>Figure 5.5 Comparison of Displacement Range before Brace Fracture.</i>	124
<i>Figure 5.6 Specimen Configurations of the Experimental Studies.</i>	129

<i>Figure 5.7 Gusset Plate Buckling Illustration .....</i>	<i>129</i>
<i>Figure 5.8 Schematic of the Midspan Fiber Section in Brace Model. ....</i>	<i>134</i>
<i>Figure 5.9 Maximum Strain Ranges as Function of Location and Number of Elements .....</i>	<i>136</i>
<i>Figure 5.10 Relationship of the Simulated Maximum Strain Range versus <math>w/t</math>, <math>KL/r</math> and <math>E/F_y</math>. .</i>	<i>138</i>
<i>Figure 5.11 Calculated and Numerical Maximum Strain Ranges for All Specimens.....</i>	<i>139</i>
<i>Figure 5.12 Relationship of the Experimental Axial Deformation Range versus <math>KL/r</math>. ....</i>	<i>141</i>
<i>Figure 5.13 Schematic of the Fracture Material Model).....</i>	<i>143</i>
<i>Figure 5.14 Comparison of the Proposed and Previous Fracture Models.....</i>	<i>145</i>
<i>Figure 5.15 Accuracy of Proposed as a Function of <math>w/t</math>, <math>KL/r</math> and <math>E/F_y</math>.....</i>	<i>147</i>
<i>Figure 5.16 The Illustration of the Single-story Frames and The Applied Loading Protocol. ....</i>	<i>149</i>
<i>Figure 6.1 Elevations and Floor Plans of 3-, 9- and 20-story Buildings. ....</i>	<i>154</i>
<i>Figure 6.2 Variation of the Steel Weight of Buildings Using <math>R=3</math> and <math>8</math>. ....</i>	<i>158</i>
<i>Figure 6.3 Illustration of the Simulation of P-delta and Gravity Frame Effects .....</i>	<i>160</i>
<i>Figure 6.4 Seismic Responses of Buildings With and Without the Gravity Frame Effect.....</i>	<i>161</i>
<i>Figure 6.5 Illustration of the R Factor as Defined by the FEMA P695 Methodology (2008).....</i>	<i>163</i>
<i>Figure 6.6 IDA Results for the 3-story Building (<math>R=6</math>).....</i>	<i>167</i>
<i>Figure 6.7 Adopted Target and the Design Spectra at Seattle. ....</i>	<i>170</i>
<i>Figure 6.8 Scaled Median Acceleration Spectra and The Corresponding Target Spectra.....</i>	<i>174</i>

<i>Figure 6.9 Seismic Responses of the 3-, 9- and 20-story Buildings with Various R Factors.....</i>	<i>175</i>
<i>Figure 6.10 Probability of Damage at the 2/50 Hazard Level with Various R Values. ....</i>	<i>179</i>
<i>Figure 6.11 Probability of Damage at the 10/50 Hazard Level with Various R Values.....</i>	<i>180</i>
<i>Figure 6.12 The Means and Standard Deviations of the Deflection Amplification Factors.....</i>	<i>183</i>
<i>Figure 6.13 The Means and Standard Deviations of the Overstrength Factors. ....</i>	<i>184</i>
<i>Figure 7.1 Typical Specimen Dimensions and Sizes for SCBF Specimen. ....</i>	<i>191</i>
<i>Figure 7.2 Hysteretic Responses of Single-story Frame Specimen HSS5 and HSS12 .....</i>	<i>192</i>
<i>Figure 7.3 Dimensions of Specimen NCBF32 and the Connection Details .....</i>	<i>193</i>
<i>Figure 7.4 Hysteretic Responses of the Pilot NCBF (NCBF32). ....</i>	<i>195</i>
<i>Figure 7.5 Illustrations of the Analytical Models of NCBFs, and Connections of NCBFs. ....</i>	<i>198</i>
<i>Figure 7.6 Illustrations of Models Representing.....</i>	<i>199</i>
<i>Figure 7.7 Comparison of Analytical and Experimental Responses, Including Fracture.....</i>	<i>201</i>
<i>Figure 7.8 Target and Median Spectra of AISC-SCBF and Pre-1988 NCBF.....</i>	<i>206</i>
<i>Figure 7.9 Seismic Performance of the Western CBF Buildings .....</i>	<i>208</i>
<i>Figure 7.10 Maximum Story Drift Range for AISC-SCBF and BDP-SCBF Buildings .....</i>	<i>209</i>
<i>Figure 7.11 IDA Results for the 3-story NCBF Building using M1 Scaling Method. ....</i>	<i>210</i>





## List of Tables

<i>Table 2.1 CBF Design Requirements.....</i>	<i>13</i>
<i>Table 2.2 Summary of Test Program .....</i>	<i>23</i>
<i>Table 4.1 Dimensions and Material Properties for Selected UW Test Specimens .....</i>	<i>80</i>
<i>Table 4.2 Dimensions and Material Properties of Braces and Gusset Plates of NCEE Tests.....</i>	<i>81</i>
<i>Table 4.3 Simulated and Measured Responses of the Single-story Frames.....</i>	<i>101</i>
<i>Table 4.4 Simulated and Measured Responses of TCBF1-1(HSS) Specimen .....</i>	<i>108</i>
<i>Table 4.5 Simulated and Measured Responses of TCBF1-2 and TCBF1-3 Specimens .....</i>	<i>109</i>
<i>Table 4.6 Simulated and Measured Responses of TCBF2-1 Specimen.....</i>	<i>110</i>
<i>Table 4.7 Simulated and Measured Responses of TCBF2-1 and TCBF2-2 Specimens .....</i>	<i>111</i>
<i>Table 4.8 Errors in Total Energy Dissipation and Maximum Story-shear Forces. ....</i>	<i>113</i>
<i>Table 5.1 Overview of the Experimental Research Programs .....</i>	<i>127</i>
<i>Table 5.2 Characteristics of the specimens and the corresponding maximum strain ranges .....</i>	<i>130</i>
<i>Table 5.3 Variations of Design Parameters .....</i>	<i>131</i>
<i>Table 5.4 Variations of Several Characteristics at Axial Deformation Level .....</i>	<i>133</i>
<i>Table 5.5 Fracture Models based on Fiber Strains.....</i>	<i>137</i>
<i>Table 6.1 Effective Seismic Weight of Structure .....</i>	<i>154</i>

<i>Table 6.2 Member Sizes of the 3-story Model Buildings .....</i>	<i>156</i>
<i>Table 6.3 Member Sizes of the 9-story Model Buildings .....</i>	<i>156</i>
<i>Table 6.4 Member Sizes of the 20-story Braced Frames with Difference R Factors.....</i>	<i>157</i>
<i>Table 6.5 Summary of Evaluations of the Buildings Using FEMA P695 IDA Procedure .....</i>	<i>168</i>
<i>Table 7.1 CBF Design Requirements.....</i>	<i>189</i>
<i>Table 7.2 Member Sizes, Material Strengths and Weights of the Three-story CBF Buildings .....</i>	<i>203</i>
<i>Table 7.3 Dimensions of the Gusset Plates in SCBF Buildings .....</i>	<i>203</i>
<i>Table 7.4 Evaluations of the SCBF and NCBF Buildings Using FEMA P695 IDA Procedure .....</i>	<i>211</i>

# Chapter 1 : Introduction and Research Objectives

## 1.1 Introduction

Braced frame systems offer an attractive solution to satisfy multiple design objectives within a performance-based earthquake engineering (PBEE) framework. Their elastic properties provide the stiffness and strength needed to achieve operational performance objectives, which are primarily defined by the performance of non-structural elements. If detailed properly, their displacement and energy dissipation capacities can meet severe inelastic deformation demands resulting from extreme events.

Concentrically braced frames (CBFs) join beams, columns, and braces at common workpoints such as shown in Fig. 1.1. Several types of CBFs have been developed, including ordinary concentrically braced frames (OCBFs), non-seismic braced frames (NCBFs), special concentrically braced frames (SCBFs), and buckling restrained braced frames (BRBFs). OCBFs are designed for larger seismic design forces and smaller deformation demands, but they are less commonly used today, because of reductions of their economical benefit in seismic design codes. NCBFs are essentially CBFs designed with no special detailing requirements. These may comply with older code requirements in regions with high seismic demands or current code requirements in R=3 frame designs for regions with low seismicity. SCBF systems allow the brace yielding and buckling and yielding of connections to achieve energy dissipation, and the systems are designed in opposing pairs to avoid asymmetrical response and to limit deterioration of resistance of

CBF system for inelastic hysteretic behavior. SCBFs are the most commonly used braced frame system for seismic design today in high seismicity regions. BRBFs have been developed as a ductile alternative to the SCBFs. BRBFs are a relatively new lateral load resisting system resembling concentric bracing. Buckling restrained braces (BRBs) are patented structural elements consisting of a yielding steel core encased by concrete or mortar cast inside a steel tube that prevents member buckling. An appropriate unbonding material is applied between the steel core and the concrete. Unlike a conventional buckling bracing system, BRBs display full hysteretic behavior and tolerate large inelastic deformations without buckling when subjected to tensile and compressive forces. As a result, BRBs are highly regarded by engineers as an effective type of bracing system, and their use is becoming more common.

SCBFs have been increasingly used by structural engineers in the past few decades, largely because of the unsatisfactory performance of special moment resisting frames (SMRF) during the 1994 Northridge Earthquake. Prior to this earthquake, SMRFs were considered to be one of the best structural systems for use in areas of high seismicity. The simple configuration and straightforward design criteria of frame structures increased the popularity of SMRF system among the engineers, architects and owners. However, the 1994 Northridge, 1995 Hyogo-ken Nanbu and other recent earthquakes have significantly reduced the confidence of engineers in these systems due to widespread brittle fractures that occurred in special welded-flange bolted-web beam-to-column connections (FEMA 2000). To avoid this premature failure of the structural systems, the Federal Emergency Management Agency (FEMA) conducted a great number of investigations and guideline development by the SAC Joint Venture (comprised of the Structural Engineers of Northern California, Applied Technology Council, and California Universities for

Research in Earthquake Engineering) (FEMA 1997a through 1997c, FEMA 2000b through FEMA 2000d). Based on these investigations and developed guidelines, more stringent requirements and restrictions are now required for the design using SMRFs, and more rigorous checks are stipulated for quality control to achieve the required ductility of beam-to-column connections. Research on SMRF systems has also demonstrated that very large story drift may occur during a severe earthquake leading to serious damage to the structural and non-structural components. Further, SMRF systems tend to be controlled by interstory drift limitations, which usually lead to much larger member sizes than those designed upon the basis of strength alone. This has resulted in cost increases, with engineers and owners now seeking more efficient and economical systems.

Currently, SCBFs are considerably more economical than SMRFs because of the decreased quantity of steel and field welding that is required. Additionally, SCBFs are inherently stiff systems and are able to resist seismic excitations with considerably less structural and non-structural deformations. For this reason, considerable research has been conducted on SCBFs with the overall goal of improving system and connection performance. However, research results have indicated that current design methods prevent braced frames with traditional and buckling-restrained braces from achieving their full potential.

For PBEE, SCBFs efficiently provides a large elastic stiffness, which resists low to moderate seismic excitations with minimal damage and inelastic deformation, to meet immediate occupancy and operational limit states. Seismic design using reduced seismic load results in nonlinear inelastic deformation of the system during the large, infrequent earthquakes. The structure must tolerate these large inelastic deformation without building collapse or loss of life. The inelastic behavior of SCBFs is highly nonlinear and

primarily governed by the severe deformations of the brace member including buckling, post-buckling and tensile yielding of the brace. To assure that the braced system can achieve these large inelastic deformations without premature failure, SCBFs require capacity design of the beams, columns and gusset plate connections joining the braces to other framing members. The gusset plate connections are designed to withstand the deformations and loads that result from brace yielding and buckling. In the current AISC Seismic Provisions (AISC 2010a), this design intent is addressed by requiring that the connection strength exceed the expected plastic capacities (both tension and compression) of the brace. Out-of-plane buckling of the brace is accommodated using geometric limits on the gusset plate relative to the end of the brace to permit brace end rotation. Typically, engineers employ a  $2t_p$  linear clearance requirement, as shown in Fig. 1.1. The  $2t_p$  clearance model usually results in large rectangular gusset plates; tapered plates are also widely used since that they reduce the size of the connections, but tapered gusset plates must typically have increased thickness to prevent gusset plate buckling, see Fig. 1.1.

However, the seismic performance of SCBF structures is still not well understood, because the dynamic behavior of the steel braced frame building system is complex and highly nonlinear. To better understand and improve the seismic performance of the braced frame system, an international project “NEES-SG: International Hybrid Simulation of Tomorrow’s Braced Frame.” was conducted. A great number of full-scale braced frames have been tests in the project, including single-story, single-bay frames (Johnson 2005, Herman 2006, Kotulka 2007, Powell 2009), two-story frames (Roeder et al. 2011a) and three-story frames (Lumpkin 2009). The research mainly focused on the design and performance of the gusset plate connections, and a new elliptical clearance model for gusset plates (Lehman and Roeder 2008) and a balanced design procedure for gusset plate

connections (Roeder et al. 2011b, Lumpkin 2009) were proposed for ensuring the desired performance of SCBF systems. The project provided a large experimental database for development and validation of analytical models of SCBF systems, and these analytical models were the basis of the researches of this dissertation.

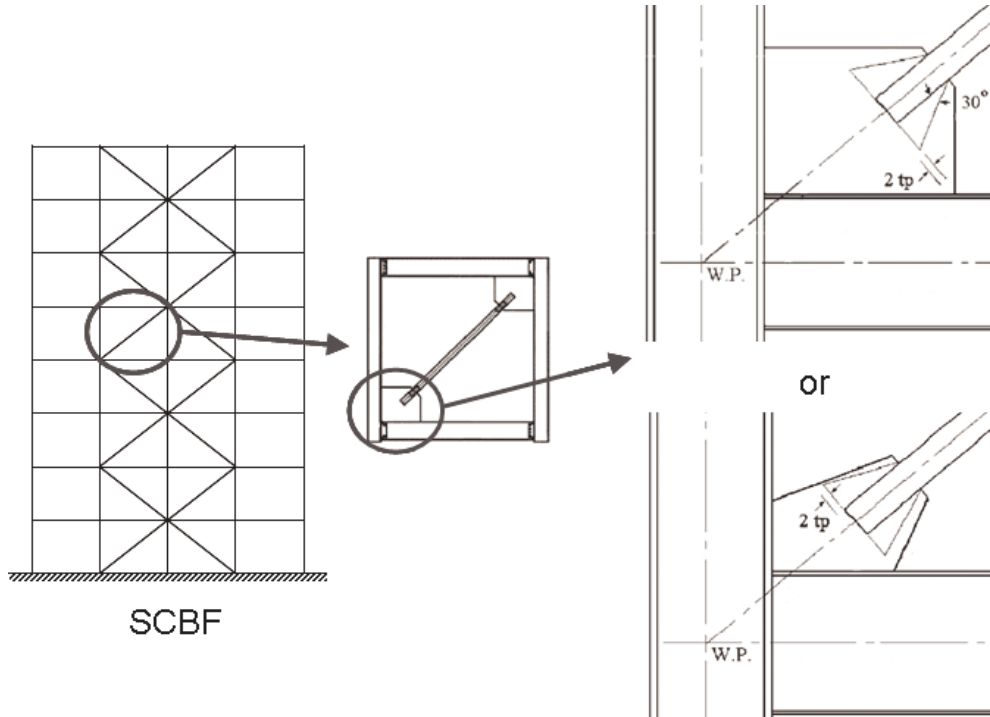


Figure 1.1 Typical SCBF System and Gusset Plate Connections

## 1.2 Research Objectives

Based on these prior experimental research efforts, the behavior of SCBF systems, components, braces and gusset plate connections, are better understood. This improved understanding can be translated into better models for predicting buckling, tensile yielding, post-buckling and fracture of the brace, yielding and deformation of the gusset connections, and the local deformation of framing elements. These diverse behaviors

must be appropriately simulated in the analytical model to ensure accurate prediction of SCBF systems. In this research, a number of analytical studies were conducted to provide a comprehensive investigation of SCBF structural systems using analytical techniques which were verified by comparison to experimental results. These models were then used to extend the understanding of SCBF performance through detailed analysis of local behavior and nonlinear dynamic analysis of SCBFs to include the full range of system behavior to brace fracture and beyond.

The scope included the development of reliable analytical models to simulate the full range of CBF system behavior and valid analytical procedures of braced frame systems. The analysis supported the experimental research program, used the experimental research to verify and document the accuracy of the models, and extended the research to investigate additional parameters beyond the experimental work. The analytical research accomplished these goals by: (1) developing reliable modeling techniques that capture the important nonlinear behavior for use in practical dynamic modeling, and (2) establishing system performance of large scale CBF structures, which included (a) capacity evaluation of CBF structures including brace fracture, post-fracture behaviors and potential collapse, (b) demand analysis of a wide range of ground motions and building configurations, and (c) performance evaluation procedures for braced frame systems.

To achieve these goals, the developed model was calibrated and verified to accurately simulate SCBF behavior. Prior model development and experimental research were used in this calibration and model development process. A new connection model was proposed to better represent the nonlinear behavior of the brace and framing systems comparing with other conventional models, pinned or fix joints. A model to accurately



simulate brace fracture and post-fracture deformation was developed, and its effect on system performance was analyzed. The final analytical models were used for comprehensive dynamic analysis over a wide range of the CBF systems. The analytical studies of CBF structures at the system level enhanced the understanding of SCBF behavior and provide recommendations for improving the current seismic provisions and design practice for the braced frames.

### **1.3 Overview of Document**

This chapter provides the introduction and background of the steel braced frame systems and research objectives of the analytical studies. A literature review of prior experimental and analytical investigations is provided in Chapter 2 including the descriptions of the new clearance model and the proposed balanced design procedure for the gusset connections developed from the experimental research.

A FE analytical study was performed prior to the multi-story frame tests used in the experimental program to aid in the design of test specimen, to confirm the performance expected of the system, and to establish a new clearance design model for midspan gusset plate connections and in-plane-buckling connections. Chapter 3 presents the establishment and validation of the FE model and the comparison with the experimental observations at both the global and local levels.

Based on the prior experimental results, an improved simulation method for SCBFs was proposed. The proposed models were extended to apply on other types of CBFs. Chapter 4 presents the development and accuracy of the improved analytical models.

Upon the improved analytical model, Chapter 5 describes a new fracture model of

the brace that was based upon the strain deformation range of the brace. The chapter describes the development of the strain-range fracture model and compares it with other previous existing fracture models.

After the development of the analytical tools, a series of dynamic analysis was performed using the proposed models to evaluate the seismic performance of large scale SCBFs. SCBF buildings with variable story height, 3-, 9- and 20-story with various response modification coefficients (R-factors), were analyzed, and other seismic performance factors were investigated, and details of the evaluation procedures are provided in Chapter 6.

In Chapter 7, the seismic vulnerability of the older CBFs (NCBFs) was evaluated and compared with the equivalent SCBFs following the current AISC design requirements and also the new balanced design procedures.

Chapter 8 concludes with a summary of results of presented herein and several recommendations of future research of the braced frame structural systems.

## **Chapter 2 : Overview of Previous Experimental and Analytical Investigations**

### **2.1 Introduction**

CBFs have been widely used throughout the world in the past few decades. For better understanding of their seismic performance, a number of experimental and analytical investigations have been conducted. The experimental investigations include the testing of component members and full systems and provide the basis of the development of new design rules (such as the SCBF design requirements), which improved the seismic performances of CBFs. Various simulation methods were created to represent the seismic behavior of CBFs based upon the results of this earlier experimental research.

Section 2.2 summarizes and compares the design requirements of CBFs from past to present. Section 2.3 provides an experimental literature review of CBFs. The review first describes the history of experimental investigations conducted in past decades; and then provides a relative detailed review of the comprehensive experimental program on SCBFs, which is the primary basis of this analytical research. Section 2.4 reviews previous analytical models of CBF systems, including modeling of braces, connections and the framing system. Those models are evaluated and related to the goals of this research in Section 2.5.

## 2.2 Seismic Design Requirements of CBFs

CBFs are commonly used for seismic design. In active seismic regions, on the west coast and in certain areas in the Midwest of the US, SCBFs are used and designed with reduced seismic forces and special detailing requirements. Prior to 1988, CBFs were designed without special detailing requirements. These frames are recognized by the earthquake engineering community as vulnerable to seismic damage and collapse, and this recognition led to substantial changes to the design philosophy and detailing requirements of CBFs in 1990s and resulted in the modern SCBF system.

Typically, braces are joined to the beams and columns of the frame through gusset plate connections. During earthquakes, the braces in the CBF system experience yielding in tension and buckling in compression. Brace post-buckling behavior places significant cyclic load and end rotation demands on these connections. With out-of-plane buckling, end rotation of the brace causes significant local rotation of and large bending demands on the gusset plate. The design of the gusset plate connection as a boundary condition of the brace directly influences the behavior and ductile capability of the brace as well as the frame system.

In SCBFs, the connections are designed to withstand the deformations and loads that result from brace yielding and buckling. In the current AISC Seismic Provisions (AISC 2010a), this design intent is addressed by requiring that the connection strength exceed the expected plastic capacities (both tension and compression) of the brace. Out-of-plane buckling of the brace is accommodated using geometric limits on the gusset plate relative to the end of the brace. Typically, engineers employ a  $2t_p$  linear clearance

requirement with rectangular or tapered gusset plates, as shown in Fig. 2.1.

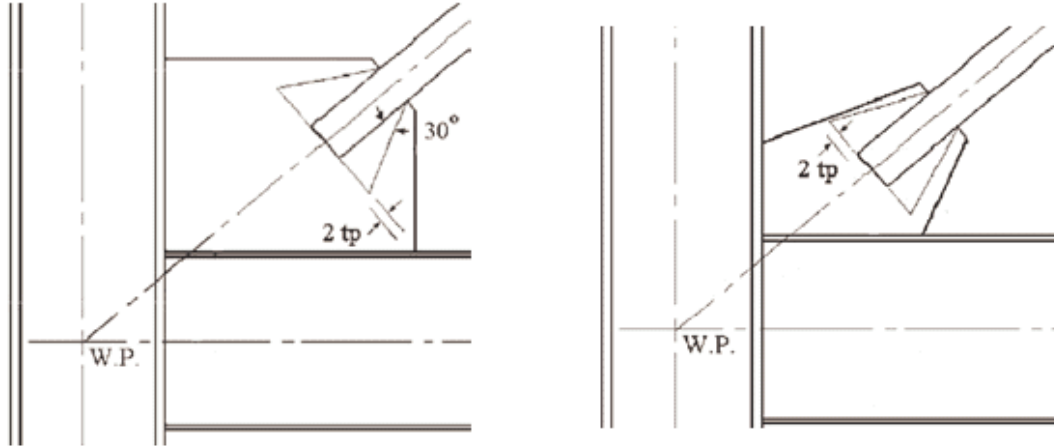


Figure 2.1 Typical Gusset Plate Connections with Current AISC Design Requirements

Recent research shows that although frames designed to the current code possess ductility, their displacement capacity is limited in that the yielding is restricted to a single element (brace) (Lehman et al 2008). Extensive research into the seismic design and behavior of braced frames indicates that a balance between brace yielding/buckling and connection yielding suggests increasing the drift capacity of the system. This research has resulted in a Balance Design Procedure (BDP), which balances the strength of the brace and the gusset plate to promote ductility and alleviate potential failure modes (Roeder et al. 2011b). A summary of the BDP method is given later in Section 2.2.1. The BDP procedure also promotes an  $8t_p$  elliptical clearance requirement for corner gusset connections and a  $6t_p$  linear clearance for midspan gusset connections, illustrated in Figs. 2.2a and b respectively. These clearance models further enhance the seismic performance and constructability by providing lighter and more compact connections. The investigation of the  $6t_p$  linear clearance through finite element analysis will be described

in Chapter 3.

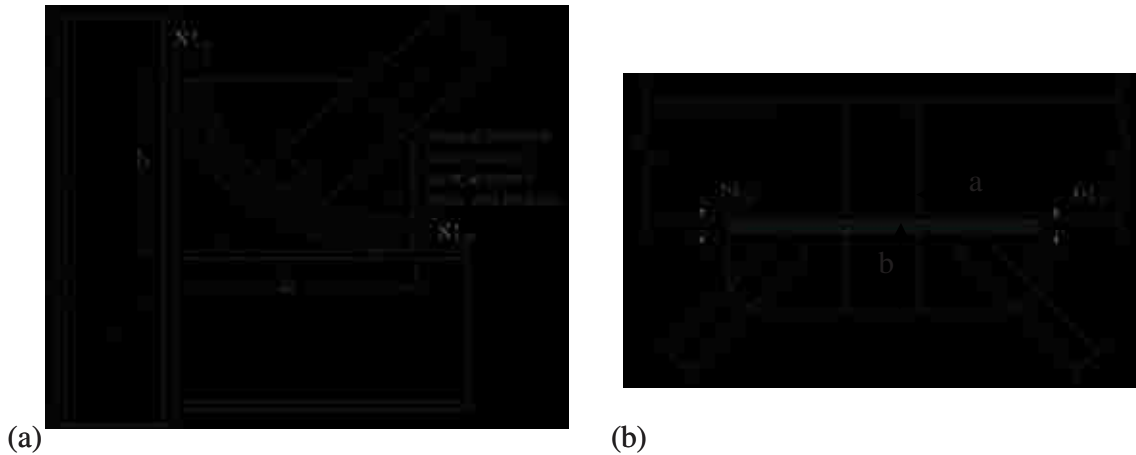


Figure 2.2 Illustrations of (a) the Elliptical Clearance Model for Corner Gusset Plate Connections and (b) the New Linear Clearance Model for Midspan Gusset Plate Connections

Prior to the 1988 UBC, CBF members and gusset plate connections were designed using the prescribed seismic forces. There was no consideration of overstrength, its impact on the connection demands, or ductile detailing in these earlier designs. As a result, these older CBFs are unlikely to exhibit ductile response because of connection failure and are defined as NCBFs. A dynamic response investigation of the vulnerability of the older braced frame was conducted and described in Chapter 7.

The 1994 UBC (ICBO 1994) introduced limited ductile detail requirements for braced frames, and the 1997 AISC Seismic Design Provisions (AISC 1997) fully developed and extended the concepts to create SCBFs, which have significant ductile detailing requirements and are designed with the response modification coefficient (R factor) of 6.

Table 2.1 CBF Design Requirements

Component	Current NCBFs (R = 3)	Pre-1988 NCBFs ( $R_w=8$ )	OCBF (R = 3.25)	SCBF (R = 6): 1997-Current
System Configs.	No limitations		No limitations (requirements for V, inverted-V and K)	K bracing not allowed, requirements for V & inverted-V
Braces	$KL/r < 200$ (recommended)		$KL/r < \sim 100$ for K, V, inverted-V configurations; seismic b/t	$KL/r < \sim 100$ with exceptions; seismic b/t
Net Section	Design for factored loads	ASD for service loads	Design for factored loads	Design for $R_y F_y A_g$ of brace
Brace Conn.	Design for factored loads	ASD for nominal brace tension or service loads without 33% stress increase	Design for minimum of $R_y F_y A_g$ of brace or amplified seismic load	Design for $R_y F_y A_g$ and $1.1 R_y P_n$ of brace & permit end rotation of brace
Beams	Design for factored loads	ASD for service loads	For V & inverted-V systems design for unbalanced load	
Columns	Design for factored loads	ASD for service loads	Design for minimum of maximum load of $1.1 R_y$ times brace strength or amplified seismic load	
Column Splices	Design for factored loads	ASD for service loads	Column design axial loads, special PJP weld requirements, flanges splice 50% of flange strength	Column design axial load, $0.5 M_p$ flexure, plastic shear strength; special PJP weld requirements

Table 2.1 compares the current design requirements for the three CBF systems, including current SCBF systems in seismically active regions (AISC 2010a and 2010b), CBFs designed in low-to-moderate seismic regions (i.e. CBFs with  $R=3$  (denoted NCBFs herein), ordinary concentrically braced frames (OCBFs)), as well as the older NCBF systems based on the 1988 UBC (ICBO 1988). Each design requirement, or lack thereof, impacts the system behavior. The more stringent slenderness,  $KL/r$ , and compactness requirements for OCBF and SCBF braces reduce post-buckling degradation with higher resistance to low-cycle fatigue. Such requirements generally result in larger, less efficient

brace sections for OCBFs and SCBFs. NCBFs and Pre-1988 NCBFs have no special detailing requirements, resulting in uncertainty in balance between the connection and brace strength, e.g., some connections will be stronger than the brace and others will be weaker. Finally, NCBF design requirements above do not establish a clear hierarchy of yielding and failure, resulting in uncertain seismic response and high susceptibility to connection failure, frame member damage and soft-story collapse relative to SCBFs.

### **2.2.1 Balance Design Procedure for SCBFs**

Improper design of connections can lead to a poor hysteretic performance of the braced frames with reduced energy dissipation and inelastic deformation capacity. An improved balanced design procedure (BDP) was developed based on the concept of balancing the yield mechanisms and failure modes of the critical elements of the structural system (Roeder 2001 and 2002). The improved design method of connections of SCBFs was proposed (Roeder et al. 2011b) to promote ductility and prevent less desirable failure modes of the SCBFs. The yield mechanism with the lowest resistance controls the response of the system, and multiple yield mechanisms resulted in increased inelastic deformation capacity and desirable seismic performance. Failure modes result in fracture or tearing, which may cause deterioration of resistance and reduction of inelastic deformation capacity. The critical failure mode should have the smallest resistance of all possible modes and be the maximum resistance of the connection. The combination of the controlling yield mechanism and the critical failure mode control the ductility and inelastic performance of the SCBF. The so-called BDP helped ensure the desired yielding and failure mechanism occur in a logical order.



A design controlling the hierarchy of yielding is achieved through the use of balance factors, called beta ( $\beta$ ) factors. These  $\beta$  factors have similar characteristics to the  $\phi$  factors (resistance factors) used in load and resistance factor design, but they are fundamentally different, because  $\beta$  factors are based on achieving ductility and inelastic deformation capacity rather than required strength under statistically extreme load combination (Roeder 2002). This procedure is possible, because the connection design force depend on the capacity of the brace and are much larger than the factored loads required for the structural design. A smaller  $\beta$  factor was used when a given yield mechanism or failure mode is difficult to predict or has undesirable consequences, while a larger  $\beta$  factor was adopted for certain desirable, ductile yield mechanisms or failure modes when the resistance can be accurately predicted and desirable inelastic deformation occurs. Equation 2.1 expresses the use of  $\beta$  factors in balancing the resistances of certain yield mechanisms, and Equation 2.2 illustrates how the balanced design procedure can prevent undesirable failure modes.

$$R_{yield,mean} = R_y R_{yield} \leq \beta_{yield,1} R_{yield,1} \leq \beta_{yield,2} R_{yield,2} \dots \leq \beta_{yield,i} R_{yield,i} \quad (2.1)$$

where  $R_y$  is the ratio of the expected yield stress to the minimum specified yield stress and  $R_{yield}$  is the nominal yield resistance of the particular yield mechanism. The optimal yielding sequences for SCBF are, in order, brace buckling, brace yielding, connection yielding and beam/column yielding.

$$R_{yield,mean} = R_y R_{yield} \leq \beta_{fail,1} R_{fail,1} \leq \beta_{fail,2} R_{fail,2} \dots \leq \beta_{fail,i} R_{fail,i} \text{ and } \beta_{yield} < \beta_{fail} \quad (2.2)$$

where  $R_{fail}$  is the nominal failure resistance of the failure mechanism. For the connection design of SCBFs, the yield mechanism is Whitmore yielding of gusset plates, and the failure modes includes Whitmore fracture, buckling, block shear of gusset plates,

excessive weld tearing and net section fracture of the brace-to-gusset connections. Different  $\beta$  factors were suggested in the study (Roeder et al. 2011b).

### **2.3 Overview of Previous Experimental Investigations**

The SCBF system may be initially designed as a vertical truss. The truss hypothesis results in economical member designs, and capacity based detailing requirements assure that the system provides sufficient stiffness and resistance to resist seismic design loads and easily meet the serviceability limit state in the concept of PBSB. For life safety and collapse prevention, SCBFs develop brace buckling and yielding and gusset plate connection yielding during large, infrequent earthquakes. After brace buckling, SCBFs have highly nonlinear and inelastic behavior. To better understand and improve the nonlinear behavior of SCBFs, many experimental investigations have been conducted since the 1970s. The focus of those experimental investigations could be categorized into three groups: tests of brace components, gusset plate connections and full braced frame systems.

In SCBFs, nonlinear behavior of bracing members mainly govern the system performance. During the 1970s and 1980s, many researches studied the post-buckling and tensile yield behavior of the brace (e.g., Workman 1969, Wakabayashi 1973, Popov et al. 1976, Kahn and Hanson 1976, Black et al. 1980, Astaneh-Asl et al. 1989, Foutch et al. 1987, Lee and Goel 1987, Aslani and Goel 1989). In those research studies, many types of braces (e.g. angles, wide-flange, hollow rectangular and built-up cross sections) with various design parameters (e.g. slenderness ratios, width-to-thickness ratios and steel types) were tested and analyzed under monotonic or cyclic loads. Based on those

experiments, several key conclusions were made:

- (1) Stockier brace members exhibited greater hysteretic energy dissipation than slender specimens.
- (2) The effective slenderness ratio appeared to be the most influential parameter in determining hysteretic behavior of bracing members.
- (3) The maximum compressive strength decreased with increasing numbers of cycles.
- (4) Shape of the cross-section was a significant parameter affecting the hysteretic behavior.
- (5) Hollow rectangular tubes tend to concentrate yield deformation at the corners of the tube and may lead to early brace fracture.
- (6) The width-to-thickness ratio influenced the fracture life of the HSS section brace.

SCBF gusset plate connections must accommodate the brace end rotation caused by brace buckling during severe seismic loading. In addition, the connections must sustain both the tensile and compression loads in the brace during these deformations. Premature failure of the connection would limit the functionality of the brace and provide poor seismic performance. Compared with component tests of bracing members, the experimental research on the gusset plate connections is relatively limited. Gusset connections were initially investigated by applying tensile loads to the connections (Whitmore 1952, Chakrabarti 1983, Hardash and Bjorhovde 1985). Those studies verified that the Whitmore method was appropriate to estimate the maximum tensile stress in the gusset plates, and the block shear model was proposed to estimate the tensile fracture capacity. Thornton (1984) investigated the compressive capacity of the gusset plates, and

proposed a method to estimate the buckling strength based on the Whitmore width and the effective length of the gusset.

Based on the Thornton and Whitmore procedure, many experimental studies were been conducted to improve the performance of the gusset plate connections using monotonic (e.g. Hu and Cheng 1987, Brown 1988, Gross and Cheok 1988, Cheng et al. 1994, Yam and Cheng 2002, Sheng et al. 2002) and Cyclic loading (e.g. Rabinovitch and Cheng 1993, Walbridge et al. 1998, Grondin et al. 2000). These studies led to several key results:

- (1) The Whitmore and Thornton method provided conservative estimate of ultimate strength for compact specimens and overestimated the strength of slender gussets.
- (2) Increasing the bending stiffness of the brace-to-gusset connection and extending it toward beam and column boundary improved the buckling strength of gusset plates.
- (3) The design of weak gusset plate-strong brace combinations resulted in larger energy dissipation than the strong gusset plate-weak brace design.
- (4) The effect of gusset plate edge stiffeners appeared to reduce the rate of decay of the post-buckling resistance for the weak gusset plate-strong brace model.

However, these tests were all gusset plate component tests that did not include the effects of frame action and brace buckling deformation.

More recent research tested full SCBF systems, consisting of bracing members with gusset plate connections at the ends of the brace, to represent the interaction of the bracing member and gusset connections (e.g. Astaneh-Asl et al. 1982, El-Tayem et al. 1985, Xu and Goel 1990, Aslani and Goel 1989). These investigations mainly studied

systems with single, double angle and double channel bracing members. They concluded that:

- (1) The buckling strength of the brace members decreased as a result of cyclic loading.
- (2) The strength and ductility of the braces were highly depended on the connection designs.
- (3) For out-of-plane buckling of the brace, the gusset plates that formed a plastic hinge showed ductile behavior.
- (4) Fixed-end connections provided more energy dissipation capacity, and higher resistance, due to a shift of the end plastic hinge from the gusset plate to the bracing member.
- (5) The boxed section configuration was found to be the most effective in dissipating energy and eliminating section distortion (Aslani and Goel 1989).

The past studies verified yield mechanisms and failure modes such as brace yielding and buckling, gusset plate yielding, brace fracture, and gusset plate weld tearing. These results improved the understanding of behavior of the components, i.e. braces and gusset plates. However, this work fails to validate the performance of the full CBF systems, including bracing members, gusset connections and framing systems, and the interaction between these individual elements. In a more recent experimental study (Uriz and Mahin 2004) on a two-story complete braced frame with HSS section braces and tapered gusset plates, the brace placed large demands on the gusset plate connections, and, in turn, the framing members. The experiment showed column yielding in the column base and column fracture at the beam-column connection. Further and more comprehensive research on complete frame systems was required to better understand the seismic

performance of the SCBF systems and the interaction between components.

### **2.3.1 Prior Experimental Program**

With the overall goal of improving the SCBF system and connection performance, a research program was started at the University of Washington (UW) in 2005. This research was funded by the National Science Foundation (NSF) under the small groups projects CMS-0301792, “Performance-Based Design of Concentrically Braced Frames,” and CMS-0619161, “NEESR-SG International Hybrid Simulation of Tomorrow’s Braced Frames”. The research program included both experimental and analytical modeling investigations. The experiments included 32 single-story single-bay CBF frames testing at UW (Johnson 2005, Herman 2006, Kotulka 2007 and Powell 2009), and six multi-story frames (3-two story and 3-three story) tested at the National Center for Research Engineering (NCREE) in Taipei, Taiwan (Clark 2009, Lumpkin 2009). All of the specimens in the experimental research were full-scale and complete systems. The test specimens and the general conclusions are summarized in Table 2.2.

The single-story single-bay tests at UW were conducted prior to the multi-story testing at NCREE to establish the design technique and base knowledge of SCBF systems, and the multi-story test specimens focused on gusset plate connection performance and utilization of the knowledge gained the single-story single-bay frame tests. The setup of the UW tests represented a single-story single-bay in a theoretical multi-level prototype structure. The testing was conducted by applying cyclic lateral loading, and the effect of gravity loads was simulated by applying axial compression loads in the columns, as shown in Fig. 2.3a. The laboratory constrained the testing to idealized boundary

conditions and did not permit inclusion of floor slabs, but the relative simplicity of the setup permitted evaluation of a wide range of gusset plate configurations, design strategies, brace types and configurations. Nearly all of the tests used HSS 5×5×3/8 braces and W16×45 and W12×72 sections for beams and columns respectively. Various gusset plate connection design parameters were investigated, including thickness and shape of the gusset plate, types and sizes of clearance on the plate and beam-column connections. Specimens with a wide-flange brace (W6×25) and larger beams (W16×89) were also investigated in this test program. The elliptical clearance model and BDP method, described previously, were proposed based on this investigation of the single story tests.

Following the single-story frame tests, three full-scale 2-story single-bay frame specimens using the multi-level X-brace configuration (Clark 2009), see Fig. 2.3b, were tested. The first two frame specimens were designed using the  $8t_p$  elliptical clearance model (see Fig. 2.2a) and BDP method. These frames included composite floor slabs with realistic test boundary conditions that the column bases were fixed on the reaction floor, while the reversed cyclic loading was applied at the roof level. The first test used HSS braces [TCBF1-1(HSS)], and the framing system was reused for the second specimen with reinstallation of new gusset plate connections and wide-flange braces [TCBF1-2(WF)]. The midspan gusset connection at the first floor beam was investigated, and edge stiffeners were added to stiffen the connection based up relative flexible boundary conditions of the connections determined from the continuum finite element analysis of the frame prior to testing. The third specimen [TCBF1-3(TG)] again reused the framing system and installed new HSS braces with tapered gusset plates designed following current AISC code, using the  $2t_p$  linear clearance model.

As the second phase of the multi-story experimental program, three full scale 3-story frames using multi-level X-brace configuration at the bottom two stories and a chevron configuration at the top story were tested, and the cyclic loading was applied on the roof level, as shown in Fig. 2.3c. The framing system included composite floor slabs, and the beams, columns, and composite slabs were reused throughout the three tests with different bracing members and gusset plate connections; the first two specimens used HSS braces and wide-flange braces with out-of-plane buckling gusset plate connections, [TCBF2-1(HSS) and TCBF2-2(WF)], respectively, and the third frame used HSS braces with an in-plane buckling connection configuration. All corner gusset plates used the  $8t_p$  elliptical clearance model, while the midspan gusset plates used the new proposed  $6t_p$  linear clearance model without edge stiffeners as illustrated in Fig. 2.2b. These designs were based on a continuum finite element investigation included as part of this dissertation. More details of investigation will be described in Chapter 3. The overall resulting conclusions reached by the experimental program, including single- and multi-story frames are summarized in the following section.

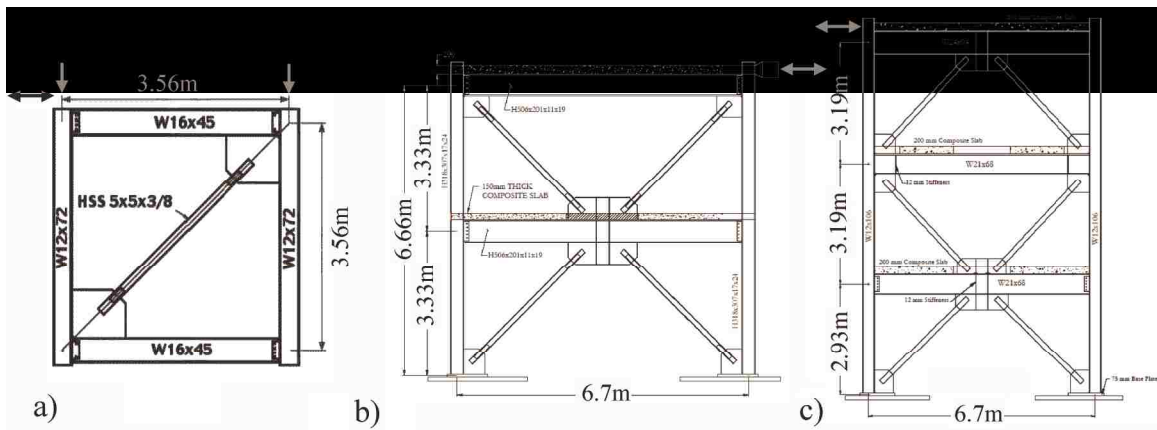


Figure 2.3 Typical Test Specimens; a) Single-Story Single-Bay SCBF, b) Two-Story Single-Bay SCBF, and c) Three-Story Single-Bay SCBF



Table 2.2 Summary of Test Program

Specimen Brace Type	Specimen Description	Gusset and Clearance	Failure Mode
HSS-1	AISC Design- fillet welds by UFM.	13mm- 2tp linear	Weld fracture
HSS-2	HSS1 w/fillet weld sized to capacity of plate	13mm- 6tp ellipse	Brace fracture
HSS-3	BDP-Fillet weld sized to capacity of plate	13m - 6tp ellipse	Brace fracture
HSS-4	BDP-Fillet weld sized to capacity of plate	13mm- 9.4tp ellipse	Brace fracture
HSS-5	BDP-Fillet weld sized to capacity of plate	10mm- 8tp ellipse	Brace fracture
HSS-6	BDP-HSS5 except fillet welds reinforced	10mm- 8tp ellipse	Brace fracture
HSS-7	BDP-Fillet weld sized to capacity of plate	22mm- 6tp ellipse	Brace fracture
HSS-8	BDP-Fillet weld sized to capacity of plate	10mm- 3tp ellipse	Brace fracture
HSS-9	BDP-CJP weld	13mm- 6tp ellipse	Brace fracture
HSS-10	BDP-Tapered gusset- fillet welds to plate cap.	13mm- 7tp ellipse	Brace fracture
HSS-11	Heavy beam-fillet welds to plate capacity	22mm- 6tp ellipse	Brace fracture
HSS-12	AISC Design - CJP weld	13mm- 2tp linear	Brace fracture
HSS-13	BDP- CJP weld	13mm- 7tp ellipse	Brace fracture
HSS-14	No net section reinf- fillet welds to pl. cap.	10mm- 8tp ellipse	Brace fracture
HSS-15	BDP-Min. block shear- fillet welds to pl. cap.	10mm- 6tp ellipse	Brace fracture
HSS-17	BDP-Tapered gusset- fillet welds to plate cap.	10mm- 9tp ellipse	Brace fracture
HSS-18	BDP-Bolted shear pl. - fillet welds to plate cap.	10mm- 8tp ellipse	Brace fracture
HSS-20	BDP-Bolted end plate	10mm- 7tp ellipse	Brace fracture
HSS-21	BDP-Bolted end plate	10mm- 7tp ellipse	Bolt fracture
HSS-22	BDP-Tapered gusset - unwelded beam flanges	10mm- 8tp ellipse	Gusset tearing
WF-23	BDP-W6x25 wide flange brace	10mm- 8tp ellipse	Weld fracture
HSS-24	BDP-3/8" gusset, 6tp elliptical	10mm- 6tp ellipse	Brace fracture
HSS-25	Heavy beam- No net section reinf.- CJP weld	22mm- 6tp ellipse	Brace fracture
HSS-26	Heavy beam- No net section reinf. - Near fault	22mm- 6tp ellipse	Net section
HSS-27	No net section reinforcement - Near fault	10mm- 8tp ellipse	Net section
HSS-28	BDP-Tapered gusset	19m - 2tp linear	Brace fracture
HSS-29	2-Channel Br. - Testing block shear of pl.	10mm- 8tp ellipse	Beam Tearing
HSS-30	Single St. X-bracing - Sandwich pl. at X-conn.	6.4mm- 8tp ellipse	Brace fracture
HSS-31	Single St. X-bracing - Thru pl. at X-conn.	6.4mm- 8tp ellipse	Brace fracture
NCBF32	NCBF gusset conn. designed to the 1988 UBC	10mm- 8tp ellipse	Conn. fracture
TCBF1-1(HSS)	BDP-Two story	10mm- 8tp ellipse	Brace fracture
TCBF1-2(WF)	BDP-Two story	10mm- 8tp ellipse	Brace fracture
TCBF1-3(TG)	AISC Design -Two story- Tapered gusset	20mm - 2tp linear	Brace fracture
TCBF2-1(HSS)	BDP-Three story	10mm - Varies	Brace fracture
TCBF2-2(WF)	BDP-Three story	10mm - Varies	Brace fracture
TCBF2-3(IP)	BDP-Three story- In plane buckling	20mm - 2tp linear	Brace fracture.

### 2.3.2 Important Insight and Improved Designs of SCBFs

The UW test program provided important insight into seismic behavior of SCBFs and their modeling requirements. These include:

- The seismic performance of SCBFs are strongly dependent upon the gusset plate connection and the brace cross-section.
- Extensive inelastic deformation of the gusset plate must be expected. In a well-designed SCBF gusset plate yielding will occur after initial yielding and buckling of the brace. Gusset plate yielding reduces local brace buckling, deformation in the beams and columns adjacent to the gusset plate, and damage to the welds between the gusset and beams and columns, and maximizes SCBF inelastic deformation capacity.
- Different methods are available for permitting and accommodating gusset plate deformation. The  $2t_p$  linear clearance, shown in Fig. 2.1, works well with tapered gusset plate connections, but it often leads to larger, thicker gusset plates, which may significantly reduce the inelastic deformation capacity of the system. The recently proposed  $8t_p$  elliptical clearance model, shown in Fig. 2.2a, often permits smaller, more compact gusset plates, in particular when rectangular gusset plates are used. The elliptical method provides increased inelastic deformation capacity and reduces the size of the relatively rigid connection stiffness zone and the damage to welds, beams and columns adjacent to the gusset. For midspan connections, a  $6t_p$  horizontal clearance zone shown in Fig. 2.2b is preferred, because the boundary conditions are different for midspan and corner connections. In the midspan connection, only the

bottom flange of the beam provides restraint to the gusset plate; in a corner connection, both the beam and column restrain the gusset connection.

- The strength and stiffness of the gusset plate connection must be adequate to develop the expected resistance of the brace, but excess strength and stiffness concentrates the inelastic deformation into a short length of the brace and causes early brace fracture.
- Tapered gusset plates behave a bit differently than rectangular gussets. They may provide good end rotational capacity for the brace, but they also result in thicker gussets or greater inelastic demands on the gusset plate and the welds.
- Wide flange braces achieve larger inelastic deformations than HSS tubes, but they do this at the cost of increased deformation demands on the gusset plate connection and the weld connecting the gusset plate to the beam and the column.
- The system performance is highly dependent on the inclusion of beams and columns. Extensive local yielding must be expected in the beam and column adjacent to the gusset plate.

These observations demonstrate that all of the components and their interaction influence the inelastic response of the SCBF system.

## **2.4 Overview of Previous Analytical Work and Modeling of SCBFs**

Beyond the experimental investigations, a number of analytical studies were conducted to enhance the understanding and improve analytical models for predicting braced frame performance, and various simulation methods have been developed and used. The primary focus of past analytical research was modeling approaches of the brace

and gusset plate connection where large and plastic deformations are expected. Those analytical investigations could be also categorized into three groups: simulation of the braces, gusset plate connections and full braced frame systems as described as follows.

### **2.4.1 Simulation of the Braces**

The inelastic seismic response of SCBFs is dominated by compressive buckling, tensile yielding and post-buckling behavior of the braces (Popov et al. 1976). The inelastic deformation of braces is complex and highly nonlinear. Therefore, simulation of the cyclic inelastic behavior of the brace plays a big role and strongly influences the overall analytical seismic response of the braced frame structures. In most of the early analytical studies, the gusset plate connections were simplified as pinned or fixed joints. Hence, the results of such analyses are largely dominated by brace behavior. Various analytical methods have been developed to represent the nonlinear cyclic buckling behavior of braces. These analytical models can be further divided into three different general categories: phenomenological, simplified phenomenological and finite element (FE) methods as depicted in Fig. 2.4.

The phenomenological method employs a prescribed physical model to simulate the cyclic behavior of the brace (Nilforoushan 1973). The phenomenological model of the brace uses simplified hysteretic rules to mimic the experimental axial force-axial displacement relationship, as shown in Fig. 2.4a. The model is simple and computationally efficient, because the method may require only one local degree of freedom, i.e. axial displacement of the brace. However, as high accuracy of simulation is needed, the models require specification of numerous empirical input parameters for each

strut. It is always difficult or uneconomical to obtain those parameters properly. Therefore, even if the phenomenological method is computationally economical, its accuracy is often uncertain and its use is limited.

For finding a more general and computationally efficient analytical approach for simulation of brace performance, physical theory brace models were developed and provided an intermediate model between the phenomenology and FE approaches (Soroushian et al. 1988; Ikeda et al. 1986). The physical theory brace model usually consists of a plastic hinge model and two elastic struts or beam-column elements as shown in Fig. 2.4b. The main assumption of the physical theory models was that all inelastic deformation of the brace are concentrated in dimensionless plastic hinges at the critical locations (generally at the mid-length) of the brace. The critical part of this model is simulation of the plastic hinges. The inelastic axial force-rotation relationships of the plastic hinge, using force (Ikeda et al. 1986), and displacement method of analysis (Soroushian et al. 1988), were adopted with simplified theoretical formulations based on physical considerations that allow the cyclic inelastic behavior of braces to be computed. Different from the phenomenological models, the required input parameters of the physical theory models are only the material properties and geometric engineering properties of the brace member. Further experiments or analyses using refined models are not required for obtaining the proper input parameters. However, based on the comparison of analytical responses of the physical theory model with the experimental results, the accuracy of representation of the analytical model still needs to be improved.

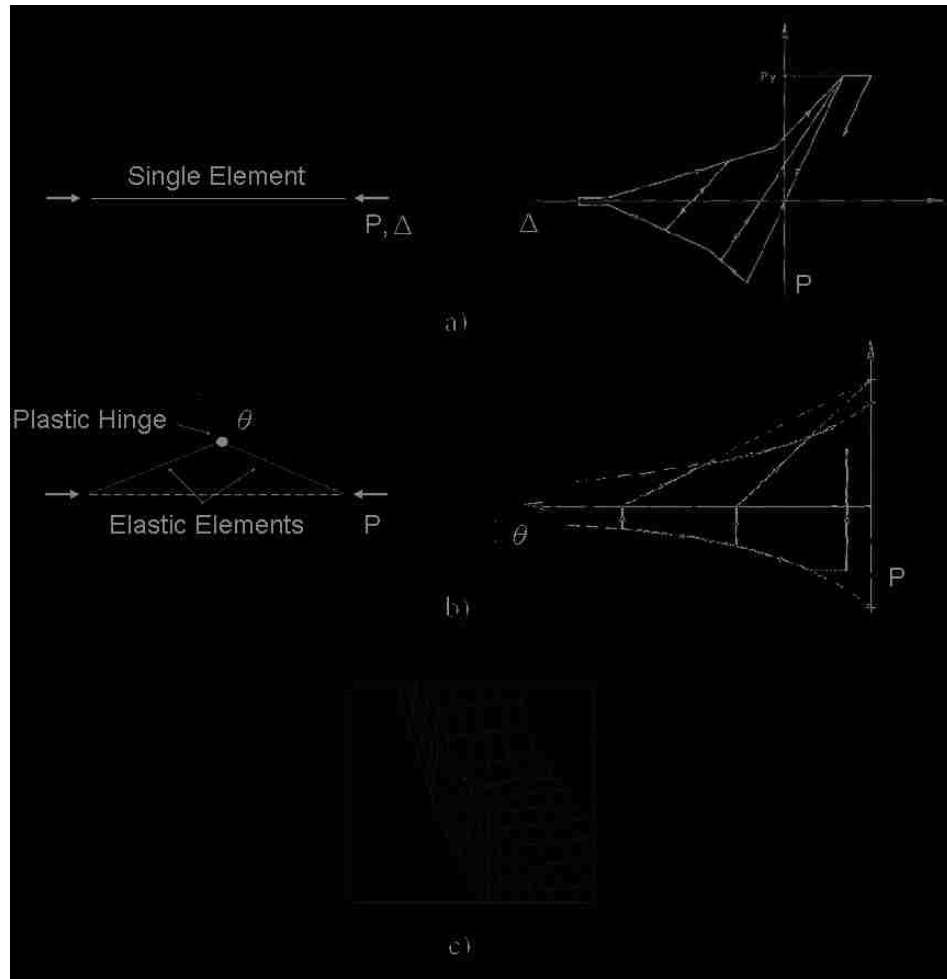


Figure 2.4 Schematics of the three categories of brace hysteretic models: (a) Phenomenological Models; (b) Simplified Phenomenological Models; (c) Finite Element Models

The FE method, also-called continuum FE analysis, subdivides the considered member into a series of elements (shell or brick elements) as illustrated in Fig. 2.4c, which have an adequate mesh size and physical characteristics needed to provide a reliable representation of member behavior. Finite Element Method (FEM) is more and more commonly adopted to achieve the simulation of the complex inelastic deformations of the braces as computational capability increased in the past decade. Haddad and Tremblay (2006) completed an analytical study on connection designs of out-of-plane

and in-plane buckling braces through FEM. A FE model of a single brace attached to gusset plate connections at the both ends was developed using ABAQUS program with eight-node brick elements; both pushover and cyclic loading analyses were applied. To induce the buckling behavior of the brace model, a small transverse displacement was imposed at mid-length of the brace to reproduce the initial imperfection of the brace tubes prior to applying compression or cyclic loading.

The FEM requires appropriate mesh size, proper element capabilities, good modeling techniques, and verification and calibration of the results. However, although FE modeling can provide a very realistic representation, it usually demands significant computation. Many simultaneous equations are required, and the nonlinear calculations may require hours or days to complete even for modest sized structures. The costly computations make it difficult to apply the procedure to relatively large structural systems and practical applications. Therefore, for analyses of relatively large structural systems, the phenomenological and simplified phenomenological methods are usually adopted.

#### **2.4.1.1 Fiber-Type Finite Element Models**

Beyond those simulation methods, Gunnarsson (2004) did a prior analytical study focusing on a less computational intensive FE brace model with line-elements and fiber section using the OpenSees framework (McKenna 1997) with the goal of achieve both of high accuracy and computational efficiency. This fiber-type FE model lies between full FE simulation and simplified phenomenological methods. The model attempts to combine the realism of FE approach and the computational efficiency of the physical theory model. Gunnarsson's brace model consists of a minimum of ten force-based

nonlinear beam-column elements in combination with the Steel02 material model, and fiber sections were used for including distributed plasticity of braces. For inducing buckling behavior of the brace, an initial imperfection of  $L/500$  was required ( $L$  is the length of the brace tubes). The single brace model was verified by matching the AISC buckling curve (AISC 2005). This model enforces plane sections remain plane deformational constraints at all nodes and integration points. However, compared to the continuum FE model, the fiber-type FE model requires fewer computations, and provides the possibility of reasonable accuracy at dramatically reduced computational cost.

Using a similar fiber-type FE approach, Tremblay (2008) analyzed a number of braces with various slenderness ratios for evaluating the influence of the brace slenderness on the axial compressive strains that lead to local buckling and brace fracture. The strain demand was examined in an attempt to assess the effect of brace slenderness on brace fracture. Uriz et al. (2008) conducted experimental and analytical study on SCBFs to assess the performance of chevron braced frame structures. They also modeled braces using the fiber-type FE model; fiber sections were used to model plastic hinge behavior including low-cycle fatigue effects. The investigation examined many parameters including: the effects of fatigue modeling parameters, the dynamic characteristics of SCBFs, as well as the response of low-rise and mid-rise braced frame buildings.

## **2.4.2 Simulation of the Gusset Plate Connections**

The brace can not be accurately simulated without combining the brace model with a correct model of the brace connections. Hence, modeling of the gusset plate connection



also plays a significant role in the simulation of SCBF structures. Gusset plate connections must tolerate large inelastic deformations, while resisting large tensile axial forces from braces and the bending moment due to brace buckling. These combined effects complicate analytical prediction of their performance. For obtaining the representation of these complex deformations of gusset plate connections in SCBFs, continuum FEM has always been employed.

Cheng et al. (1994) created FE models for single gusset plates using the ANSYS computer program for predicting the buckling strength of the connections. The FEM was also used for studies of brace-gusset plate and beam-brace-column connections (Fu et al. 2007, MacRae et al. 2004). MacRae et al. built FE models of beam-brace-CFT column connections using the ABAQUS program for evaluating the transfer and distribution of force to the joint. Fu et al. (2007) also used ABAQUS to model brace-gusset plate connections for investigating the inelastic seismic responses of typical slotted net section connections with round pipe.

Rather than using refined models, the gusset plate connection was usually simplified as a pinned or fixed joint in other structural analyses using line-elements simulation approach (Tremblay. 2008; Ikeda et al. 1986, Uriz et al. 2008). However, gusset plate connections in real structures do not usually act like a perfect pinned or rigid joint. For accurate simulation of SCBF behavior, detailed modeling of the gusset plate connections is required.

### **2.4.3 Simulation of the Full Systems**

Boundary conditions are always critical in FE modeling of SCBF components and

systems, (i.e. the braces or gusset plate connections), because both braces and gusset plate connections have large inelastic deformations after brace buckling. These large deformations lead to variable boundary condition for each component (e.g. changed orientation of the brace axial force for the gusset plate components and changed bending resistance of the gussets for the brace components). The variability of boundary conditions was usually not included in the continuum FE analysis of components.

To include the correct boundary conditions for the bracing member and the gusset plate connections, the simulation of the full SCBF system is needed. Yoo (2006) developed a continuum FE model for the braced frames using the ANSYS program, and he validated his model by comparison to experimental results from a series of the single-bay single-story testing at UW. A fine element mesh and detailed modeling of all connections were required. These complex models provide accurate representation of both global and local behavior of the system, and numerous comparisons were made between local and global behavior in analysis and experiments, as illustrated in Fig. 2.5. This model provided good representation of the local behavior, and the FE model was extended to include consideration of initiation of cracking and fracture. (Yoo et al. 2008, Yoo et al. 2009).

Beyond the brace model using the fiber-type FEM described previously, Gunnarsson (2004) also simulated the full braced frame system and compared the results to a limited number of tests. Several simplified models of the gusset plate connections, consisting of rigid links and spring model of the gusset joint, were investigated. The rotational stiffness values of the spring model were estimated by the empirical formulas given by the Yoo's (2006) FE investigation for qualification of joint stiffness.

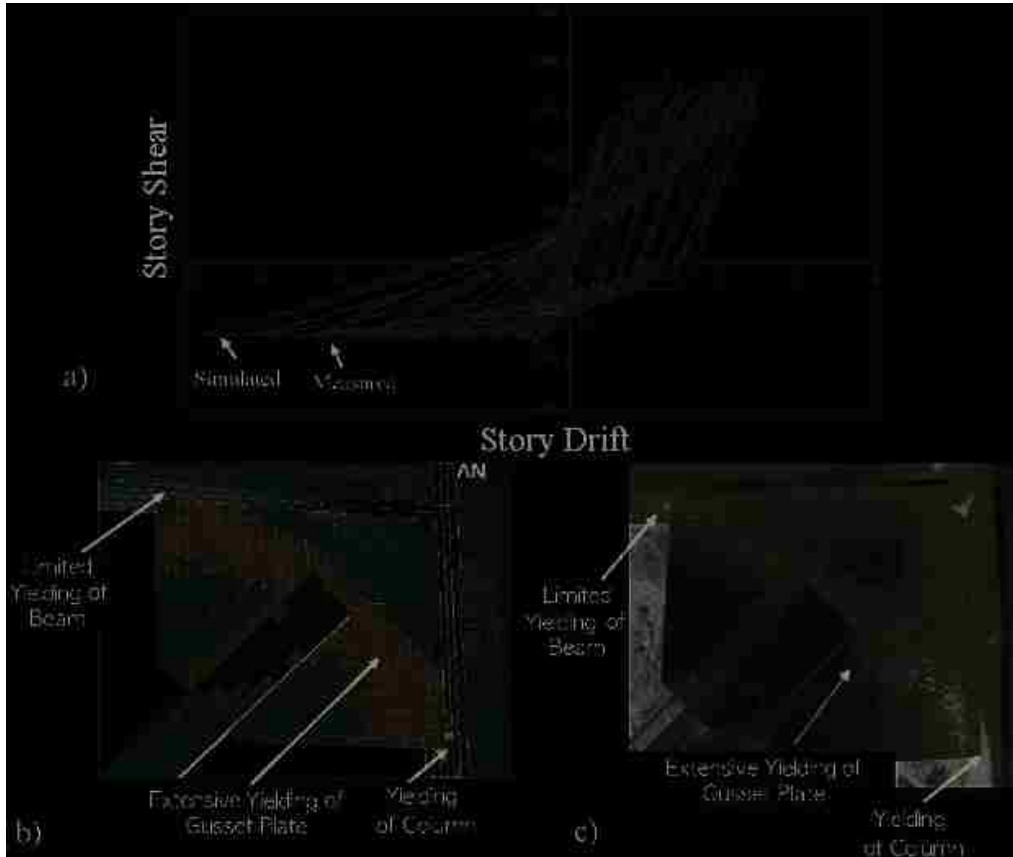


Figure 2.5 Comparison of Results of Detailed Analysis with Experiments; a) Measured and Computed Force-Deformation Behavior, b) Computed Stress Distribution, c) Experimentally Observed Yielding



## **Chapter 3 : Continuum Finite Element Analysis on Three-Story SCBF Systems**

### **3.1 Introduction**

A series of 3-story, single-bay SCBF experiments, including two out-of-plane buckling braced frames using HSS (TCBF2-1) and wide-flange (TCBF2-2) braces and one in-plane buckling braced frames using HSS braces (TCBF2-3), were conducted as a part of the experimental work in the braced frame project.

Prior to the tests, those frame specimens were investigated through a continuum FE analytical study (1) to confirm the design of test specimen and (2) to establish the  $6t_p$  linear clearance design for midspan gusset plate connections and the in-plane-buckling connections. The FE investigation here is an extension of the prior analytical study by Yoo (2006), who conducted the continuum FE investigation on the single-story (UW tests) and two-story braced frames (TCBF1), using the ANSYS computer program. The finite element mesh and detailed modeling of connections used in these analyses were similar to those used by Yoo (2006). However, two modifications were made to improve the FE model of the brace buckling and the composite concrete slabs. With the improvements, the continuum FE model (denoted ANSYS model herein) accurately simulated the measured and observed responses of the multi-story frame specimens at both global and local levels.

The dimensions and design of the test specimens are given in Section 3.2. The details of the extended FE model in the study and the modifications made are described in Section 3.3, and the applications of the FE model with the modifications are presented in Section 3.4. Section 3.5 will present the resulting response simulation of those 3-story frames and comparison with measured and observed test results. The design, test setup and primary test results of the 3-story frame specimens with the analytical study using this extended FE model were also addressed in a published journal paper as documented in Appendix A.

## **3.2 TEST SPECIMENS**

The three-story frame test program was undertaken to further investigate midspan gussets and multi-level SCBFs with different brace configurations, connection and brace types. Each specimen utilized a multi-story X brace configuration in the bottom two stories and a chevron (or inverted V) brace configuration in the top story. The first and second tests had HSS rectangular tube (TCBF2-1) and wide flange braces (TCBF2-2) with an out-of-plane buckling brace configuration, respectively, and the third frame had HSS rectangular tube braces with an in-plane buckling brace configuration (TCBF2-3). Extensive nonlinear analysis preceded the experiments to evaluate alternatives and to improve the midspan gusset plate connection design. Together, they provide the basis for a new method for detailing these connections. The tests also provide confirmation of past design recommendations, validation of the analytical methods, and evaluation of the distribution of inelastic deformation between different stories.

The test specimen all utilized the same brace configuration. For economy, all tests

were performed on the same frame; each specimen retained the same slab, beams and columns. The braces and gusset plate connections were replaced. Figure 3.1 gives dimensions and member sizes of the specimens. The repeated test components included W12x106 columns, W21x68 first and second story beams and a larger W24x94 third story beam to resist the unequal forces in chevron or inverted V-bracing after brace buckling. All of the beam and columns were US sizes.

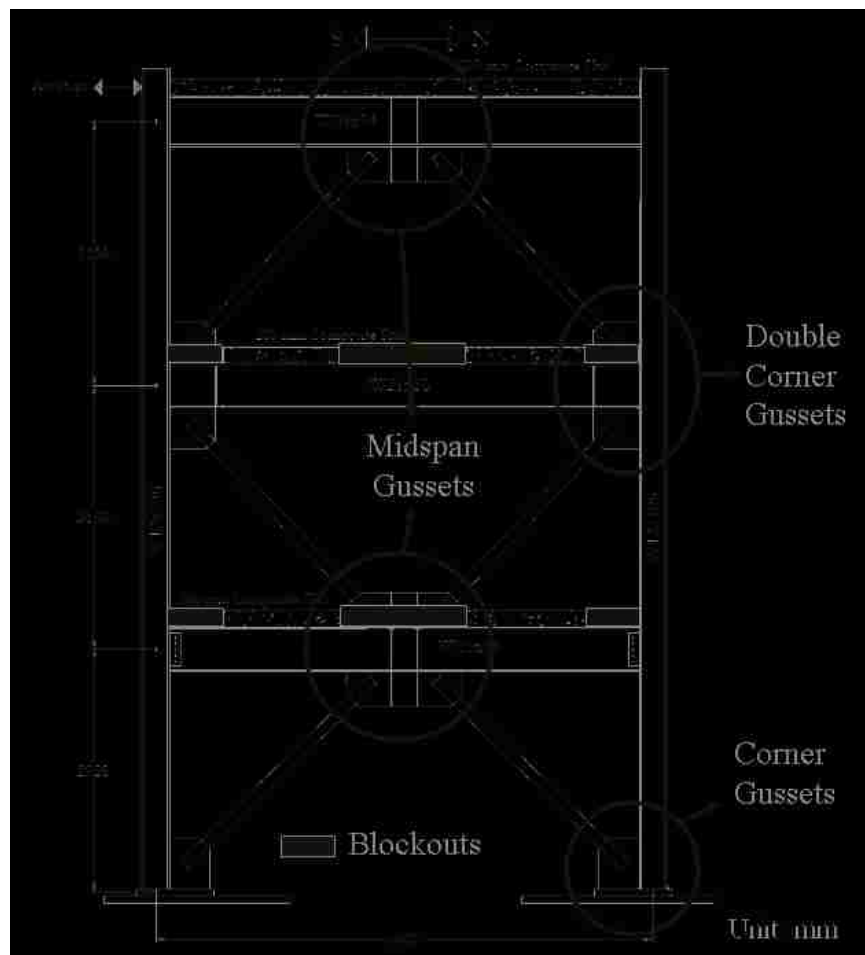


Figure 3.1 Typical TCBF2 Specimen Configuration.

For TCBF2-1 and TCBF2-3, the braces were A500B/C HSS 5x5x3/8 sections ( $A_g = 3987. \text{ mm}^2$ ). TCBF2-2 retained the same beams and columns but Taiwanese steel was

utilized, specifically H175x175x7.5x11 ( $A_g = 5121. \text{ mm}^2$ ) wide flange braces. These member sizes are typical of those used in a low to mid-rise structure. The total work point-to-work point height was 9.31 m; the first story was slightly shorter than the upper two stories to achieve approximately equal brace lengths on all three stories. The beam-to-column connections on the first story were shear plate connections, but the upper two stories had welded-web-welded flange beam-to-column connections. Composite (200-mm thickness) concrete slabs reinforced with 0.50% steel fiber were used on each story, since the lateral loads were transferred from the actuators through the slab to the frame during testing. More details of design and test results of the specimens can be found in the reference (Lumpkin 2009).

### **3.3. Continuum Finite Element Model with Modifications**

The ANSYS model for the multi-story frame specimens in this study used the similar mesh sizes and details modeling of connections of Yoo's FE model (Yoo 2006). All of the members were constructed using four-node quadrilateral shell elements (SHELL181 provided in ANSYS). The four-noded element has 6 degrees of freedom at each node and is suitable for analyzing thin to moderately-thick shell structures and large strain nonlinear applications. Figure 3.2a shows the typical element mesh and boundary conditions used for these three-story frames. The frame model was fully restrained at the base plates and restrained out-of-plane at the floor levels simulating the lateral supports of the test specimens. The shear-tab connections were simulated by constraining the shear-tab to the beam web at the locations of connecting bolts as shown in Fig. 3.2a.

Moreover, a large-displacement formulation was used to simulate buckling behavior;



a bilinear, kinematic hardening material model was adopted to simulate the inelastic behavior of steel under cyclic loading. Concrete slabs were also simulated in the model by using elastic shell elements with the elastic modulus of concrete. Figure 3.2b presents the approximate mesh sizes for each member. Among all members, the gusset plate has relatively refined mesh due to that the behavior of gusset plates is complex and highly nonlinear behavior, especially beyond the brace ends.

For improving the FE model and increasing the accuracy of the simulation for the multi-story tests, modifications used to model brace buckling and the composite slab are discussed in greater detail.

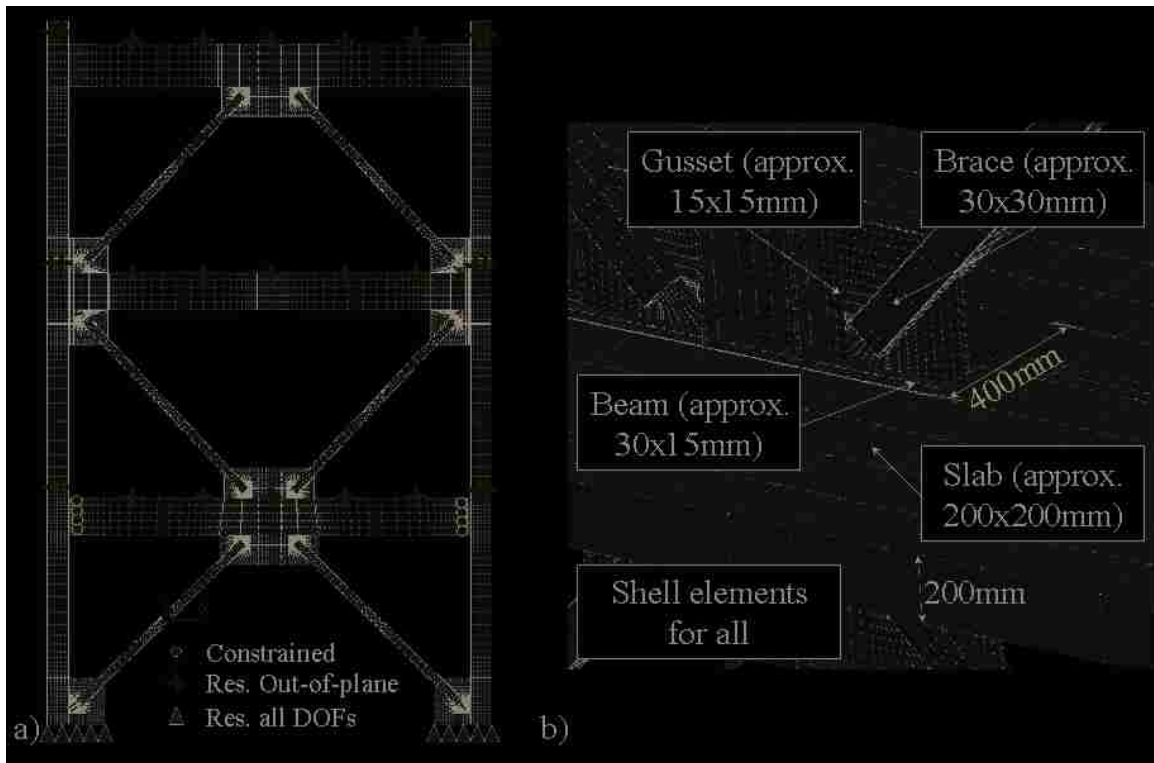


Figure 3.2 (a) The Typical Applied Element Mesh and the Boundary Conditions, (b) Approximate Mesh Sizes for Each Component.

### 3.3.1 Modeling Approach of Brace Buckling

The experimental program and Yoo's analytical study (2006) for the single-story single-bay frames employed brace eccentricity to induce and control the direction of brace buckling. However, in the multi-story frame specimens, brace eccentricity was not used in the test specimens. To simulate brace buckling in the continuum FE models for those multi-story frames, a small transverse force was applied at the mid-length of the braces, as shown in Fig. 3.3, instead of an initial eccentricity. Without the initial deformation of the brace, the brace buckling behavior would not be consistently triggered in the computer model. The applied forces were relatively small (a total of 18kN) with the purpose of providing an initial crookedness or imperfection to initiate brace buckling in the computer model, and the forces were applied at the corner of the brace cross section, as shown in the figure. These small force remained in place through the entire sequence of cyclic loads. The mesh size around the mid-length of the brace was uniformly distributed with an approximated mesh size of 30-by-30mm. The direction of brace buckling in the computer model was controlled by the direction of the given transverse force. Comparisons between this approach and the prior method of using an eccentric offset of the entire brace show that the modified modeling approach provided better simulation of brace performance.

The experimental results of the prior first 2-story braced frame, TCBF1-1(HSS), was used to verify this modeling approach for brace buckling. Figure 3.4 shows the experimental story drift distributions of the frame and the analytical responses using the two difference approaches at the average story drift of 1.6%.The results show that the modified model provided more accurate simulation of the complete frame behavior,

which is mainly controlled by the simulation of the buckling and post-buckling behavior of the braces, than the model with brace eccentricity. Using the eccentric offset of the brace, the FE model overestimated the deformation concentration at the bottom story and didn't predict the buckling of the second story braces due to the significant underestimate of the second story drift, and this prediction is essentially different from the experimental observation.

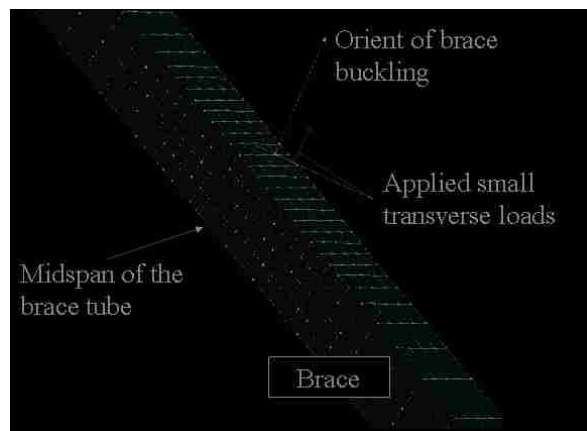


Figure 3.3 Mesh and the Applied Loads at Midspan of the Brace

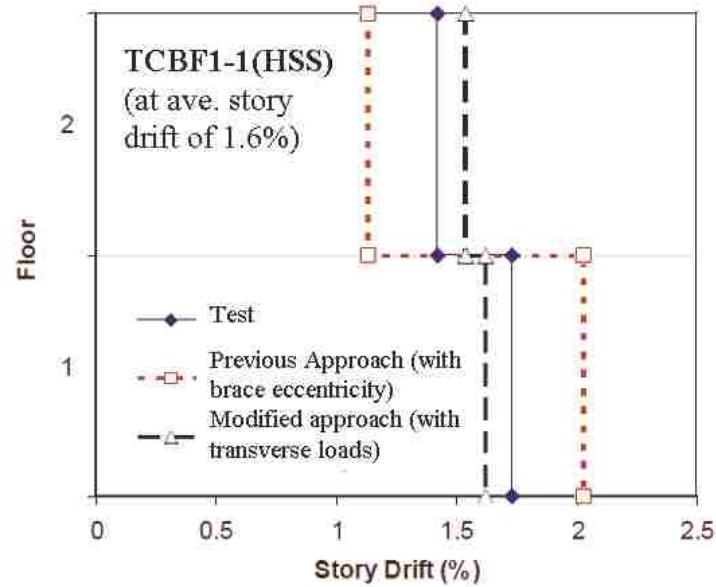


Figure 3.4 Comparison of the Story Drift Distribution of TCBF1-1(HSS) with Different Approaches of Modeling Brace Buckling.

### 3.3.2 Modeling Composite Slab

The two-story and three-story frame specimens had a composite slab at each floor level, which significantly increased the stiffness and strength of the beams, thus the effect of the composite slab must be included in the continuum FE model.

In the experimental observation, no severe creaks occurred on the concrete slab except the slab adjacent to shear-tab connections. The slab was assumed to retain elastic in the frame models, shell elements using an elastic material model with the elastic modulus of concrete were added on the top of the upper flange of the beam, as depicted in Figs. 3.5 and 3.2b, to include the stiffness of concrete slab. The simulation of the severe creaks of slab adjacent to the shear-tab connections were evaluated and discussed later in this chapter.

The concrete slab model had identical thickness (200mm) and width (2060mm) as

the test specimens. The slab model was constrained to the beam through the nodes arranged according to the location of the shear studs at the top flange of the beam in the specimen and to the column through the nodes at the intersection of the slab and the ends of column web.

In the three-story frames, a number of blockout regions in the slab were arranged for multiple use of the frame using variable brace configurations, as shown in Figs. 3.2b and 3.5a. Those blockout regions were wider than the beam member. Figure 3.1 indicates the locations of all blockout regions in the frame specimens. For correctly representing the composite slab, those blockout regions were also included in the ANSYS model as shown in Fig. 3.5b. The support beams (see Fig 3.5a) beneath the concrete slab in the transverse direction of the frame were neglected in the model with the assumption that they have a minor effect on the system behavior.

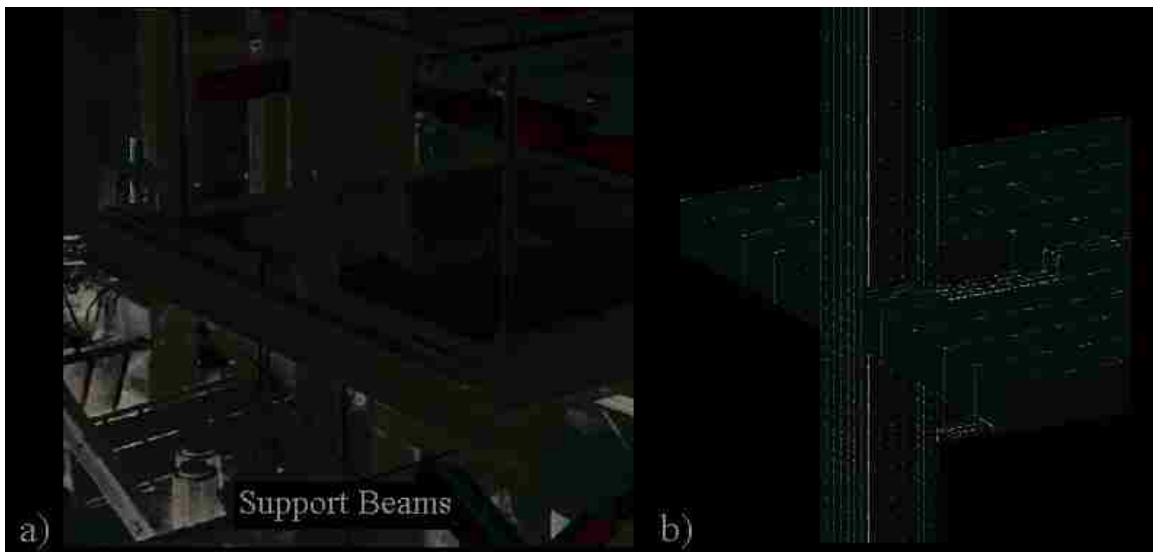


Figure 3.5 (a) The Photo and (b) the Mesh of the Composite Slab with the Blockouts.

### **3.4 Applications of the Extended Finite Element model**

The extended FE model for the multi-story frames was verified by the first two-story braced frame test, TCBF1-1(HSS), as described above, and used to check the design of the three-story frame specimens and predict their behavior before the tests. This was especially important for the connections that only appeared in the multi-story frames, such as the midspan gusset plate connections, the double-corner-gusset plate connections (see Fig. 3.1), and the in-plane buckling connections for the TCBF2-3(IP), since there was no prior single story test data for these connections. The evaluations of those particular connections are described as follows.

#### **3.4.1 Clearance Design of Midspan Gusset Plate Connections**

The midspan gusset plate connections in the two-story frame tests, TCBF1-1 and TCBF1-2, used the  $8t_p$  elliptical clearance design with edge stiffeners as mentioned previously. The midspan connections for these two specimens did not develop elliptical yielding band as shown in Fig. 3.6 and provided adequate but less than desired performance. Prior analysis (Yoo et al. 2009) suggested that this was a result of the edge stiffeners. The edge stiffeners increased the out-of-plane stiffness of the connection and resulted in twisting of the composite beam at the 1<sup>st</sup>-floor level caused by the buckling braces. To improve the design of the midspan connections and avoid the twisting of composite beams, a new design with uniform horizontal off-set clearance zone and no edge stiffeners was developed for the design of the three-story specimens through this analytical investigation.



Figure 3.6 Photo of the Midspan Gusset Plate Connection with Edge Stiffeners in Specimen TCBF1-1(WF).

A finite element analysis to evaluate this particular midspan connection was conducted. Horizontal clearance zones with a vertical clearance of 2 to 8 times of the thickness of gusset plate ( $t_p$ ), parallel to the bottom flange of the beam as illustrated in Fig. 2.2b, were evaluated using the TCBF1-1(HSS) test specimen configuration and modifying the design of the middle gusset plate. The cyclic loading protocol of TCBF1-1 in the test was applied. The equivalent plastic strain (EPS) was evaluated to indicate the potential failure of the gusset-to-beam and column connections based on prior FE study (Yoo et al. 2008). The results of the study based upon the single-story frames (UW tests) showed that significant weld tearing at the gusset-to-column welds occurred as the EPS value reached the range of 0.0732 and 0.0832, and the weld tearing at gusset-to-beam welds occurred as the EPS value increased to 0.0554.

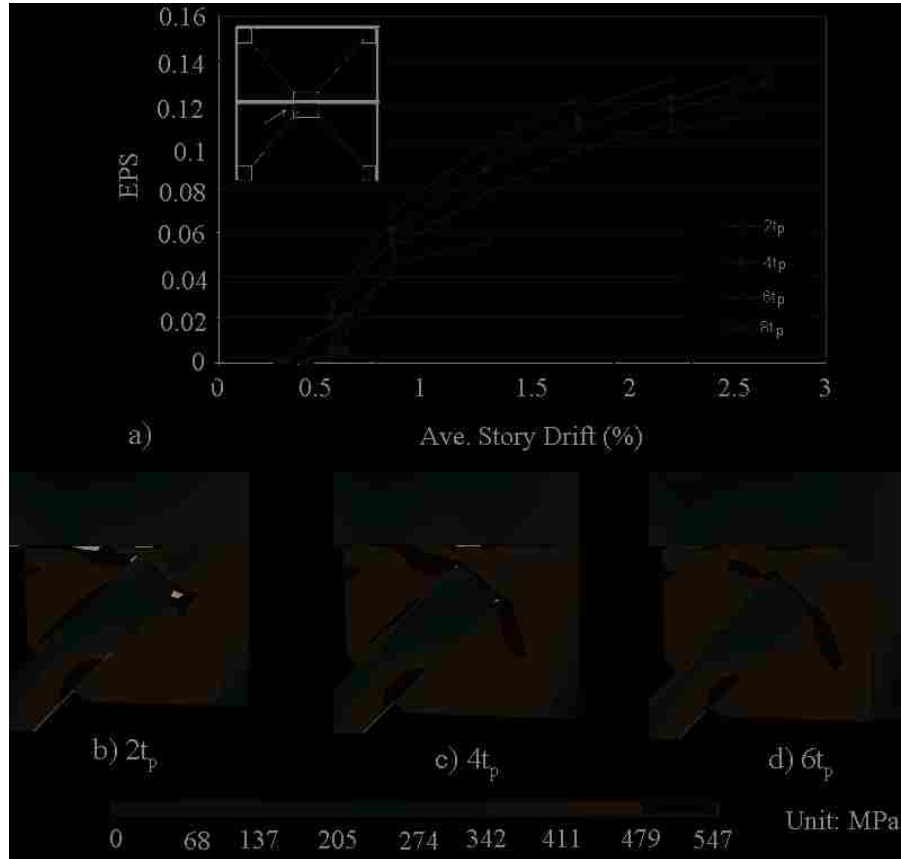


Figure 3.7 (a) The EPS Responses of the Midspan Gussets-to-Beam Weld in the Two-story Frame with Various Linear Clearances; the Equivalent Stress Distributions of the Midspan Gusset Plates with Clearances of (b)  $2t_p$ , (c)  $4t_p$  and (d)  $6t_p$ .

The EPS value was used to estimate the strain demand and the potential for weld fracture of the midspan gusset-to-beam weld in the two-story frames based upon the criteria proposed by Yoo et al. (2008). Figure 3.7a shows the EPS values of the middle gusset-to-beam weld at the gusset plate edge versus average story drift using the various clearances, from  $2t_p$  to  $8t_p$ . These developed EPS values for the clearance of  $2t_p$  to  $6t_p$  were over the limit value of 0.0554 proposed by Yoo et al. (2008) at less than the average story drift of 1.0%. The results suggested that the Yoo's EPS limits for predicting weld fracture, which were validated by the experiments of corner gusset plates, were likely not



suitable for the midspan gusset plates. The analyses of the  $8t_p$  linear clearance failed to converge analysis for story drifts larger than 1.5%. The failure to converge may reflect purely computational concerns, but deformation and instability of the gusset plate with this larger clearance is also a likely cause. The target deformation of these frames is greater than an average 1.5% drift, and so the  $8t_p$  clearance was eliminated from consideration. Figure 3.7a show that increasing the linear clearance decreases the EPS demand at the gusset-to-beam welds and beam webs. Further, Figures 3.7b, c and d show significantly increasing stress concentration with the smaller clearance values. As a result, the  $6t_p$  horizontal clearance design was used for the design of the three-story specimens. The linear clearance design for the midspan gusset plate connections was verified by the experimental results. Figure 3.8a shows the elliptical yield shape of the midspan gusset plate connection in the test, which well agreed with the analytical prediction of the frame as shown in Fig. 3.8b. Based on the analytical evaluation and test results, using the horizontal clearance design for the midspan gusset plate connections successfully prevents the twisting of the composite beam mentioned above.

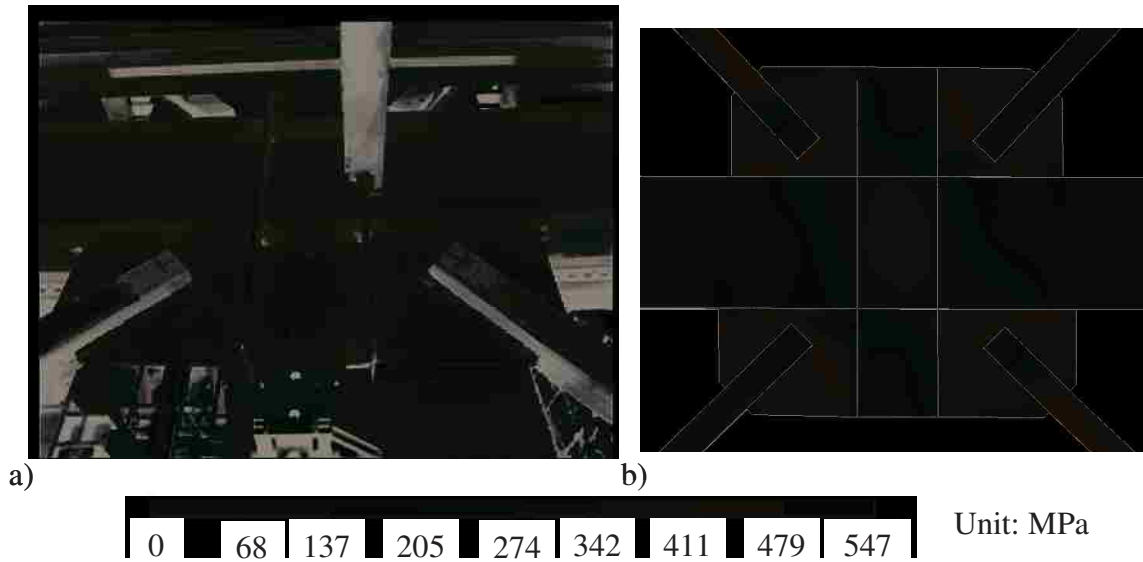


Figure 3.8 (a) Photo of Gusset Plate Yielding and (b) Analytical Equivalent Stress Distribution of the Midspan Gusset Connection of TCBF2-1(HSS)

### 3.4.2 Design of Double Corner Gusset Connections

In the preparation of the three-story frame tests, the FE model of the three-story specimen was also used to predict the performance of other aspects, i.e. double-corner gusset plate connections, of the frame behavior at both the local and global levels.

The analytical results indicated that the double-corner-gusset plate connections at the ends of the second floor beam formed severe stress concentration at the edge of gusset-to-beam connections and warped the bottom beam flange, which would be potentially damaging to the framing system, as shown in Fig. 3.9a. For the multiple use of the framing system, a stiffener was added to the beam web at the edge of the gusset plate to prevent premature failure of the connection.

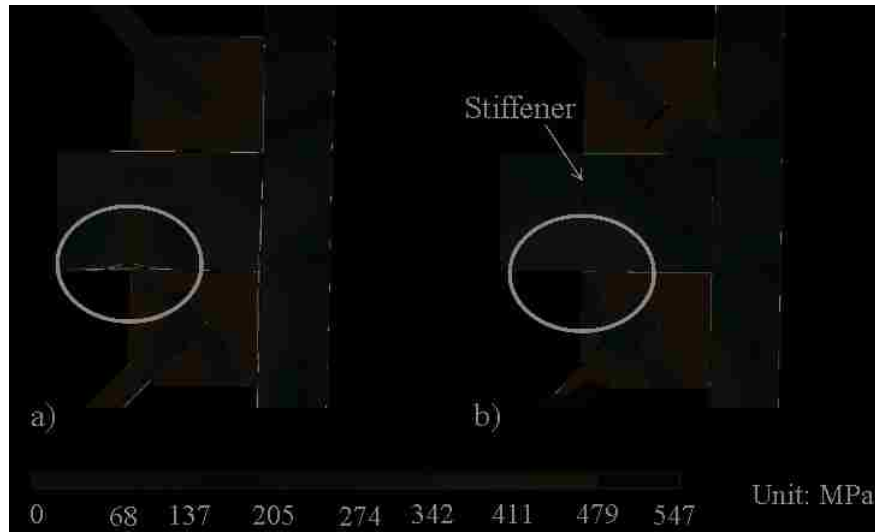


Figure 3.9 Comparison of the Equivalent Stress Distribution (a) With and (b) Without Adding the Stiffener at Average Story Drift of 2.0 %

The analytical results confirmed that adding the stiffener effectively reduced the stress at the beam and prevented warping of the beam flange. Figure 3.9 shows the equivalent stress distribution of the particular connection with and without the web stiffener at the average frame story drift of 2.0%. It is apparent that with the stiffener welded at the beam web, this double-corner gusset plate connection performed similarly to the other corner gusset connections.

### 3.4.3 Design of In-plane Buckling Connections

The in-plane buckling brace configuration was used in the TCBF2-3 as mentioned previously. The in-plane buckling connection was designed to transfer the brace axial load through a knife plate, as illustrated in Fig. 3.10a. This in plane buckling connection had not been analyzed or tested before, therefore FE analysis was performed to investigate the connection prior to the experiment.

Thicknesses of the knife plates,  $t_{kp}$ , and linear clearances,  $Nt_{kp}$ , were evaluated in the analytical research (see Fig. 3.10a). Two thicknesses of 20 and 25mm and two linear clearances of  $1t_{kp}$  and  $2t_{kp}$  were analyzed. Figures 3.10b to d show the dimensions of the knife plates and the resulting equivalent stress distributions.

Comparison of the stress distributions with different clearances using the 260-by-20mm knife plate (see Figs. 3.10b and c) shows that the  $1t_{kp}$  clearance dramatically increases the magnitude of the stress demand on the hinge region. This small clearance led to the concentration of inelastic strain and deformation into a relatively small area of the knife plate. The  $2t_{kp}$  clearance distributes the rotational and tensile strain and deformation demand to a larger area and larger hinge region (see Figs. 3.10c and d). Therefore, the  $2t_{kp}$  clearance model was used for the design of the knife plate.

Moreover, with different thickness of knife plate using the  $2t_{kp}$  clearance, the 260-by-20mm knife plate more effectively spread the yielding to other areas of the knife plate and decrease the demand on the hinge region than the narrower (210-by-20mm) knife plate. Based upon the analytical results, a  $2t_{kp}$  clearance on a hinge region with cross-sectional dimensions of 260-by-20mm was used for the design.

The end of the knife plate was tapered, as shown in Fig. 3.10a, since the corners were lightly stressed and the taper produced a cleaner detail. The FE analysis of this changed geometry was also performed, and comparison of Fig. 3.10e and d shows that the taper improves the stress flow from the brace to the hinge region, because of the elimination of the sharp transitions between stress contours. To assure uniform stress in the plastic hinge zone of the knife plate, the taper was stopped a distance of  $2t_{kp}$  from the brace end.

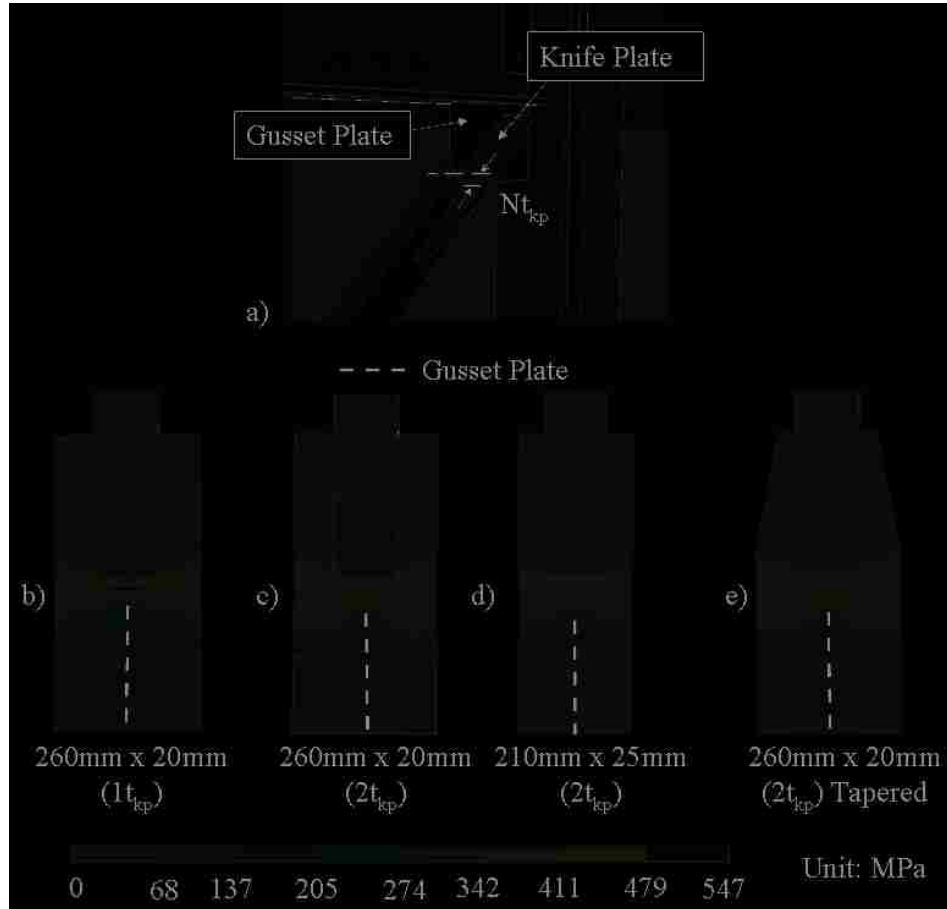


Figure 3.10 (a) A Schematic of the In-Plane Buckling Connections; the Equivalent Stress Distributions of the Knife Plate with (b-d) Various Thickness and Clearance, and (e) Final Tapered Design for TCBF2-3(IP).

### 3.5 Analytical Responses of the 3-story Braced Frames

The extended FE model using the results of the investigations on those particular connections as described above was performed to simulate the series of the 3-story frame tests. The analytical responses are presented and compared with the experimental results at both global and local levels in this section.

### 3.5.1 Analytical Results of TCBF2-1 with OOP HSS Braces Buckling

During testing of TCBF2-1, severe cracks were observed at the two ends of the first floor concrete slab, as shown in Fig. 3.11a, at average frame drift of 0.7%. Figure 3.11b show the post-test crack map. The severe cracks resulted from the large rotational demand of the shear-tab connections underneath the slab and the blockout placed in the slab. The concrete slab was not repaired for subsequent test specimens, and so this damage was present prior to all other tests. The cracks were considerable, and there was concern that this prior damage would have a significant impact for subsequent tests which was not captured in the composite slab model described previously.

To investigate the influence of the severe slab cracking on the frame system behavior, two cases of slab modeling, titled Case I and Case II as shown in Fig. 3.12a, were analyzed and compared. Case I assumed no cracks occurred on the slab during the test, while the Case II model simulates the specimen with severe slab cracking by simply removing the slab elements near the shear-tab connections. Figure 3.12b shows analytical story drift distribution of the TCBF2-1 for the two models and compare the predictions with experimental results. The results at three different drift levels, 0.33, 0.67 and 1.67%, are shown in the figure.

At the 0.33% drift level, both of the models agree well with the measured results. However, the analytical responses at drift of 0.67 and 1.67% showed that the composite slab had a more significant effect on the frame stiffness and story drift distribution throughout the story height. Compared with the experimental response, the Case II model was overall a better model of specimen behavior after the severe cracks occurred early in the test. As a result, the Case II slab model was consistently used for the simulations of

the entire series of the 3-story frames.

Figure 3.13 shows a comparison of the analytical and experimental hysteretic responses of the TCBF2-1 for the frame and individual stories. In the test, the first brace fractured at the first cycle to reach the average story drift of 2%. No fracture model was included in the FE model, therefore the comparison is shown until the cycle prior to brace fracture with the frame drift of 1.67%.

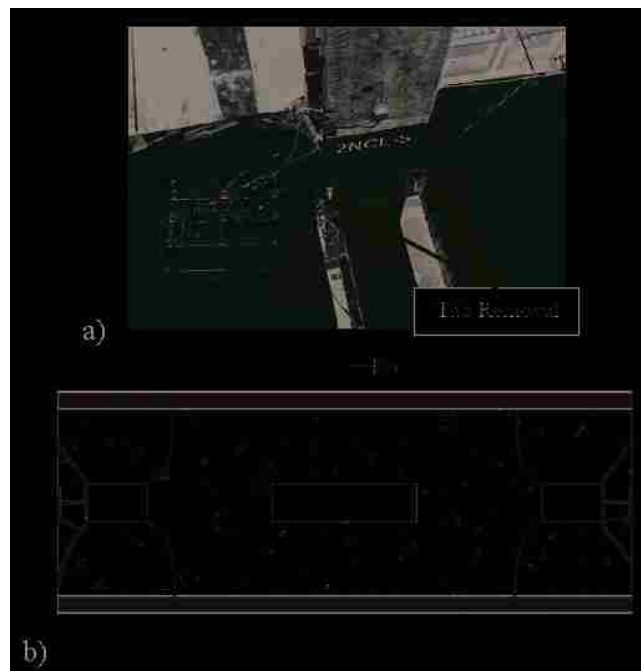


Figure 3.11 (a) Photo and (b) the Crack Map of the Outer Corner Blockout Crack on the 1st-story Slab After the Test.

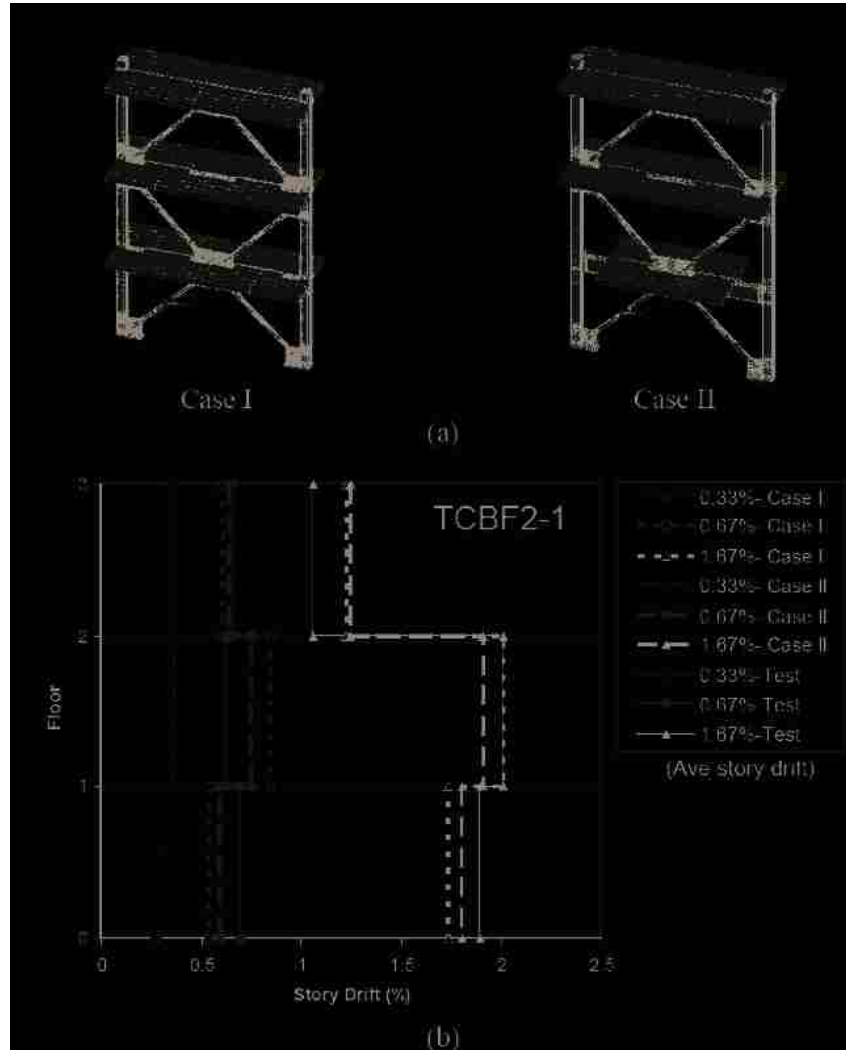


Figure 3.12 (a) Schematics of the FE model of two cases regarding the simulation of slabs, and (b) comparisons of story drift distribution between test results and analytical responses of the two cases

The comparison shows that the improved FE model simulated the specimen performance well both for the frame strength and lateral stiffness. It is apparent that the model simulated the highly nonlinear behaviors of the frame system and captured the measured story drift distribution through the height of the structure. The lateral loads were only applied at the roof level, but both the analysis and experiments show that there was considerable variation in deformation over story height. Figures 3.14a and b show



the experimental and analytical individual story drifts versus the average story drift, respectively. During the cycles of the average drift of 1.67%, the model slightly overestimated the deformations at the top story, while the test showed more deformation concentration at the bottom two stories.

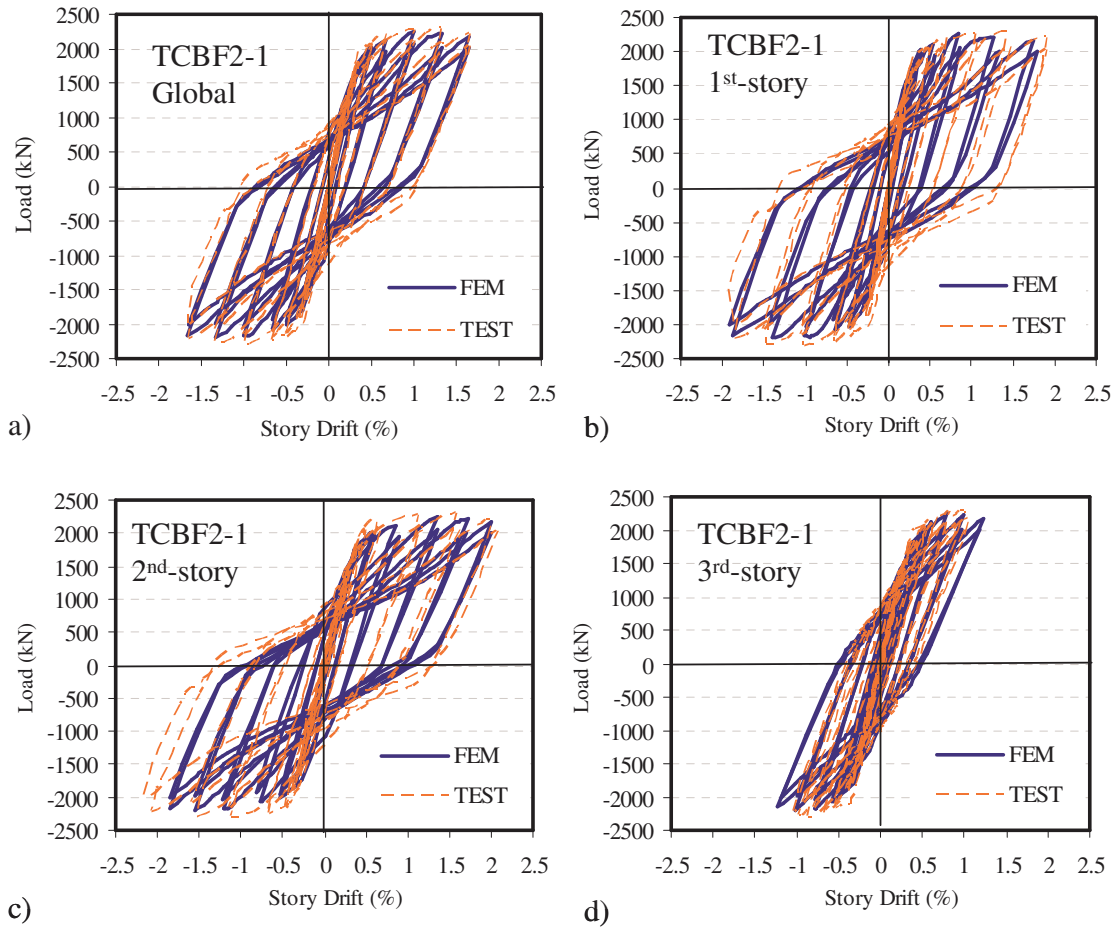


Figure 3.13 Comparison of experimental and analytical hysteretic responses of TCBF2-1

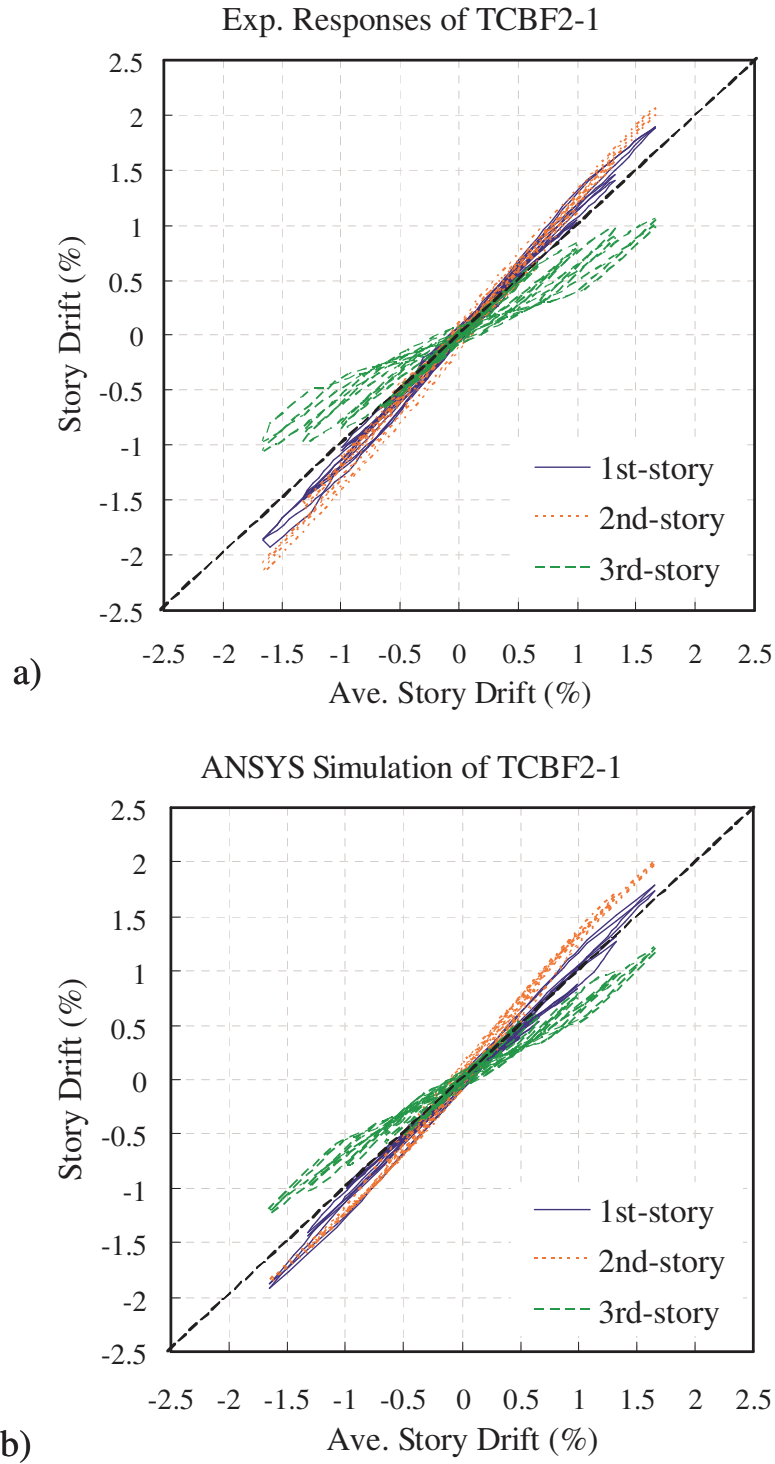


Figure 3.14 (a) Experimental and (b) analytical individual story drifts versus the average story drifts of TCBF2-1.

The continuum FE simulation not only accurately represented the global behavior but also the local deformation of the braced frame system. Figure 3.15 compares the local deformed shape of the experimental and analytical plastic hinge region at the midlength of the brace. The cupping behavior of the steel tube was well represented in the FE model. The results showed the high stress of over 547MPa was developed at the corner of the brace tube on the compression side, as shown in the figure, where the fracture initiation occurred in the experiments.

In terms of the local behavior of the beams, the most critical location was the second floor beam near the double-corner-gusset connections where the stiffeners were added based on the prior FE analysis for the connection design. Severe yielding was observed at the bottom beam flange near the edge of the gusset plate throughout the entire test. This severe yielding was captured by the FE model. Figures 3.16a and b show bottom and top views of the stress distributions at this location and compare them with the experimental observations, respectively. It is apparent that high stresses in excess of the yield strength of the steel (411Mpa) were predicted at the location where the yielding was observed in the test.

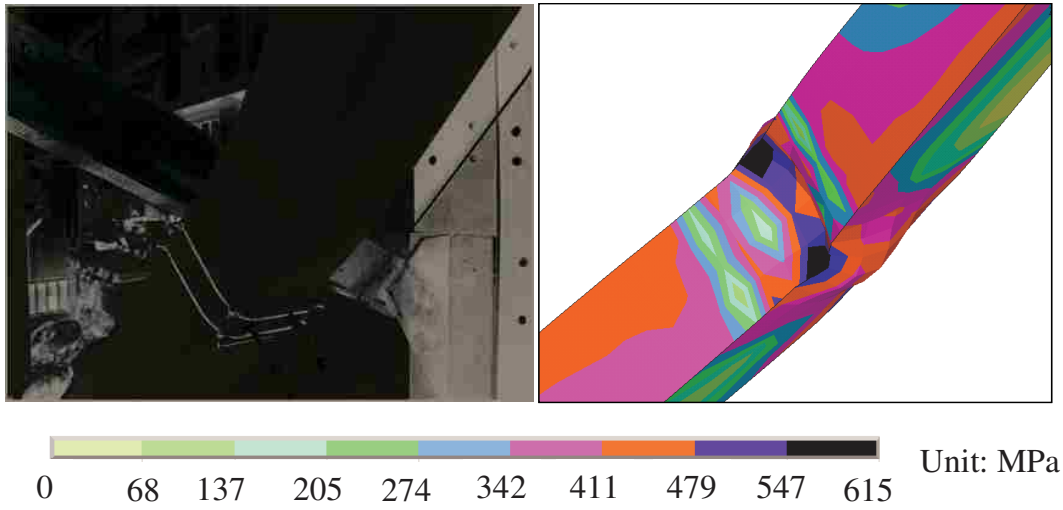


Figure 3.15 Comparison of experimental and FE analytical responses of the brace of TCBF2-1.

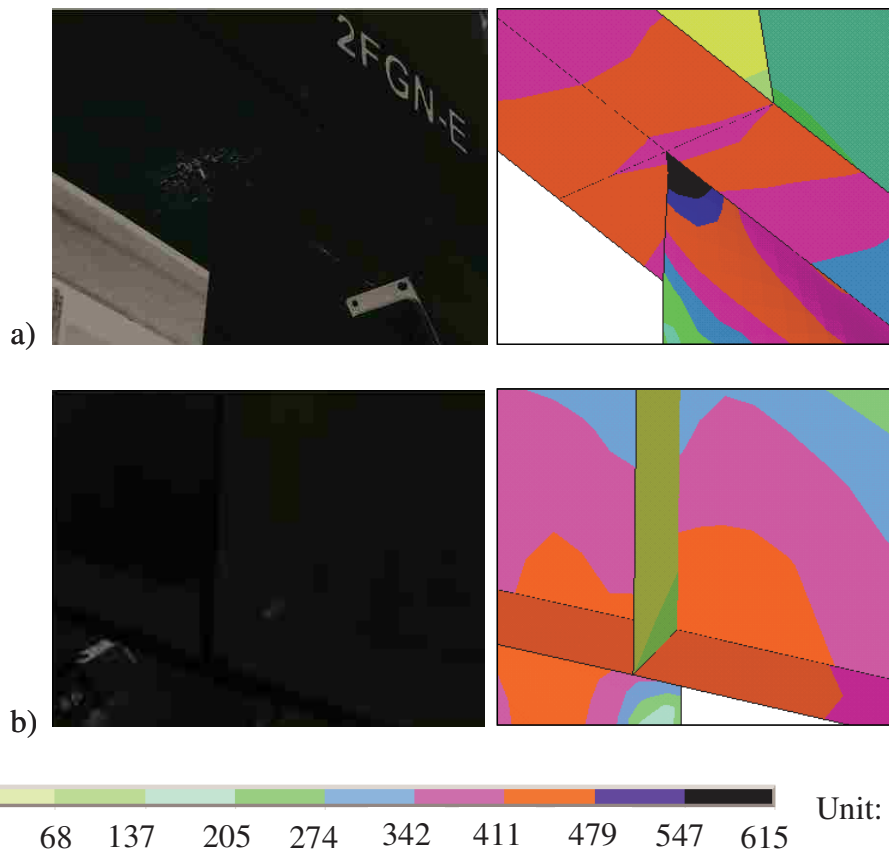


Figure 3.16 Comparison of experimental and FE analytical responses of the beams of TCBF2-1.

Severe yielding was observed at the column base during the tests, this was also predicted by the FE model. Figures 3.17a and b show the comparisons of the observed yielding and the analytical stress distributions at the column web and the column flange, respectively. Again the FE model predicted the yield behavior at the critical location well.

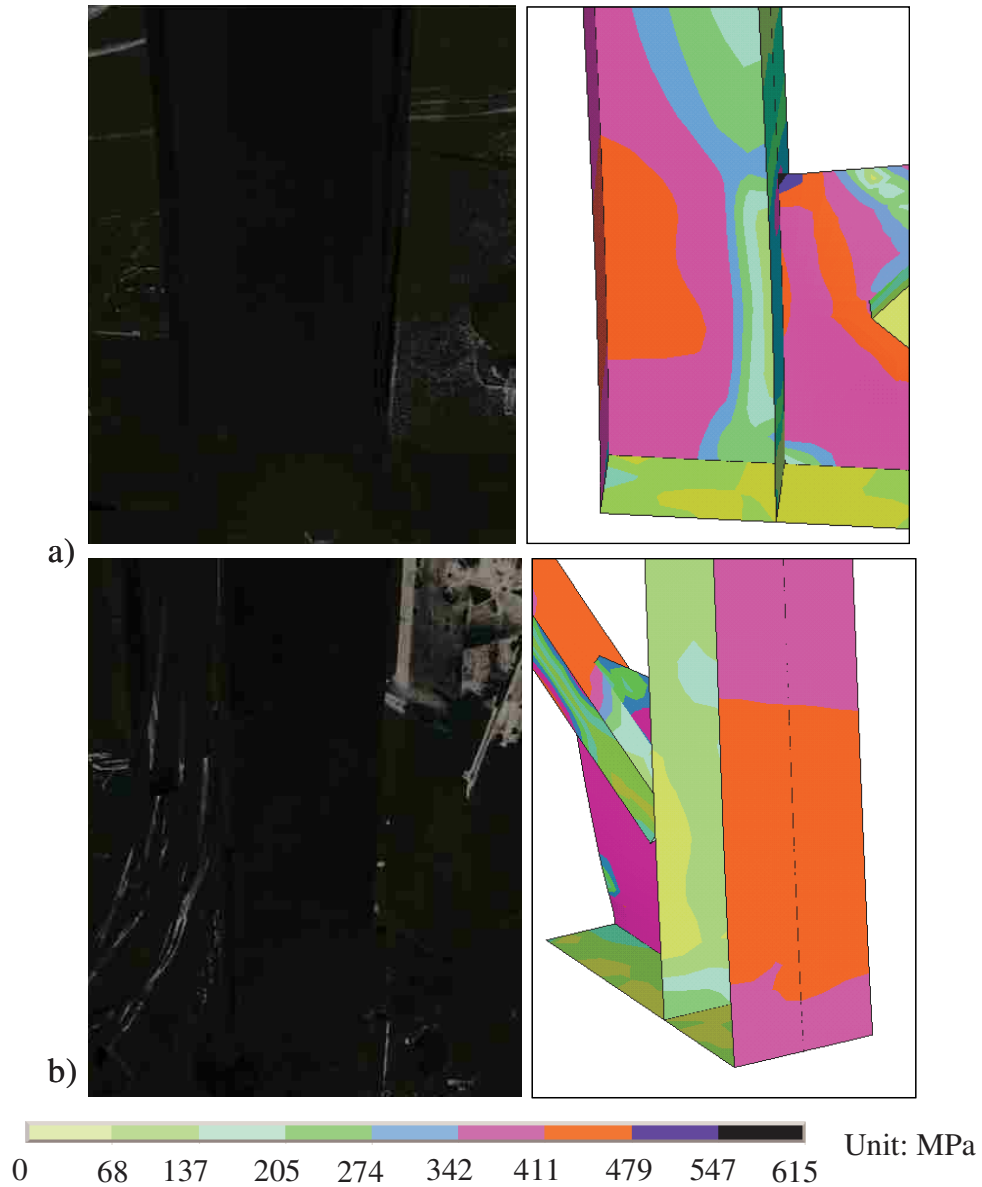


Figure 3.17 Comparison of experimental and FE analytical responses of the columns of TCBF2-1.

The gusset plate tolerates the end rotation of the braces and transfers the forces from the braces to the framing system, therefore, it played a significant role in the test frames and the computer predictions. Figures 3.18a, b and c compare the experimental observations and analytical results of the midspan gusset plates at the 1<sup>st</sup>, 2<sup>nd</sup> and 3<sup>rd</sup> story of the specimen, respectively. The computer prediction shows the elliptical yield bending of gusset plates as observed in the test results.

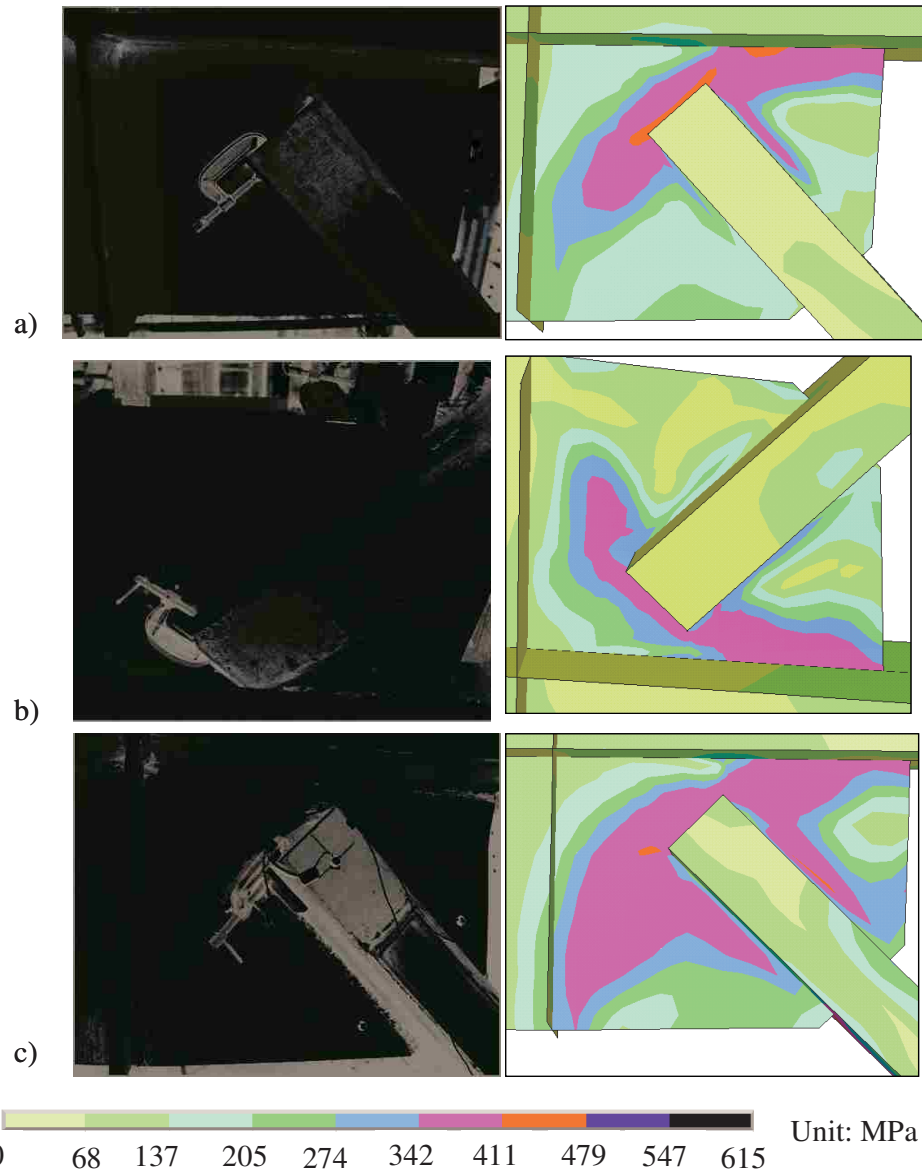


Figure 3.18 Comparison of experimental and FE analytical responses of the midspan gusset plates of TCBF2-1.

Figures 3.19a and b show the comparisons of the experimental and analytical results of the corner gusset plates at the first and third stories, respectively. The second story gusset not shown here has quiet similar deformed shape with the 3<sup>rd</sup>-story as having identical geometry and boundary conditions. The predicted deformed shape agreed with the experimental results as shown in the figures.

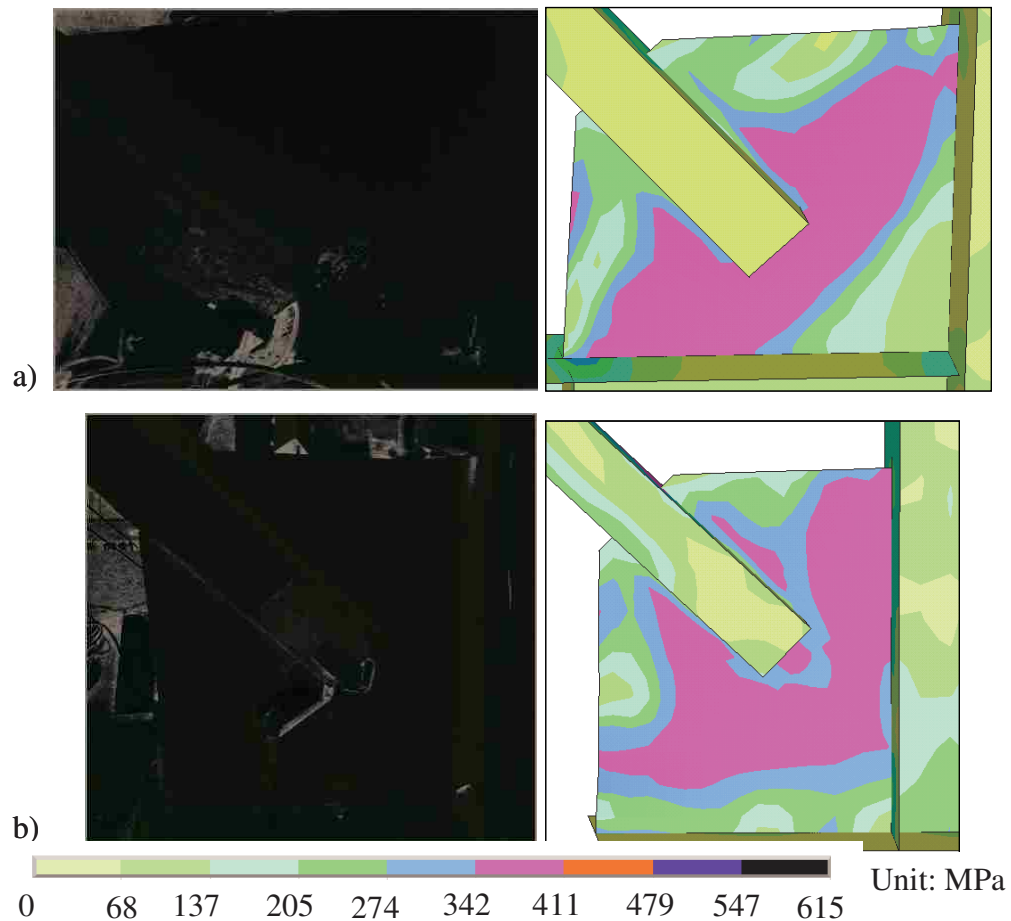


Figure 3.19 Comparison of experimental and FE analytical responses of the corner gusset plates of TCBF2-1.

Moreover, the reversed out-of-plane deformation of the braces resulted in the gusset plate being bent repeatedly during the cyclic loading test. This repeated action led to the distortion at the corner of the gusset plates near the beam and column surface. The distortion was observed in the experiments and also captured by the FE model. For instance, Figures 3.20a, b and c show the comparisons of the experimental observations and the analytical predictions of the gussets attaching the columns, beams and the base plates, respectively. It is apparent that the FE model simulated this local deformation



accurately.

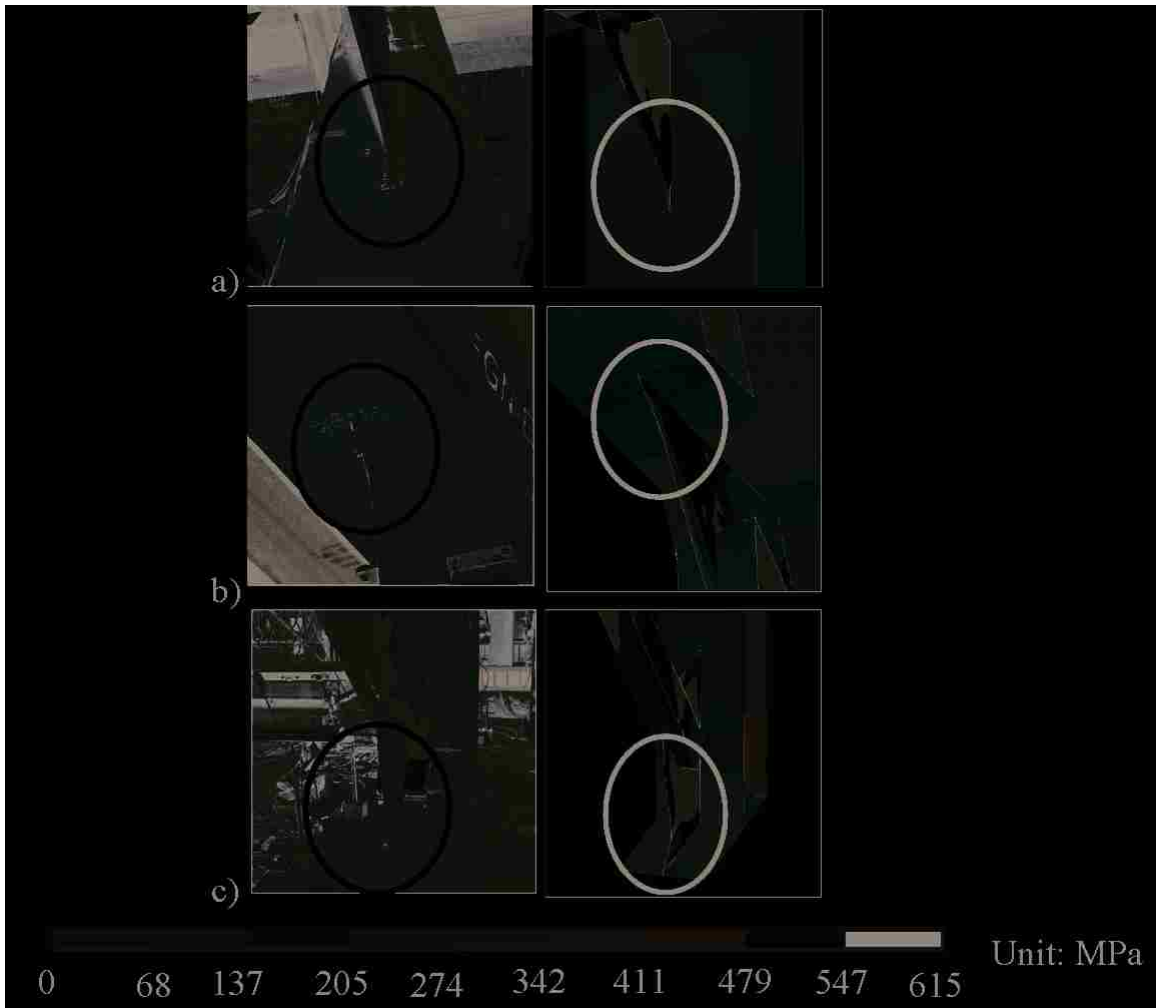


Figure 3.20 Comparison of experimental and FE analytical responses of distortions of gusset plates of TCBF2-1.

### 3.5.2 Analytical Results of TCBF2-2 with OOP WF Braces Buckling

As mentioned previously, after testing TCBF2-1, the braces and gusset plate connections were replaced for the next test of TCBF2-2(WF). Residual forces within the framing system at the end of prior test were ignored at the start of this test. The

consideration of the multiple use of the framing system (e.g. residual forces and deformations within the frame) was not included in the FE simulation. All following frames were simulated as brand new frames.

Figure 3.21a compares the analytical hysteretic story drift response of the TCBF2-2 with the measured results. With the use of the wide-flange braces, the test results showed that the frame dramatically lost resistance immediately after initial brace buckling. The FE model was unable to capture this observed sharp drop-off of the frame resistance at 0.33% drift, which implied the model underestimated the brace buckling capacity. The underestimation likely resulted from the modeling approach used to initiate brace buckling (i.e. use of transverse force at the midlength of the brace). Reducing the applied transverse forces may increase the predicted buckling capacity of the brace, however it could lead to increased difficulty in achieving convergence of the analysis. The inaccurate simulation of the brace buckling capacity led to different order and sequence of brace buckling in the computer model.

However, the FE model still accurately predicted the frame strength during the post-buckling response. Figures 3.21b, c and d compare the experimental and analytical response of the 1<sup>st</sup>, 2<sup>nd</sup> and 3<sup>rd</sup> stories, respectively. The model predicted the ultimate story drift of the first story accurately, while it underestimated at the second story and overestimated at the third story deformation. Based on those comparisons, it is apparent that the FE model predicted the lateral stiffness and resistance of each individual story, but the accuracy of the prediction of story drift distribution was reduced from that achieved with the first test, especially at the upper two stories.

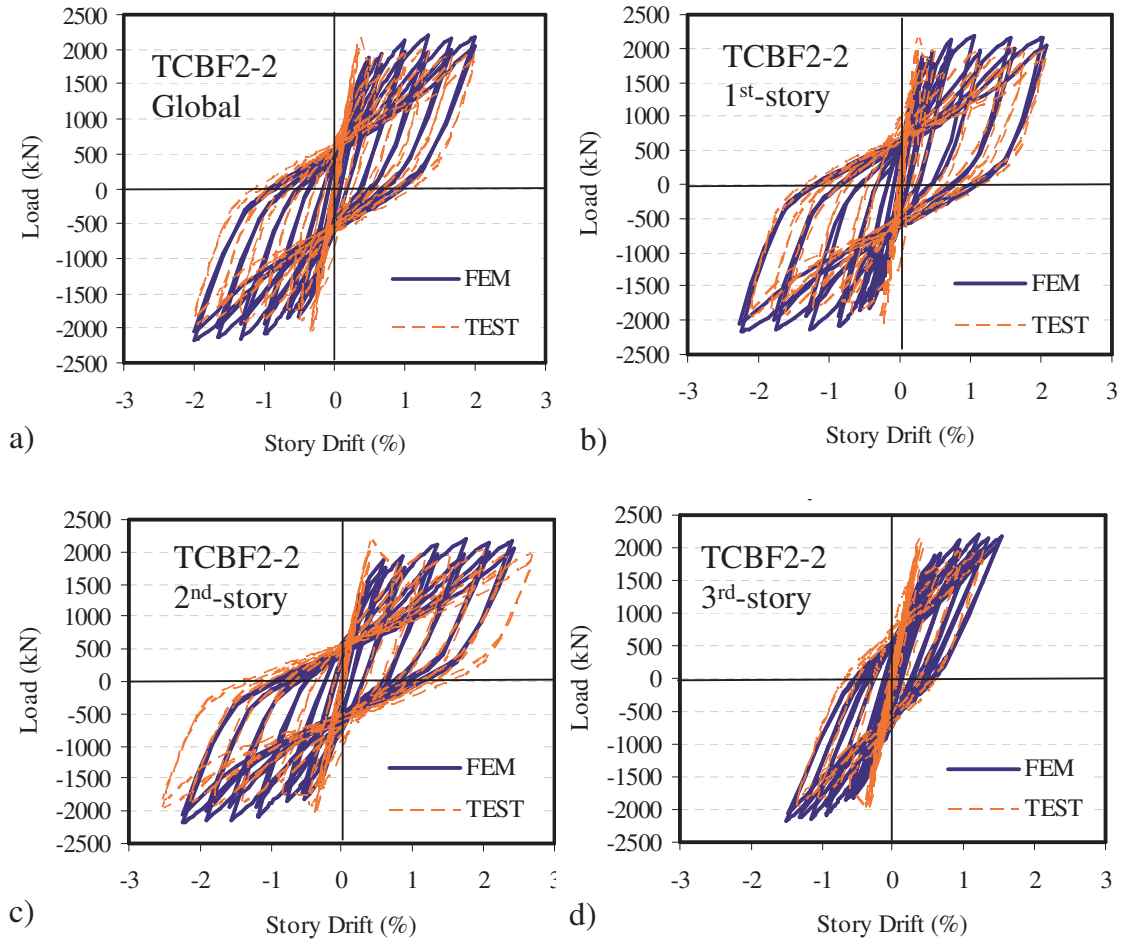


Figure 3.21 Comparison of experimental and analytical hysteric responses of the TCBF2-2

It is likely that the reused framing system was more flexible during this second test due to the yielding of the column bases, because of the severe concrete slab cracking near the shear-tab connections of the first floor beam, and the elongation of the bolt holes of the shear-tab connections observed after the first frame test. The increased flexibility of the frame led to the slight reduction of the frame stiffness and possible reduction in apparent resistance, and the combined effects lead to changes in the distribution of the deformation in the frame.

Figure 3.22 shows the experimental and analytical story drifts at each level versus the average drift. The experimental results showed greater deformations at the second story and smaller deformation at the third story than the analytical prediction throughout the entire test.

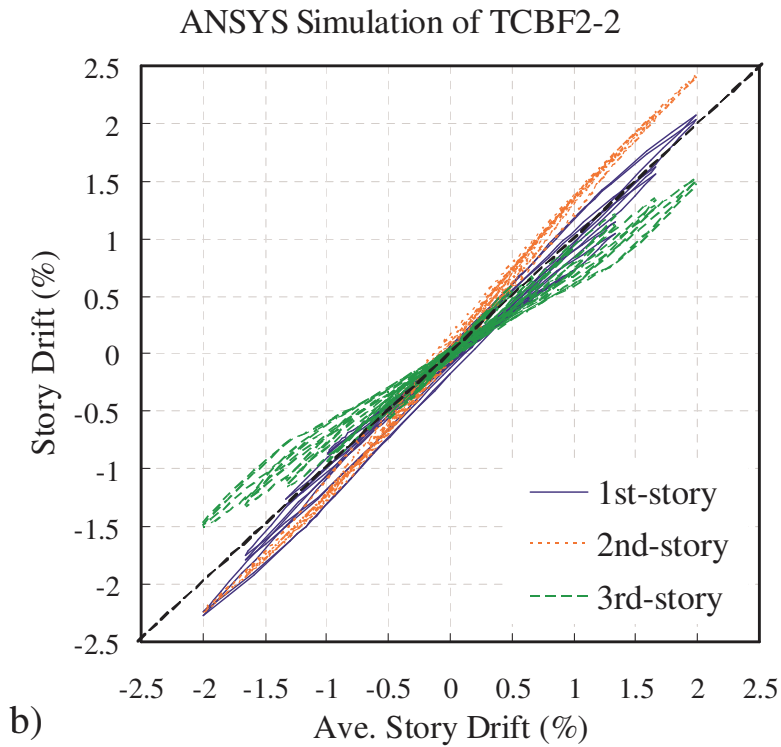
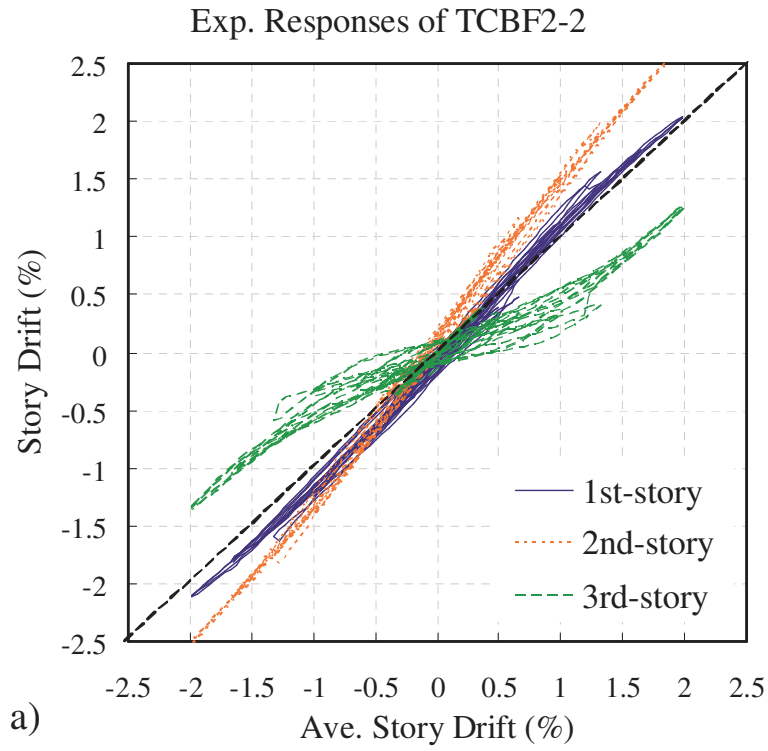


Figure 3.22 (a) Experimental and (b) analytical individual story drifts versus the average story drifts of TCBF2-2.

Figure 3.23 compares the measured and predicted local deformation of the plastic hinge of the brace in the midlength of the brace. No additional transverse force (to give a deformation imperfection for inducing local buckling) was used in the FE model. The local buckling of the flanges at the plastic hinge was predicted at the location observed in the test, while the buckling orientation was different as shown in the figure. The orientations of local buckling in the experiments were arbitrary, while the orientation in the computer model was always toward the interior of the section as shown in the figure. This is likely controlled by the direction of the small transverse forces applied to induce global buckling of the brace at the opposite side of the flanges, and retained throughout the analysis.

The test of TCBF2-2(WF) confirmed that both the elliptical clearance design model for corner gusset plates and the horizontal clearance design model for midspan gusset plates functioned well with wide-flange braces. The nonlinear behavior of those connections was captured by the FE model. Figures 3.24a, b and c show the comparisons of the experimental and analytical results for the midspan gusset plate connections at the 1<sup>st</sup>, 2<sup>nd</sup> and 3<sup>rd</sup> stories, respectively; and Figures 3.25a, b and c show the comparisons for the corner gusset plates at the 1<sup>st</sup>, 2<sup>nd</sup> and 3<sup>rd</sup> stories respectively. It is apparent that the test results and analytical responses compared well to each other.

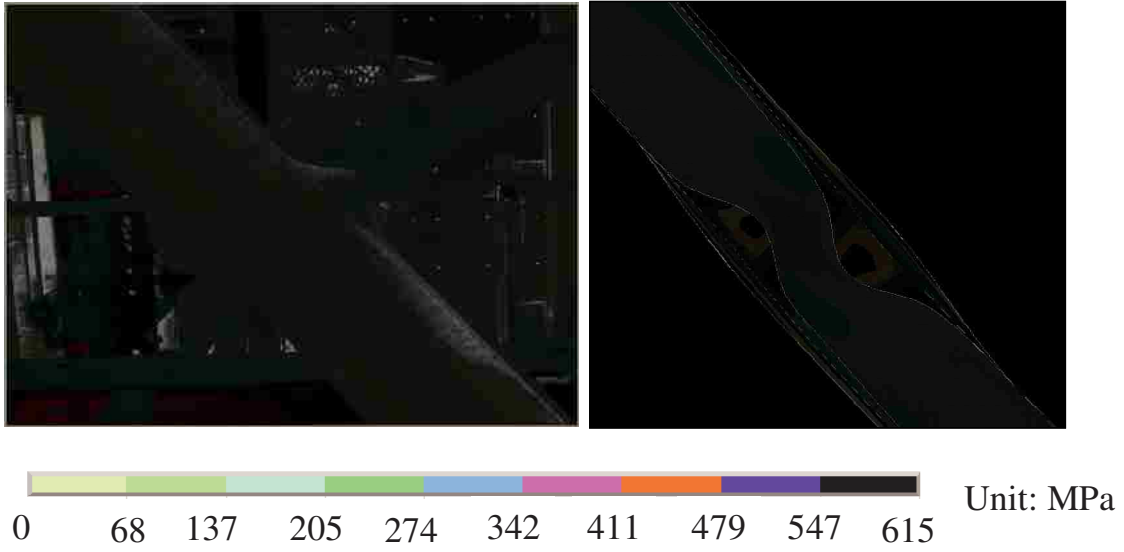


Figure 3.23 Comparison of experimental and FE analytical responses of the brace of TCBF2-2.

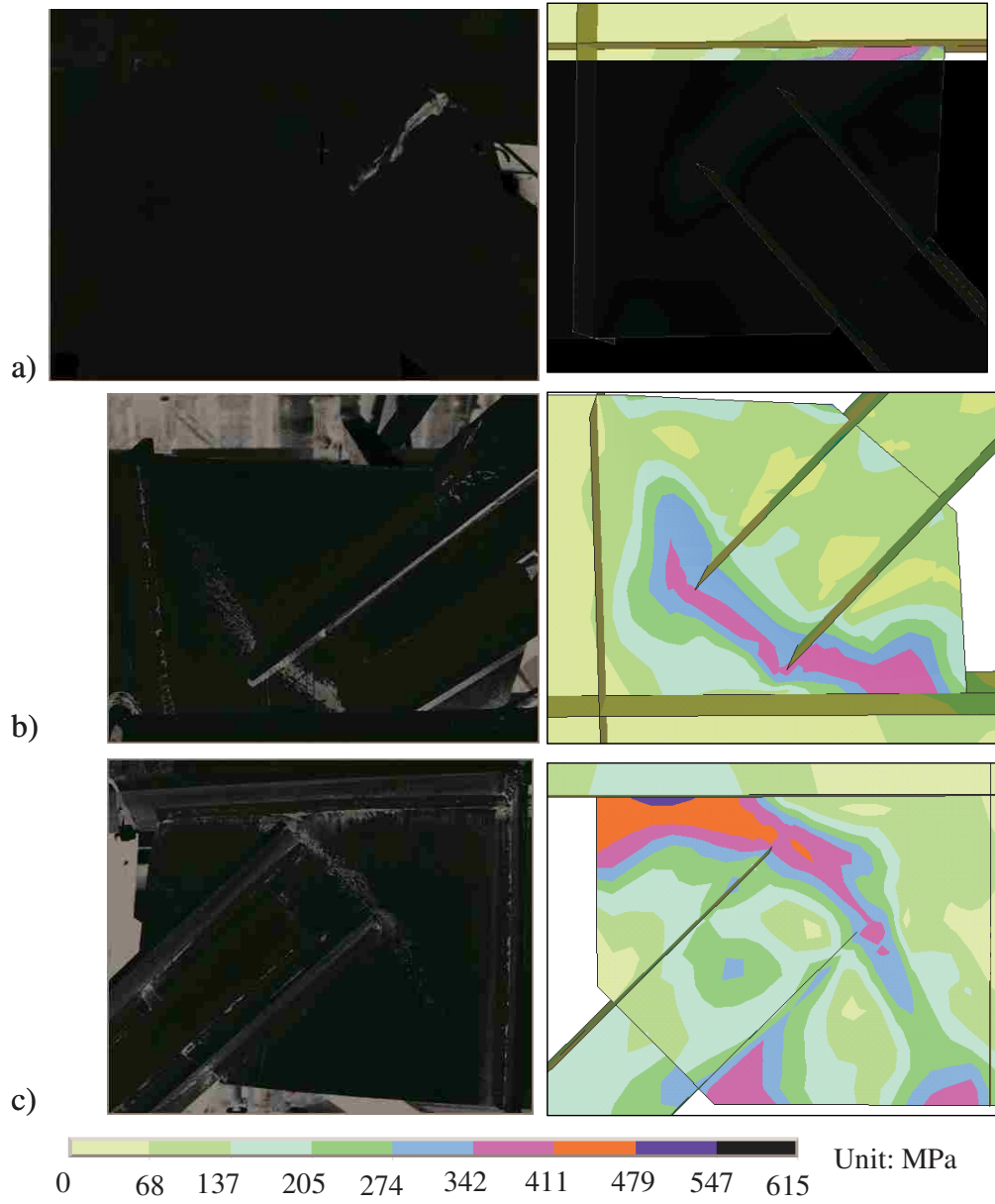


Figure 3.24 Comparison of experimental and FE analytical responses of the midspan gusset plates of TCBF2-2.



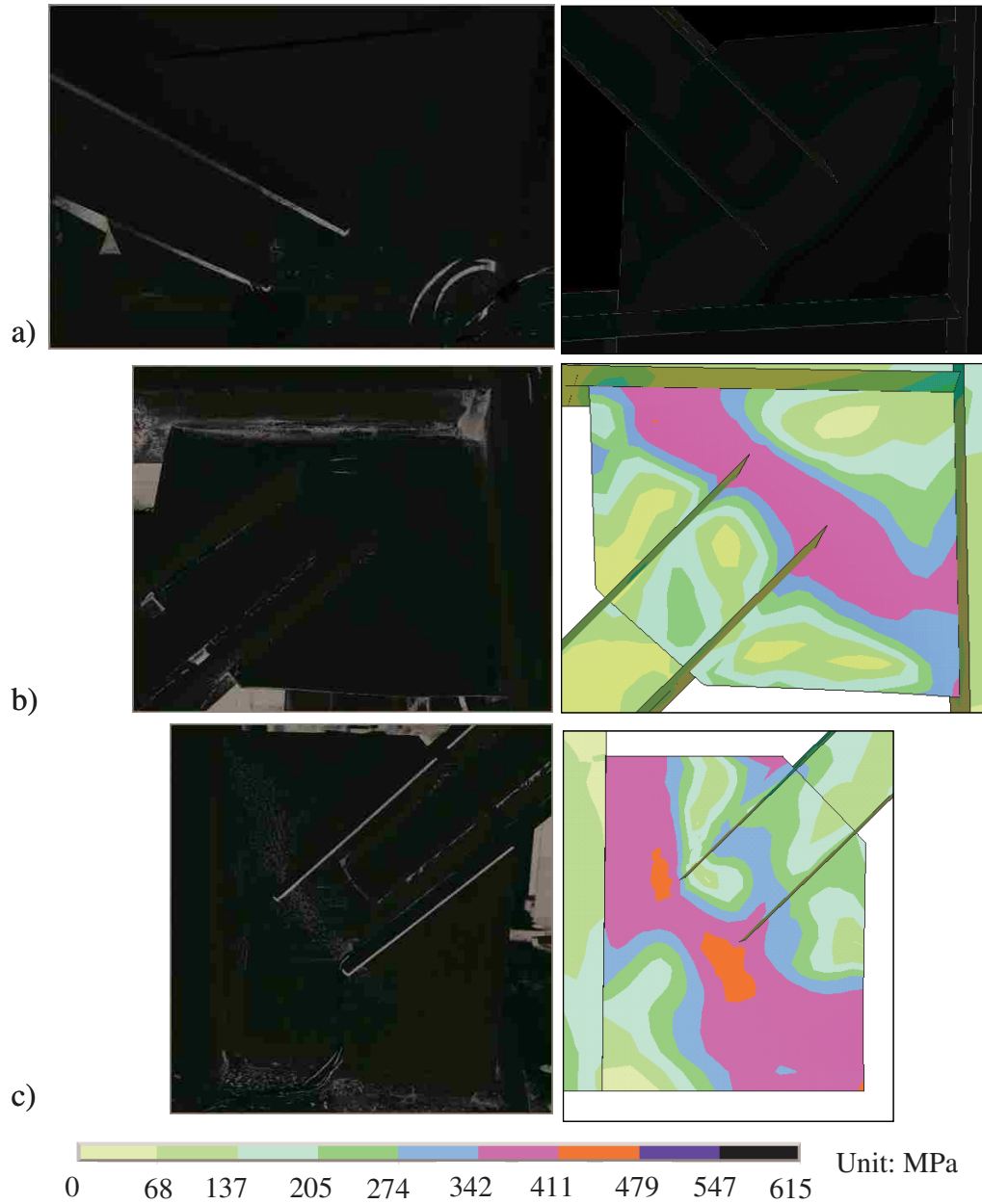


Figure 3.25 Comparison of experimental and FE analytical responses of the corner gusset plates of TCBF2-2.

### 3.5.3 Analytical Results of TCBF2-3 with IP HSS Braces Buckling

The FE model was also used to simulate the cyclic behavior of the TCBF2-3, which used an in-plane (IP) buckling brace configuration with HSS braces. The small transverse

forces were applied in plane to induce brace buckling. Figure 3.26a compares the analytical and experimental story drift response. The model accurately simulated the buckling capacity and the post-buckling behavior, including the strength and stiffness of the frame. Figures 3.26b, c and d show the measured and predicted force-deformation response of the 1<sup>st</sup>, 2<sup>nd</sup> and 3<sup>rd</sup> story, respectively. The results show that the model slightly overestimated the drift at the first and third stories, and underestimated the second story drift, which is similar with the simulated trend in the prior wide flange specimen.

Figures 3.27a and b show that the experimental and analytical story drift of the three stories versus the frame drift. It is apparent that accuracy of the simulation was decreasing at the second story compared with the previous two tests due to the multiple use of the framing system. As noted earlier, residual stresses, increased looseness of bolts, slab cracking and other damage may change the stiffness distribution and result in reduced local resistance due to repeated testing, and this is not captured by the FE model.

In terms of the local behavior of the frame, even though the brace end rotations all concentrated on the knife plates, there was slight yielding on the gusset plates, which connect the knife plates to the frame, as shown in Fig. 3.28. Similar with the previous tests, some yielding at the beam and column flanges adjacent to the gusset plate edges was also observed and predicted as shown in the Figs. 3.28a and b.

Figures 3.29a, b and c compare the analytical and experimental performance of the knife plates for the 3 stories of the frame. The analytical responses again compared well with the test results in that the yielding and rotation were mainly concentrated at the linear clearance region of the knife plates, and the highest stress occurred in the knife plate at the location right beyond the gusset plates as shown in the figures.

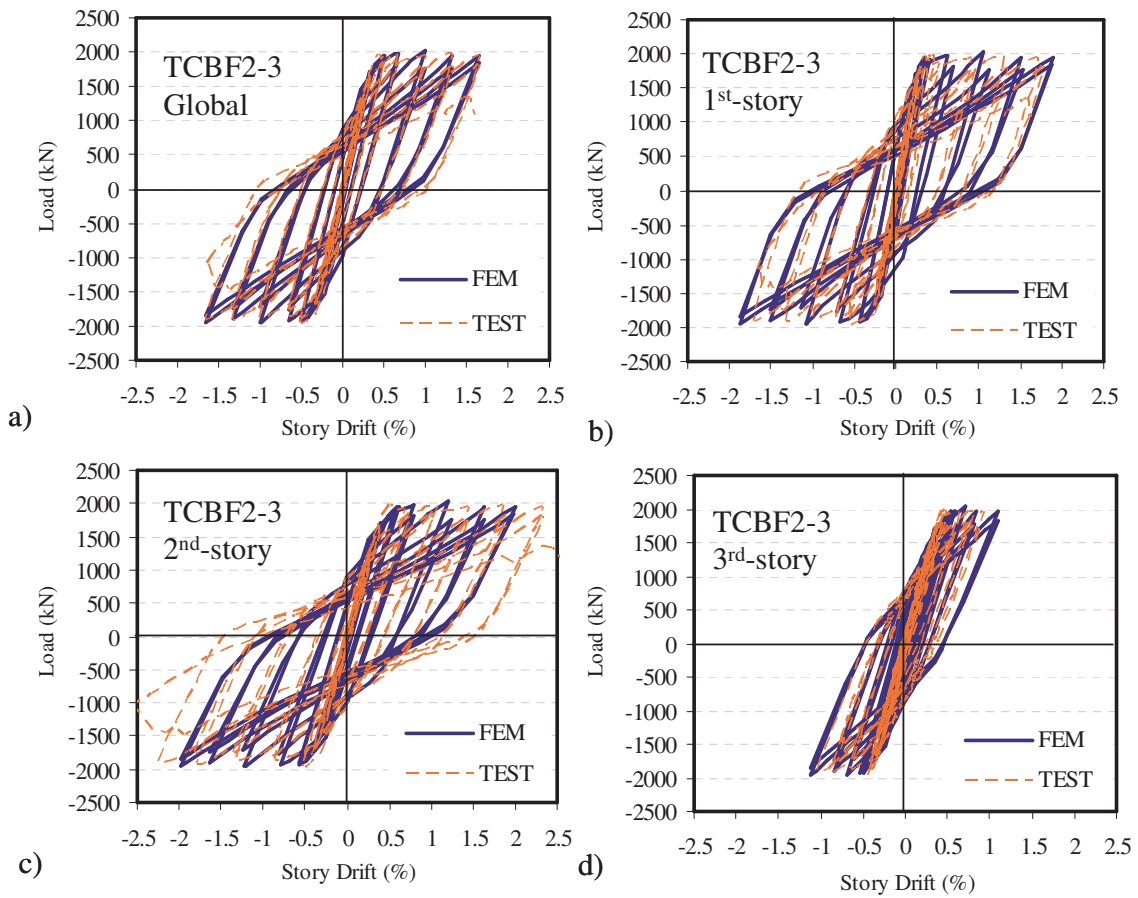


Figure 3.26 Comparison of experimental and analytical hysteresis responses of the TCBF2-3

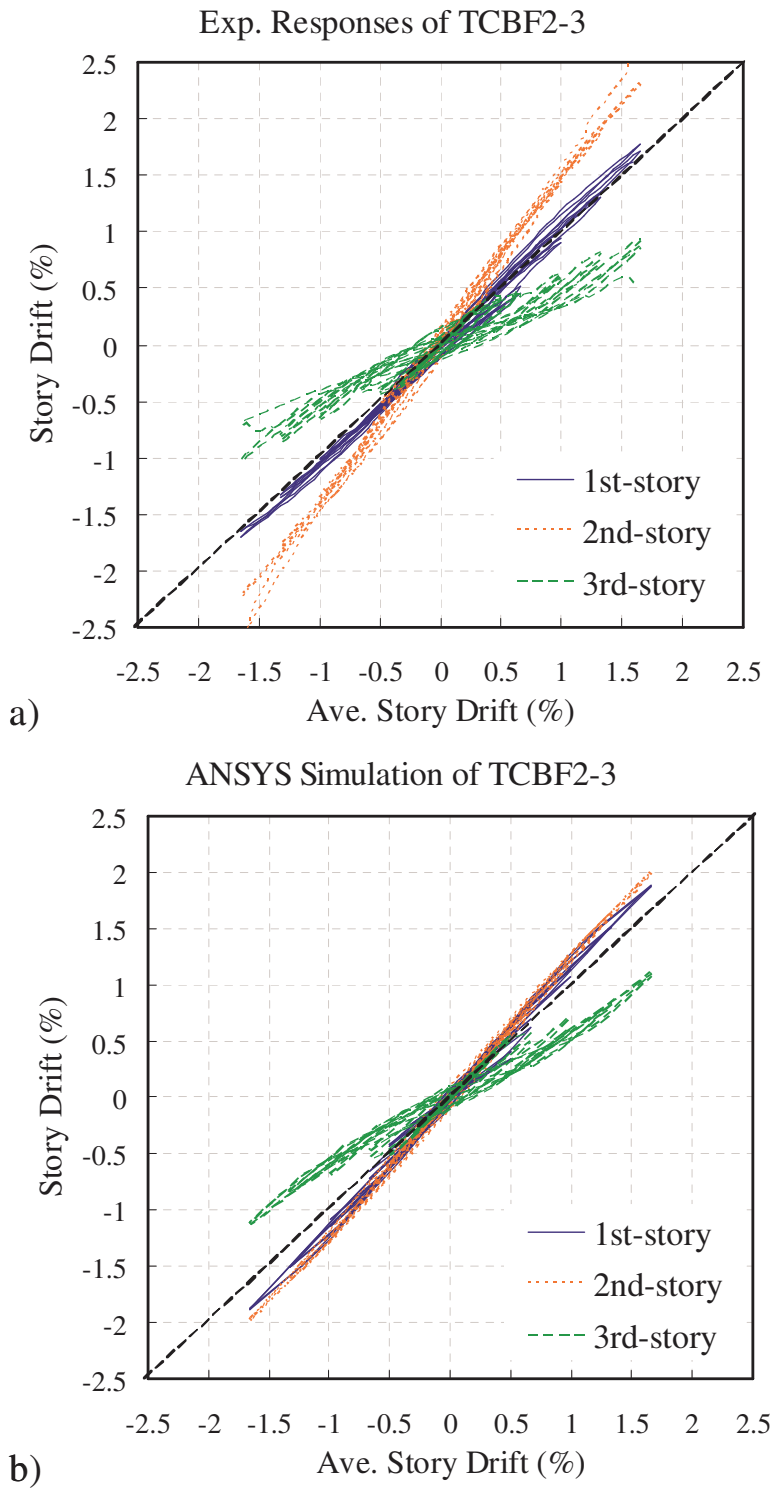


Figure 3.27 (a) Experimental and (b) analytical individual story drifts versus the average story drifts of TCBF2-3.

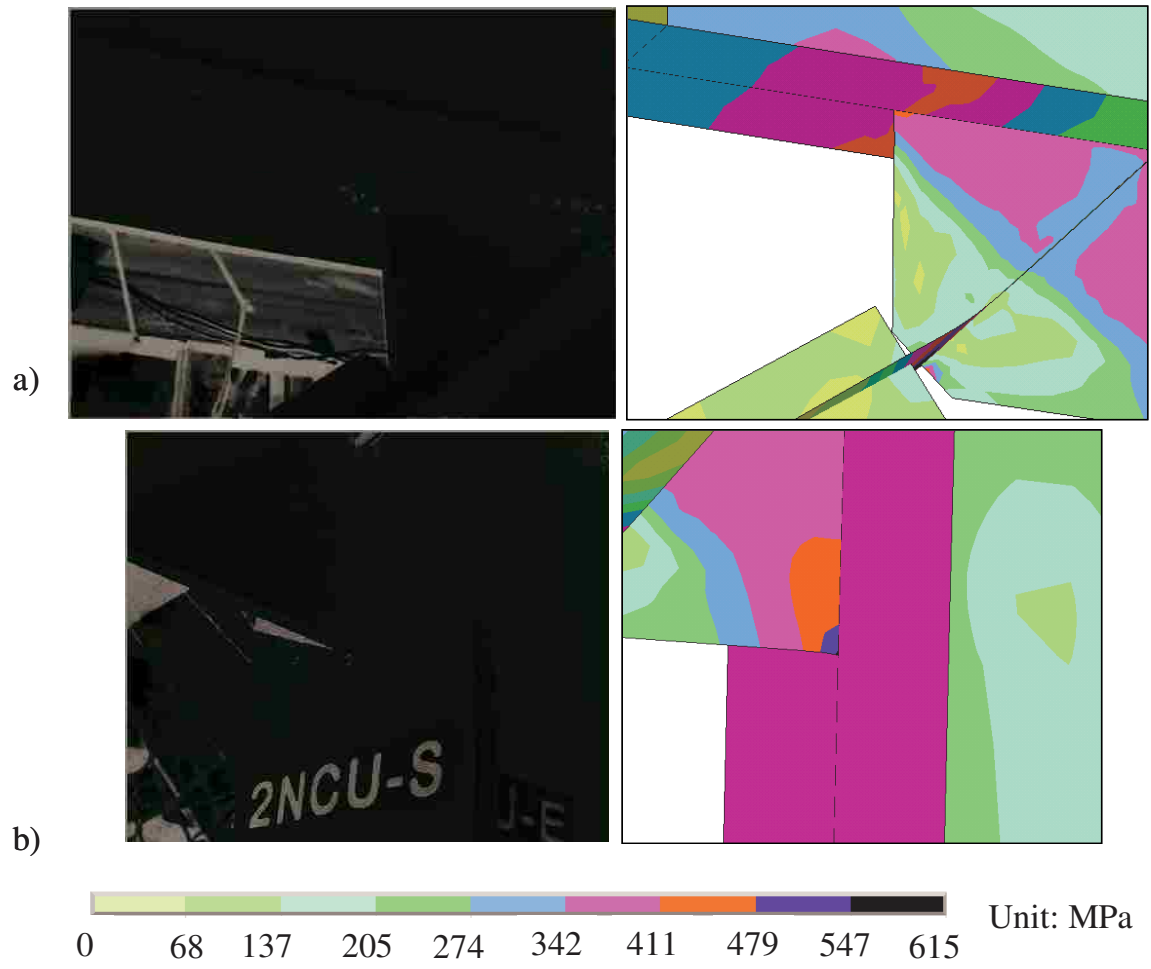


Figure 3.28 Comparison of experimental and FE analytical responses of (a) the gusset-to-beam and (b) the gusset-to-column connections of TCBF2-3

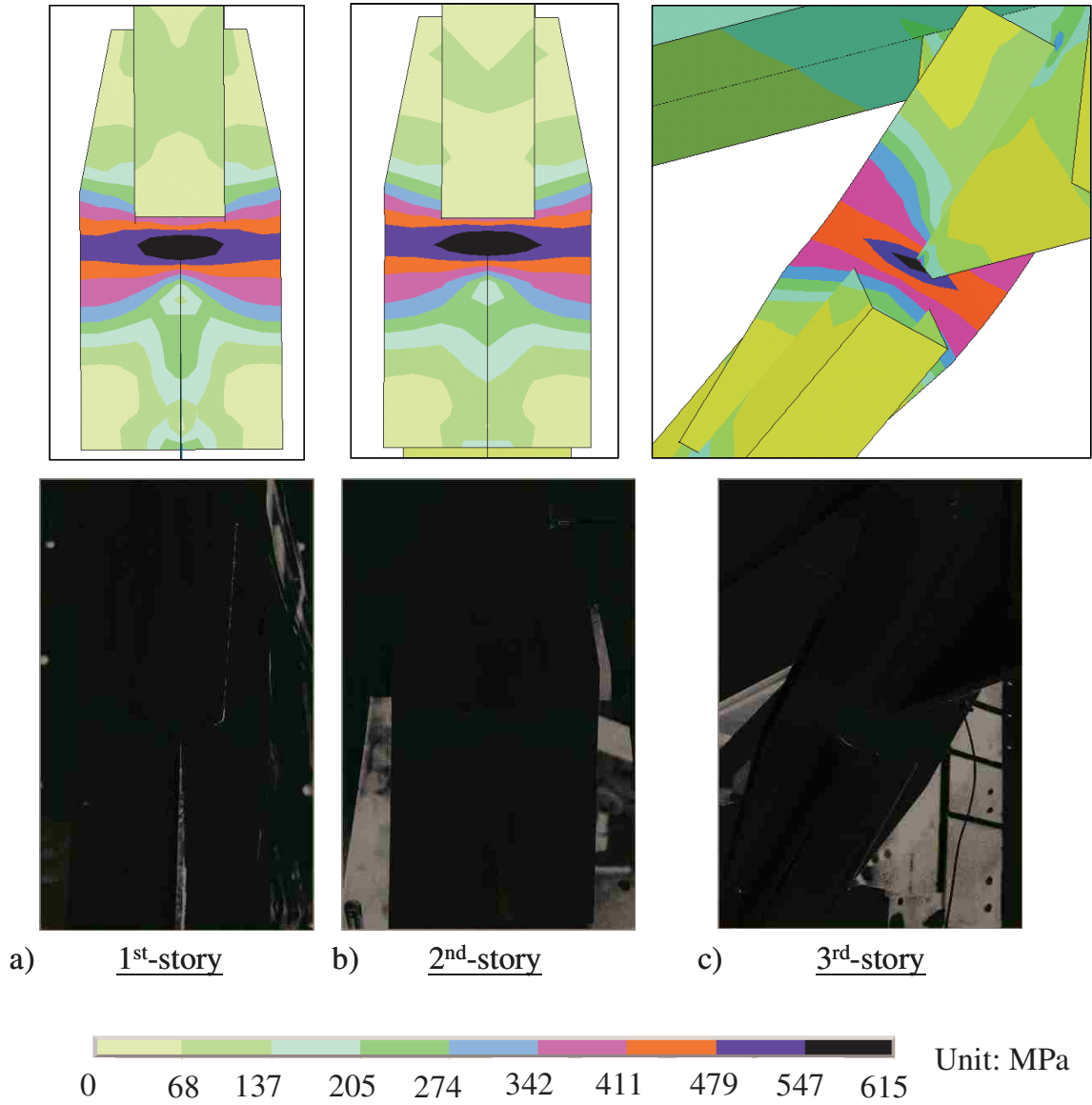


Figure 3.29 Comparison of experimental and FE analytical responses of (a) the 1st-, (b) 2nd- and (c) 3rd-story knife plates of TCBF2-3.

## **Chapter 4 : Improved Analytical Model of SCBF Systems**

### **4.1 Introduction**

The large strength and stiffness of SCBFs usually result in an economical system that easily meets serviceability limit states for Performance Based Seismic Design (PBSD). During large, infrequent earthquakes, SCBFs must assure life safety and collapse prevention performance states, and this requires simulation of the nonlinear behavior. As a result, theoretical models for PBSD must reliably predict both elastic and inelastic performance. Chapter 3 developed a high resolution nonlinear model for this purpose, and validated this model by comparison with experiments. The high resolution finite element model include large deformation theory for simulation of both local and global buckling, and some studies extended the models to include consideration of initiation of cracking and fracture based upon the strains, components of strains, or stress-strain history computed in the analyses (Huang et al. 2010, Shaw et al. 2010, Yoo et al. 2008, Yoo et al. 2009). The effort required to develop these models is substantial, since some had more than 20,000 shell elements and a much larger number of degrees of freedom. Nonlinear analyses of these complex models required considerable computing and were very expensive for typical professional practice. Further, they are not suitable for completing nonlinear static and dynamic analysis for PBSD of larger braced frame systems. Simpler methods are needed. Unfortunately, most simple models result in

significant loss in accuracy in predictions of SCBF performance.

In this chapter, a simplified but relatively accurate nonlinear method is developed using the OpenSees computer program with line-elements combined with fiber sections. The model utilizes fundamental concepts of engineering mechanics to estimate properties of key components, which are based on and evaluated using measured performance of braced frame experiments.

In this chapter, a detailed description of the proposed improved models are provided, while the primary content of the chapter was addressed in a journal paper as documented in Appendix B. All of the modeling parameters and their influence on the analytical responses will be described. The accuracy of the proposed model is verified by comparing to the results of the past experimental program, and comparisons are made with other common computer models to show that the proposed model provides improved accuracy over current methods and permits reliable prediction of seismic performance of SCBF systems. An error analysis on the current and the improved models is given and described at the end of the chapter.

## **4.2 Simulated SCBF Tests for Development of Analytical Models**

A wide range of analyses including the full nonlinear shell element analyses as well as the simplified analyses described in this chapter were performed on each of the 38 test specimens in the braced frame project, including 32 single-story frames testing in UW (UW tests) and 6 multi-story frames testing in NCREE at Taiwan (NCREE tests), as described previously. The specimens cover a wide range of analytical parameters. For brevity, a group of 14 specimens were selected from these 38 tests to reflect the range of



observed SCBF performance. Critical data for these specimens is provided in Tables 4.1 for nine single-story single-bay frames (HSS1, HSS2, HSS5, HSS7, HSS10, HSS11, HSS12, HSS17 and WF23). The typical frame configuration for these specimens is shown in Fig. 2.3a, and these tests were used for development and verification of the improved simplified analytical model. Table 4.2 for multi-story specimens with the geometric parameters illustrated in Figs 2.2a and b for various type of gusset plate connections respectively.

The 14 specimens included a wide range of engineering parameters. In particular:

- Specimens HSS1 and HSS12 simulated current AISC design practice (AISC 2005). They employed current AISC design requirements including the  $2t_p$  linear clearance (Fig. 2.1), and as a result had larger and thicker gusset plates. Specimen HSS1 was detailed with a fillet weld at the gusset plate to beam and column; Specimen HSS12 utilized a CJP weld at that connection. Relative to the other tests, these specimens had different failure modes (HSS1) and reduced drift capacity, demonstrating that the size and thickness of gusset plates strongly influence system performance.
- Specimens HSS2 and HSS5 were designed using the elliptical clearance method (Fig. 2.2a) and utilized thinner more compact gusset plates. These tests had large drift capacities and stable response.
- Specimens HSS10 and HSS17 had a tapered gusset plates using the elliptical clearance model.
- Specimens HSS7 and HSS11 studied variations on the elliptical clearance method. Both specimens used a gusset plate that was thicker than the minimum required. Specimen HSS11 also utilized heavier beams than required. The specimens had

diminished drift capacity, indicating that the strength and stiffness of the connection and framing members strongly influences SCBF performance.

- Specimen WF23 had a wide flange brace with the gusset plates using the elliptical clearance model. This test shows, as prior research has also shown, that wide flange braces can sustain larger inelastic deformations and place greater inelastic demands on the connections than rectangular HSS tubes.

Taken as a whole, these parameters address key conclusions noted from the experimental research (Johnson 2005, Herman 2006, Kotulka 2007, Powell 2009) and represent a wide range of variation in the design parameters. The ability of computer models to capture these differences is important.

Table 4.1 Dimensions and Material Properties for Selected UW Test Specimens (Figs. 2.1, 2.2a and 2.3a)

Spec.	Beam		Column W12×72 F <sub>y</sub> (MPa)	Brace HSS5× 5×3/8 F <sub>y</sub> (MPa)	Gusset Plate			F <sub>y</sub> (MPa)	Clearance	
	Size	F <sub>y</sub> (MPa)			a (mm)	b (mm)	t <sub>p</sub> (actual) (mm)		Type	N (t <sub>p</sub> )
HSS1	W16x45	407.1	410.5	479.0	864	762	13	814.3	Linear	2
HSS2	W16x45	401.7	385.2	479.0	635	533	12	450.9	Elliptical	6
HSS5	W16x45	392.1	405.8	500.9	635	533	10	450.2	Elliptical	8
HSS7	W16x45	392.1	405.8	442.7	724	622	22	403.7	Elliptical	6
HSS10*	W16x45	409.2	405.1	450.2	475	419	13	469.4	Elliptical	6
HSS11	W16x89	393.4	401.0	450.2	724	622	23	431.8	Elliptical	6
HSS12	W16x45	366.1	337.3	450.2	864	762	13	220.3	Linear	2
HSS17*	W16x45	381.1	355.1	450.2	526	413	10	286.7	Elliptical	6
WF23 <sup>#</sup>	W16x45	392.1	405.8	362.7	556	508	10	286.7	Elliptical	8

\* : tapered gusset plates; <sup>#</sup>: wide-flange brace (W6x25)

Table 4.2 Dimensions and Material Properties of Braces and Gusset Plates of NCREE Tests

Specimen	Brace		Gusset Plate			
	Section	$F_y$ (MPa)	Shape	Clearance	$t_p$ (mm)	$F_y$ (MPa)
Phase I - Two-story frames						
TCBF1-1 (HSS)	HSS125x125x9 (mm)	446.8	Rectangular <sup>#</sup>	8- $t_p$ elliptical	10	403.7
TCBF1-2 (WF)	H175x175x7.5x11 (mm)	320.2	Rectangular <sup>#</sup>	8- $t_p$ elliptical	10	406.4
TCBF1-3 (TG)	HSS125x125x9 (mm)	442.0	Tapered	2- $t_p$ linear	20	346.9
Phase II - Three-story frames						
TCBF2-1 (HSS)	HSS5x5x3/8 (in.)	314.8	Rectangular	8- $t_p$ elliptical at corner & 6- $t_p$ linear at mid-span gussets	10	396.2
TCBF2-2 (WF)	H175x175x7.5x11 (mm)	340.1	Rectangular	8- $t_p$ elliptical at corner & 6- $t_p$ linear at mid-span gussets	10	383.2

<sup>#</sup>: using edge stiffeners at the midspan gusset plate connections

Three two-story single-bay frames (Fig. 2.3b), TCBF1-1(HSS), TCBF1-2(WF) and TCBF1-3(TG), and two three-story single-bay frames (Fig. 2.3c), TCBF2-1(HSS) and TCBF2-2(WF), were included in the analytical study. Their design member sizes and material properties are shown in Table 4.2. These multi-story frame tests evaluated the interaction of the braces and connections. More importantly, mid-span connections were studied and composite floor slabs and different boundary conditions were simulated.

The two-story frame tests (TCBF1) used a single frame (e.g., the beams and columns were retained for all 3 tests and only the braces and gusset plates were replaced). The tests used Taiwanese hot rolled shapes, H506x201x11x9 and H318x307x17x24 for beams and columns, respectively. The three-story frame test series (TCBF2) used a different frame, which was built from US shapes, W21x68, W24x94 and W12x106 sections for beams at bottom two floors, beams at roof level and columns, respectively. Similarly, lateral cyclic loads were only applied at the top level of concrete slab through

the load beams, and the framing members were reused through each entire phase, TCBF1 and TCBF2. Only the braces and gusset plates were replaced between the tests. Additional details of the test setup and dimensions of the multi-story frame tests may be found in Chapter 2 and elsewhere (Clark 2009, Lumpkin 2009).

### **4.3 The Improved Line-element Model of SCBFs**

Tensile yielding, buckling and post-buckling behavior of the brace are highly nonlinear behaviors and key elements in the seismic response of the SCBF system. Significant deformation and yielding of the gusset plate connections are also present, and local yielding of the beams and columns adjacent to the gusset plate occurs. All of these must be simulated in a nonlinear model to accurately represent system performance. Continuum finite element analysis, such as the detail nonlinear shell element model described earlier, accurately simulates these behaviors, however, these complex finite element simulations are computational expensive and time consuming. Further, for large structural systems this modeling approach is impractical for nonlinear dynamic analysis of complete systems.

Instead, improved models of CBF performance were developed in the OpenSees framework (McKenna 1997), and simplified discrete component models including beam-column elements and concentrated springs were used to simulate the system behavior. Similar OpenSees models have been used in other recent research (e.g. Aguero et al. 2006, Uriz et al. 2008).

### 4.3.1 Braces, Beams and Columns

Force-based nonlinear beam-column elements with four integration points were used to model the brace, beam and column members. The Giuffre-Menegotto-Pinto model, Steel02 material model in OpenSees, was the nonlinear constitutive law used for all members. The effect of rigid end zones was also included in the model at beam-column and beam-column-brace connections.

This work built upon prior research (Gunnarson 2004) where a minimum of ten segments (or elements) along the length of the brace and an initial displaced shape in the form of a sine function with the apex equal to 1/500 of the length of the brace were used to efficiently simulate brace buckling behavior. One element having four integration points and no out-of-plane imperfection was used for the beam and column members to capture the yielding mechanism of the framing system observed in the tests.

Fiber cross sections were employed, which enable the creation of the various steel cross sections with the assumption of plane strain compatibility. The required number of the fibers through the cross section of the brace was also investigated. As shown in Fig. 4.1a, the HSS tube was discretized using four fibers along the thickness in each direction at each of eight quadrilateral patches. This discretization accurately predicted the brace performance for the sizes studied here. For wide-flange braces, a 2 (thickness) by 10 (flange or web length) fiber discretization was used, as shown in Fig. 4.1b. The finer mesh of fibers was arranged in the buckling direction of the cross section, as shown in the figure. Significant local yielding in beam and column members adjacent to gusset plate connections occurs in the SCBF experiments. To simulate the nonlinear behavior of the beams and columns, beam-column elements with fiber sections were also employed. For

both beams and columns, cross sections were discretized using 2 fibers along the thickness and 4 fibers along the length within each flange and web. Additional fibers were arranged in the bending direction in the cross section (Fig. 4.1c). In addition, composite action was considered for specimens that included a slab, which included the beams in the multi-story tests. To consider the composite effect of the concrete slabs in the simulation of the multi-story frame specimens, the slab was included by modifying the cross section, as illustrated in Fig. 4.1c. The true dimensions of the slab in the specimens were used in the model, and an elastic material model, which did not develop tensile stress, was used for representing the concrete behavior.

As a result, a total of 128 fibers through the brace cross sections and 24 fibers through the beam and column cross sections were adopted.

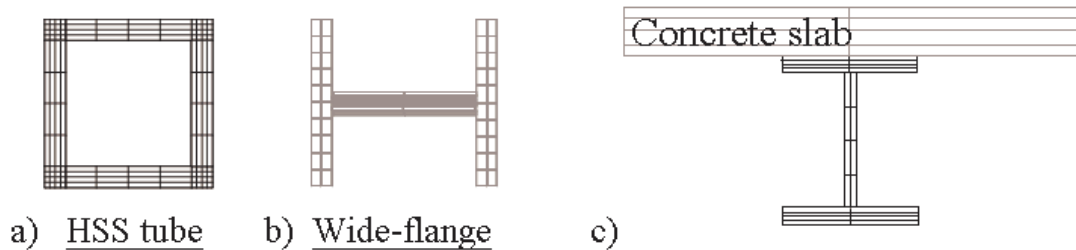


Figure 4.1 Fiber Discretization used for (a) HSS and (b) Wide-flange Brace Members and (c) the Composite Beam Members.

### 4.3.2 Gusset Plate connections

Gusset plate connections are neither pinned nor fixed joints, and these connections have a significant effect on the stiffness, resistance and inelastic deformation capacity of the SCBF system. Hence, accurate simulation of these connections is required and

carefully considered in the study.

A wide range of alternatives were considered in developing an accurate simulation. To simulate the nonlinear out-of-plane rotational behavior of the gusset plate connections, single and multiple springs along the brace axial direction at and beyond the end of the brace were investigated. Rotational spring stiffness, ranging from fully pinned to fully rigid, was evaluated. For the nonlinear springs, different yield strengths were used. It was found that increased initial spring stiffness increased the predicted buckling capacity of the brace. Hence, the correct estimate of the gusset plate stiffness is required to accurately predict the buckling capacity of the brace.

Figure 4.2 shows the analytical modeling approach for the gusset plate. The rotational spring was located at the physical end of the brace. Rigid links were used to simulate the remainder of the gusset plate, as shown in Figure 4.2. A zero-length nonlinear rotational spring element using Steel02 material model at the end of the brace simulated the out-of-plane deformational stiffness of the connection. Therefore the stiffness of this rotational spring was based upon the geometry and properties of the gusset plate. A rational estimate of gusset stiffness is provided in Eq. 4.1. The expression was verified using results from a continuum finite element study (Yoo 2006). This spring stiffness is:

$$K_{cal}^{rotational} = \frac{E}{L_{ave.}} \left( \frac{W_w t_p^2}{12} \right) \quad (4.1)$$

where E is Young's modulus of steel plate,  $W_w$  is the Whitmore width defined by a  $45^\circ$  projection angle,  $L_{ave.}$  is the average of  $L_1$ ,  $L_2$  and  $L_3$  as shown in Figure 4.2, and  $t_p$  is the thickness of the gusset plate.

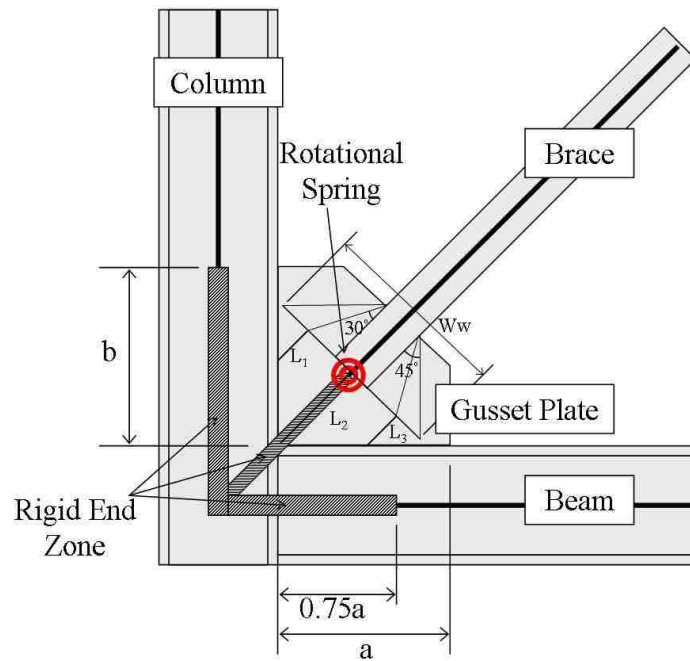


Figure 4.2 Proposed Connection Model

These expressions are empirical with a basis in engineering mechanics. Gusset plates are designed for stress levels averaged over the Whitmore width of the gusset, and so this width represents the portion of the gusset that is considered effective in resisting the loads and deformations of the brace. The rotational stiffness in Eq. 4.1 is effectively  $EI/L$ , or the rotational stiffness of a cantilever beam with the properties of the gusset. The stiffness is affected by the thickness and properties of the gusset. In addition, the flexural strength of the nonlinear rotational spring mode is also based on the Whitmore width; this method is effective in computing the capacity of Whitmore cross section of the gusset plates as shown in Eq. 4.2. The post-yield stiffness is 1% of the initial rotational stiffness. Note that for a tapered gusset plates, the actual width is used if the actual width is smaller than the Whitmore width. The resistance is defined by:



$$M_y = \left( \frac{W_w t_p^2}{6} \right) F_{y, \text{gusset}} \quad (4.2)$$

where  $F_{y, \text{gusset}}$  is the yield strength of steel of the gusset plate. Figure 4.3 illustrates the material model of the nonlinear rotational springs.

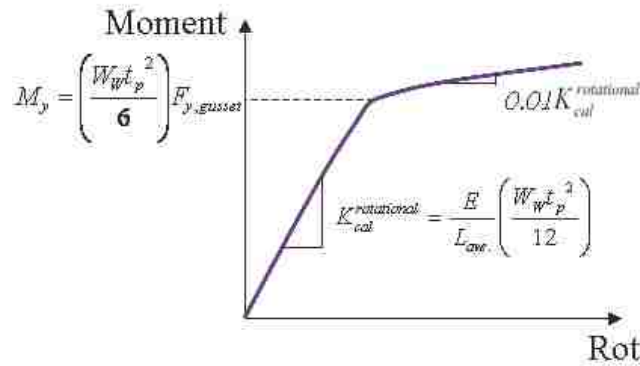


Figure 4.3 Illustration of the Zero-length Rotational Spring Model

The gusset plate sustains minimal in-plane deformation relative to other deformations modes of the frame, and therefore rigid links were used to simulate this rigidity. Three rigid zones are used. The first extends from the work point of the connection to the physical end of the brace. The second extends from the work point to the physical end of the gusset along the length of column. The third extends from the work point along the length of the beam, however, it only extends out to 75% of the dimension "a" on the beam (Fig. 4.2) to permit some limited deformation within the "rigid" zone (as noted in Fig. 4.1). The rigid link at the ends of the brace makes the brace length identical to the actual length and provides the most accurate estimate of brace buckling resistance. Experiments show that some in-plane deformation of the gusset occurs due to diagonal stress fields, and therefore the ideal rigid zone is somewhat

smaller than the full size of gusset.

The analytical results of the study showed that the adopted size of rigid zone on the beams and columns defined above was the size found to best represent the experimental behavior for all test specimens. Tapered gussets have smaller dimensions “a” and “b” than rectangular gussets, and hence greater deformation is permitted. The analytical results also confirmed that the fiber elements joining to the rigid links on the beams and columns permit yielding that reflects the local yielding observed in experiments. Those rigid links were simulated by using elastic beam-column elements with extremely large stiffness in OpenSees program. The combined effect of these modeling attributes led to significant improvements in the accuracy of the prediction of SCBF system performance.

### **4.3.2 Beam-to-Column Connections**

Beam-column connections at beam-column-brace connections usually were welded-flange welded-web connections. As a result, they were treated as fully restrained connections with the simplified fixed connection models.

The beam-to-column connections at locations without a gusset plate were usually shear-plate (or shear-tab) connections in the specimens in this brace frame project. The shear-tab connections did not include a slab in the single-story single-bay test specimens but included a slab (with block outs) in the multi-story specimens. The connections were simulated as illustrated in Fig. 4.4a. The model is a combination of the zero-length nonlinear spring element and the Pinching4 material model (both available in OpenSees), which simulates degradation of strength and stiffness as shown in Fig. 4.4b.

The moment-rotation model developed by Liu and Astaneh-Asl (2004) was used to

estimate the initial rotational stiffness and the maximum positive and negative moment capacities for the shear-tab connections with and without slabs. The composite shear-tab connection model includes composite action for shear tabs with composite slabs bearing against the face of the column. All of the parameters of the bending moment and rotation capacity in the figures were based upon Liu and Astaneh-Asl's study (2004). Figures 4.4c and d illustrate the backbone moment-rotation models for bare-steel and composite shear-tab connections, respectively.

The ultimate rotation capacity for positive bending,  $\theta_{ult}^+$ , and for negative bending,  $\theta_{ult}^-$ , are calculated according to the dimension of the shear tab and the gap between the beam web and column flange. Maximum positive moment capacity,  $M_{max}^+$ , and maximum negative moment capacity,  $M_{max}^-$ , are calculated based on the design shear load of the connection and geometric properties of the shear-tab and composite slab.

The initial rotational stiffness of the shear-tab connection is determined by two parameters, the moment at which connection slips,  $M_{slip}$ , and the corresponding rotation,  $\theta_{slip}$ . According to the experimental results from Liu and Astaneh-Asl's study,  $M_{slip}$  was typically 25% of  $M_{max}^+$  for the shear-tab connection with slab, and was 50-60% of  $M_{max}^+$  for bare-steel shear-tab connections. The corresponding rotation,  $\theta_{slip}$ , was 0.0042 rad. on average for all specimens. The values for the rest of the parameters, including  $\theta_{max}^+$ ,  $\theta_{max}^-$ ,  $\theta_{drop}$ , and  $M_{drop}$  (presented as a fraction of  $M_{max}^+$ ), are based on a compilation and averaging of backbone curves of moment-rotation for typical shear tab connections tested.

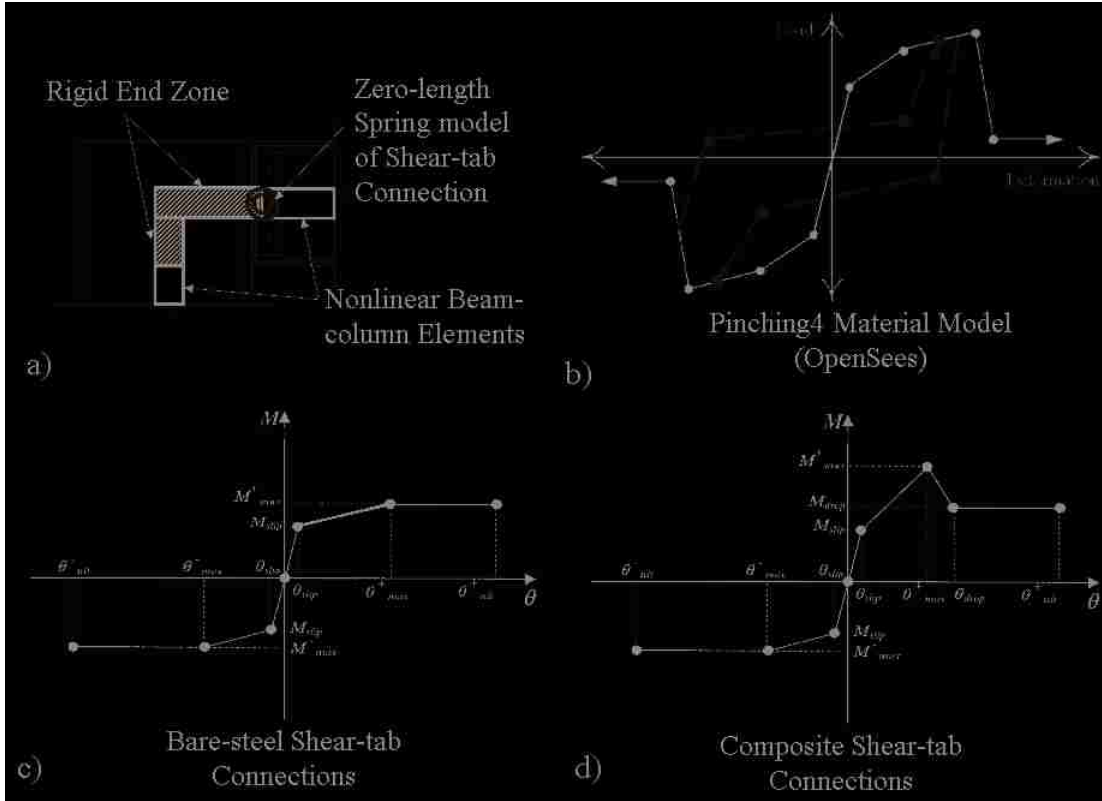


Figure 4.4 Illustration of (a) the Shear-tab Connection Model, (b) the Pinching4 Material Model in OpenSees, and the Liu's Moment-rotation model for (c) the Bare-steel Shear-tab and (d) the Composite Shear-tab connections.

Beyond these models of the connections, the additional detail of the modeling approaches and quantification of the important variables used for other components of the braced frame, e.g. braces, beams (with and without composite slab) and columns, are provided in Appendix B. The OpenSees model was also used to evaluate and compare with nonlinear models with pinned or rigid joints, which are the conventional modeling approaches for the brace-beam-column connections of CBFs.

### 4.3.3 Processing Functions of Members

In the OpenSees framework, the input files for the model are built using Tcl/Tk

programming language. The proposed model required multiple discrete elements through the length of each member. Two processing functions for the brace, beam and column, respectively, e.g. `BraceMake( )` and `BeamColumnMake( )`, were developed to automatically generate all of the required elements on each member. These routines were developed to facilitate the use of this by practicing engineers and future research. The operation of those functions is described here and the source codes are provided in Appendix C.

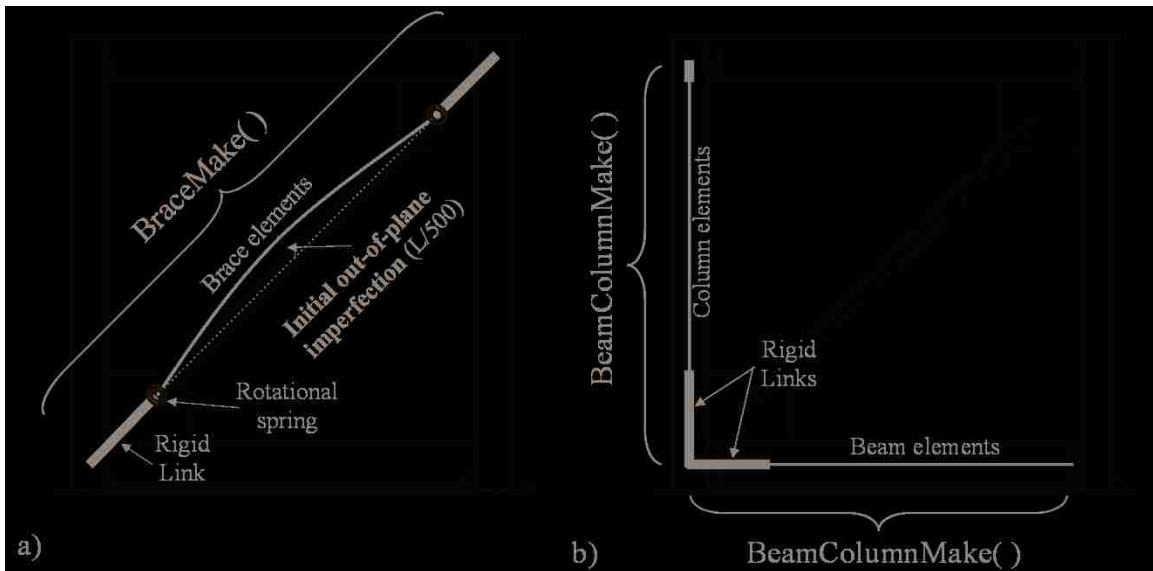


Figure 4.5 Illustrations of the Model Created by the Functions of (a) `BraceMake( )` and (b) `BeamColumnMake( )`.

`BraceMake( )` automatically generate all needed commands for every nodes and elements within a bracing member (see Appendix C.1) by employing a series of analytical parameters which are associated with the information of the brace and its gusset plate connections. This module establishes dimensions, geometric, material properties, initial out-of-plane imperfection, nonlinear rotational spring elements and

rigid end zones at brace ends, as illustrated in Fig 4.5a. BeamColumnMake( ) (see Appendix C.2) generate the code needed for creating all nodes and elements for the beam or column members, including beam-column elements and rigid end zones, as illustrated in Fig 4.5b. Even though the proposed improved model required a number of elements to capture the highly nonlinear behavior of the systems, each component is established efficiently by a single command in the input files using those processing functions.

#### **4.3.4 Model Setup of The Brace Frame Specimens**

The group of 14 SCBF tests described previously were simulated using the proposed modeling approach. The details of the model setup of those tests are presented here.

Figure 4.6 illustrates the typical model setup of the single-story, single-bay frames tested in UW laboratory. In the test setup, the lateral load was transferred to the top beam of the frame through a loading beam made from a much heavier wide-flange section. The loading beam was simulated with several rigid elements as shown in the figure. The frame model was fully restrained at the location of shear transfer connection used to anchor the frame to the reaction beam in the test setup as shown in Fig. 4.6. The column bases were simulated as rollers, and the 350kips (1545kN) axial loads were applied to the top of the columns as in the tests. In addition, the frame model was restrained against out-of-plane movement at the nodes of the intersection of the beams and columns.

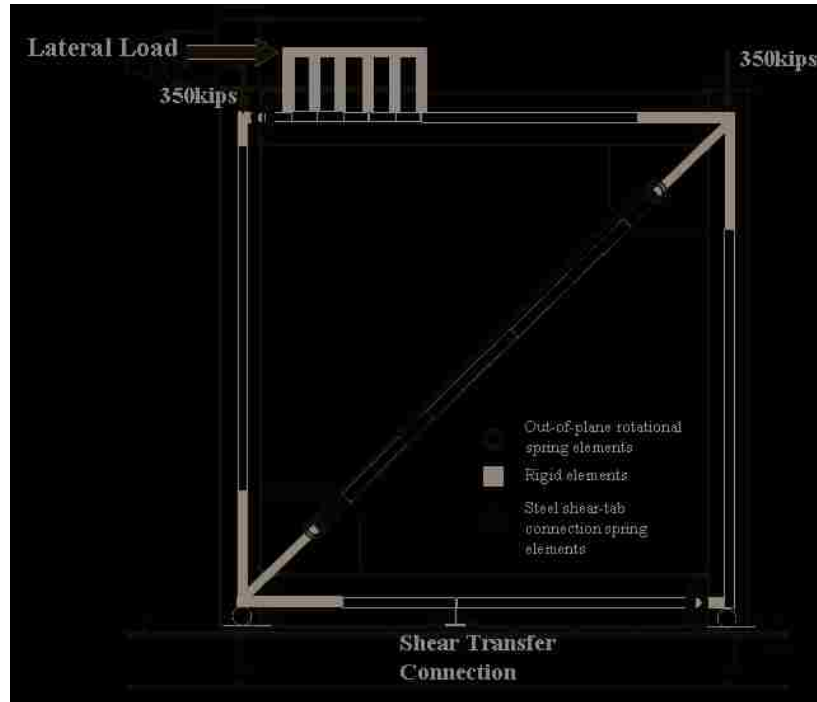


Figure 4.6 Illustration of the Typical Model Setup for the Single-story Specimens

Figure 4.7 illustrates the model developed for the two-story frames tested at NCREE. The composite slab is simulated in the model using additional fiber sections using an elastic no tension material model, which has the young's modulus of concrete, through the beam cross section. The shear-tab connections at the ends of the first floor beam were simulated using the moment-rotation model with slab proposed by Liu and Astaneh-Asl (2004) as described previously.

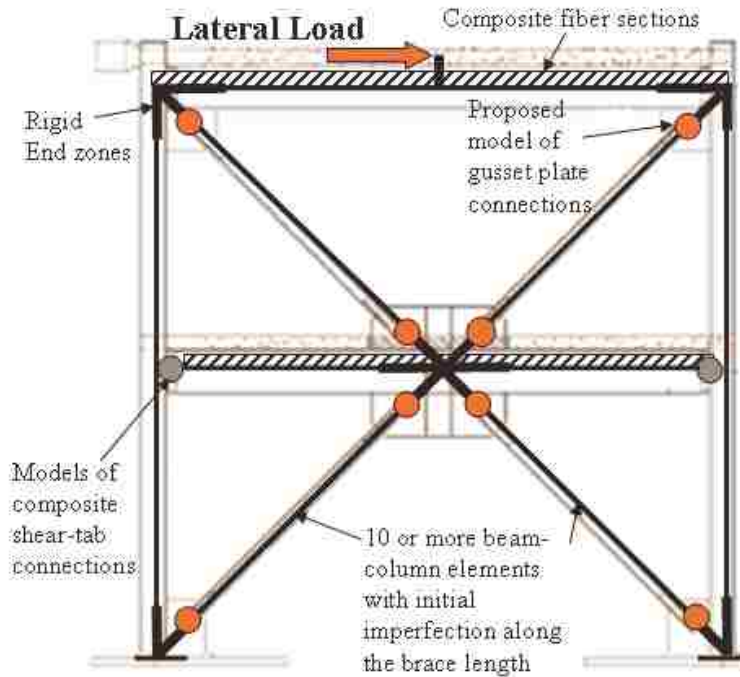


Figure 4.7 Illustration of the Typical Model Setup for the Two-story Specimens

In the specimens TCBF1-1(HSS) and TCBF1-2(WF), the midspan gusset were reinforced with edge stiffeners. The stiffened connections reduced the out-of-plane rotation of the gusset plates. To simulate this, the out-of-plane rotational stiffness and strength of those edge stiffeners were included in the model, and it led to approaching fixed end restraint to the ends of braces at the mid-span gussets.

The lateral loads were applied only on the top level of the frame through the composite slab in the tests. An additional rigid element was used at the middle of the top beam as illustrate in the figure to apply the lateral loads and simulate this test condition. In addition, the two column bases were fully restrained, while the nodes at beam-to-column connections and mid-span of the beams were restrained against out-of-plane movement and deformation.

Using a similar modeling process, the three-story frames were also simulated using



the proposed model. Figure 4.8 illustrates this model used. In particular, more and wider block-out regions were used in the three-story specimens, therefore, the effect of the block-out areas were considered in the model. The bare beam was used within the block-out areas, while fiber section of composite slab was used for the rest of beams, as shown in Figure 4.8.

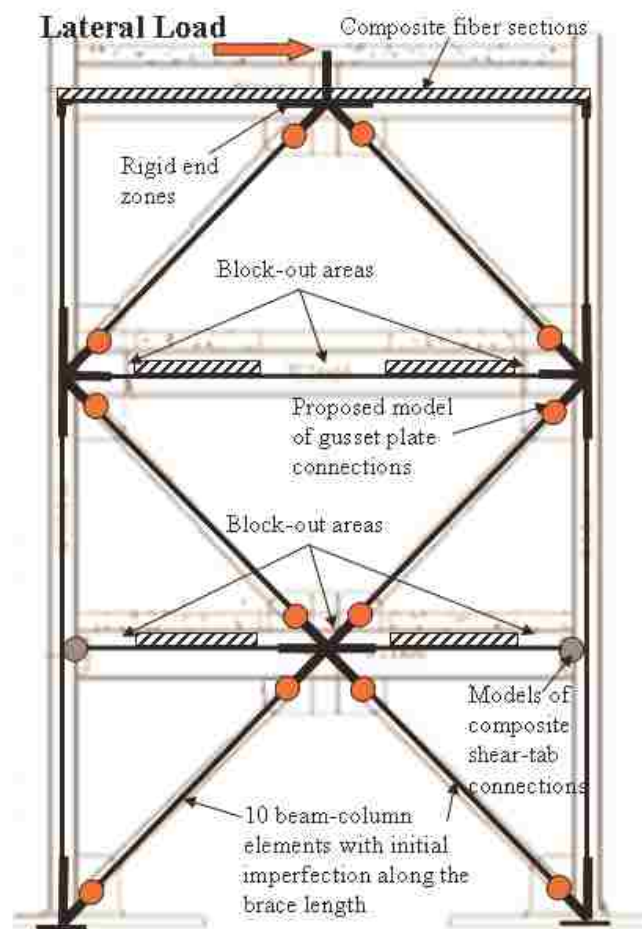


Figure 4.8 Illustration of the Typical Model Setup for the Three-story Specimens

## 4.4 Comparative Approaches

While the proposed improved model is simpler than the complex shell element models described in Chapter 3, it is more involved than the current modeling approaches used in engineering practice. To investigate accuracy afforded by the introduction of the fully proposed modeling approach, two additional modeling approaches, which better reflect nonlinear analyses used in practice, are compared. The primary differences of these approaches and the proposed approach are the connections models. In engineering practice, gusset plate connections maybe simulated as pin connections with various beam-column connections options. In other cases, rigid fully restrained connections may be employed. In practice, one of two variations is selected: the ends of the brace are either pinned or rigid restrained. Although the approach to modeling brace buckling is similar, the boundary conditions of the brace for these models are not.

To study the impact of these more conventional approaches, the two models were investigated, and are depicted in Fig. 4.9. The first is designated as the pinned model, and uses Liu and Astaneh-Asl's connection model (2004) for shear-tab beam-column connections, a rigid connection for beam-column connections at the brace gusset-plate connections, and pin connections at the work point with no rigid offsets, as illustrated in Fig. 4.9. The second is designated as the fixed model and uses rigidly restrained connection instead of pin connections at the work point, as illustrated in the figure. In all other manners, the models were identical to the improved model described earlier. While the pinned and rigid models included in the study use simplified assumptions for the connections, they continue to employ the full benefits of nonlinear modeling and analysis provided by OpenSees, even though many commonly used computer programs have

significantly less capabilities for simulating material and geometric nonlinearities. However, for simplicity, this more advanced approach was used. The two alternate connections reflect the variation that is expected in practice, and they are compared to theoretical predictions with the proposed improved model, which is also illustrated in Fig. 4.9, to demonstrate the effect of variations in analytical model on the accuracy of the predicted results.

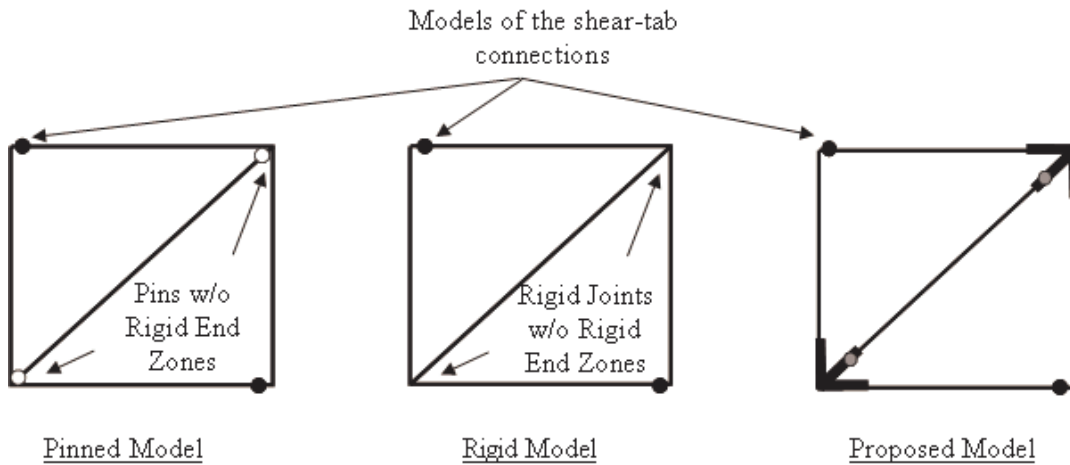


Figure 4.9 Illustrations of the Pinned, Rigid and Proposed Models

## 4.5 Simulation results

The 14 selected experiments were simulated using the three models mentioned above and compared to the test results to investigate the relative accuracy of the different theoretical predictions.

### 4.5.1 Single-story Frames

The 9 single-story single-bay frames were analyzed, and a comparison of the global responses is provided in Table 4.3. All models provided similar predictions of tensile resistance and stiffness of the frame. Significant differences lie in the accuracy of the simulated compressive response. The pinned model always significantly underestimated the buckling capacity of the brace. The rigid model always significantly overestimated the brace buckling capacity, and it also predicted more dramatic loss of resistance during post-buckling deformation. The proposed model consistently provided a more accurate prediction of the buckling capacity of the brace due to using the real length of the brace and proper modeling of the gusset plate connection.

This result is very important as the component models for the three approaches were identical, with the only difference being the approach used to model the connections. This suggests that the connection modeling approach has a significant impact on the global response of the frame.

A number of individual differences and comparisons are of note:

- Specimen HSS1 reflected the current design provisions, with a fillet weld connection joining the gusset plate to the beam and column. Failure of the specimen resulted from fracture of the weld. The model of this specimen had a relatively large rigid length effect since the gusset plate was large. The improved proposed model slightly overestimated the initial stiffness and tensile strength of the frame. The pinned and rigid joint models, which did not include rigid offsets, better captured the initial stiffness and the tensile strength of the frame, but had significant error in the compressive resistance. Specimen HSS12 had the same

dimensions of Specimen HSS1, but used CJP welds at the gusset to beam and column connections. The CJP welds avoided the early weld fracture noted with Specimen HSS1. As a result, the proposed model more accurately predicted the behavior of the specimen.

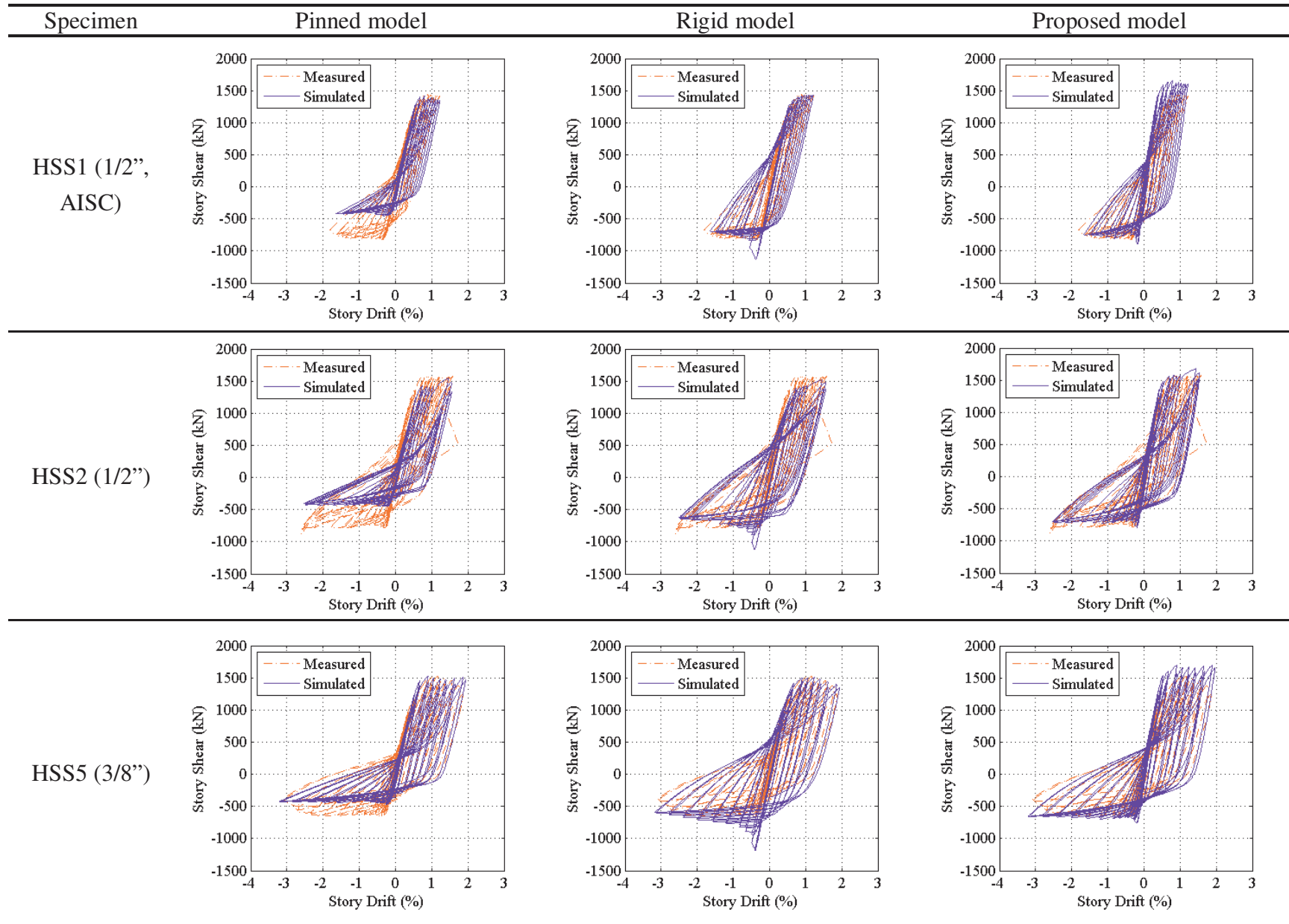
- Specimen HSS2 was designed using the elliptical-clearance model, and it had a thinner, more compact gusset plate relative to Specimens HSS1 and HSS12. The proposed modeling approach provides a more accurate estimate of stiffness and compressive and tensile resistance than the pinned or rigid joint models. Specimen HSS5 also had thin gusset plates with 8tp-elliptical-clearance gusset plates, which provided greater ductility and deformation capacity than other specimens. The proposed model slightly overestimated the initial stiffness and the tensile strength compared to the traditional models.
- Specimens HSS7 and HSS 11 had thicker gusset plates and the proposed improved model provided consistently better estimates of stiffness and resistance than the pinned and rigid models.
- Specimen HSS10 had tapered gusset plates. As a result, the model has shorter rigid lengths on the beams and columns. The proposed model had better estimates of compressive behavior than the pinned and rigid joint models. The tensile resistance was again overestimated by a modest amount.
- Specimen HSS17 had thin and tapered gusset plates, and the proposed model again predicted the overall behavior of the frame more accurately than other models.
- Specimen WF23 had wide-flange brace with thin gusset plate designed by the 8tp elliptical clearance model. The proposed model accurately predicted the buckling

capacity and the post-buckling behavior of the brace, but overestimated the strength with the brace in tension.

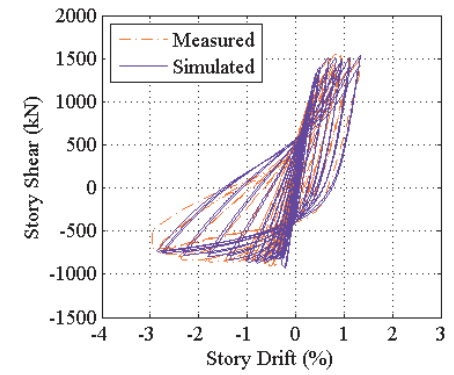
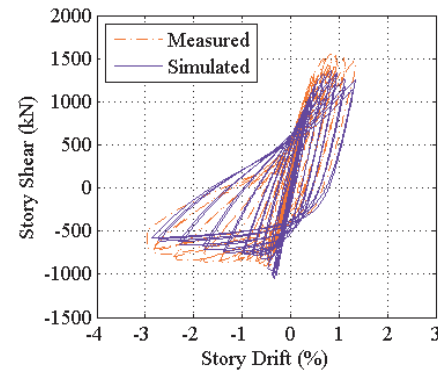
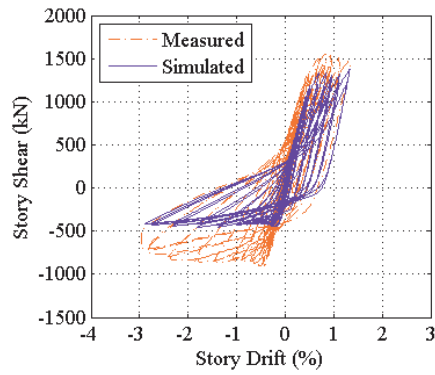
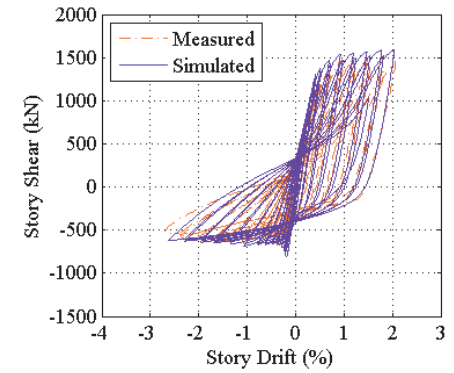
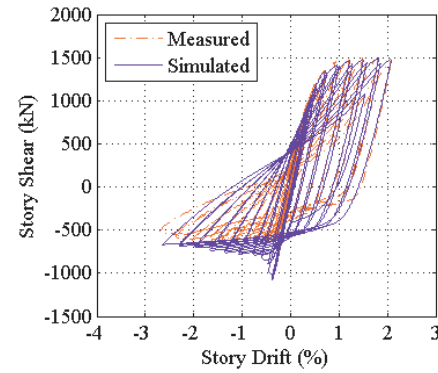
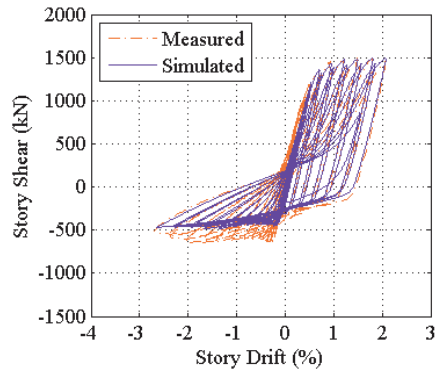
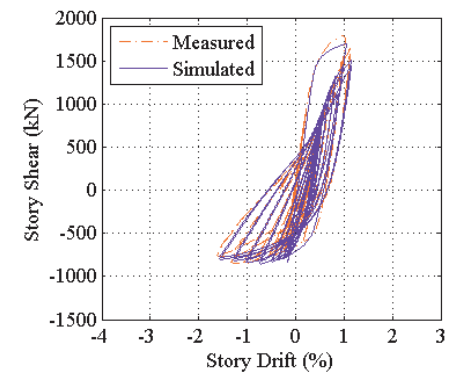
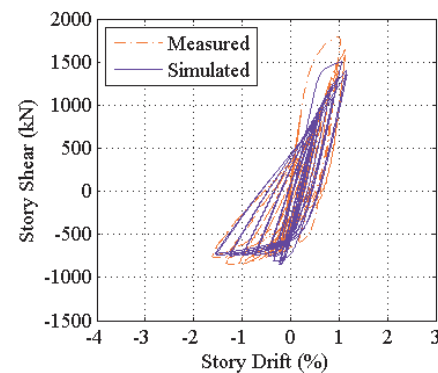
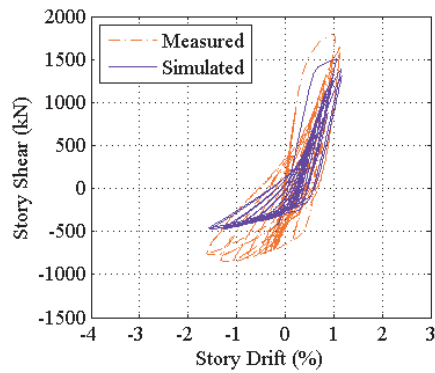
The results described above confirm that the proposed model provided better simulation of the axial compressive response of the braces than the pinned and rigid models.

The fiber model are incapable of simulating many local behaviors, such as local buckling, but some local deformations are accurately simulated. To further compare the models and experimental results, three specimen comparisons are highlighted. The three specimens have different thicknesses and geometries. Specifically, Specimen HSS5 had rectangular 9.5mm thick gusset plates, Specimen HSS7 with a 22.2mm thick, rectangular gusset plate, and Specimen HSS10 with a 12.3mm thick, tapered gusset plate. Figures 4.10a, b and c show the comparison between the measured and simulated out-of-plane brace deformations for all three specimens. The figure shows that the model is capable of capturing this local response mechanism for all of the gusset plates studied.

Table 4.3 Simulated and Measured Responses of the Single-story Frames

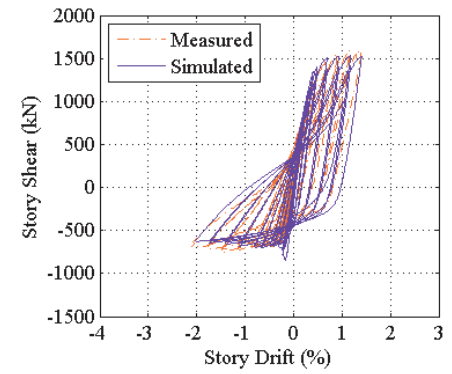
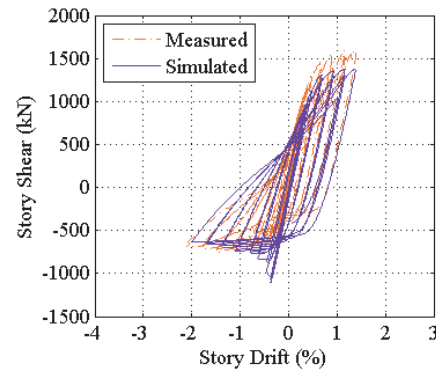
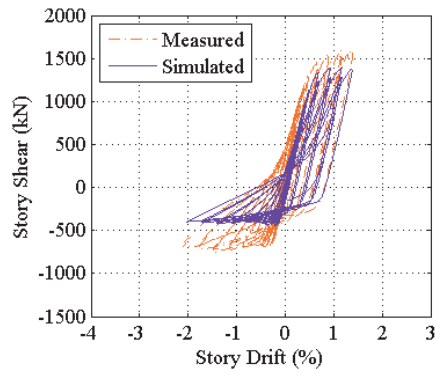


HSS7 (7/8")

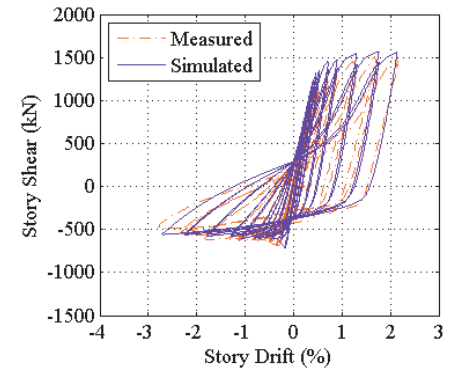
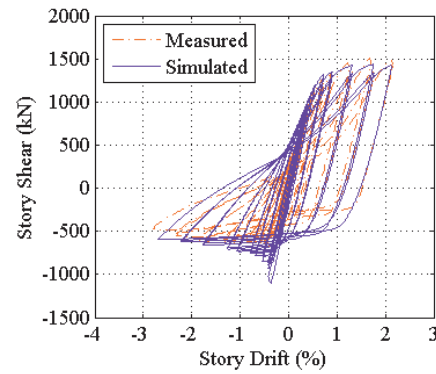
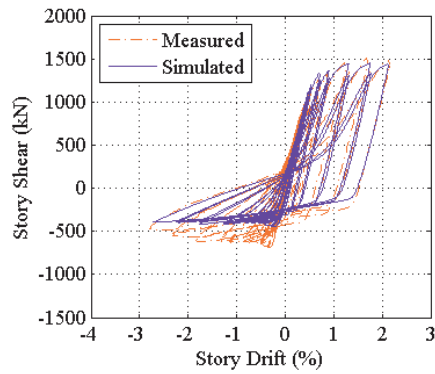
HSS10 (1/2",  
tapered)HSS11 (7/8",  
larger beam)



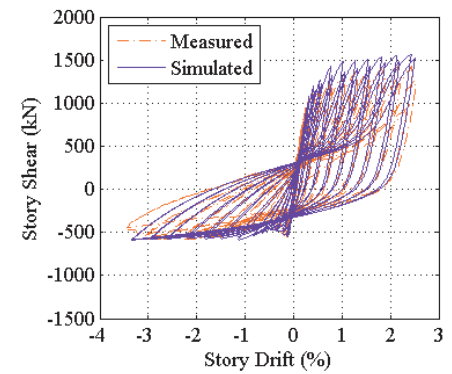
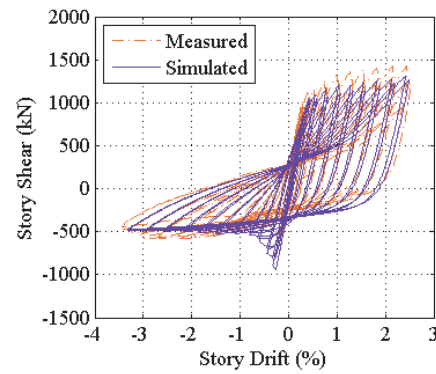
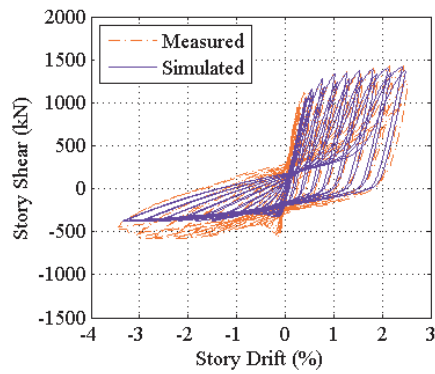
HSS12 (1/2",  
CJP welding)



HSS17 (3/8",  
tapered)



WF23 (3/8")



Figures 4.11a, b and c present the analytical responses of the proposed spring model for the same three specimens. (The rotation is positive for compression in the brace.) The results show that in the computer model, the connections started developing the inelastic rotation deformations early in the small drift of the frames. The models reach the plastic moment capacity of gusset plates ( $W_w t_p 2/4$ ), which is indicated with a solid line in the figures. The results also shows that at similar story drift, the connections with thinner or tapered gusset plates led to larger end rotation but smaller residual end rotation of the brace.

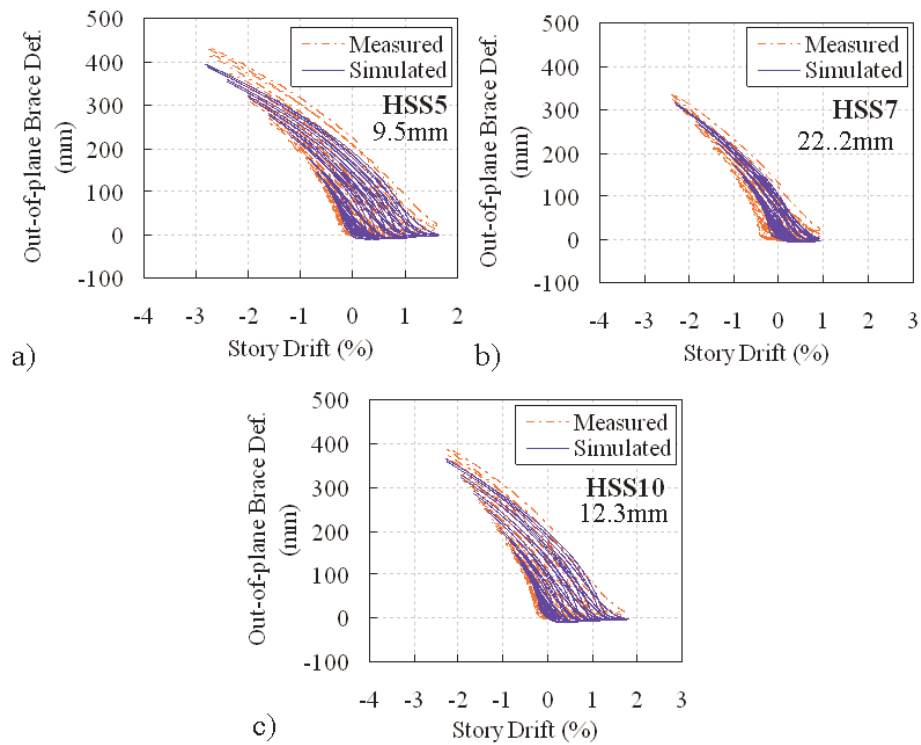


Figure 4.10 Comparisons of Experimentally Measured and Simulated Out-of-plane Deformation at Midspan of the Braces for the Specimens with (a) Thinner (HSS5), (b) Thicker (HSS7), and (c) Tapered (HSS10) Gusset Plates.

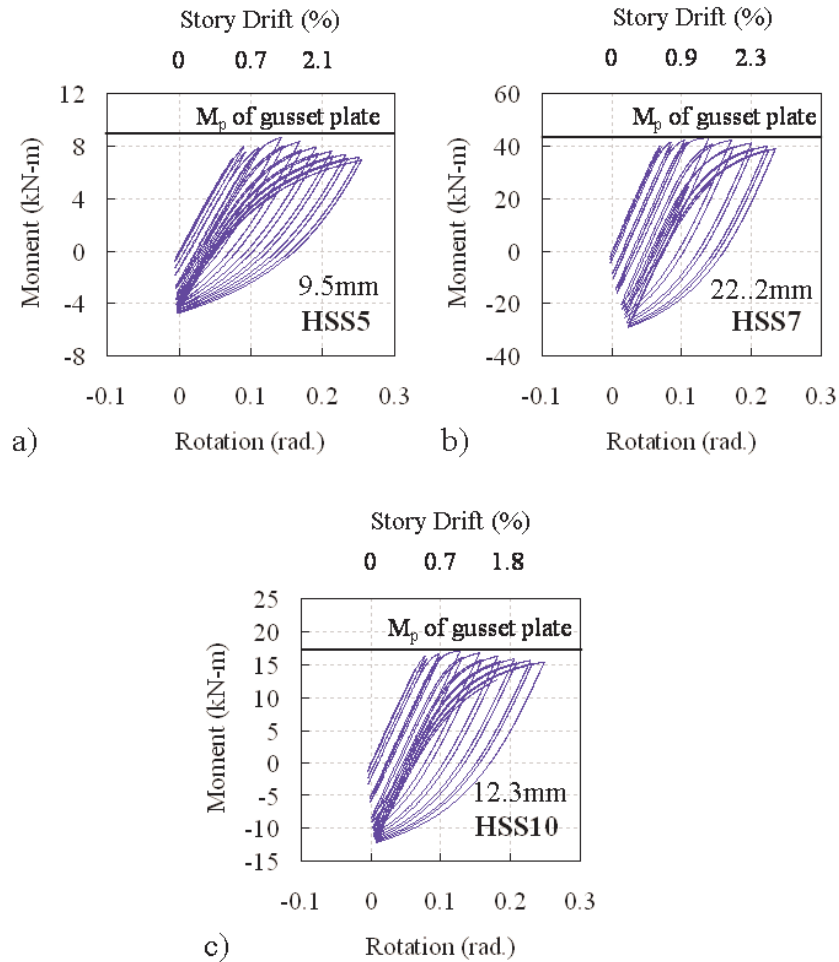


Figure 4.11 Analytical Moment-Rotation Hysteretic Responses Using the Proposed Connection Model for the Specimens with (a) Thinner (HSS5), (b) Thicker (HSS7), and (c) Tapered (HSS10) Gusset Plates.

## 4.5.2 Multi-story Frames

The multi-story frames were also simulated using the prior results as a basis. The theoretical predictions of the two alternate and the proposed modeling approaches were again compared with test results for all multi-story specimens. The composite effect of the concrete slab was included in the model except the block-out regions which was used for the installation of the gusset plate connections due to the reuse of the framing system,

as shown in Fig. 3.1. For the connection model of the mid-span gusset plates in the two-story frame specimens, the out-of-plane rotational stiffness was increased to simulate effect of the edge stiffeners, which restrained the gusset plate substantially and eliminated gusset plate deformation. (Note that these stiffeners were not included in the three story specimens).

The overall specimen and individual story measured responses and the results using the three modeling approaches are shown in Table 4.4 for TCBF1-1(HSS). Specimen TCBF1-1(HSS) was a two-story with rectangular HSS braces. The table shows that the proposed model accurately predicted the hysteretic behavior of the specimen both at the roof level and individual stories; while the conventional models had relative low accuracy at both levels. This finding is important since the distribution of demands over the height of a braced frame building will greatly impact its seismic performance.

The results of the proposed model for TCBF1-2(WF) and TCBF1-3(TG) specimens are shown in Table 4.5. Specimen TCBF1-2(WF) used same frame of Specimen TCBF1-1(HSS) but had wide flange braces and comparably detailed gusset plates. The frame had a sharp drop in resistance, which corresponded to initial brace buckling, and this was simulated by the modeling approach. However, there were residual forces, moments and stresses in the beams and columns of the frame after completion of the first test and these were not simulated. As a result, the predicted frame strength was slightly larger than the experimental results due to the prior loading history.

Similar results were found for Specimen TCBF1-3(TG), which had a new set of HSS-section braces and tapered gusset plates with reduced edge stiffeners around the mid-span gusset plates. The proposed model predicted the average top story displacement well. However, the 1st-story inter-story drift was slightly underestimated, while the

2nd-story inter-story was overestimated by a similar amount. The frame strength was again overestimated because the model did not consider the damage, deterioration and residual effects accumulated during the prior two tests.

The 3-story single-bay frames were also analyzed; the theoretical predictions of the conventional approaches for TCBF2-2(HSS) are provided in Table 4.6, and that of the proposed model for both two three-story frames are shown in Table 4.7. The results are similar to the two-story specimens. The pinned model was unable to represent the cyclic behavior both at the roof level and individual stories, while the rigid model provided a better prediction of the behavior at the roof level but had reduced accuracy at the individual stories. Specimen TCBF2-1(HSS) was tested first (virgin test frame), and the proposed model accurately represented the initial stiffness, lateral resistance and the distribution of stiffness and deformation over the height of the frame. TCBF2-2(WF) was the second test, and the beams, columns, and their connections were reused for economy of the testing. As a result, the proposed model slightly overestimated the frame resistance. However, the proposed model estimated the distribution of deformation for the various floor levels.

Table 4.4 Simulated and Measured Responses of TCBF1-1(HSS) Specimen

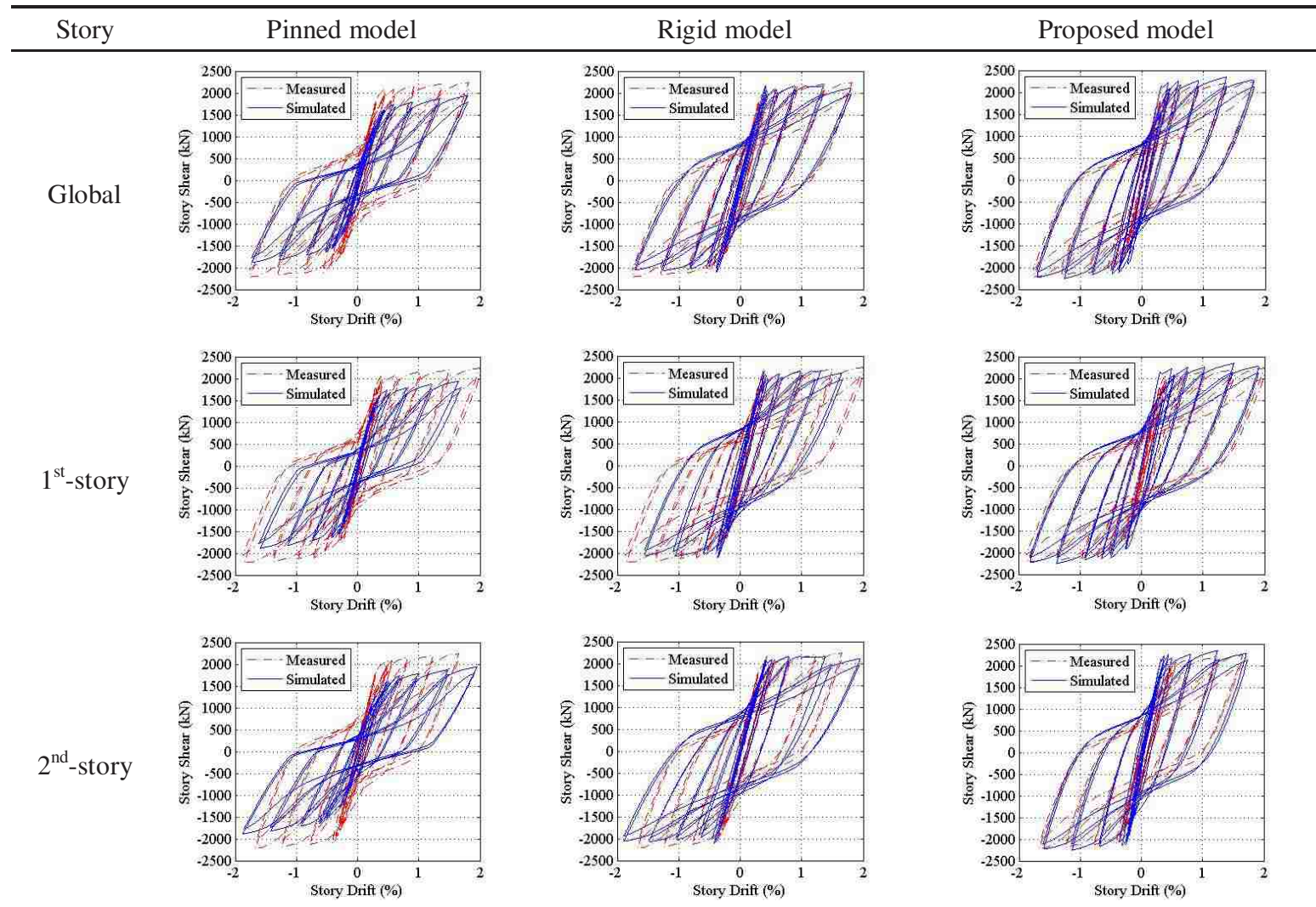




Table 4.5 Simulated and Measured Responses of TCBF1-2 and TCBF1-3 Specimens

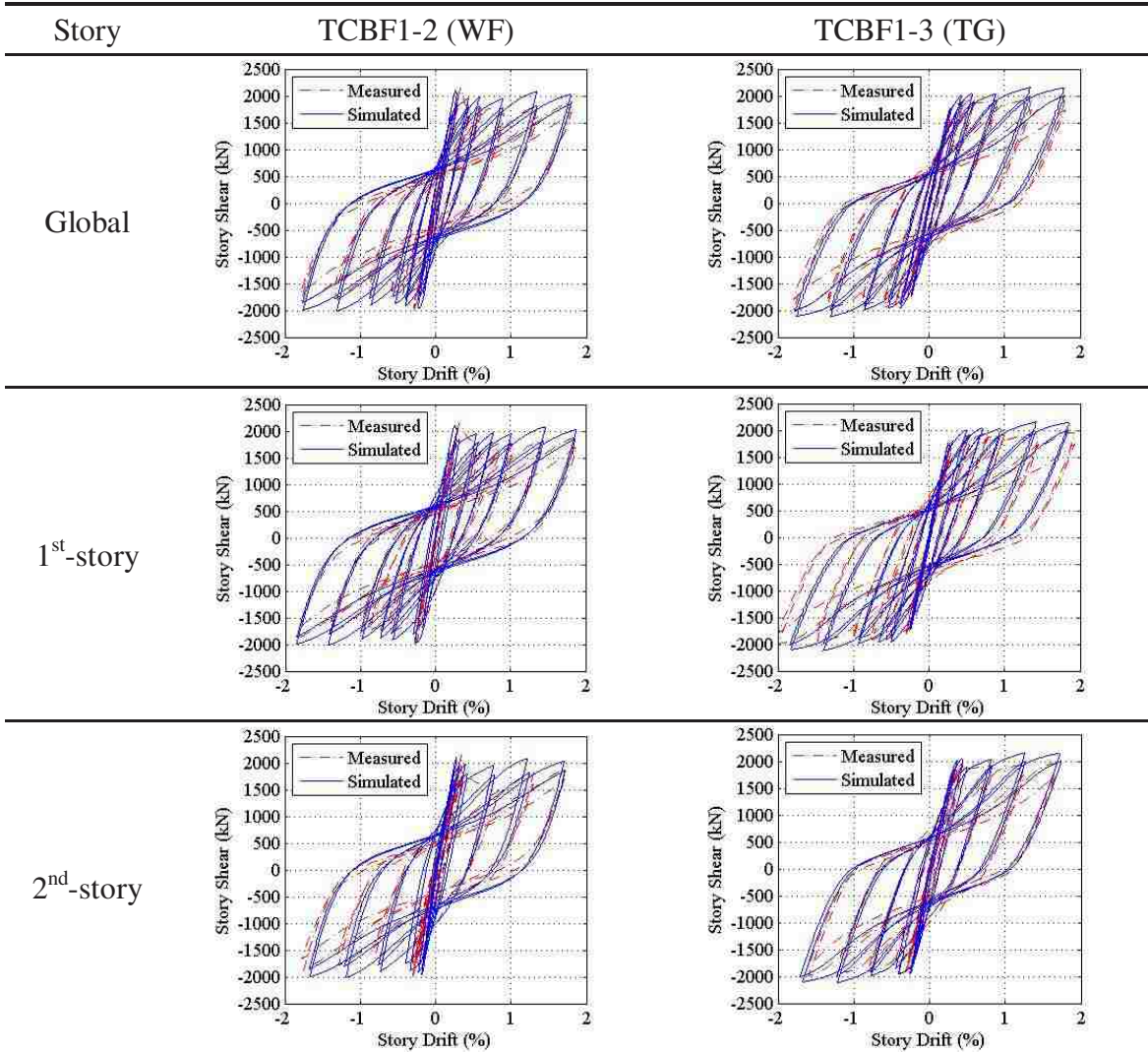


Table 4.6 Simulated and Measured Responses of TCBF2-1 Specimen

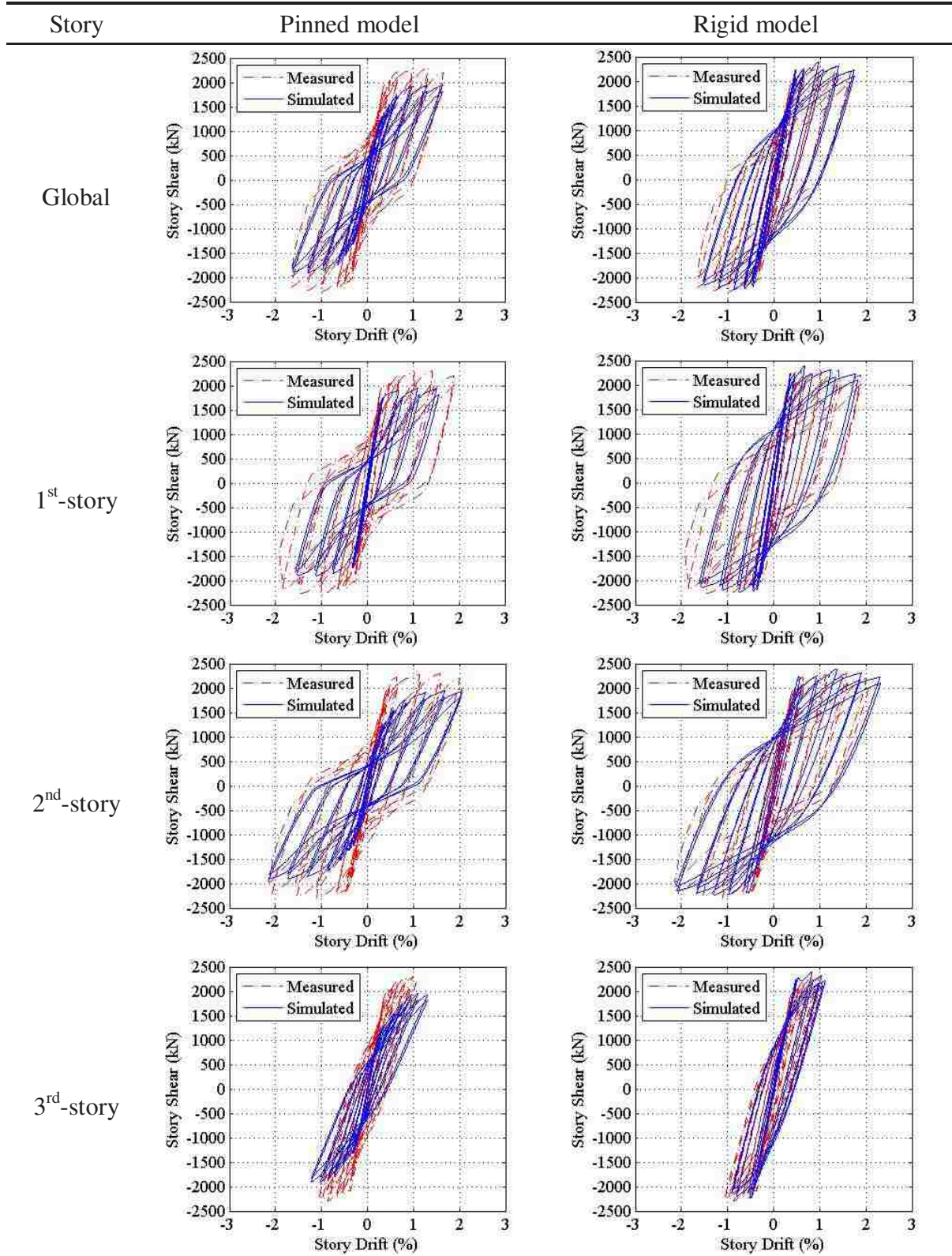
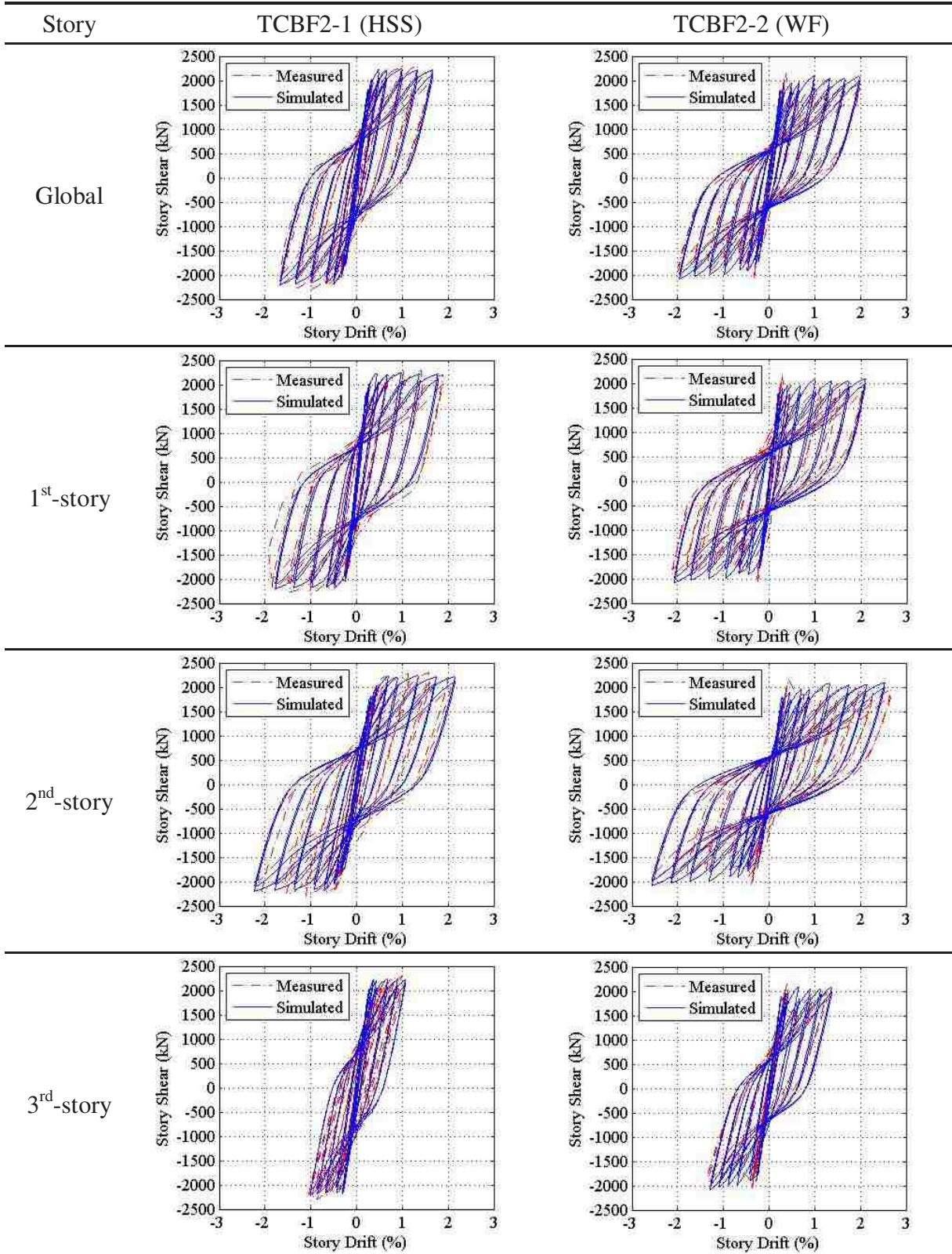




Table 4.7 Simulated and Measured Responses of TCBF2-1 and TCBF2-2 Specimens



## 4.6 Error Evaluation

To quantify the difference between the analytical responses and the experimental results, an error analysis was conducted. The errors in prediction of the total energy dissipation, maximum story-shear forces were calculated by integrating the area of each cycle and summing them and the results are shown in Table 4.8. The analyses and experiments were displacement controlled, and so the applied story drift history was identical, and therefore the differences in the total energy dissipation values reflect the accumulated errors of the predicted story-shear force of the frames. On average, the errors were approximately 13% by the proposed model, and 42% and 20% by the pinned and rigid models, respectively.

Comparison of the measured and predicted maximum story-shear force for the single-story frames and the multi-story frames show that the proposed model consistently provided a better estimate of the frame resistance than the pinned or rigid models. In the single-story frames, the pinned joint consistently underestimated maximum story-shear force for the brace in compression, while the rigid joint model consistently overestimated the story shear force. The proposed model slightly overestimated the maximum story-shear for brace in compression with the frame having very thin gusset plates.

Moreover, the proposed model provided significantly better estimates of buckling and post-buckling behavior than the pinned and rigid joint models in the single-story frames. For multi-story frames, the pinned joint models provided relatively poor estimates, while the proposed model and the rigid joint model were relatively comparable.

Table 4.8 Errors in Total Energy Dissipation and Maximum Story-shear Forces for Brace in Tension and Compression of the Simulations.

Specimen	Error in Total Energy Dissipated (%)			Error in Max. Story-shear Force For Brace in Tension (%)			Error in Max. Story-shear Force For Brace in Compression (%)		
	Prop.	Pinned	Fixed	Prop.	Pinned	Fixed	Prop.	Pinned	Fixed
HSS1(1/2", AISC)	24.2+	50.2-	18.2+	15.3+	1.6-	0.5-	7.7+	45.5-	36.3+
HSS2 (1/2")	3.7-	48.6-	8.2+	6.7+	2.0-	3.2-	10.1-	48.9-	27.1+
HSS5 (3/8")	14.1+	29.8-	44.6+	11.7+	0.3-	1.3-	12.8+	28.1-	82.8+
HSS7 (7/8")	11.1+	46.6-	15.8+	1.2-	11.3-	12.0-	3.5+	49.2-	17.5+
HSS10 (1/2", tapered)	28.6+	23.6-	48.5+	5.8+	0.1+	0.3-	23.4+	24.7-	67.1+
HSS11(7/8", large beam)	12.1+	52.6-	6.1+	4.8-	15.8-	15.8-	0.3+	44.1-	0.9-
HSS12(1/2", CJP)	11.7+	39.7-	29.6+	2.4-	13.5-	14.1-	4.2-	40.2-	47.1+
HSS17(3/8", tapered)	24.5+	24.7-	52.8+	3.4+	4.4-	5.1-	4.1+	35.3-	59.9+
WF23 (3/8")	4.6+	38.0-	3.3+	9.7+	0.7-	8.2-	1.8+	33.9-	63.3+

Specimen	Ave. /Story	Error in Total Energy Dissipated (%)			Error in Max. Story-shear Force (%)		
		Proposed	Pinned	Fixed	Proposed	Pinned	Fixed
TCBF1-1 (10mm, HSS)	Ave.	6.3 <sup>+</sup>	47.8 <sup>-</sup>	8.3 <sup>-</sup>	4.6+	13.6-	3.2-
	1st	6.9+	57.6-	23.0-			
	2nd	5.5+	35.6-	9.9+			
TCBF1-2 (10mm, WF)	Ave.	16.4 <sup>+</sup>	42.0-	7.2+	2.0-	18.2-	0.0+
	1st	13.6+	51.4-	13.8-			
	2nd	20.1+	29.6-	34.9+			
TCBF1-3 (20mm, AISC, TG)	Ave.	8.3 <sup>-</sup>	41.3-	8.4+	10.2+	1.1-	13.5+
	1st	14.7-	54.0-	13.3-			
	2nd	0.4+	24.2-	37.7+			
TCBF2-1 (10mm, HSS)	Ave.	2.0 <sup>+</sup>	47.5 <sup>-</sup>	2.7 <sup>-</sup>	2.2-	15.2-	4.0+
	1st	9.2-	60.3-	16.1-			
	2nd	21.1+	38.8-	25.7+			
	3rd	10.0-	38.6-	27.7-			
TCBF2-2 (10mm, WF)	Ave.	0.6 <sup>+</sup>	60.0-	22.2+	3.4-	19.3-	0.1+
	1st	7.3-	67.5-	12.7+			
	2nd	2.9-	62.2-	17.7+			
	3rd	37.0+	33.3-	66.6+			

+ Overestimated, - Underestimated



## **Chapter 5 : A Model to Simulate SCBFs Beyond Brace Fracture**

### **5.1 Introduction**

In large earthquakes, the bracing members of SCBFs may be subjected to large axial deformations resulting in severe global and local buckling deformations, and tensile yielding. This inelastic response permits the systems to sustain large, cyclic drift demands. Eventually, failure of one of the components will occur. The design philosophy predicates brace fracture as the primary failure mode. (Experimental research indicates that the local buckling deformations, typically at the center of the brace, eventually lead to tearing of the brace.) Although fracture is never desirable in a structure system, a system will fail if the demand is large enough. To maintain gravity-load carrying capacity, it is necessary to define a fracture mode that will not compromise the structure integrity. For braced frames, loss of a column or connection would not meet this criterion. Therefore, brace fracture is the desired fracture mode.

While the concept of PBSO is widely accepted, capacity evaluation of SCBF structures including fracture and collapse is difficult to conduct in a practical manner. In particular, it is difficult to predict brace fracture, which is the desired failure mode of SCBFs, and therefore its prediction is central to accurate PBSO of SCBFs.

During testing, severe out-of-plane deformation due to the buckling behavior

typically resulted in brace fracture. This behavior is illustrated in Fig. 5.1. The out-of-plane displacement of brace increases with the story drift of the frame, which results in a concentration of inelastic deformation at the midlength of the brace and eventual formation of a plastic hinge, as shown in Figs. 5.1a to c. At the location of the formed plastic hinge, cupping at the center of the brace tube (Fig. 5.1d) occurred first, which leads to crack initiation (Fig. 5.1e) at the cupped location after a few additional cycles. The crack grew as the brace sustained tensile force again in the following cycles and eventually fully fractures (Fig. 5.1f).

An investigation of the brace fracture was conducted based on these observations, and a modeling approach was developed and implemented in the OpenSees framework. To correctly evaluate the seismic behavior of SCBFs, all members and their connections must be accurately modeled. The well developed and validated modeling approach for the nonlinear analysis using line-element models, as described in the previous chapter, was used to model the structure, and to establish the modeling approach and loading criteria for brace fracture. This portion of the study was undertaken to develop a practical yet accurate model to predict the onset and impact of brace fracture. In turn, the combination of the line element model and brace fracture model then were used to evaluate the impact of brace fracture on the system performance.

The brace fracture model was based on a great number of past experimental studies. Those test specimens varied widely in their slenderness ratio, width-to-thickness ratio and yield strength of the bracing members, and these parameters were specifically included in the fracture model. Although different structural steel sections may be used as bracing members (e.g., wide flanges, angles, channels and tube sections), this study focused on rectangular HSS braces, because they are economical and widely used in practice. The

primary content of the chapter was addressed in a journal paper as documented in Appendix D.

An overview of the prior fracture simulation models is provided in Section 5.2. The details of experimental data set used for the development of the fracture model are summarized in Section 5.3. Section 5.4 presents the evaluation of fatigue life prior to brace fracture at axial- and strain-deformation levels. A material model for implementation in OpenSees is described in Section 5.5. The resulting model was compared with other previous models for predicting brace fatigue life in Section 5.6, and the impact of design parameters of predicted fracture was evaluated in Section 5.7.

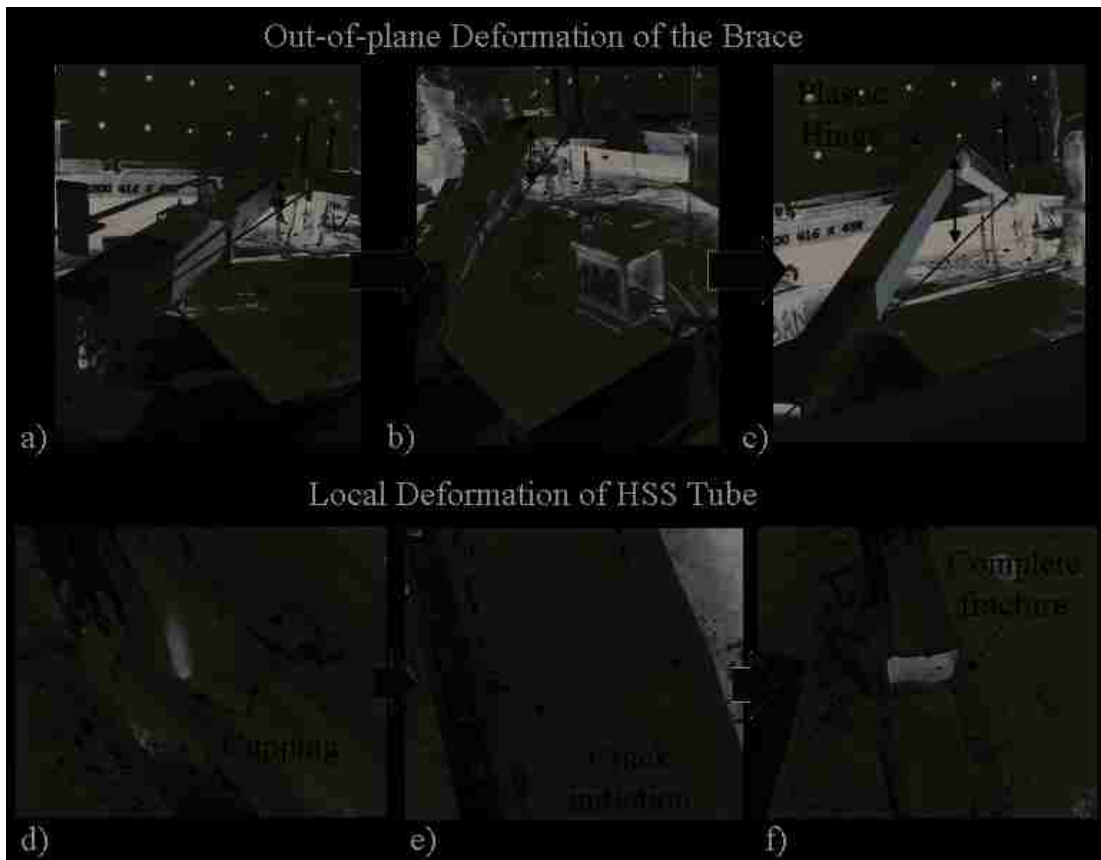


Figure 5.1 The Global and Local Behavior Resulting in Brace Fracture

## 5.2 Prior Brace Fracture Simulation Models

Brace fracture is the primary failure mode of SCBFs with proper design (Lehman and Roeder 2008). In past studies, several different approaches had been developed to predict the fracture life of the braces under cyclic loading. In the case of continuum FE analysis, the EPS has been calibrated to predict brace fracture, e.g., Yoo et al. (2008) and Fell et al. (2009). In this study, the focus was on modeling approaches to simulate brace fracture that are appropriate for use in nonlinear analyses using line-elements.

Several research studies have developed these types of models and a brief discussion of the selected models follows. Models that link brace fracture to the global response include those by Lee and Goel (1987), Shaback and Brown (2001) and Tremblay (2003). Uriz and Mahin (2008) link the local deformation response of the brace to predict the onset of fracture.

Some previous studies experimentally investigated the relationship between global axial deformations and fracture life of the brace. Lee and Goel tested thirteen full-scale hollow and concreted-filled square tubular bracing members with different effective slenderness and cross-sectional slenderness ratios. Six specimens from this experimental study and three specimens from a prior study (Liu and Goel 1987) that utilized HSS tubes were combined to develop a model to predict the brace fracture life of HSS braces. The researchers postulated that the cyclic deformation demands on the brace resulted in low-cycle fatigue fracture. To simulate the observed response, the cyclic axial deformation response of the HSS tube was used as the primary parameter in the brace fracture model.

Figure 5.2a shows a typical cyclic normalized axial force-deformation response from



a single cycle of a test on an isolated brace. Two normalized axial deformations are defined. The compressive portion of the normalized axial deformation  $\Delta_1$  is the displacement that ranges from the maximum displacement in the compressive loading direction to the displacement corresponding to a tensile force of  $P_y/3$ , as shown in the figure. The normalized axial deformation  $\Delta_2$  is the remaining portion of the displacement range. These two deformations are used to quantify the defined non-dimensional parameter of the fracture life,  $\Delta_f$ , using the defined weights, as indicated in Eq. 5.1, where  $n$  is the number of cycles achieved before the brace fracture. Equation 5.2 provides the fracture limit, which was based on the experiments.

$$\Delta_f = \sum_{j=1}^n (0.1\Delta_1 + \Delta_2) \quad (5.1)$$

$$\Delta_{f,pred.1} = C_{s.1} \frac{(315/F_y)^{1.2} \left( \frac{4b/d + 1}{5} \right)}{[(b-2t)/t]^{1.6}} \quad (5.2)$$

In Eq. 5.2,  $b$ ,  $d$  and  $t$  are the width, depth and thickness of the HSS tube, respectively;  $F_y$  is the yield strength of the brace, in MPa; and  $C_{s.1}$  is an experimentally determined non-dimensional constant. The fracture life was related to three primary variables:  $F_y$ ,  $b/d$ , and  $(b-2t)/t$ , or the yield strength, cross-sectional aspect ratio, and cross-sectional slenderness. The experimental data set had effective slenderness ratios,  $KL/r$ , between 35 and 77 and cross-sectional slenderness ratios,  $(b-2t)/t$ , between 14 and 30, where  $L$  and  $r$  are the length and the ratio of gyration of the tube, and  $K$  varied between 0.50 and 0.85. All of the experiments used ASTM-A500, Grade B structural tubes. According to the test results, the corresponding  $C_{s.1}$  values varied from 1160 to 1508, and a mean value of 1335 was suggested for use. Figure 5.2b shows the comparison between the fracture life measured during the tests,  $\Delta_{f,test}$ , and the fracture life predicted using Eq. 5.2,  $\Delta_{f,pred.1}$ .

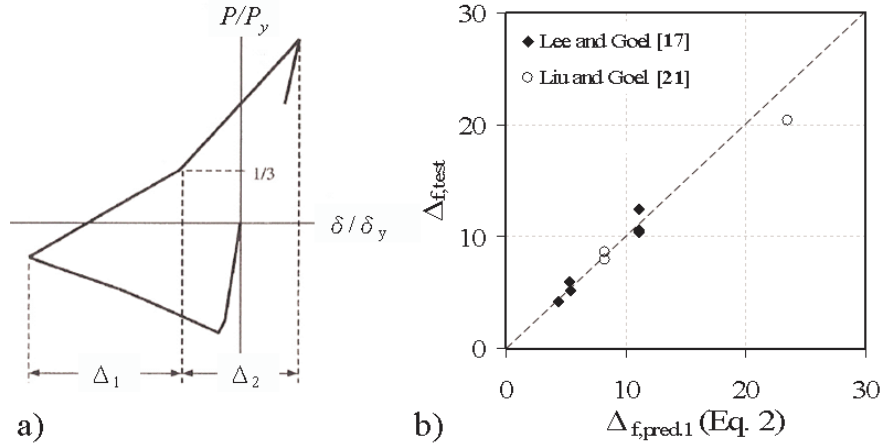


Figure 5.2 (a) Definition of Displacement Components  $\Delta_1$  and  $\Delta_2$  from; (b) Comparison of Predicted and Experimental Measured Fracture Life (Lee and Goel 1987)

Shaback and Brown (2001) also proposed an empirical equation to predict fracture life of an HSS brace. Equation 5.1 by Lee and Goel was adopted, but different limits were developed in this later study. Instead of Eq. 5.2, a pair of equations was proposed to estimate the fracture life (Eqs. 5.3a and 5.3b) and to describe the dependence of brace fracture on the slenderness ratio; all other variables were the same.

$$\Delta_{f,pred.2} = C_{s,2} \frac{(350/F_y)^{-3.5}}{[(b-2t)/t]^{1.2}} \left( \frac{4b/d-0.5}{5} \right)^{0.55} (70)^2 \text{ for } \frac{KL}{r} < 70 \quad (5.3a)$$

$$\Delta_{f,pred.2} = C_{s,2} \frac{(350/F_y)^{-3.5}}{[(b-2t)/t]^{1.2}} \left( \frac{4b/d-0.5}{5} \right)^{0.55} \left( \frac{KL}{r} \right)^2 \text{ for } \frac{KL}{r} \geq 70 \quad (5.3b)$$

$C_{s,2}$  is an experimentally determined non-dimensional constant, and the researchers proposed a value of 0.065. This model was based on different data, and the researchers used a combined data set with nine full-scale HSS-tube braces tested by Shaback and Brown. These tests had cross-sectional slenderness ratios,  $(b-2t)/t$ , between 12 and 18 and effective slenderness ratios,  $KL/r$ , between 52 and 66, where  $K$  varied between 0.66 and

0.77. Brace tests conducted by Archambault (1995) were also included. Figure 5.3 shows the comparison between the fracture life measured during the tests,  $\Delta_{f,test}$ , and the fracture life,  $\Delta_{f,pred,2}$ , predicted using Eqs. 5.3a and b.

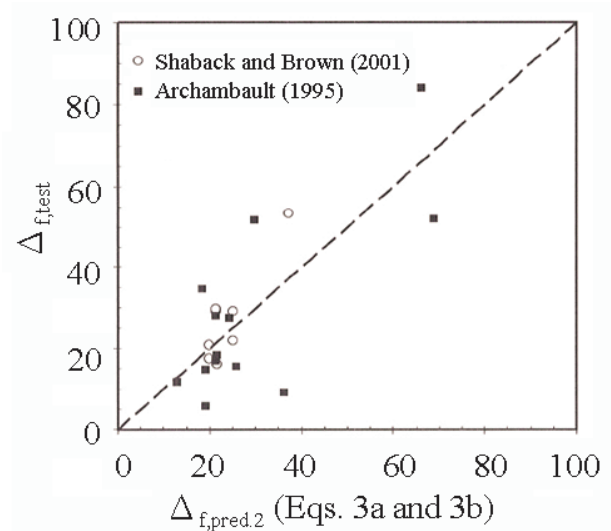


Figure 5.3 Comparison of Predicted and Experimental Measured Fracture Life (Shaback and Brown 2001)

Tremblay et al. (2003) conducted a total of 24 cyclic tests, including full-scale single-story braced frames with X-bracing and single diagonal bracing configurations, and based fracture on a limiting value of the brace-end rotational deformations for rectangular hollow sections. A combined data set was developed, including 22 tests with brace fracture from their test program and 24 tests from other studies on single bracing members from the following test programs: Gugerli 1982, Lee and Goel 1987, Liu and Goel 1987, Walpole 1996, Shaback and Brown 2001. In this combined data base,  $KL/r$  varied from 60 to 143, and the width-thickness ratios,  $b_o/t$  and  $d_o/t$ , varied from 8 to 13 and 7 to 23, respectively, where  $b_o$  and  $d_o$  are the flat width and depth of the cross section.

The end rotation is related to the total ductility of the bracing member by Eqs. 5.4 and 5.5, where  $L_H$  is the brace length using the assumption that the ends are simply supported as illustrated in Fig. 5.4a. The axial movement of the brace under compression,  $\delta_c$ , (shown in Fig. 5.4a) is defined by Eq. 5.5, where  $\mu_c$  and  $\mu_t$  are the peak compression and tensile ductility values and  $\delta_y$  is the axial yield deformation of the bracing member.

$$\theta_f = \sqrt{\frac{2\delta_c}{L_H}} \quad (5.4)$$

$$\delta_c = (\mu_c + \mu_t - 1)\delta_y \quad (5.5)$$

The maximum end rotations corresponding to brace fracture,  $\theta_{f,pred}$ , was derived from the database of cyclic tests and are given by Eq. 5.6.

$$\theta_{f,pred} = 0.091 \left( \frac{b_o}{t} \frac{d_o}{t} \right)^{-0.1} \left( \frac{KL}{r} \right)^{0.3} \quad (5.6)$$

Figure 5.4b shows the comparison of the experimental and their predicted end rotations corresponding to the onset of brace fracture.

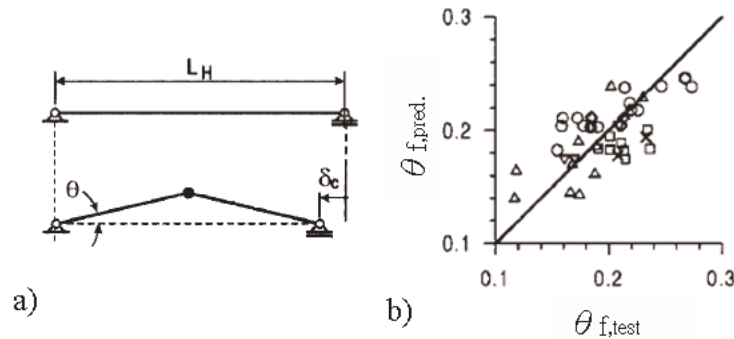


Figure 5.4 (a) Simplified deformed shapes for prediction of out-of-plane deformations for single bracing and (b) experimental versus predicted values. (Tremblay et al. 2003)

Uriz (2005) used an accumulative strain limit to develop a prediction for initiation of

brace fracture based on low-cycle fatigue. The model was implemented in the OpenSees structural analysis software platform. The low cycle fatigue modeling approach was based on Miner's rule (ASTM 2003, Fisher et al. 1997), which is expressed as the damage index,  $DI$ , given in Eq. 5.7. In the equation, the damage index at each cycle amplitude is estimated by dividing the number of cycles at that amplitude,  $n(\varepsilon_i)$ , by the number of cycles at that amplitude necessary to cause failure, under constant amplitude testing,  $N_f(\varepsilon_i)$ . The Coffin-Manson relationship (ASTM 2003, Fisher et al. 1997) expressed in Eq. 5.8, was used to determine the relationship between strain amplitude and the number of constant amplitude cycles necessary to cause failure. In this equation,  $N_f$  is the number of cycles at strain amplitude  $\varepsilon_i$  resulting in failure, and the parameters of  $m$  and  $\varepsilon_o$  are empirical constants, where  $\varepsilon_o$  is the failure strain for a single reversal, while  $m$  is known as the fatigue ductility exponent.

$$DI = \sum_{j=1}^n \left( \frac{n(\varepsilon_i)}{N_f(\varepsilon_i)} \right)_j \quad (5.7)$$

$$\varepsilon_i = \varepsilon_o (N_f)^m \quad (5.8)$$

Following this approach, the value of  $DI=0$  indicates that there is no damage, and a value of  $DI=1$  indicates failure. For this research, a modified rainflow cycle counting method was used to determine the amplitudes of each cycle and the number of cycles for all types of symmetric, asymmetric and arbitrary cyclic history.

Uriz used experiments performed by Yang on full-scale bracing members (Yang and Mahin 2005) to calibrate and validate the modeling approach. This calibration led to the parameters,  $m = -0.5$  and  $\varepsilon_o = 0.095$ . Figure 5.5 shows the comparison between the predicted and measured maximum axial displacement before brace fracture.

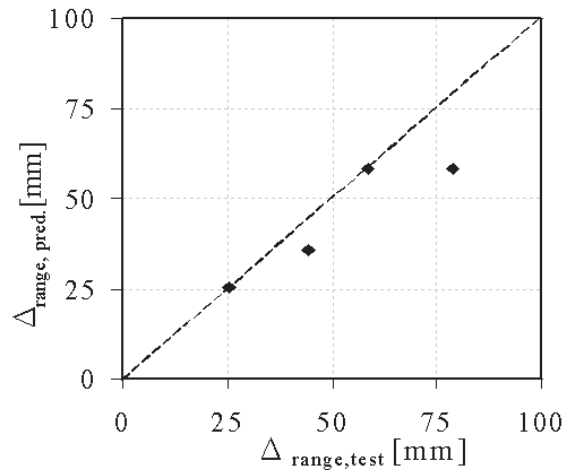


Figure 5.5 Comparison of Predicted and Experimental Displacement Range before Brace Fracture (Uriz 2005)

All of these previous brace fracture models were evaluated in a comprehensive study on prediction of brace fracture, as described in Section 5.4, for a broader experimental data set, as shown in Section 5.3.

### 5.3 Experimental Data Set

Experimental data from prior studies were gathered to evaluate the previous models and evaluate a newly proposed model. The following criteria were used for selection of the data set:

- (1) The test must use square HSS tubes for the bracing members.
- (2) The test must exhibit brace fracture.
- (3) Sufficient information regarding the geometry, material properties and test loading must be available to permit simulation of the braced and its boundary conditions.

The experimental data set included not only the frame tests in the prior experimental program, as mentioned in Section 2.3.1 (Johnson 2005, Herman 2006, Kotulka 2007, Powell 2009, Clark 2009, Lumpkin 2009), but also the tests of other past experimental studies on brace components and braced frames (Lee and Goel 1987, Shaback and Brown 2001, Tremblay et al. 2003, Yang and Mahin 2005, Uriz 2005, Goggins et al. 2006, Fell et al. 2009, Han et al. 2007).

A total of forty-four (44) specimens included in the data set, The tests include a range of configurations including: (1) component tests consisting of only the brace and gusset plate connections (Lee and Goel 1987, Shaback and Brown 2001, Tremblay et al. 2003, Yang and Mahin 2005, Goggins et al. 2006, Fell et al. 2009, Han et al. 2007), and (2) single- and multi-story frame tests including the beams, columns, braces and gusset plate connections simulating a lateral frame configuration (Johnson 2005, Uriz 2005, Herman 2006, Kotulka 2007, Powell 2009, Clark 2009, Lumpkin 2009).

Prior experimental studies suggest that the fracture life of the HSS bracing members depends on the slenderness ratio of the bracing members, the width-to-thickness ratio of the cross-section, the yield strength of the steel, the restraint and boundary condition of the brace, and the imposed displacement history. Synthesis of the experimental studies indicates that smaller width-to-thickness ratios (Lee and Goel 1987, Shaback and Brown 2001, Tremblay et al. 2003, Fell et al. 2009, Goggins et al. 2006, Han et al. 2007) and larger slenderness ratio (Shaback and Brown 2001, Tremblay et al. 2003, Fell et al. 2009, Goggins et al. 2006) increase brace ductility. As much as possible, the data set was developed that included a wide range of these important design variables. Table 5.1 summarized the specimen configurations and study variables of specimens involved in the experimental data set.

An example of a full-scale, single-story one-bay braced frame as shown in Fig. 5.6a; these tests were conducted at UW laboratory (Johnson 2005, Herman 2006, Kotulka 2007, Powell 2009). Examples of full-scale two-story and three-story frames are shown in Fig. 5.6b and c; these frames were tested at NCREE laboratory (Clark 2009, Lumpkin 2009). A different, brace configuration two-story frame test is shown in Fig. 5.6d; this example frame was tested at University of California (UC) Berkeley (Uriz 2005). Figure 5.6e, shows an example isolated brace (or component) test; this type of test was conducted at UC Davis (Fell et al. 2009), UC Berkeley (Yang and Mahin 2005), University of Dublin in the United Kingdom (Goggins et al. 2006) and University of Calgary in Canada (Shaback and Brown 2001). Figure 5.6f shows an example test of an inclined brace test; this type of test has been conducted at Hanyang University in Korea (Han et al. 2007), University of Michigan (Lee and Goel 1987) and Ecole Polytechnique in Canada (Tremblay et al. 2003).



Table 5.1 Overview of the Experimental Research Programs

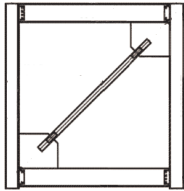
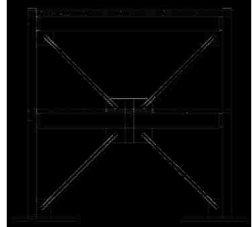
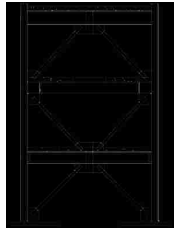
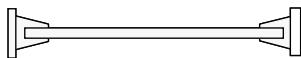
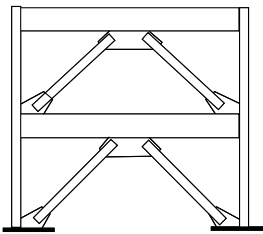
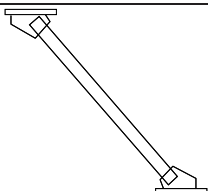
Research Program (No. of Spec. included in this study)	Specimen Configuration	Study Variables Involved
Johnson 2005 (4), Herman 2006 (4), Kotulka 2007 (5), Powell 2009 (3)		<ul style="list-style-type: none"> <li>• Brace slenderness ratio</li> <li>• Yield strength of the steel</li> <li>• Displacement history</li> </ul>
Clark 2009 (2)		<ul style="list-style-type: none"> <li>• Brace slenderness ratio</li> </ul>
Lumpkin 2009 (1)		<ul style="list-style-type: none"> <li>• Brace slenderness ratio</li> </ul>
Fell et al. 2009 (3), Yang and Mahin 2005 (2), Shaback and Brown 2001 (8), Goggins et al. 2006 (2)		<ul style="list-style-type: none"> <li>• Brace slenderness ratio</li> <li>• Width-to-thickness ratio</li> <li>• Yield strength of the steel</li> <li>• Displacement history</li> </ul>
Uriz 2005 (1)		<ul style="list-style-type: none"> <li>• Brace slenderness ratio</li> </ul>
Han et al. 2007 (1), Tremblay et al. 2003 (1), Lee and Goel 1987 (6)		<ul style="list-style-type: none"> <li>• Brace slenderness ratio</li> <li>• Width-to-thickness ratio</li> <li>• Yield strength of the steel</li> <li>• Displacement history</li> </ul>

Table 5.2 provides primary details of these specimens, including size, geometry and material. The braces encompass a wide range of HSS sections, from SHS20x20x2.0 (mm) to HSS6x6x3/8. These sizes result in a wide range of width-to-thickness ratios,

consistently defined as  $w/t=(b-3t)/t$  here according to the definition in the AISC manual of steel construction (AISC 2010b), which ranged from 7 to 28 for the test specimens included. The effective slenderness ratios,  $KL/r$ , of the braces ranged from 34 to 167. The effective length factor,  $K$ , of all specimens here was determined using the method proposed by Jain et al. (1978), in which  $\beta$  is obtained using the ratio of flexural stiffness of the bracing member and gusset plates  $\beta_m$  and  $\beta_\theta$  respectively, using Eqs. 5.9a-d.

$$\beta_\theta = \left( \frac{EI_g}{l_{ave}} \right)_{gusset\ plate} \quad (5.9a)$$

$$\beta_m = \left( \frac{EI_b}{L} \right)_{bracing\ member} \quad (5.9b)$$

$$\frac{\tan \alpha}{\alpha} = -2 \frac{\beta_m}{\beta_\theta} \quad (0.5\pi \leq \alpha \leq \pi) \quad (5.9c)$$

$$K = \frac{\pi}{2\alpha} \quad (5.9d)$$

In the expressions,  $E$  is modulus of elasticity,  $I_g$  is the moment inertia of the Whitmore section of the gusset plate, and  $I_b$  is the moment inertia of the cross section of the tube for the bracing members,  $l_{ave}$  is average of the three buckling lengths,  $l_1$  to  $l_3$ , as illustrated in Fig. 5.7 modified from Thornton method (1984), and  $L$  is length of the brace tube. The variable  $\alpha$  is between  $0.5\pi$  and  $\pi$ . The measured yield strength of the steel,  $F_y$ , is reported herein. Table 5.3 shows the mean and deviation of the design parameters computed using the 44 tests.

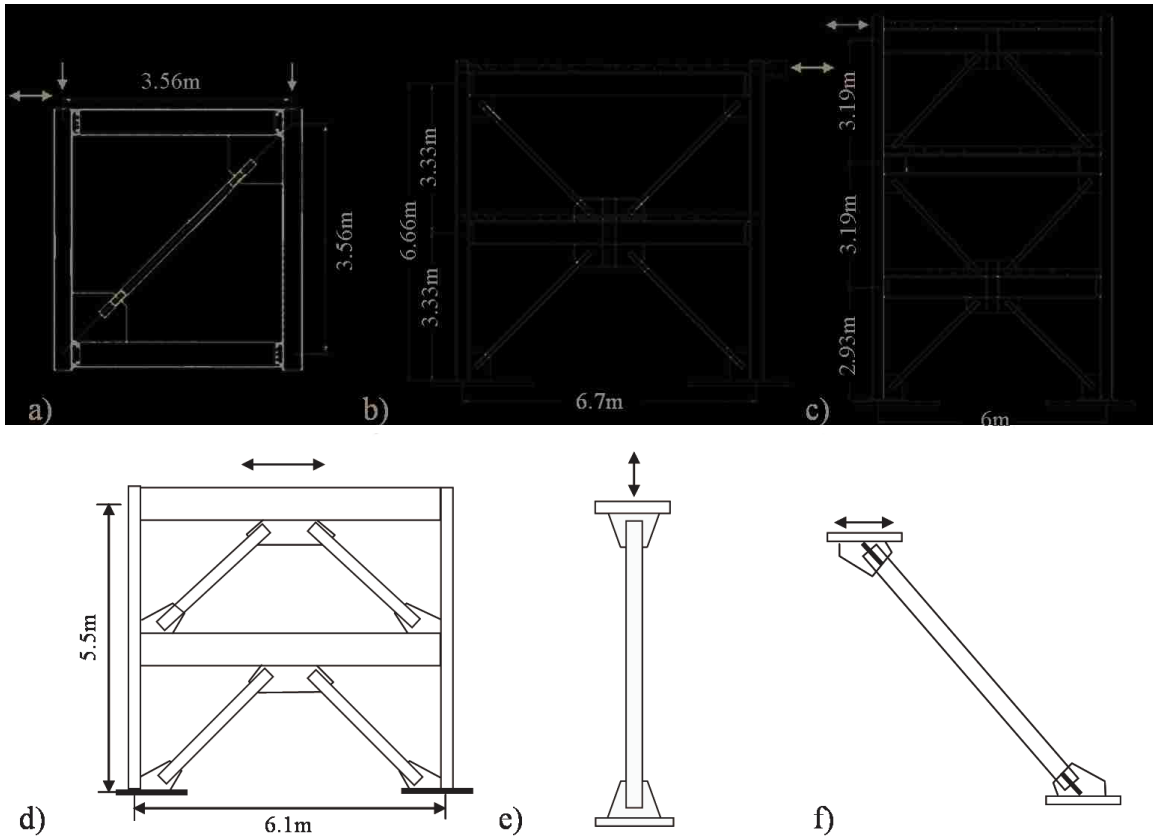


Figure 5.6 Specimen Configurations of the Experimental Studies (a) Single-story Braced Frame, (b) Multi-story X-braced Frame, (c) Three-Story Braced Frame, (d) Chevron Braced Frame, (e) Brace Tests, and (f) Inclined Brace Test

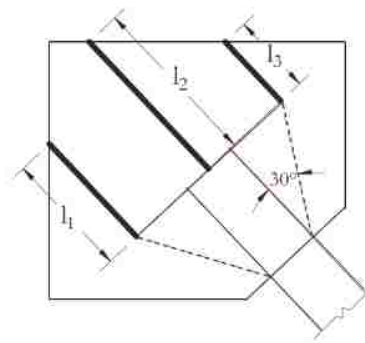


Figure 5.7 Gusset Plate Buckling Illustration

Table 5.2 Characteristics of the specimens and the corresponding maximum strain ranges

Study	Specimens	Brace Shape	Steel	$A_g$ (mm <sup>2</sup> )	$w/t$	$KL/r$	$E/F_y$	Max. $\epsilon_{range, simul}$
Johnson 2005	HSS2 <sup>S</sup>	HSS5x5x3/8	A500, Gr. B	3987	11.3	77.6	414.3	0.0443
	HSS3 <sup>S</sup>	HSS5x5x3/8	A500, Gr. B	3987	11.3	77.2	414.3	0.0493
	HSS4 <sup>S</sup>	HSS5x5x3/8	A500, Gr. B	3987	11.3	77.7	396.2	0.0520
	HSS5 <sup>S</sup>	HSS5x5x3/8	A500, Gr. B	3987	11.3	81.0	396.2	0.0605
Herman 2006	HSS6 <sup>S</sup>	HSS5x5x3/8	A500, Gr. B	3987	11.3	81.2	448.2	0.0467
	HSS7 <sup>S</sup>	HSS5x5x3/8	A500, Gr. B	3987	11.3	66.1	448.2	0.0606
	HSS8 <sup>S</sup>	HSS5x5x3/8	A500, Gr. B	3987	11.3	75.8	448.2	0.0512
	HSS9 <sup>S</sup>	HSS5x5x3/8	A500, Gr. B	3987	11.3	77.1	448.2	0.0469
	HSS10 <sup>S</sup>	HSS5x5x3/8	A500, Gr. B	3987	11.3	77.8	440.7	0.0534
Kotulka 2007	HSS11 <sup>S</sup>	HSS5x5x3/8	A500, Gr. B	3987	11.3	64.8	440.7	0.0438
	HSS12 <sup>S</sup>	HSS5x5x3/8	A500, Gr. B	3987	11.3	70.1	440.7	0.0492
	HSS13 <sup>S</sup>	HSS5x5x3/8	A500, Gr. B	3987	11.3	81.8	440.7	0.0480
	HSS14 <sup>S</sup>	HSS5x5x3/8	A500, Gr. B	3987	11.3	81.0	440.7	0.0460
	HSS15 <sup>S</sup>	HSS5x5x3/8	A500, Gr. B	3987	11.3	82.7	440.7	0.0426
Powell 2009	HSS17 <sup>S</sup>	HSS5x5x3/8	A500, Gr. B	3987	11.3	81.7	440.7	0.0486
	HSS24 <sup>S</sup>	HSS5x5x3/8	A500, Gr. B	3987	11.3	81.0	448.2	0.0508
	HSS25 <sup>S</sup>	HSS5x5x3/8	A500, Gr. B	3987	11.3	66.1	448.2	0.0535
Clark 2009	TCBF1-1	HSS125x125x9	A500, Gr. B	3967	11.3	56.4	450.0	0.0589
	TCBF1-3	HSS125x125x9	A500, Gr. B	3967	11.3	69.6	448.8	0.0488
Lumpkin 2009	TCBF2-1	HSS5x5x3/8	A500, Gr. B	3987	11.3	64.7	431.8	0.0512
Fell et al. 2006	Kavinde-1	HSS4x4x1/4	A500, Gr. B	2174	14.2	60.2	630.4	0.0550
	Kavinde-2 <sup>S</sup>	HSS4x4x1/4	A500, Gr. B	2174	14.2	60.2	630.4	0.0613
	Kavinde-4	HSS4x4x3/8	A500, Gr. B	3084	8.5	67.4	630.4	0.0692
Yang and Mahin 2005	Yang-4 <sup>S</sup>	HSS6x6x3/8	A500, Gr. B	5213	14.2	39.3	483.3	0.0607
	Yang-5	HSS6x6x3/8	A500, Gr. B	5213	14.2	39.3	483.3	0.0647
Uriz 2005	Patxi-SCBF-1	HSS6x6x3/8	A500, Gr. B	5213	14.2	45.8	478.5	0.0617
Goggins et al. 2006	Broderick-S1-40H	40x40x2.5SHS	S235JRH	375	13.1	35.8	741.2	0.0693
	Broderick-S4-20H	20x20x2.0SHS	S235JEH	144	6.7	74.4	621.3	0.0577
Shaback and Brown 2001	Shaback-1B	RHS127x127x8.0	G40.21-350W	3620	12.9	53.9	453.7	0.0477
	Shaback-2A	RHS152x152x8.0	G40.21-350W	4430	16.0	53.3	457.0	0.0458
	Shaback-2B	RHS152x152x9.5	G40.21-350W	5210	13.5	52.4	443.4	0.0476
	Shaback-3A*	RHS127x127x6.4	G40.21-350W	2960	16.7	64.8	425.2	0.0384
	Shaback-3B	RHS127x127x8.0	G40.21-350W	3620	13.6	65.8	453.7	0.0409
	Shaback-3C	RHS127x127x9.5	G40.21-350W	4240	10.5	61.6	438.2	0.0397
	Shaback-4A	RHS152x152x8.0	G40.21-350W	4430	15.8	63.5	457.0	0.0403
	Shaback-4B	RHS152x152x9.5	G40.21-350W	5210	13.6	59.7	436.7	0.0411
Han et al. 2007	Han-S77-28*	HSS100x100x3.2	SPSR400	1239	28.3	76.9	497.5	0.0248
	Lee-1* <sup>S</sup>	RHS5x5x0.188	A500, Gr. B	2271	25.7	63.0	469.3	0.0320
Lee and Goel 1987	Lee-2* <sup>S</sup>	RHS5x5x0.188	A500, Gr. B	2271	25.7	34.4	464.7	0.0345
	Lee-4* <sup>S</sup>	RHS4x4x0.125	A500, Gr. B	1226	31.5	77.1	500.0	0.0452
	Lee-5 <sup>S</sup>	RHS4x4x0.250	A500, Gr. B	2316	14.2	79.0	391.9	0.0555
	Lee-6 <sup>S</sup>	RHS4x4x0.250	A500, Gr. B	2316	14.2	45.1	391.9	0.0698
	Lee-7 <sup>S</sup>	RHS4x4x0.250	A500, Gr. B	2316	14.2	45.1	391.9	0.0593
Tremblay et al. 2003	Tremblay-S3A#	RHS76x76x4.8	G40.21-350W	1310	12.8	166.7	510.1	0.0490

\*: Width-thickness ratio do not satisfy the current AISC requirements

#: Slenderness ratio do not satisfy the current AISC requirements

§: Applied by unsymmetrical loading history.

Table 5.3 Variations of Design Parameters

	$w/t$	$KL/r$	$E/F_y$
Mean	13.7	67.6	468.3
Str. Dev.	3.1	13.4	48.0
Str. Dev./Mean	22.2%	19.8%	10.2%

## 5.4 Evaluation of Fracture Life of the Brace

In addition to the geometric and material variations, the cyclic deformation history of the brace can impact its fracture life. Using the experimental data set, the axial deformations of the bracing member and local strain deformation computed for critical location (i.e. the plastic hinges at the midlength of brace) were investigated as possible parameters to predict the measured fracture life.

The majority of the experiments did not measured strain deformations. Therefore, to ensure consistency analogy all test programs, the simulated responses were computed using the improved modeling approach described in Chapter 4. The test specimens were simulated using the loading protocol used for the test until the drift (or other global deformation measure) corresponding to the reported onset of brace fracture was reached. The resulting analytical global hysteretic responses and local strain deformations were then used to evaluate the brace fracture life.

### 5.4.1 Brace Axial Deformations

A study was initially conducted to examine the influence of the drift history on fracture life by evaluating seven parameters, including:

- (1) The maximum axial deformation range of the bracing member for the entire history, which correlates to the maximum end rotation of the brace (Tremblay et al. 2003).
- (2) The maximum axial deformation range for a single cycle.
- (3) The maximum tensile axial deformation.
- (4) The maximum compressive axial deformation.
- (5) The accumulated axial deformation counted using the counting approach proposed by Lee and Goel (1987) as expressed in Eq. 5.1.
- (6) The accumulated axial deformation derived by pure summation of all deformations.
- (7) The accumulated axial deformation counted using the rain-flow counting method.

The axial deformations,  $\Delta_1$  and  $\Delta_2$ , were determined based on the analytical hysteretic responses. Table 5.4 shows the results. The variables that were based on solely on axial deformations had large variability, from 27% to 66% (Detailed data are listed in Appendix D.2), which is larger than the variation in the design parameters ( $w/t$ ,  $KL/r$ , and  $E/F_y$ ), shown in Table 5.3. Therefore using axial deformation as the sole parameter was deemed unreliable. Similarly, the axial deformation parameters were considered having a relatively weak relationship with the brace fracture. This also illustrates possible limitations of several of the past brace fracture prediction methods (Shaback and Brown 2001, Lee and Goel 1987, Tremblay et al. 2003).

Table 5.4 Variations of Several Characteristics at Axial Deformation Level

	Max. Axial Def. Range (%)		Max. Axial Def. (%)		Accumulated Axial Def. (%)		
	Entire History (Tremblay et al. 2003)	For a Given Cycle	Ten.	Comp.	$\Sigma \Delta_f$ (Lee & Goel 1987)	$\Sigma \Delta_{\text{rain-flow}}$	$\Sigma \Delta$
Mean	2.3	2.0	1.3	1.0	51.2	21.9	41.9
Str. Dev.	0.7	0.5	0.4	0.4	33.5	11.5	21.7
Str. Dev./Mean	30.1%	27.4%	29.7%	44.3%	65.5%	52.4%	51.8%

### 5.4.2 STRAIN-RANGE FRACTURE MODEL

As illustrated in Fig. 5.1, fracture of an HSS brace results from the large strains and local deformation demands at the middle of the brace during reverse cyclic demands. These experimental observations were used to develop the basis for the proposed fracture model. Specifically, the local strain demands at the midlength of the brace were used to predict the onset of brace fracture. Each test specimen was simulated. The strain demands prior to the onset of fracture behavior were determined analytically.

Nonlinear beam-column elements with fiber sections are used to simulate the braces, beams and columns. Modeling formulation of the element assumes a linear-strain distribution across the cross-section. Therefore the model can simulate plastic hinging behavior and the out-of-plane deflection at the mid-span of the brace length, both of which contribute to the onset of brace fracture. However, the line-element model does not simulate local strain concentrations resulting from local deformations, such as the cupping depicted in Fig. 5.1d. Therefore, the model cannot capture the full local strain. However, it captures a significant portion of the local strain, and these computed strains were evaluated and calibrated to predict brace fracture.

The simulated strain history for Specimen HSS24 is used as an example to illustrate

typical strain response of the brace, as shown in Fig. 5.8. The plotted strain history shows the strain on the tension and compression sides (Fig. 5.8a) of the plastic hinge region (at midspan of the brace in this case). The strain deformation at the compression side of the brace during plastic rotation experienced wider range of strain as shown in the figure.

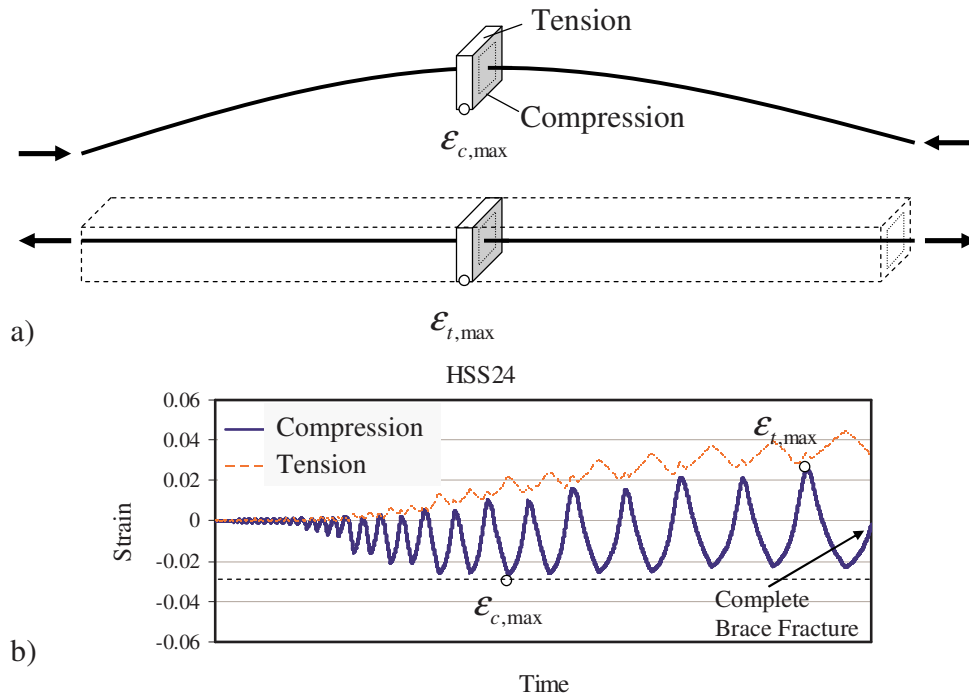


Figure 5.8 (a) Schematic of the Midspan Fiber Section in Brace Model; and (b) Typical Strain History of the Fibers at Midspan of the Brace for Specimen HSS24.

Prior to the investigation of the magnitude of the strains in individual fibers, the strain demand along the entire brace length and the stability of the demand were investigated. Specimen HSS24 (Powell 2009) is used to illustrate typical trends over the 44 tests here. Figure 5.9a shows the simulated maximum strain range (occurred at midspan of the brace in this case) over entire cyclic history,  $\text{Max. } \epsilon_{\text{range}}$ , through the depth of the tubular cross section and at two integration points away from midspan of the brace.



The results verified that the maximum demand occurred at the plastic hinge associated with brace buckling at the extreme fiber on the compression side of the hinge, as shown in Fig. 5.9a. It should be noted that midspan buckling is not guaranteed; the method shown in Fig. 5.9 is streamlined for the similar boundary conditions at each brace end. For the specimens with different gusset plate design at each end, such as Specimen TCBF1-1 and TCBF2-1 in Table 5.2, the demands at the developed plastic hinge has been considered in the study.

Uriz (2005), using a similar brace model, showed that the strain history of the brace fibers varying with the number of the brace segments. The influence of the number of the brace segments on the maximum strain range was investigated here. Figure 5.9b shows the relationship of the simulated (or computed) maximum strain range at the critical location and the number of elements used to model the brace. The results suggest that using 16 segments along the brace length (with four integration points for each element) results in a tolerable error (less than 1.2% in the example shown here). This mesh size was used throughout the study.

Four different demand parameters were developed and evaluated using the maximum simulated strains as the basis parameter, including: (1) maximum tensile strain,  $\varepsilon_{t,max}$ , (2) maximum compression strain,  $\varepsilon_{c,max}$ , (as shown in Fig. 5.8b) (3) the maximum strain range for a given cycle, and (4) the summation of maximum strain range over the entire time history, which is a summation of the absolute values of the maximum tensile and the maximum compressive strains.

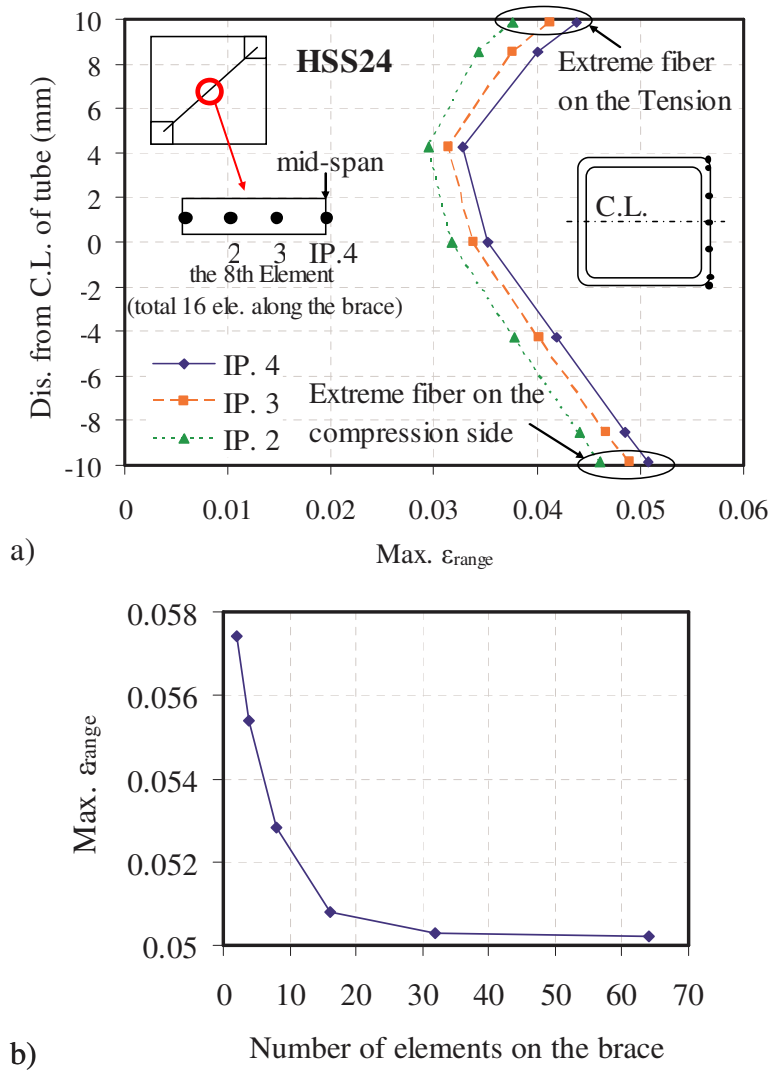


Figure 5.9 Maximum Strain Ranges as Function of (a) Location and (b) Number of Elements

In addition to the maximum values, accumulated strain was also evaluated. Two expressions were developed. The first calculated the accumulated strain and  $DI$  using the rain-flow counting method, given by Eqs. 5.7 and 5.8 with values for the parameters of  $m$  and  $\epsilon_o$  as determined by Uriz (2005). A second accumulate strain model used summation of strain from every cycle with three exponential powers of 1, 2 and 3 applied the strains

before summation.

Table 5.5 Fracture Models based on Fiber Strains

	Max. Strain		Max. Strain Range		Accumulated Strain				
	$\epsilon_{t, \max}$	$\epsilon_{c, \max}$	For a Given Cycle	Entire History	$\Sigma\epsilon_{rain-flow}$	$DI_{rain-flow}$	$\Sigma\epsilon$	$\Sigma\epsilon^2$	$\Sigma\epsilon^3$
Mean	0.019	0.031	0.041	0.050	0.467	1.052	0.873	0.0292	0.00115
Str. Dev.	0.008	0.009	0.010	0.008	0.158	0.532	0.349	0.0121	0.00053
Str. Dev./Mean	41.4%	29.4%	24.4%	15.7%	33.9%	50.6%	40.0%	41.4%	46.4%

For each expression, the strain or damage index values were computed at the measured drift corresponding to fracture. Table 5.5 presents the mean and coefficient of variation values for each expression for the 44 tests (Detailed data are listed in Appendix D.2). Using the maximum strain range through the entire history has the lowest coefficient of variation of 15.7% of all of the methods. The maximum strain and accumulated strain have the variations more than 29% and 34%, respectively. In terms of the accumulated damage approach using rainflow-counting method, the mean value of the damage index throughout the tests was close to 1.0, however, the results had a large coefficient of variation of over 50%. Therefore, the maximum strain range through entire history was considered as the best and most reliable variable for prediction of brace fracture.

The simulated maximum strain range from the strain analysis described above,  $\epsilon_{range, simul}$ , is listed for each specimen in Table 5.2. For specimens with multiple braces (in multi-story frames), the maximum strain range of the first brace to predicted to fracture was reported. The data were used to develop a regressive expression for predicting the limiting maximum strain range.

As discussed previously, the deformation corresponding to the onset of brace fracture depends on the width-to-thickness ratio of the cross section ( $w/t$ ), the slenderness ratio of the bracing member ( $KL/r$ ) and the ratio of the elastic modulus to the yield strength of the steel ( $E/F_y$ ). For the data set, Figures 5.10a, b and c show the relationships and trend lines between the Max.  $\epsilon_{range, simul}$  and the  $w/t$ ,  $KL/r$  and  $E/F_y$  ratio, respectively.

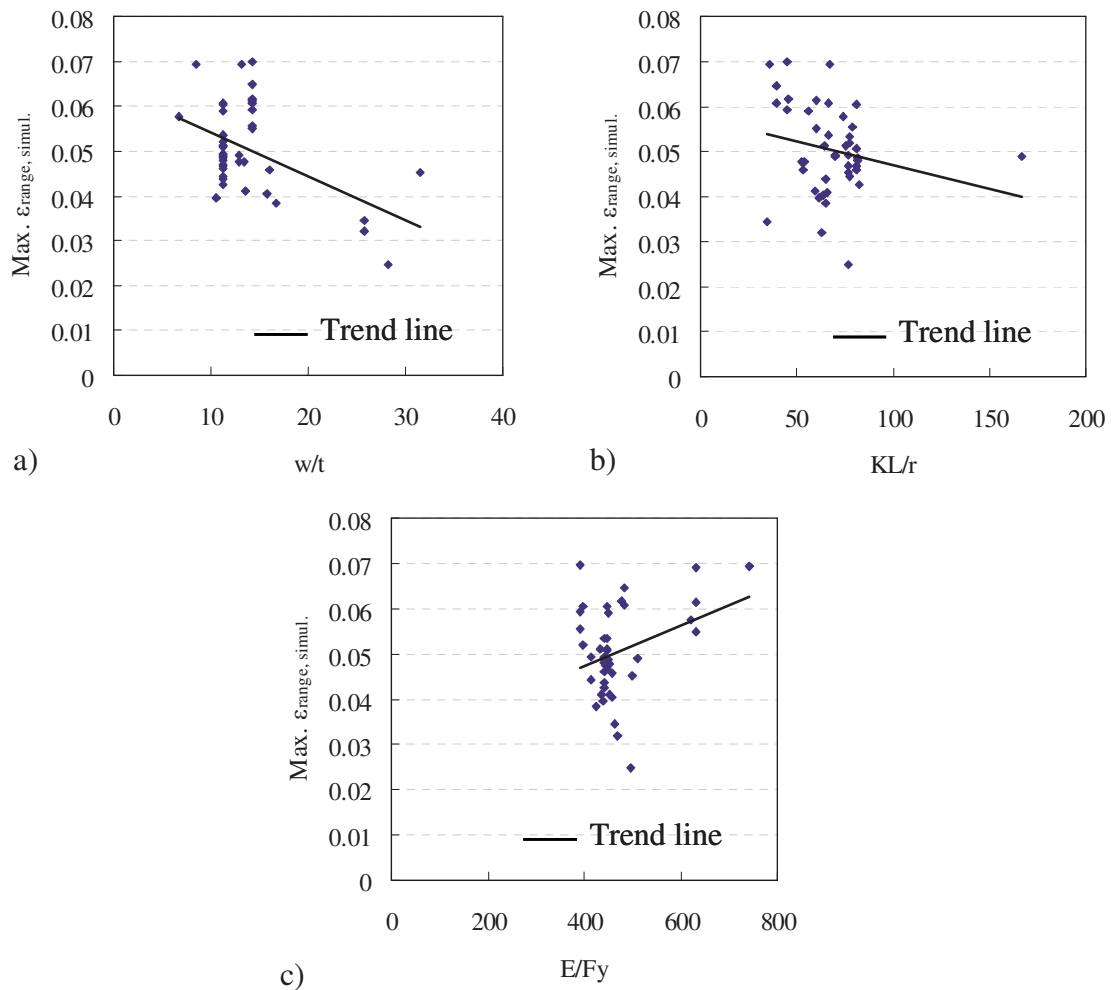


Figure 5.10 Relationship of the Simulated Maximum Strain Range versus (a)  $w/t$ , (b)  $KL/r$  and (c)  $E/F_y$  ratios.

Furthermore, the values of these design parameters were related to the simulated

maximum strain range values to create a statistic equation for predicting brace fracture,  $Max. \epsilon_{range, pred.}$ , as given by Eq. 5.10. Figure 5.11 shows the comparison between the predicted strain range limit and the calculated strain range for the brace deformation at fracture.

$$Max. \epsilon_{range, pred.} = 0.1435 \left( \frac{w}{t} \right)^{-0.4} \left( \frac{KL}{r} \right)^{-0.3} \left( \frac{E}{F_y} \right)^{0.2} \quad (5.10)$$

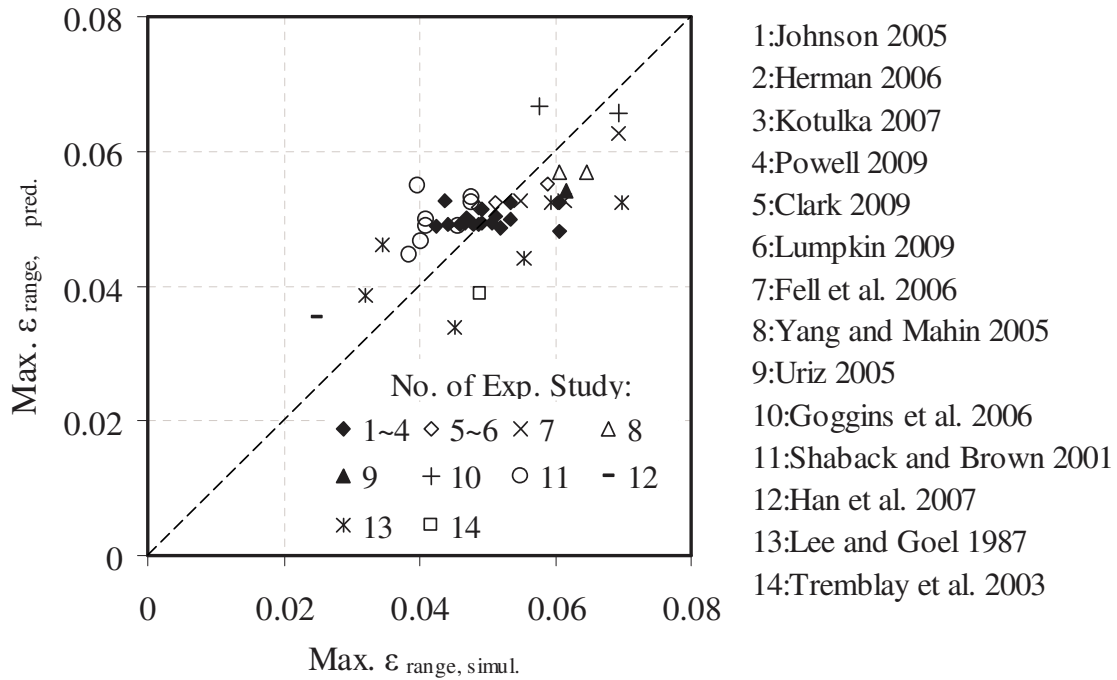


Figure 5.11 Calculated and Numerical Maximum Strain Ranges for All Specimens.

The equation was calibrated using the full data set (total of 44), and this data set is larger and more diverse than the data sets used in the development of prior fracture models. The impact of each variable is considered:

- The negative power for the ratio  $w/t$  agrees with the trend as shown in Fig. 5.10a and in the previous models (e.g. Eqs. 5.2, 5.3 and 5.6).

- There is a negative power for the ratio  $KL/r$ . On the surface, this appears to be contrary to the previous models (e.g. Eqs. 5.3 and 5.6). However, the maximum strain range on the brace does not directly correlate with the global deformation of the brace, which is the parameter used for the other models. Figures 5.10b and 5.12 show these opposite trends. Figure 5.10b shows the simulated maximum strain range versus  $KL/r$ , and this relation is negative. Figure 5.12 shows that experimental axial deformation range increases with increasing  $KL/r$ , and the trend line has a positive slope.
- Moreover, in Eq. 5.10, the positive power of ratio  $E/F_y$ , implies that stronger steel would lead to earlier fracture and compromise ductility, which agree with the trend as shown in Fig. 5.10c and Lee and Goel's model (Eq. 5.2). In contrast for Eqs. 5.3a and b, it is raised to a negative power, which suggests stronger steel will delay fracture and increase ductility. This difference is likely caused by the relatively small variation in the  $E/F_y$  ratios in past tests (as shown in Table 5.3), and the fact that the two programs used different test data to calibrate their models. A further discussion focusing on the relationship between the story drift and the maximum strain range and the impact of the design parameters on the maximum strain range is provided in Section 5.7.

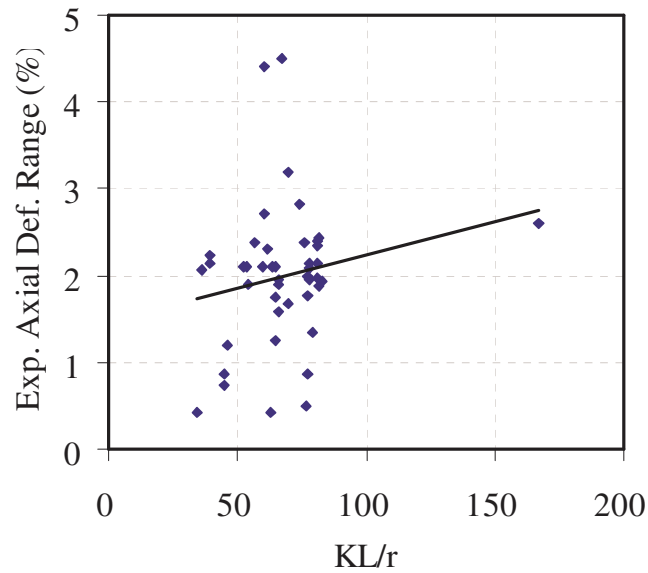


Figure 5.12 Relationship of the Experimental Axial Deformation Range versus  $KL/r$ .

## 5.5 Constitutive Model for Brace Fracture Simulation

The fracture expression was implemented in the OpenSees framework. A new fracture material model was integrated with the Steel02 constitutive material model available in OpenSees, and operates independently on each fiber in the cross section. The description and source code of the developed fracture material model are provided in Appendix E.

The fracture model monitors the maximum strain range of the fibers and reduces the stress of the fibers at the limiting value estimated by Eq. 5.10, as illustrated in Fig. 5.13a. For strains beyond the fracture strain, an elastic constitutive model with a very small effective modulus of 0.001ksi is used to ensure post-fracture convergence and allow post-fracture simulation, as shown in the figure.

A further limitation was placed on the fracture model to ensure that the fracture occurs only if the stress in the model is in tension, since experimental observations

indicate that initial fracture occurs when the brace is in tension. The fracture model is applied to all fibers through entire length at each integration point of the brace elements. Simulated fracture is triggered at the layer of fibers having largest maximum strain range on the brace, which always occurred at the extreme fiber on the compression side of the plastic hinge of the brace as mentioned previously. The model ultimately simulates fully fracture of cross section, since fracture of the initial fiber would sequentially increase the strain range in the adjacent fibers until the full rupture of the cross section. Therefore, the proposed fracture material model is capable of simulating initiation of tearing and fracture and as well as conducting the analysis beyond brace fracture.



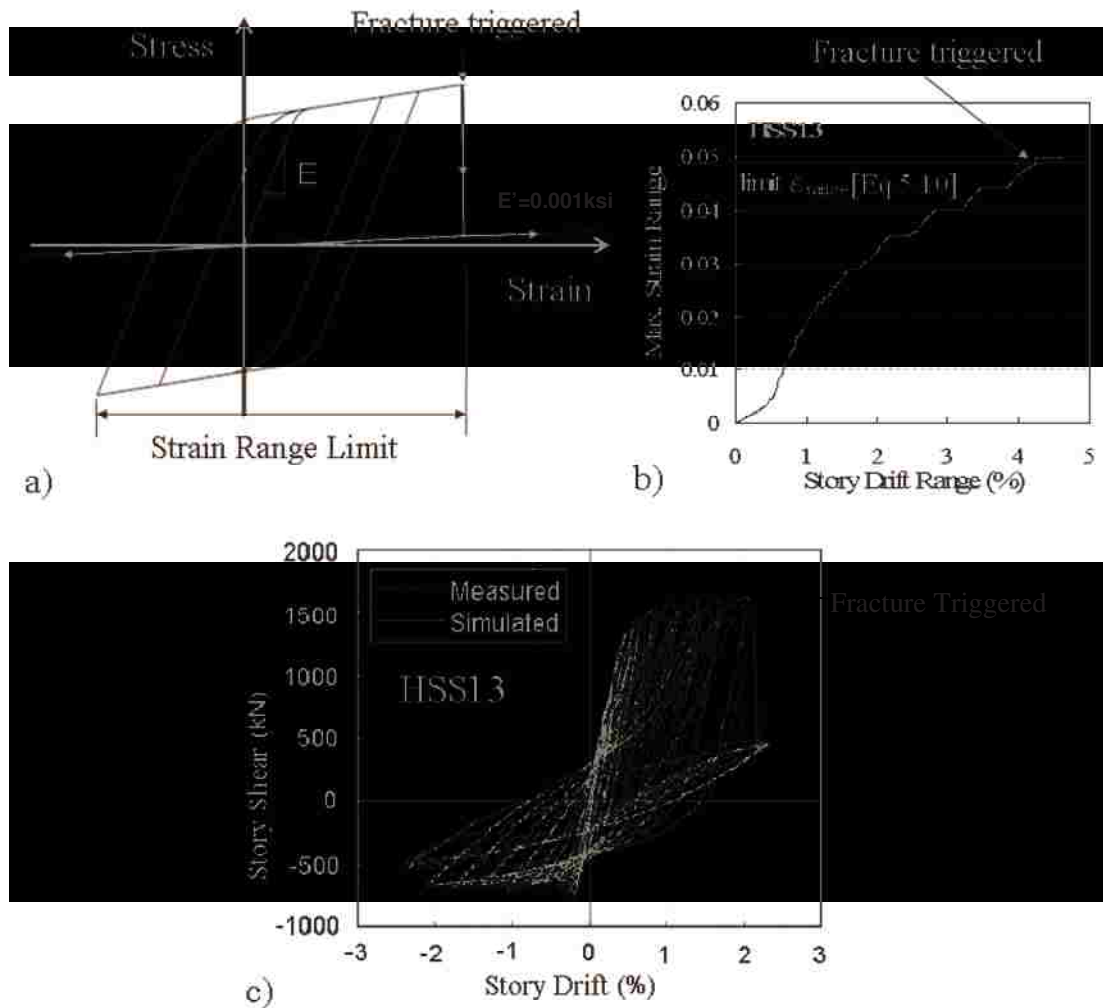


Figure 5.13 (a) Schematic of the Fracture Material Model, (b) Relationship of the Maximum Strain Range versus Story Drift Range (for Specimen HSS13), and (c) the Analytical and Measured Responses (for Specimen HSS 13).

Figure 5.13b presents the relationship of the maximum strain range at the critical location of initial fracture versus the story drift range of Specimen HSS13 (Kotulka 2007). The model permits analysis beyond brace frame as demonstrated in Fig. 5.13c for Specimen HSS13, for which testing was continued for cycles beyond complete brace fracture. System stability, stiffness and strength after brace fracture depends on secondary capacity provided by moment resistance developed through the braced-frame gusset-plate

connections. The model predicted the brace fracture at the correct story drift and accurately represented the post-fracture behavior.

## 5.6 Comparison of Prior and Proposed Fracture Models

The 44 specimens of the experimental database (Table 5.1) were simulated using the improved modeling approach with the proposed fracture model discussed above. In addition, the accuracy of four other existing brace fracture models was assessed including: (1) the accumulated axial-deformation model developed by Lee and Goel (1987) and used by Shaback and Brown (2001), (2) the maximum end-rotational model developed by Tremblay (2003) and (3) the strain fatigue model developed by Uriz (2005).

Figure 5.14a shows the resulting values using the proposed fracture model and the results calculated by Lee and Goel's and Shaback and Brown's models, which were based on accumulated axial deformations, Eqs. 5.2 and 5.3. The results were compared with the simulated accumulated axial deformation,  $\Delta_{f, simul.}$ , corresponding to observed braced fracture in the test. The figure shows that the proposed model accurately predicted the fracture life of the braces through a wide range, while the models using Eqs. 5.2 and 5.3 significantly underestimated the fracture life for specimens that sustained accumulated axial-deformations larger than 40.

The proposed fracture model was also compared with the Tremblay et al.'s model (Eq. 5.6) (2003), which uses the end-rotation as the demand parameter. Figure 5.14b compares the end-rotations predicted by the proposed fracture model and the Tremblay et al.'s model versus the experimental end rotations corresponding to observed brace fracture ( $\theta_{f, test}$ ). The maximum end-rotations for the proposed model were estimated using

Eqs. 5.4 and 5.5 and the ductility of the braces corresponding to the predicted brace fracture. The results show that the proposed model is more accurate. The Tremblay's model underestimated fracture especially for the specimens for which the measured end-rotation exceeded 0.25 radians.

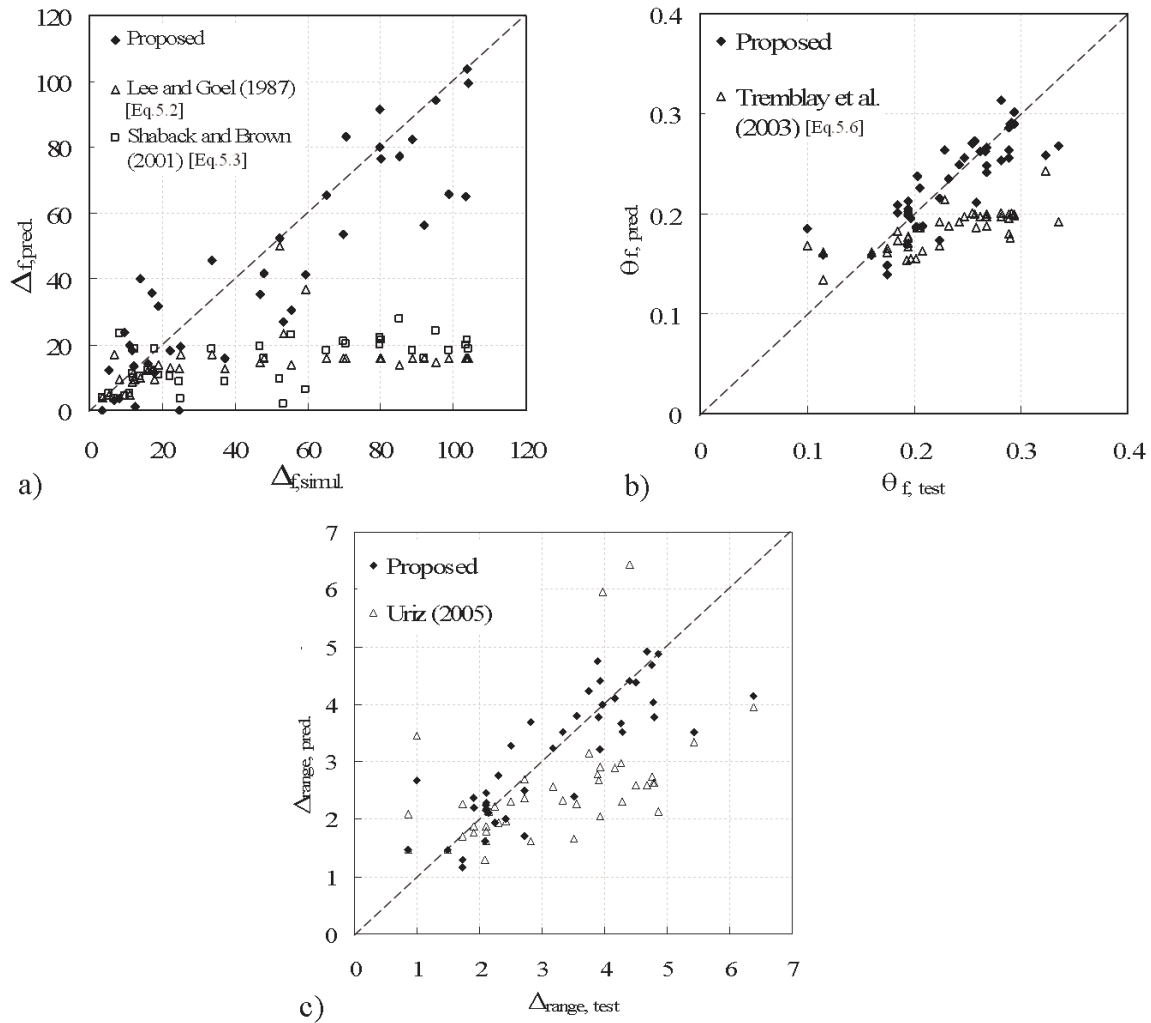


Figure 5.14 Comparison of the Proposed and (a) the Accumulated Axial-deformation, (b) the Maximum End-rotational, and (c) the Strain Fatigue Models

The proposed model was also compared with the model developed by Uriz (2005).

The models were compared using axial brace deformation, which directly correlates to

the drift capacity. The predicted axial deformation range was compared with the measured axial deformation range, as shown in Fig. 5.14c. In the figure,  $\Delta_{range,pred.}$  is the maximum axial deformation range predicted by the models, and  $\Delta_{range,test}$  corresponds to the fracture drift observed in the test. The Uriz model results were calculated using an available fatigue material model in OpenSees framework developed by Uriz (2005), using parameters values of -0.5 and 0.091 for  $m$  and  $\varepsilon_o$  respectively. The comparison shows that the proposed model provides an improved prediction of brace fracture on average, and it had smaller variation in the deformation at fracture than the fatigue model.

Figures 5.15a, b and c show the accuracy of the proposed model as a function of the slenderness ratio, width-to-thickness ratio and yield strength of the brace, respectively. The limiting values of the AISC seismic requirements are also shown. For each point, the ordinate is the ratio of the simulated maximum story drifts range prior the brace fracture relative to the experimental values and the abscissa is the value of the design parameter for a test specimen.

Figure 5.15b shows the model accuracy relative to the  $w/t$  ratio and indicates that the accuracy is reduced for width-to-thickness ratios exceeding 25, which exceed the AISC seismic design requirements (AISC 2005). The specimens that meet the AISC width-to-thickness requirements are accurately predicted. The study verified that the proposed fracture model based on the maximum strain range of the brace has best correlation to the rupture of braces of all available models.

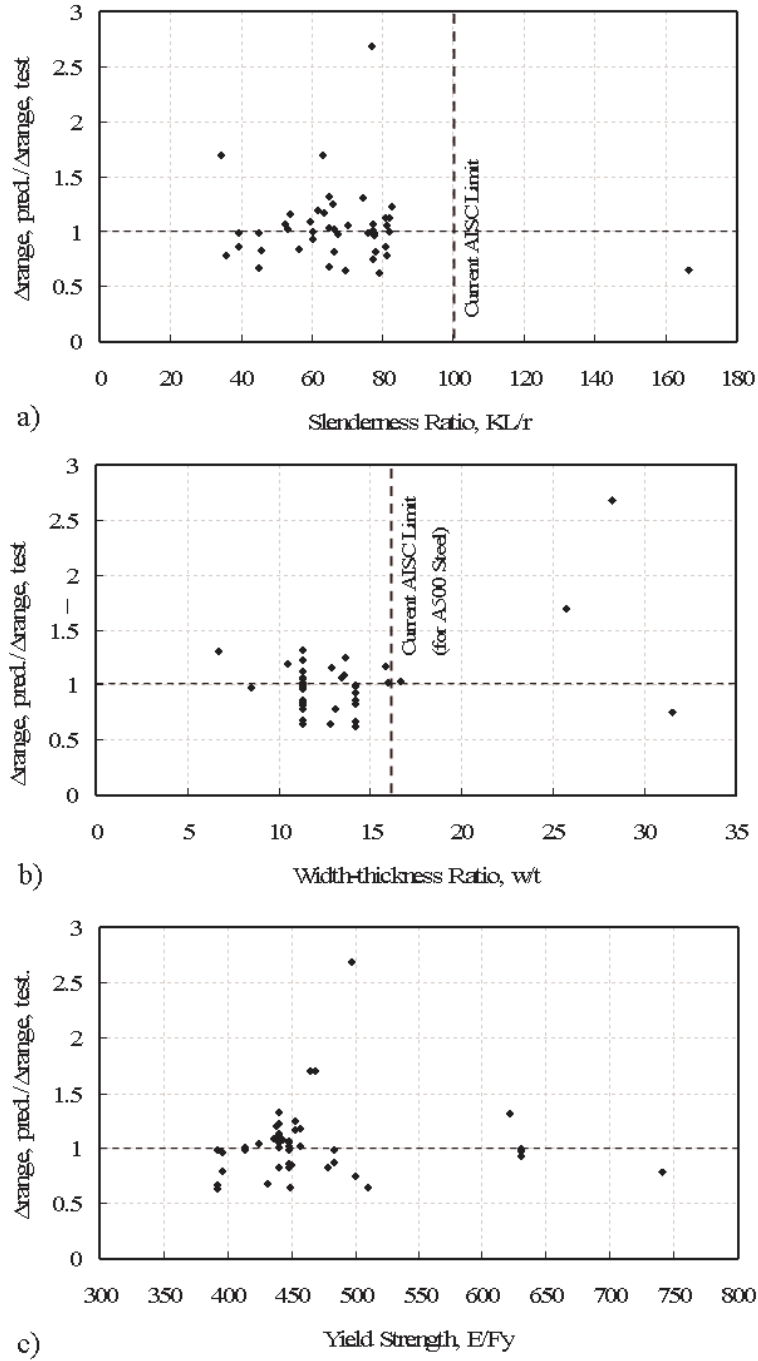


Figure 5.15 Accuracy of Proposed as a Function of (a) Slenderness Ratios, (b) Width-thickness Ratios and (c) Yield Strength

## 5.7 Impact of Design Parameters of Predicted Fracture

To investigate the impact of the design parameters, including width-thickness and brace slenderness ratios,  $w/t$  and  $KL/r$ , on the maximum strain range and fracture potential, a series of single-story, single-bay braced frames were analyzed with the length and thickness varied, as described below. Figure 5.16a shows an illustration of the frame model. A single diagonal brace with 45-degree angle was used. The analysis focused on the brace response, and the beam and column members were assumed to be pinned and to remain elastic.

The brace was modeled using the approach described previously. The gusset plate design used in Specimen HSS10 (Herman 2006) was 12mm thick and tapered. The connection had a rotational stiffness of 224kN-m/rad. and yield moment of 16.8kN-m. The reference analysis model had a story height,  $H$ , of 2.54m with HSS5x5x3/8 brace.

Two parameter studies here conducted. In the first, the  $w/t$  ratio was varied by changing the tube thickness,  $t$  (7.9 and 6.4mm) to ensure a constant  $KL/r$ . The second increased the brace length by changing the story height and span (note they are equal),  $H$  (to 3.81m and 5.08m). The latter only varied the  $KL/r$  ratio, and the effective length ratio,  $K$ , was 1.0 for all cases. It should be noted that radius of gyration,  $r$ , approximately equal to  $0.4b$  for an HSS cross section. Varying the brace width simultaneously changes both  $w/t$  and  $KL/r$ . Therefore, the brace width,  $b$ , remained constant to isolate the impact of two design parameters.

The analysis was performed using OpenSees program without including the fracture model, and a single symmetric cycle with various story drift ratios, SDR, of 1%, 2% and 3%, was applied to each frame in sequence. The maximum strain ranges at the extreme

fiber on the compression side of the plastic hinge at midspan were computed and compared. Figures 5.16b and c show the results of the two studies. In addition, the estimated limiting strain-range values, calculated by Eq. 5.10, are also shown in the figures. It is apparent that varying the brace thickness,  $t$ , (or  $w/t$  ratio) did not have significant impact on the computed maximum strain range, while increasing the brace length,  $L$ , (or  $KL/r$  ratio) significantly decreased the computed maximum strain range at each story drift level. As noted in Fig. 5.16c, the proposed fracture model predicts more drift capacity for frames with smaller  $w/t$  and larger  $KL/r$  ratios, which agreed with the trends observed in the past experiments and the prior fracture models.

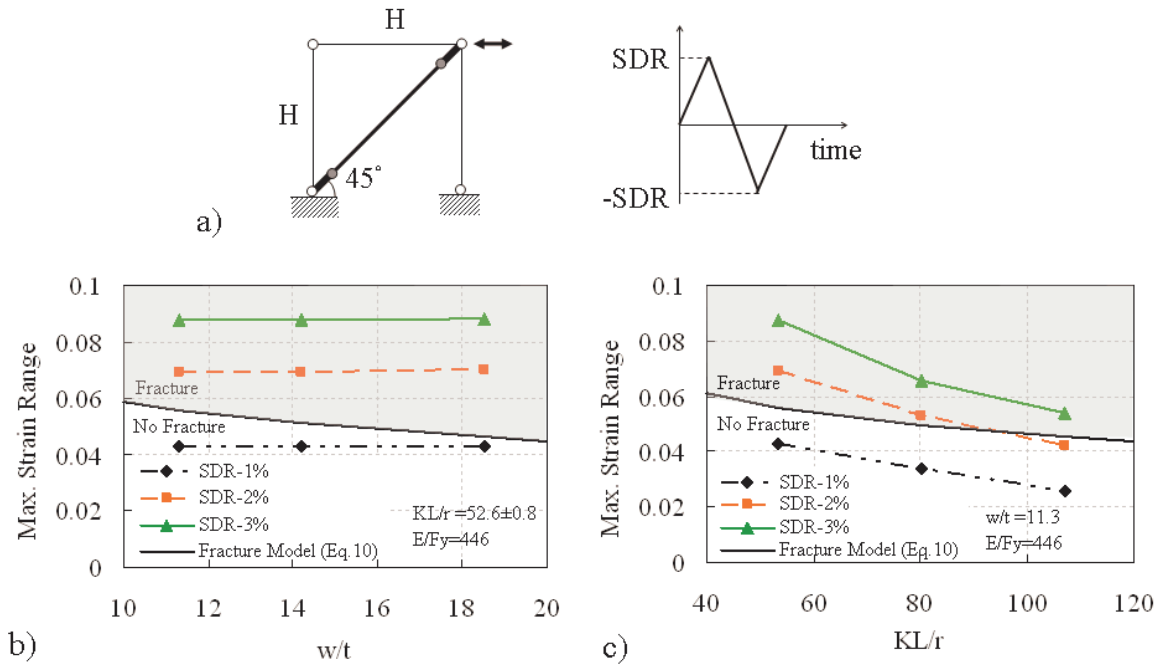


Figure 5.16 (a) The Illustration of the Single-story Frames and The Applied Loading Protocol; (b) The Variation of Max. Strain Range with  $w/t$  Ratios and (c)  $KL/r$  Ratios.





## Chapter 6 : Evaluation of the Collapse Potential & Response Modification Coefficient of SCBFs

### 6.1 Introduction

Design of SCBFs depends on several Seismic Performance Factors (SPFs). In particular, the response modification coefficient ( $R$  factor), which is used to reduce the elastic seismic design loads to those used for member design, significantly influences the design and, therefore, would be expected to influence the performance of SCBFs.  $R$  factors were originally derived in an ATC-3-06 report (1978), with the historic values determined from engineering judgment and qualitative comparisons with the known response capabilities of a relatively few, well-understood seismic-force-resisting systems. In general, these  $R$  values were also related to the  $R_w$  values used in the Uniform Building Code for allowable strength seismic design. In the most recent provisions, the National Earthquake Hazards Reduction Program (NEHRP) Recommended Provisions for Seismic Regulations for New Buildings and Other Structures (FEMA 450 2004) provided the  $R$  factors for more than 75 different seismic-force-resisting systems including SCBFs. However, the  $R$  values were somewhat arbitrarily assigned without quantifiable verification of their seismic response characteristics. It has become clear that a more rational assessment of the  $R$  value is needed for all seismic resisting systems, including SCBFs.

In modern design, large, nonlinear inelastic deformations are expected during large seismic loads and the system must be detailed to sustain these demands. However, the seismic design forces must be large enough to provide sufficient strength and stiffness needed to minimize yielding or structural damage during frequent seismic events.

An analytical study was undertaken to evaluate the seismic performance and  $R$  values for SCBF systems. SCBF systems, including 3-, 9- and 20-story structural buildings, were designed using current AISC seismic design procedures supplemented by the proposed BDP (Roeder et al. 2011b), and then nonlinear dynamic analyses were performed using the validated models described in Chapters 4 and 5. The improved models of SCBFs combined with ATC-58 fragility curves (Roeder et al. 2009) provide the best current prediction of all performance limit states, such as no repair, possible brace replacement, brace fracture, and potential collapse, in the performance evaluations.

The impact of the  $R$  value was studied by evaluating the full seismic performance, including collapse. A series of SCBF buildings were designed using a range of  $R$  values, including: (1)  $R$  of 3, 4, 5, and 6 for the 3-story buildings, (2)  $R$  of 3, 6, 7 and 8 for the 9-story buildings, and (3)  $R$  of 3, 4, 6, and 8 for the 20-story buildings. Current codes employed an  $R$  value of 6 for SCBF systems.

The building designs were assessed with two nonlinear dynamic analysis methods. The first method used the FEMA P695 Incremental Dynamic Analysis (IDA) procedure (FEMA P695 2008) to estimate collapse potential. This method was proposed to develop  $R$  values that resulted in a constant collapse probability. The second method used a suite of 20 acceleration records for the 10% and 2% in 50 year seismic hazards that were scaled to the seismic hazard levels for the building site, and the predicted system performance was used to propose appropriate  $R$  factors, deflection amplification factor,

$C_d$ , and system overstrength factor,  $\Omega_o$ , for SCBF structural systems. Both methods used the same analysis model. Both methods used SAC ground motion record sets, including 10/50 and 2/50 events, assembled for Seattle (each set consists of 20 acceleration records) (FEMA 355C 2000b, Somerville et al. 1997).

The design of the model buildings with various story heights is presented in Section 6.2. An overview of the analytical modeling for the SCBF system in the study is described in Section 6.3, including a discussion of the effect of the gravity frames on various story heights. The evaluation of collapse potential of these model buildings using FEMA P695 methodology is presented in Section 6.4, and then an alternative evaluation procedure based upon multi-performance levels of the system is presented in Section 6.5. The evaluation of deflection amplification and overstrength factors of SCBFs based upon the results using the alternative evaluation procedure is presented in Section 6.6. The results of the two evaluation methods are discussed in Section 6.7. The primary content of the chapter was addressed in a journal paper as documented in Appendix F

## **6.2 Design of the Model Buildings**

A series of 3-, 9- and 20-story buildings were designed using the equivalent lateral force procedure (ASCE/SEI 7-10, AISC 2005). The buildings were based on the model buildings used as part of the SAC Steel project (FEMA 355C 2000b). These designs adopted the basic floor plan, story height, and gravity loads. Appropriate modifications were made to translate the buildings to SCBFs. Figure 6.1 shows the typical elevations and floor plans of the different buildings considered in this study.

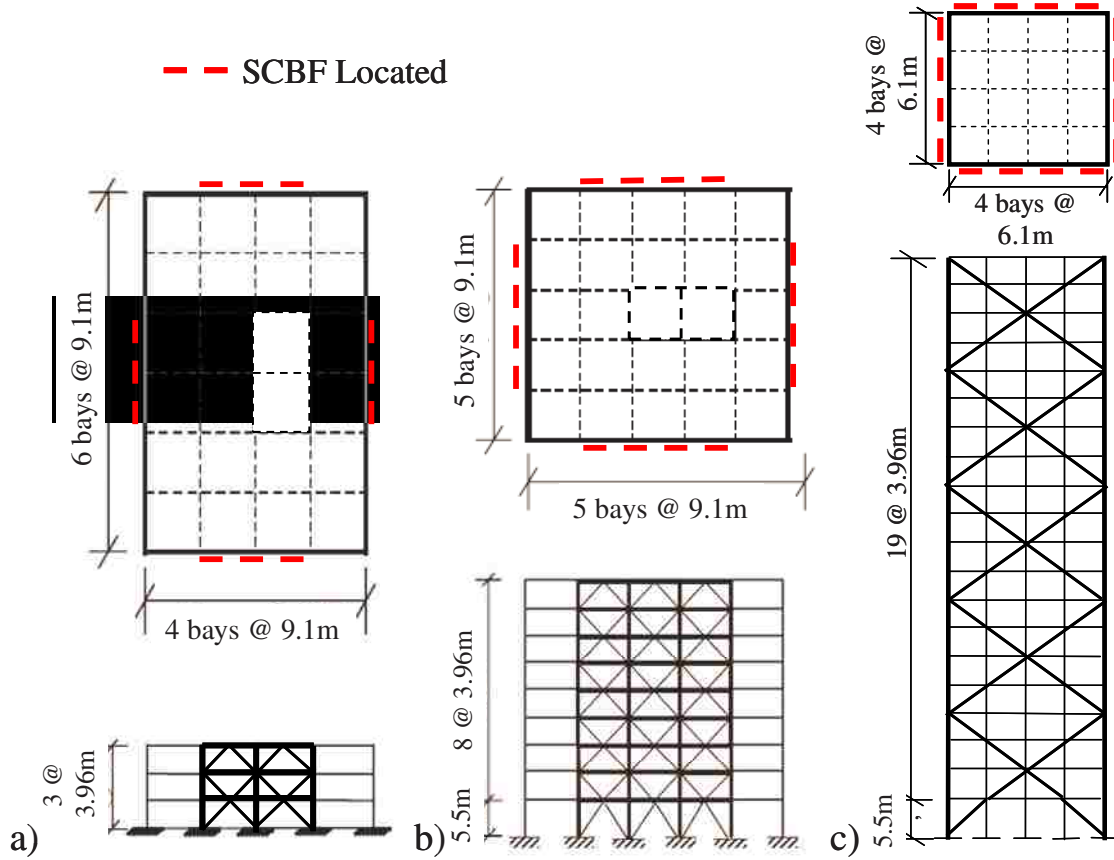


Figure 6.1 Elevations and Floor Plans of (a) 3-, (b) 9- and (c) 20-story Buildings.

The basic design R value was 6, and this value was used to adjust the design spectrum, but as noted earlier, alternate R values were also employed. All of the buildings were designed for a location in Seattle, WA, using Seismic Design Category D with soil Site Class C. The 3-story buildings had 4-by-6 bays with identical story height, while the 9- and 20-story buildings have 5-by-5 and 4-by-4 bays, respectively and with a taller bottom story to reflect typical midrise construction, as shown in Fig. 6.1.

Table 6.1 Effective Seismic Weight of Structure

Model Buildings	Gravity Loads (psf)	
	Floor	Roof
3-Story	98.4	94.5
9-Story	97.9	93.8
20-Story	92.4	104.5

The braced bays were placed on the perimeter of the buildings in a symmetric plan configuration using a multi-level X-bracing configuration, as illustrated in the figure. Table 6.1 summarizes the effective seismic weight for individual floors and the roof for each building configuration. The buildings were designed to meet the ASCE-7 design spectrum using the updated 2008 United States Geological Survey's (USGS) mapped spectral acceleration values at 2% in 50 years hazard level for the building site. The short period spectral acceleration,  $S_S$  was 1.4g and spectral acceleration at the 1 second period,  $S_I$  was 0.53g. The site class coefficients  $F_a$  and  $F_v$  are 1.0 and 1.3, respectively, and the damped spectra were adjusted to 2% of critical damping by applying damping adjustment factor  $\beta_S$  and  $\beta_I$  of 0.8 (FEMA 273, 1997a). The resulting design spectral acceleration parameters were  $S_{DS}$  of 1.17g and  $S_{DI}$  of 0.57g. The buildings were considered to be general office buildings, and an occupancy importance factor,  $I$ , of 1.0 was used.

Tables 6.2, 6.3 and 6.4 give the resulting design member sizes of the 3-, 9- and 20-story buildings, respectively. The braces were all rectangular Hollow Structural Sections (HSS) and satisfied the AISC seismic compactness criteria (AISC 2010b). The gusset plate connections were rectangular and designed using the BDP by Roeder et al. (2011b). All of the beam-to-column connections of the frames were designed as welded-flange welded-web connections. Framing members were designed to develop the expected capacity of the braces. For the three  $R=6$  designs (current code design), the fundamental periods of the resulting frames were 0.38, 0.84 and 1.85 seconds for 3-, 9- and 20-story buildings, respectively.

Table 6.2 Member Sizes of the 3-story Model Buildings

R	Story	Brace	Beam	Exterior Col.	Interior Col.
6	1	HSS 6x6x5/8	W21x93	W14x90	W14x90
	2	HSS 6x6x1/2	W21x93	W14x90	W14x90
	3	HSS 5x5x1/2	W24x104	W14x90	W14x90
5	1	HSS 6x6x5/8	W21x93	W14x109	W14x90
	2	HSS 6x6x5/8	W21x93	W14x109	W14x90
	3	HSS 6x6x1/2	W24x117	W14x109	W14x90
4	1	HSS 7x7x5/8	W21x101	W14x109	W14x90
	2	HSS 7x7x1/2	W21x101	W14x109	W14x90
	3	HSS 6x6x1/2	W24x117	W14x109	W14x90
3	1	HSS 8x8x5/8	W21x101	W14x120	W14x90
	2	HSS 8x8x1/2	W21x101	W14x120	W14x90
	3	HSS 6x6x5/8	W24x131	W14x120	W14x90

Table 6.3 Member Sizes of the 9-story Model Buildings

R	Story	Brace	Beam	Exterior Col.	Interior Col.
3	1	HSS 10x10x5/8	W21x101	W14x370	W14x370
	2	HSS 9x9x5/8	W21x93	W14x370	W14x370
	3	HSS 9x9x5/8	W21x93	W14x370	W14x370
	4	HSS 9x9x5/8	W21x93	W14x257	W14x257
	5	HSS 8x8x5/8	W21x93	W14x257	W14x257
	6	HSS 8x8x1/2	W21x93	W14x145	W14x145
	7	HSS 7x7x1/2	W21x93	W14x145	W14x145
	8	HSS 6x6x5/8	W21x93	W14x90	W14x90
	9	HSS 5x5x1/2	W21x111	W14x90	W14x90
6	1	HSS 8x8x1/2	W21x93	W14x283	W14x283
	2	HSS 7x7x1/2	W21x83	W14x283	W14x283
	3	HSS 7x7x1/2	W21x83	W14x283	W14x283
	4	HSS 7x7x1/2	W21x83	W14x193	W14x193
	5	HSS 6x6x5/8	W21x83	W14x193	W14x193
	6	HSS 6x6x1/2	W21x83	W14x120	W14x120
	7	HSS 6x6x3/8	W21x83	W14x120	W14x120
	8	HSS 5x5x1/2	W21x83	W14x74	W14x74
	9	HSS 5x5x5/16	W24x104	W14x74	W14x74
7	1	HSS 7x7x5/8	W21x93	W14x233	W14x233
	2	HSS 6x6x5/8	W21x93	W14x233	W14x233
	3	HSS 6x6x5/8	W21x101	W14x233	W14x233
	4	HSS 6x6x1/2	W21x93	W14x145	W14x145
	5	HSS 6x6x1/2	W21x93	W14x145	W14x145
	6	HSS 6x6x3/8	W21x93	W14x99	W14x99
	7	HSS 6x6x3/8	W21x101	W14x99	W14x99
	8	HSS 5x5x3/8	W21x93	W14x61	W14x61
	9	HSS 4x4x1/2	W24x104	W14x61	W14x61
8	1	HSS 7x7x1/2	W21x93	W14x211	W14x211
	2	HSS 6x6x1/2	W21x83	W14x211	W14x211
	3	HSS 6x6x1/2	W21x83	W14x211	W14x211
	4	HSS 6x6x1/2	W21x83	W14x145	W14x145
	5	HSS 6x6x3/8	W21x83	W14x145	W14x145

6	HSS 6x6x3/8	W21x83	W14x90	W14x90
7	HSS 5x5x1/2	W21x83	W14x90	W14x90
8	HSS 5x5x5/16	W21x83	W14x61	W14x61
9	HSS 4x4x3/8	W24x104	W14x61	W14x61

Table 6.4 Member Sizes of the 20-story Braced Frames with Difference R Factors

Story	R = 3		R = 4		R = 6		R = 8		Beam (for all)	Int. Col. (for all)
	Brace	Ext. Col.	Brace	Ext. Col.	Brace	Ext. Col.	Brace	Ext. Col.		
1	HSS10x10x5/8	W14x455	HSS 8x8x5/8	W14x370	HSS 7x7x5/8	W14x311	HSS 7x7x1/2	W14x257	W18x50	W12x65
2	HSS 9x9x5/8	W14x455	HSS 8x8x1/2	W14x370	HSS 7x7x1/2	W14x311	HSS 6x6x1/2	W14x257	W18x50	W12x65
3	HSS 9x9x5/8	W14x455	HSS 8x8x1/2	W14x370	HSS 7x7x1/2	W14x311	HSS 6x6x1/2	W14x257	W18x50	W12x65
4	HSS 9x9x5/8	W14x455	HSS 8x8x1/2	W14x370	HSS 7x7x1/2	W14x311	HSS 6x6x1/2	W14x257	W18x50	W12x65
5	HSS 9x9x5/8	W14x370	HSS 8x8x1/2	W14x342	HSS 7x7x1/2	W14x211	HSS 6x6x1/2	W14x193	W18x50	W12x53
6	HSS 9x9x5/8	W14x370	HSS 8x8x1/2	W14x342	HSS 6x6x5/8	W14x211	HSS 6x6x1/2	W14x193	W18x50	W12x53
7	HSS 9x9x5/8	W14x370	HSS 7x7x5/8	W14x342	HSS 6x6x5/8	W14x211	HSS 6x6x1/2	W14x193	W18x50	W12x53
8	HSS 8x8x5/8	W14x370	HSS 7x7x5/8	W14x342	HSS 6x6x5/8	W14x211	HSS 6x6x1/2	W14x193	W18x50	W12x53
9	HSS 8x8x5/8	W14x211	HSS 7x7x5/8	W14x193	HSS 6x6x5/8	W14x145	HSS 6x6x3/8	W14x132	W18x50	W12x40
10	HSS 8x8x5/8	W14x211	HSS 7x7x5/8	W14x193	HSS 6x6x5/8	W14x145	HSS 6x6x3/8	W14x132	W18x50	W12x40
11	HSS 8x8x5/8	W14x211	HSS 7x7x5/8	W14x193	HSS 6x6x1/2	W14x145	HSS 6x6x3/8	W14x132	W18x50	W12x40
12	HSS 8x8x1/2	W14x211	HSS 7x7x1/2	W14x193	HSS 6x6x1/2	W14x145	HSS 6x6x3/8	W14x132	W18x50	W12x40
13	HSS 7x7x5/8	W14x132	HSS 7x7x1/2	W14x120	HSS 6x6x1/2	W14x90	HSS 6x6x3/8	W14x90	W18x50	W12x40
14	HSS 7x7x5/8	W14x132	HSS 6x6x5/8	W14x120	HSS 6x6x3/8	W14x90	HSS 5x5x1/2	W14x90	W18x50	W12x40
15	HSS 7x7x1/2	W14x132	HSS 6x6x5/8	W14x120	HSS 6x6x3/8	W14x90	HSS 5x5x1/2	W14x90	W18x50	W12x40
16	HSS 7x7x1/2	W14x132	HSS 6x6x1/2	W14x120	HSS 5x5x1/2	W14x90	HSS 5x5x3/8	W14x90	W18x50	W12x40
17	HSS 6x6x1/2	W14x68	HSS 6x6x3/8	W14x61	HSS 5x5x1/2	W14x43	HSS 5x5x5/16	W14x43	W18x50	W12x40
18	HSS 6x6x3/8	W14x68	HSS 5x5x1/2	W14x61	HSS5x5x5/16	W14x43	HSS 5x5x5/16	W14x43	W18x50	W12x40
19	HSS 5x5x1/2	W14x68	HSS5x5x5/16	W14x61	HSS 4x4x1/2	W14x43	HSS 4x4x1/2	W14x43	W18x50	W12x40
20	HSS 5x5x5/16	W14x68	HSS 4x4x3/8	W14x61	HSS 4x4x1/4	W14x43	HSS 4x4x1/4	W14x43	W18x50	W12x40

These designs resulted in very different amounts of steel. To present the variation of the steel weight with various design  $R$  values, which directly influence the construction cost of the buildings, total steel weights of the lateral-load resisting frames in a single direction were calculated and normalized (dividing the total steel weights by the seismic weight of whole building, which is independent of  $R$  factors). Figure 6.2 compares the normalized steel weights for buildings using  $R=3$  and 8 with the normalized building weights with  $R=6$  respectively. The comparison shows that reducing the  $R$  value from 6 to 3 for the 3-story buildings increased the total steel weight by 0.27% of the seismic weight of the building. This impact for 3-story (low-rise) buildings was relatively lower than the impact for 9- and 20-story (mid- and high-rise) buildings.

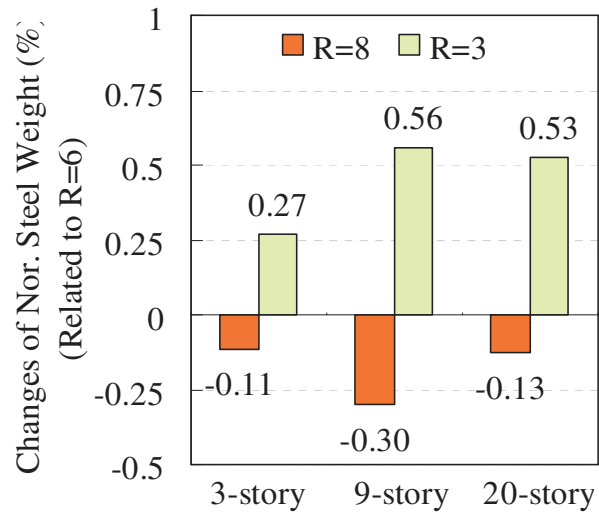


Figure 6.2 Variation of the Steel Weight of Buildings Using R=3 and 8 Comparing with That of R=6.

### 6.3 System Modeling

To assess the seismic performance of SCBFs and the  $R$  value in a rational manner, comprehensive nonlinear dynamic analysis models are required. These models must include every yield mechanism and failure mode that impacts the seismic response of the frame and must be capable of simulating the response beyond initial fracture. These requirements are met by the modeling technique proposed in previous chapters. All of the braced frame systems of the buildings in the study here were modeled using the proposed simulation model of SCBFs, which included the proposed models of the gusset plate connection (Chapter 4), and the brace-fracture model (Chapter 5).

#### 6.3.1 Effect of Gravity Frames

The gravity loads and second order effect (P-delta) effects were included in the



simulation by employing a leaning column connected to the frame by rigid links, as illustrated in Fig. 6.3. Analyses were performed with and without contributions of the gravity framing to study its impact.

The gravity frame was modeled using shear-connection springs simulating the total rotational strength and stiffness of gravity beam-column connections (shear-tab connections), which were located between the rigid link and the leaning column. The gravity loads at each floor level were placed on the gravity frame. For each seismic frame half of the gravity load was applied to each frame, since each building model used two seismic frames in each direction to resist the lateral loads, as shown in Fig. 6.1.

The properties of these shear-connection springs were based upon Liu's model of shear-tab connections with composite slabs (Liu and Astaneh-Asl 2004). The springs were simulated using the Pinching4 material model in OpenSees. Each spring element had a stiffness and strength that were equivalent to the number of the gravity bays contributing to the seismic weight. For the buildings modeling here, that is half of the total frames. A multiplier of 12 was used for the 3-story model buildings to simulate the contribution of half of the total number of gravity connections.

The rigid beams used in the gravity frame model, which had the same length of the gravity bay, were supported by rollers. The nodes at the end of the rigid beams were slaved to the nodes at the middle of the braced frame in horizontal translation at each level as illustrated in Fig. 6.3. When this secondary resistance was excluded, the springs were replaced by pins, and therefore no rotational stiffness was included.

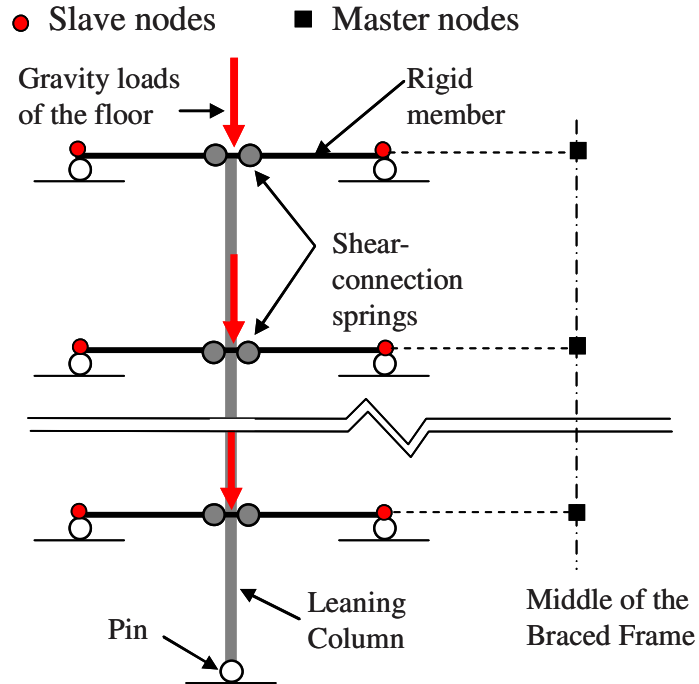


Figure 6.3 Illustration of the Simulation of P-delta and Gravity Frame Effects

The base of the leaning column was pinned. Wide-flange sections W10x49 and W12x65 were used for the gravity columns of the 3- and 9-story buildings throughout the height, respectively. The gravity columns of the 20-story buildings varied; the smallest wide flange section was a W8x31 and the largest wide-flange section was a W14x90. To represent the overall contributions, such as initial axial and bending stiffness and strength, of the gravity columns to the lateral-load resisting system, a particular cross section of the leaning column was adopted with a cross-sectional area, moment of inertia and plastic moment capacity equal to the total of the gravity columns contributing to the seismic weight. A multiplier of 11.5 was used for the 3-story model buildings to simulate the contribution of half of the total number of gravity columns.

The effects of the gravity framing were investigated. The results are shown in Fig. 6.4. The ratios plotted are the maximum story displacement without the lateral resistance

of the gravity framing,  $MSD_{w/oGF}$ , divided by the maximum story displacement with the lateral resistance with gravity framing,  $MSD_{w/GF}$ . This ratio illustrates the impact of the gravity frame on the computed seismic response. Three building models are considered, including 3-, 9- and 20-story buildings, designed using an  $R$  value of 6. The 20 ground motions were scaled to 2% in 50 year seismic hazard level using the fundamental period of the structures.

As indicated in the figure, the gravity frames can impact the computed response. The effect was significant in 3-story buildings, and much less significant on the mid-rise (9-story) and high-rise (20-story) buildings. For consistent comparisons, this effect of gravity frames was included in all analyses

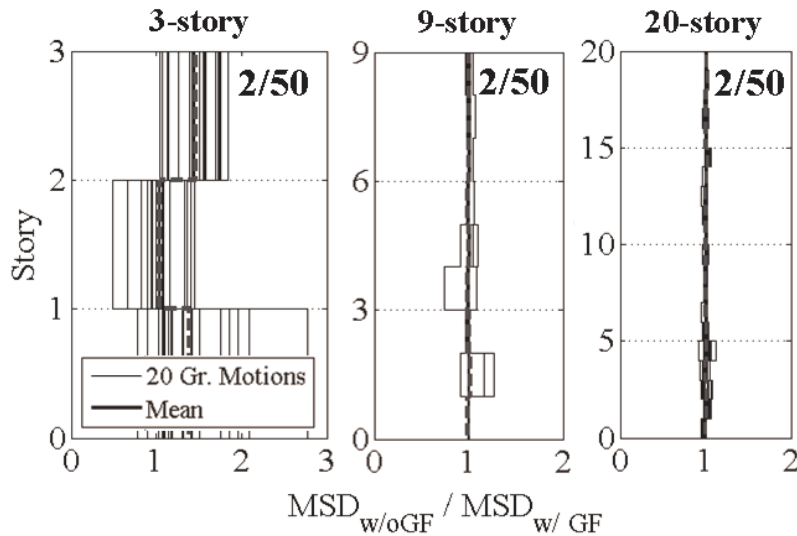


Figure 6.4 Ratios of Seismic Responses of Buildings With and Without the Gravity Frame Effect.

## 6.4 Collapse Assessment Using FEMA P695 Methodology

### 6.4.1 An Overview of FEMA P695 Methodology

The P695 methodology was developed for evaluating building system performance and response parameters for buildings with different seismic-force-resisting systems with the goal of achieving equivalent safety against collapse in earthquakes. The methodology consists of structure archetype development, nonlinear modeling of the archetypes, nonlinear analysis of the archetypes and evaluation of seismic performance factors for the systems. The procedures and the results for SCBF systems based on the methodology to determine the collapse potential and the R factor are used in this study.

Based on the methodology, archetypes are defined to capture the essence and variability of the performance characteristic. Building heights, structural framing configurations, framing bay sizes, magnitude of gravity loads of the system of interest and member and connection design and detailing requirements are appropriate characteristics for consideration.

In terms of potential collapse assessment and evaluation of R factor of the systems, the following the procedures used with the P695 methodology. Further information is found in the reference report (ATC-63 2008). Figure 6.5 illustrates the fundamental hypothesis used in the methodology based upon the pushover concept. The conversion to spectral coordinates is based on the assumption that 100% of the effective seismic weight of the structure,  $W$ , participates in fundamental mode of the system with a period of  $T_1$ .  $S_{MT}$  is the Maximum Considered Earthquake (MCE) spectral acceleration at the period of the system;  $\hat{S}_{CT}$  is the median 5%-damped spectral acceleration of the collapse level ground motions at the period of the system; and the term  $C_s$  is the seismic response

coefficient ( $V/W$ , the ratio of the design base shear and the weight of the structure); and the term  $C_d$  is the deflection amplification factor.

Two additional important design assumptions are included. The ratio of  $S_{MT}$  to the seismic response coefficient,  $C_s$ , is equal to 1.5 times of the  $R$  value accounting for the two-thirds reduction of MCE ground motion used in the ASCE/SEI 7-10 provisions. The other is that the  $C_d$  factor is equal to the  $R$  factor due to that it is reasonable for most conventional systems with effective damping approximately equal to the nominal 5% level used to define response spectral acceleration and displacement.

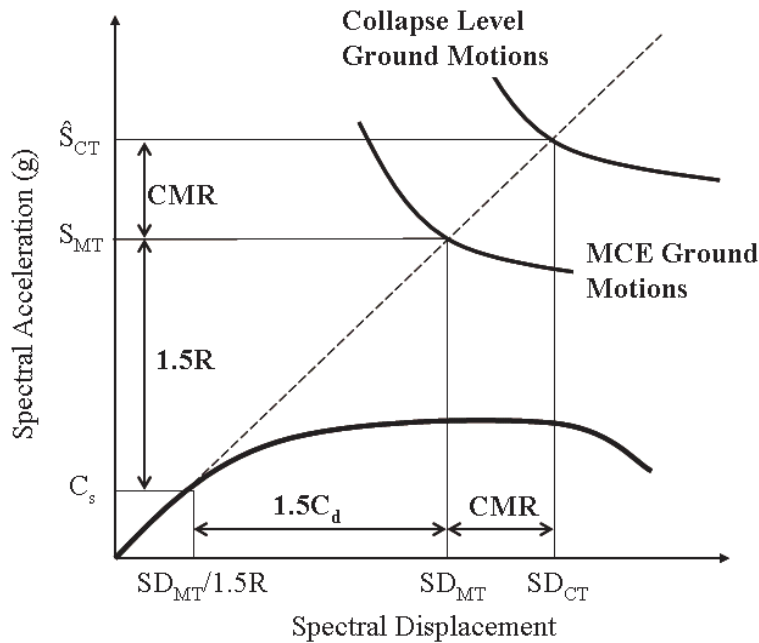


Figure 6.5 Illustration of the R Factor as Defined by the FEMA P695 Methodology (2008)

To assess the collapse margin, the Collapse Margin Ratio (CMR) is defined as the ratio of  $\hat{S}_{CT}$  to  $S_{MT}$ , as shown in the figure. To determine  $\hat{S}_{CT}$ , each archetype, designed for the reduced design base shear ( $V=C_s * W$ ) with a given R-factor, is evaluated by

conducting nonlinear dynamic analysis over a group of ground motions using the IDA method. The collapse potential of the archetype is estimated by increasing the intensity of ground motions with the dynamic simulation until the maximum roof displacement response increasing rapidly increased, which implies the softening of the system and incipient collapse. The ground motion intensity (i.e.  $\hat{S}_{CT}$  or  $SD_{CT}$ ) corresponds to seismic excitation inducing system collapse is based on flattening of the acceleration-displacement response curve. The  $\hat{S}_{CT}$  is defined as the median value of the resulting spectral acceleration capacities over the ground motion record set.

. To account for statistical variation in the records, the CMR is multiplied by a simplified Spectral Shape Factor (SSF) to obtain the Adjusted Collapse Margin Ratio (ACMR). The SSF values are specified in the report, and depend on the structural period and the inelastic deformation capacity of the building according to a pushover analysis. The method accounts for the frequency content (spectral shape) of the ground motions, and a consistent set of ground motion variation parameters is defined for different sites, hazard levels and structural periods (Baker and Cornell 2006), where  $\hat{S}_{CT}$  is determined using the forty-four selected acceleration records which satisfy the ground motion selection criteria.

Finally, the archetype is evaluated by comparing the calculated ACMR to an acceptable ACMR, which is specified according to the uncertainty factors of structural system, including the quality of design requirements, test data, numerical modeling, and a prescribed set of ground motions. By the FEMA P695 procedure, the acceptable ACMR should reflect conditional probability of collapse of 20% for individual archetype (AMCR20%) and 10% for the combination of all systems within the category. The ACMR of an individual archetype must be greater than the corresponding acceptable

AMCR to pass the trial. If the determined ACMR was less than the Acceptable ACMR, the R value of the performance group does not meet the performance requirements of collapse prevention.

#### **6.4.2 Collapse Assessment of the SCBF Model Buildings**

An application of the FEMA P695 methodology was conducted in this research project. Two idealized building models, including the 3- and 20-story buildings, were evaluated following the FEMA P695 method and were used as the archetypes for the system, and R values of 3 and 6 were compared. The nonlinear modeling of the archetype buildings follows the simulation approach of the SCBF systems previously described in Section 6.3.

The 3- and 20-story buildings were evaluated using the FEMA P695 IDA procedure with design spectral acceleration,  $S_{DS}$ , of 1.17g, which is slightly greater than the value of 1.0g suggested by the methodology and  $S_{DI}$  of 0.57g. The SAC ground motion set for 2% in 50-year seismic hazard level in Seattle was used in place of the 44 ground motion records provided by the methodology. Originally, the SAC ground motion records had been scaled to fit the USGS mapped spectral acceleration values at multiple period points (FEMA 355C 2000b). For suitable use in this research, all of the SAC acceleration records were scaled back to original ground motion records prior to the IDA process, and they were subsequently increased until collapse was predicted for each record.

Two methods for scaling the intensity of ground motions were investigated. The first method, designated Method M1, collectively increased the entire set of ground motion records using a single magnification value corresponding to the median spectral

acceleration of the record set at the fundamental period. The value is referred to as the Record Set Intensity (RSI),  $S_T(T_1)$ , according to the methodology. Using this method, the value of  $\hat{S}_{CT}$  was defined as the RSI of the group when 50% of the records predicted collapse by the IDA procedure.

The second method, designated Method M2, scaled each record individually in the IDA procedure (FEMA 355F 2000c). Using this method,  $\hat{S}_{CT}$  was defined as median spectral acceleration of the response spectra at the period  $T_1$ ,  $Sa(T_1)$ , which results in predicted collapse.

Figures 6.6a and b show the resulting IDA curves of the three-story buildings using the methods M1 and M2, respectively. In an actual building, collapse will depend on the resistance of the gravity frame as well as the residual resistance of braced frames. Braced frames dramatically lose most of their resistance and sustain increasing story drift after prediction of brace fracture. In many IDA evaluations, the collapse prediction is based on flattening of the IDA responses curves, such as those shown in Fig. 6.6. As evident in Fig 6.6, some brace fracture curves flatten at relatively low spectral accelerations while others do not flatten at all. This is partly caused by the irregular characteristics of acceleration response spectra and the large increases or decreases that may occur with modest changes in period. In addition, a braced frame has significantly different seismic performance from a moment frame, which the IDA method was originally developed upon. Braced frames beyond the brace buckling and brace fracture, while moment frames retain their resistance with moderate strain hardening and smooth reduction in stiffness until connection failure occur.

In this research, a collapse limit state corresponding to 5% drift was selected for three reasons. First, the nonlinear analyses were deemed to have sufficient accuracy to



approximate system performance up to 5% story drift. Second, experimentation indicates that most connections do not retain sufficient resistance beyond this drift level. Third, braced frame tests that included SCBF gusset plate connections indicate that they retain moment resistance well beyond brace fracture (Lehman and Roeder 2008), but this integrity cannot be assured for drift levels larger than 5%. Therefore, this limiting story drift capacity was combined with flattening effect to determine  $\hat{S}_{CT}$ .

In Figs. 6.6a and b,  $\hat{S}_{CT}$  was determined when the results for 10 out of 20 ground motions (50%) had a story drift greater than 5%. The resulting  $\hat{S}_{CT}$  values are different ( $\hat{S}_{CT}=1.88g$  with method M1 and  $\hat{S}_{CT}=2.5g$  with method M2), which suggests that the collapse potential depends on the scaling method.

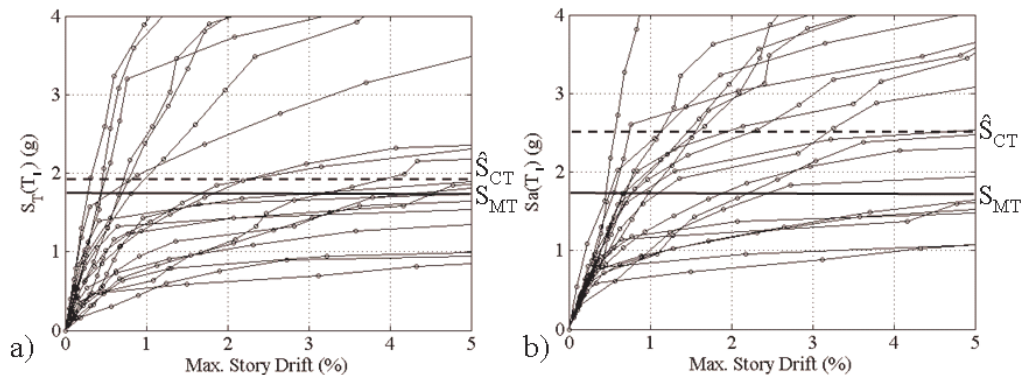


Figure 6.6 IDA Results for the 3-story Building (R=6) using (a) M1 and (b) M2 Scaling Methods with Collapse Story Drift Capacity of 5%.

The results shown in Fig. 6.6 were compared with the acceptable ACMR20% values in FEMA P695 to evaluate the collapse resistance of each system, as shown in Table 6.5. The P695 method requires an estimate of the system ductility and the structural fundamental period to determine the acceptable ACMR20%. Based on the prior experimental results (Johnson 2005, Herman 2006, Kotulka 2007, Powell 2009, Lumpkin

2009), buckling is expected at a story drift of 0.3% and fracture occurs at a story drift of 2.5% as an upper bound, which led to the story-drift ductility of 8.3. The corresponding SSF values, required to scale to CMR to determine the ACMR, were 1.4 and 1.65 for 3- and 20-story buildings, respectively (Values for structures with ductility capacity exceeding 8). An acceptable ACMR20% of 1.73 was determined, in which the 3-story and 20-story buildings were regarded as an archetype and the quality ratings for design requirements, test data, and numerical modeling were all quantified as “B-Good”. The resulting total uncertainty factor was 0.65. Table 6.5 summarizes the parameters and the results of the evaluations for the 3- and 20-story buildings with design  $R$  values of 6 and 3.

Table 6.5 Summary of Evaluations of the 3- and 20-story Buildings Using FEMA P695 IDA Procedure

Scaling Methods	M1 [ $S_T(T_I)$ ]				M2 [ $S_a(T_I)$ ]			
	3-Story		20-Story		3-Story		20-Story	
Model Buildings	3	6	3	6	3	6	3	6
R Factors	6	3	6	3	6	3	6	3
$S_{MT}$ (g)	1.76	1.76	0.65	0.65	1.76	1.76	0.65	0.65
$\hat{S}_{CT}$ (g)	1.88	2.8	0.55	0.82	2.5	3.35	0.65	0.93
CMR	1.07	1.60	0.85	1.26	1.42	1.91	1.00	1.43
SSF	1.4	1.4	1.65	1.65	1.4	1.4	1.65	1.65
ACMR	1.39	2.07	1.10	1.64	1.85	2.48	1.30	1.86
Acceptable ACMR20%	1.73	1.73	1.73	1.73	1.73	1.73	1.73	1.73
Pass/Fail	Fail	<b>Pass</b>	Fail	Fail	<b>Pass</b>	<b>Pass</b>	Fail	<b>Pass</b>

Decreasing the  $R$ -factor increased the CMR for all systems studied. However, the values using the two scaling methods are not the same and therefore the collapse probability differs. Using Method M1 (FEMA P695 method), the only system that “passes” the evaluation criteria is the 3-story system designed using an  $R$ -factor of 3. This

result suggests that SCBF systems meeting current design are vulnerable to collapse. In contrast, using scaling method M2, only the 20-story building designed with  $R=6$  fails to meet the acceptable ACMR20%. The M1 scaling method results indicate that  $R$  factor of 3 for 3-story SBF building is not vulnerable to collapse, and a designed  $R$  value smaller than 3 is required to mitigate collapse of a 20-story building. The M2 scaling method indicate that  $R$  factor of 6 is appropriate for 3-story SCBFs, while an  $R$  value of 3 is needed for 20-story SCBFs.

In particular, the analysis for both scaling methods M1 and M2 predicted greater potential for collapse with the 20-story SCBF than for the 3-story SCBF. These results are contrary to findings from prior earthquakes and other studies, in which low rise SCBFs have been deemed more vulnerable (Chen and Mahin 2010).

## 6.5 Multi-performance Level Evaluation Procedure

The results of the P695 analyses revealed ambiguities in the method. To study these further and potentially eliminate them, an alternate evaluation approach for SCBFs was investigated. All structural performance levels were evaluated including the collapse limit state and other damage dependant limit states of SCBFs (ATC-58 2009). Using this method, a range of system performance limit states was evaluated (e.g., brace buckling, brace fracture) as opposed to only collapse potential. In this method the collapse of the structure was again assumed if the computed inter story drift of any floor exceeded a 5% story drift.

The 20 SAC Seattle ground motions were scaled to the 2/50 hazard level (MCE level). In addition, the seismic performance at the 10/50 hazard level was evaluated,

using a suite of records for Seattle from the SAC ground motion set scaled to a 10% in 50 year seismic hazard (FEMA 355C 2000b). The target spectra for each hazard level were computed using the ASCE 7 (2005) using the corresponding USGS mapped spectral acceleration values that represent the 10/50 and 2/50 hazard levels. The 2/50 target spectrum is 1.5 times of the design spectrum, while the 10/50 target spectrum is slightly smaller than the design spectrum, as shown in Fig. 6.7a.

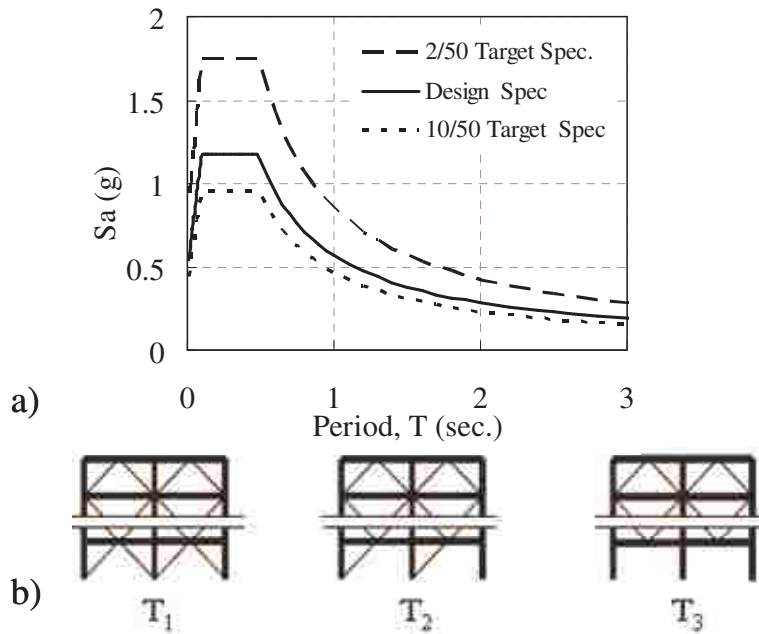


Figure 6.7 (a) Adopted Target and the Design Spectra at Seattle; (b) Illustrations of the Corresponding Frames for the Three Periods,  $T_1$ ,  $T_2$  and  $T_3$ .

In addition to the 3- and 20-story SCBFs idealized buildings, for this portion of the study, the idealized 9-story SCBFs was investigated. For each building, a number of  $R$  values were evaluated.

Because the evaluation of the P695 procedure revealed ambiguities associated with scaling ground motions, the research team considered the use of various scaling

approaches. Prior studies have scaled records using a single period, multiple periods, or a period range (FEMA 355C 2000b). For this study multi-period scaling was used because SCBFs are initially stiff structures which have a short period. However, the structural period for the system shifts significantly beyond brace buckling and again beyond brace fracture. Brace buckling invariably occurs with the 2% in 50 year hazard level and occasionally occurs with 10% in 50 year hazard. Therefore, an approach of scaling the ground motions to match the response spectra prior to and beyond the brace fracture was used.

The conclusions were substantiated by a preliminary study. Initially all of the idealized buildings were analyzed using earthquake records scaled to the first mode only. These analyses demonstrated that significant brace damage (buckling, yielding, and eventually fracture) was sustained in the 3 and 9-story building models. There was more limited brace damage in the 20-story building models, but these models exhibited significant higher mode effects. Therefore, for the 20-story buildings, these higher modes must be included in the scaling procedure. As a result two different scaling approaches were used.

For the structures primarily governed by the fundamental mode prior to damage, i.e. the 3- and 9-story buildings, the following approach was used. For the 10/50 target spectrum, minimal nonlinearity was observed from the preliminary analysis, and each ground motions was independently scaled to meet the 10/50 target spectrum using only the first (fundamental) period ( $T_1$ ) of the structure. The scaling was conducted for each story height and R factor.

The dynamic analyses with 2% in 50 year seismic hazard indicated that the bottom story was critical for the 3- and 9-story building models. The braces commonly buckled

and occasionally fractured, and this damage mode impacted the structural period. Therefore, multi-period scaling was used. Three periods were used. 1) The fundamental period ( $T_1$ ), 2) the second period ( $T_2$ ) corresponded to loss of braces in one-direction at the critical story, and 3) the third period ( $T_3$ ) corresponded to loss of all braces at the critical story. These three states are illustrated in Fig. 6.7b.

The scaling expressions used weighted combination of the  $Sa_i$  values,  $f_{10/50}$  and  $f_{2/50}$ , for the 10/50 and 2/50 events, respectively.

$$f_{10/50} = \frac{Sa_{1,t}}{Sa_{1,g}} \quad (6.1)$$

$$f_{2/50} = \frac{Sa_{1,t}}{Sa_{1,g}} w_1 + \frac{Sa_{2,t}}{Sa_{2,g}} w_2 + \frac{Sa_{3,t}}{Sa_{3,g}} w_3 \quad (6.2)$$

The expression is a weighted function of the spectra accelerations at the periods of interest. In the expression,  $Sa_{i,t}$  is the target elastic spectral acceleration, value corresponding to the  $T_i$  period ( which was established as described previously),  $Sa_{i,g}$  is the spectral acceleration value of the ground motion at the period  $T_i$ , and  $w_i$  is the weight for the  $T_i$  period points. The weights were 0.55, 0.35 and 0.1 for  $T_1$ ,  $T_2$  and  $T_3$ , respectively. The adopted weight were determined by assuming that the structures are mainly controlled by the fundamental period of the system and the probability of occurrence for the system losing all braces ( $T_3$ ) is less than the system losing one-direction braces ( $T_2$ ). The resulting median scaled acceleration spectra corresponding to 10/50 and 2/50 hazard levels are shown in Figs. 6.8a and b. The corresponding target spectra are also shown. The values of three periods of interest ( $T_1$  to  $T_3$ ) are indicated in the figures.

The preliminary analysis of the 20-story building models indicated significant contributions of the second mode in top and bottom stories with the first mode governing

the response of the remainder of the building. To include the second-mode effects, a modified scaling approach was adopted to scale the ground motions for use in the 20-story building analysis. For the 20 story buildings, the scaling function was based on the first two modal periods for both hazard levels. Because significant damage was not observed in high-rise building, the larger periods resulting from brace damage were not included. The resulting scaling factors,  $f_{m,10/50}$  and  $f_{m,2/50}$ , given in Eq. 6.3, were used to scale the ground motions for both of the 10/50 and 2/50 events of these taller systems.

$$f_{m,10/50} \text{ and } f_{m,2/50} = \frac{Sa_{m2,t}}{Sa_{m2,g}} w_{m2} + \frac{Sa_{m1,t}}{Sa_{m1,g}} w_{m1} \quad (6.3)$$

In the expression,  $Sa_{mi,t}$  is the target elastic spectral acceleration value for the  $i^{th}$  modal period ( $i=1$  and  $2$ ),  $Sa_{mi,g}$  is the spectral acceleration value of the ground motions at the  $i^{th}$  modal period. For the second expression, weights of  $w_{m2}=0.6$  and  $w_{m1}=0.4$  were used. Figure 6.8c shows the median scaled acceleration spectra for 10/50 and 2/50 hazard levels and the corresponding target spectra for the 20-story SCBF building. The values of the first two mode periods,  $T_{M1}$  and  $T_{M2}$ , used for scaling were indicated in the figure. All used scaling factors of the ground motions for different building heights are listed in Appendix F.2.

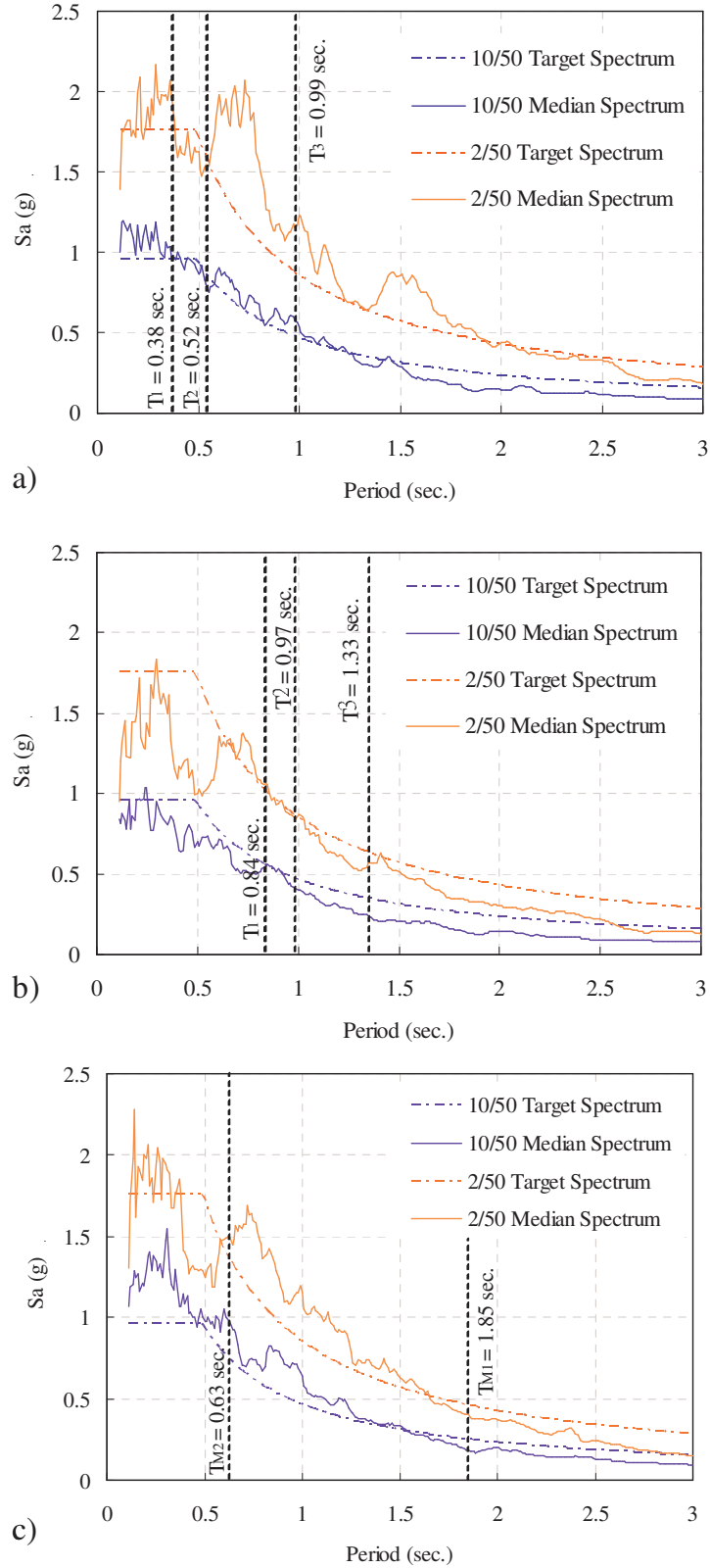


Figure 6.8 Scaled Median Acceleration Spectra and The Corresponding Target Spectra for (a) the 3-, (d) 9- and (e) 20-story



The scaled 2% and 10% in 50 year (2/50 and 10/50) ground motions were used to compute the nonlinear response of the building models. Figures 6.9a, b and c show the average Maximum Story Drifts (MSD) computed for the 3-, 9- and 20-story SCBFs for the 10/50 and 2/50 hazard levels, respectively. As noted in the figures, different building designs, which depended on the  $R$  value, were conducted. The studied  $R$  values were 3 and 6 for the 3-story building models, and 3, 6, and 8 for the 9- and 20-story building models.

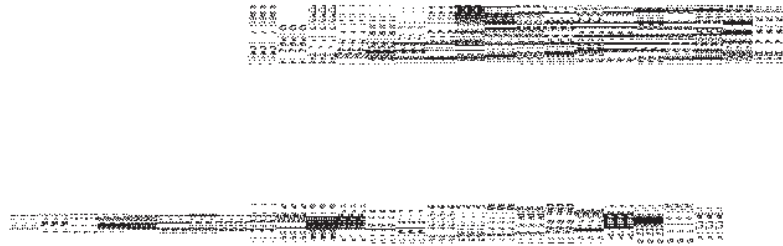


Figure 6.9 Seismic Responses of (a) the 3-story, (b) 9-story and (c) 20-story Buildings with Various  $R$  Factors at 10/50 and 2/50 Hazard Levels.

For all building types, in the 10/50 events, the average MSDs over the building height varied between 0.3% and 0.5%. Fragility curves show that brace fracture does not

occur at these drift levels. The results show that the earthquakes at this hazard level cause very limited deformation and little concentration of inelastic deformation over the building height.

For the 2/50 level analyses, the average MSD values increased significantly and severe concentration of deformation occurred in some cases. The three story-height SCBF buildings designed with  $R$  value varying between 3 and 6 had much more severe deformation than the taller SCBF buildings. The average MSD for the 9- and 20-story building models had similar peak values (1% and 1.5%) as designed with  $R$  value of 3 and 6, respectively. This consistency was not retained for 9- and 20- story buildings designed with  $R$  value of 8, as shown in Figs. 6.9b and c, due to the different distribution of deformation in the two different building heights.

The 3- and 9-story SCBF buildings had similar distribution of drift over the building height. Both sustained larger inelastic deformation in the first story, which always resulted from predicted brace buckling and occasional brace fracture at that story, while the 20-story building models had quite different distribution.

The response of the 20-story building models differed significantly from the 3-story and 9-story building models in three ways. First the upper stories sustained the largest deformations for the 20-story models. The maximum story drift and inelastic deformation occurred in both the bottom and upper stories of the 20 story due to the higher mode effects and the brace damage that resulted. Second, the distribution of deformation along the height of the building depends on  $R$ . The peak average MSDs occurred at different story height with different  $R$  values. Third, the resulting peak average MSDs varied between 1.0% and 1.3%, and these are significantly lower than those noted with shorter buildings. These results suggest improved structural performance with increasing

building height.

The average maximum story drift distributions shown in Fig. 6.9 provide interesting and valuable information. In addition to predicting global force and drift demands, the analytical models (Chapters 4 and 5) are capable of predicting the local performance including out-of-plane brace displacement and the onset of brace fracture. This modeling approach allows a comprehensive evaluation of all performance levels.

Several performance limit states were considered:

- 1) Initial brace buckling: The brace buckling was computed in the analysis model, and prior experiments show the initial brace buckling always occurred at approximately 0.3% story drift.
- 2) Excessive brace buckling requiring replacement of the brace: Requirements for possible replacement of the brace were defined as: (a) the maximum out-of-plane displacement of the braces exceeded three times the brace depth or (b) prediction of brace fracture. These damage states related to definitions developed in a prior study on fragility curves of CBFs (ATC-58 2009). The out-of-plane displacement and the brace fracture were predicted by the analysis model as described in Chapters 4 and 5.
- 3) Brace fracture: The fracture was predicted by the analysis model.
- 4) Incipient collapse: A story drift limit of 5% was adopted to predict the onset of incipient collapse, the prior experiments show that braced frames have considerable inelastic deformation capacity after brace fracture. Therefore basing collapse solely on brace fracture is unduly conservative. Other experiments also show that the gravity connections are unlikely to be reliable at drifts much greater than 5%. This performance prediction offers greater confidence than the P695

evaluation procedure, because the damage states are based upon experimental observation rather than an unverified analytical procedure.

All analytical responses were assembled to determine the probability of occurrence for these four performance limit states. Figures 6.10a, b and c show these probabilities for the 3-, 9- and 20-story buildings for each  $R$  factor at the 2/50 hazard level (MCE level), respectively. As expected a reduction of  $R$  reduces the probabilities of all damage limit states beyond brace buckling. Brace buckling occurs in the 2%-in-50 year event, for all  $R$  values studied.

The number of stories impacts the SCBF performance. In general, the 20-story building sustains less damage than the 3-story building for a given  $R$  factor. These results suggest that a smaller  $R$  factor may be needed for consistent performance of shorter SCBF buildings. This clearly contradicts the prediction from the P695 IDA evaluation, but it is consistent with other prior analytical studies.

Figure 6.11 shows similar damage level comparisons for the 10/50 hazard level. Figure 6.7a shows that the 10/50 hazard level is very close to the design spectrum (2/3 of the MCE). Results show that the probability of brace buckling was high, but little additional damage was predicted regardless of the  $R$  value or building height.

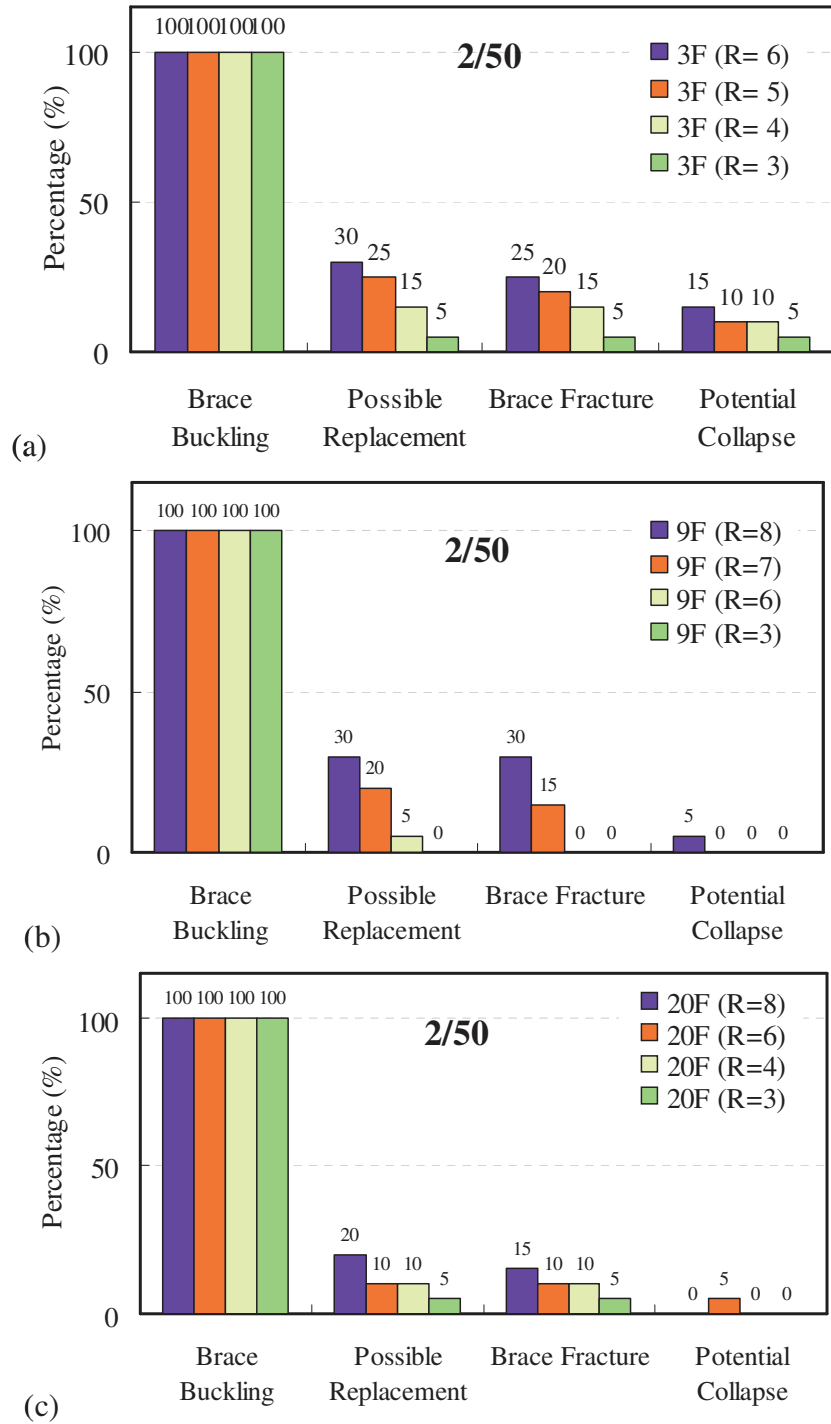


Figure 6.10 Probability of Damage at the 2/50 Hazard Level with Various R Values (a) 3-story SCBF, (b) 9-story SCBF, and (c) 20-story SCBFs.

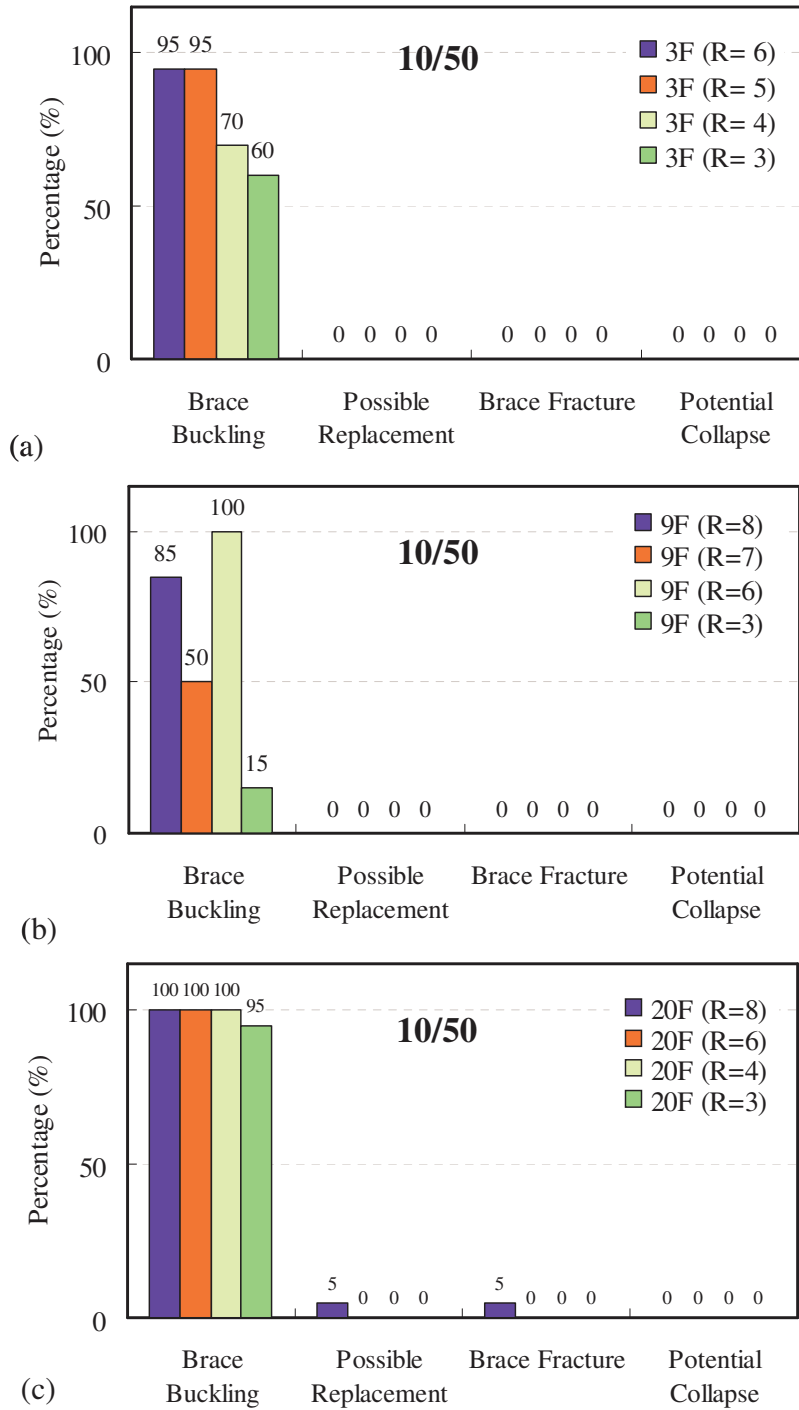


Figure 6.11 Probability of Damage at the 10/50 Hazard Level with Various R Values (a) 3-story SCBF, (b) 9-story SCBF, and (c) 20-story SCBFs.

## 6.6 Deflection Amplification and Overstrength Factors

The deflection amplification,  $C_d$ , and overstrength,  $\Omega_o$ , factors were also computed and investigated for each of the building models. The results of those analyses are presented here.

The deflection amplification factor was calculated as the ratio of the maximum displacement at the 2/50 hazard level,  $SD_{max}$ , to the elastic deformations under the design equivalent lateral forces,  $SD_{ELF}$ , as shown below.

$$C_d = \frac{SD_{max}}{SD_{ELF}} \quad (6.4)$$

Figures 6.12a, b and c show the mean and standard deviation of the deflection amplification factors for 3-, 9- and 20-story buildings, respectively. In all cases, the bottom story had larger value than the upper stories, although the deviations for a given story and among the stories are less for the taller structures.

The mean value of  $C_d$  and standard deviation of  $C_d$  decrease with decreasing  $R$  factors. The current value of  $C_d = 5$  for SCBFs appears appropriate for the upper stories of SCBF frames but underestimates the inelastic story drift of the bottom stories by a considerable amount for all but the tallest structures.

The overstrength factor is used to define the required resistance of certain capacity-controlled components. The overstrength factor was computed as the ratio of the maximum story shear computed from the dynamic analysis corresponding to the 2/50 hazard level,  $V_{max}$ , to the design story shear computed using the equivalent lateral force method,  $V_{ELF}$ , as given by Eq. 6.4.

$$\Omega_o = \frac{V_{max}}{V_{ELF}} \quad (6.4)$$

Figures 6.13a, b and c show the mean and the standard deviation values of the

calculated overstrength factors for 3-, 9- and 20-story buildings, respectively. The overstrength values also decrease with a decrease in the  $R$  factors. For the 3-story building model, the overstrength values were similar over all stories. For the 9- and 20-story building model, the overstrength factors in the lower stories were similar to the values computed in the 3-story building models and increased in the upper stories. The increased values in the upper stories likely resulted from selection of a less efficient brace cross section for these stories, resulting in larger design overstrength involved. With an  $R$  factor of 3 for low-rise buildings and an  $R$  factor of 6 for the mid- and high-rise structures (as well as neglecting the increase of the overstrength at the upper stories for mid- and high-rise buildings), an overstrength value of 2 is recommended, and this recommendation is consistent with current design code.



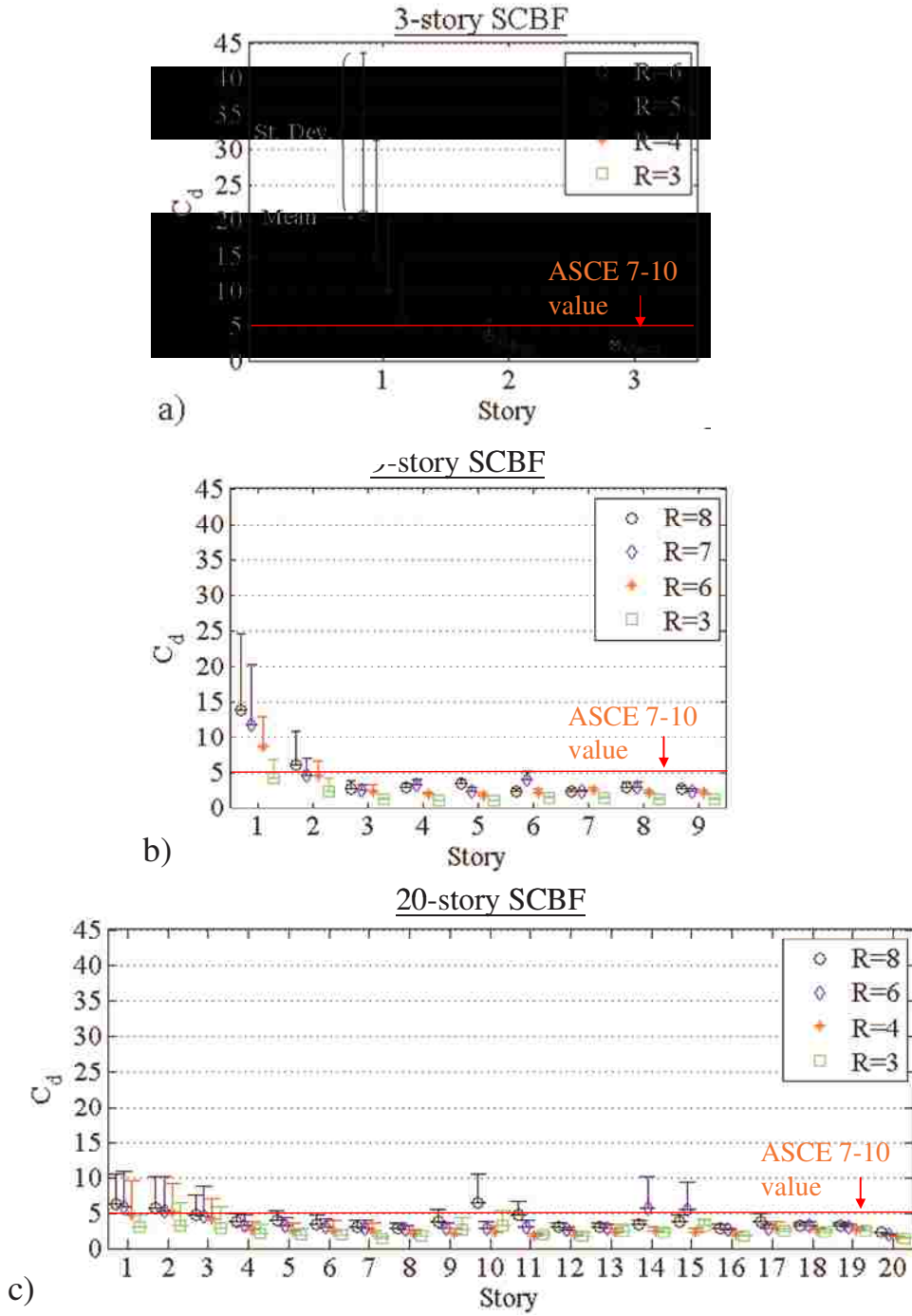


Figure 6.12 The Means and Standard Deviations of the Deflection Amplification Factors for (a) 3-, (b) 9- and (c) 20-story Buildings with Various R Factors.

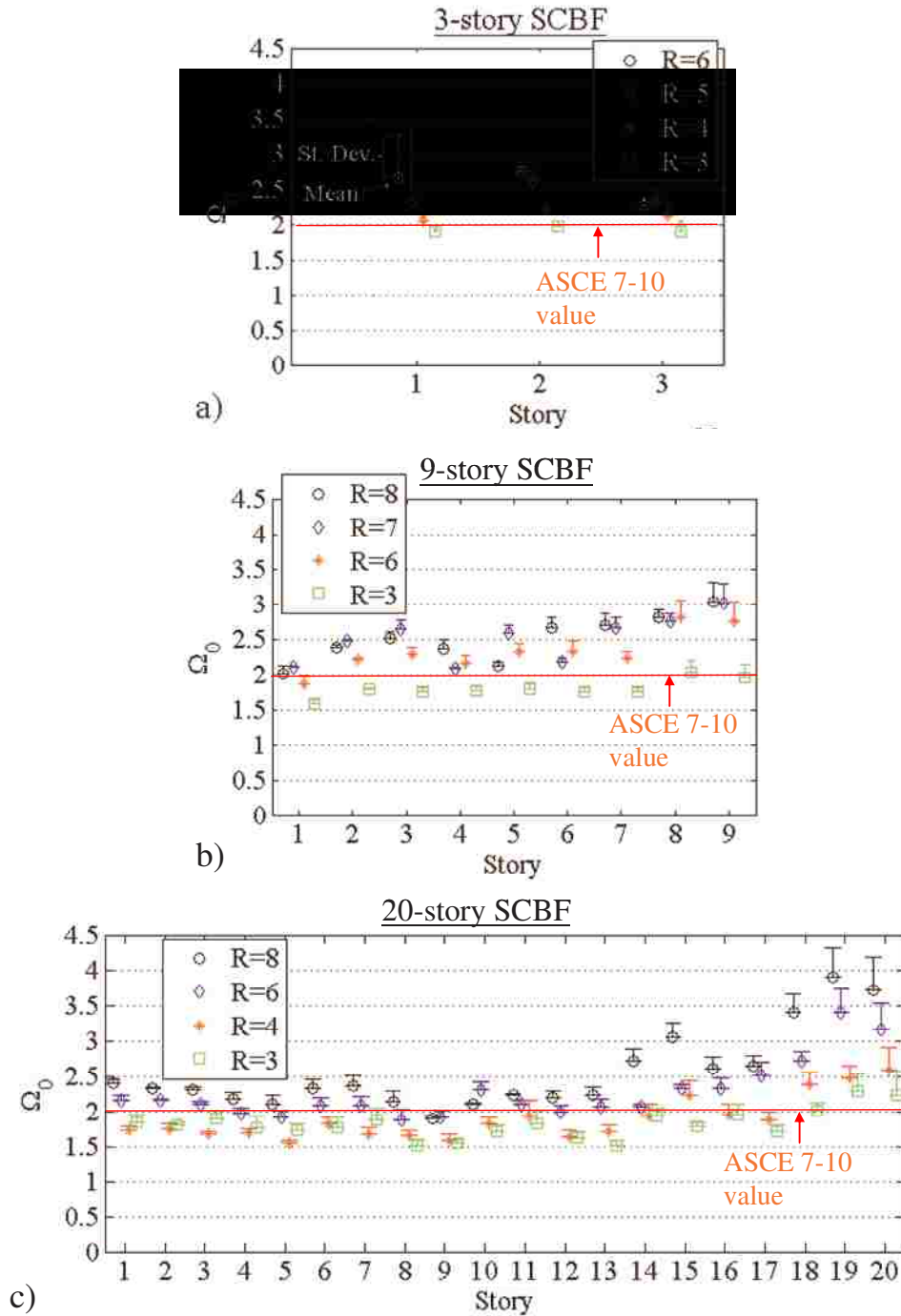


Figure 6.13 The Means and Standard Deviations of the Overstrength Factors for (a) 3-, (b) 9- and (c) 20-story Buildings with Various R Factors.

## 6.7 Comparison of the Proposed and FEMA P695 Procedures

Comparison of the FEMA P695 methodology with the alternate method described here raises several major concerns about accuracy and reliability of the FEMA P695 procedure for evaluation of braced frames. In particular:

- 1) The probability of the potential collapse estimated by the P695 methodology was significantly higher for the 20-story building models than for the 3-story building models. In stark contrast, the alternate analysis procedure clearly showed that the 3 story frames had much larger story drift demands with increased structural damage and brace fracture (for the hazard level corresponding to the 2% in 50 year event). This later finding is consistent with findings from other research (Chen and Mahin 2010).
- 2) The FEMA P695 procedure would suggest relatively a smaller R value is required for the 20-story (high-rise) buildings compared with the 3-story building. This is clearly different than the large body of existing knowledge of earthquake engineering, and it is in direct opposition to the alternate analysis performed here.
- 3) The FEMA P695 procedure is sensitive to the scaling methods used in IDA evaluation as shown by the different results achieved from scaling methods M1 and M2 in Table 6.5. This sensitivity increases the ambiguity of the method.

The results show that of the two evaluation methods, the proposed evaluation procedure is more reliable, for two reasons. First, the FEMA P695 focuses on an imperfect collapse assessment, which is difficult to validate. The alternate method evaluates validated multiple limit states. Furthermore, the alternate method considers the full range of seismic damage.

Second, the alternate method provides a rational mechanism for scaling the earthquake ground motions to meet both the seismic hazard level and expected structural performance. Higher mode effects are considered in the evaluation of the high-rise buildings; effects of structural damage on the dynamic response are incorporated as appropriate. Further, the alternate method captures a wide range of performance states that are 1) documented by experimental observations, 2) important to the building owner and occupants, and 3) ignored by the P695 method.

Both methods used a modeling approach, which employed the most accurate modeling of braced frame behavior used to date, since the models were validated to simulate the full range of behaviors and damage states, including brace fracture, observed in experiments. This final point emphasizes the primary limitation with the P695 procedure. Focusing solely the stability or toppling aspects of collapse does not provide a reliable method to provide consistent performance among building types. Collapse prediction is a highly uncertain response mechanism, difficult to fully simulate in a nonlinear dynamic response analysis, and its validation is not possible with the current experimentation. The P695 procedure extends this uncertain prediction with statistical predictions that imply great accuracy and reliability of the prediction. Engineers and building owners are more concerned by the probability of brace fracture, reparability of the structure, and other structural performance states that impact building performance. The alternate procedure provides a mechanism to estimate structural performance for SCBF systems and provide a consistent level of performance using the  $R$  value method.

## **Chapter 7 : Seismic Vulnerable of Older CBF Systems**

### **7.1 Introduction**

In high seismic regions, including those on the west coast and in certain areas in the Midwest of the US, SCBFs are required. SCBFs are designed with reduced seismic forces and special detailing requirements. Prior to 1988, CBFs were designed with reduced seismic design loads but without special detailing requirements (ICBO 1988), and these older CBFs are referred to herein as Non-seismic concentrically braced frames or NCBFs.

NCBFs may comply with older code requirements in high seismic regions or current code requirements in low seismicity regions. Many are still in service throughout the US, even in regions of high seismicity. Prior research described in Chapters 4, 5 and 6 focused on SCBFs, which have improved seismic performance relative to older frames. Although it is known that the seismic performance of NCBFs is substandard. There is significant uncertainty regarding quantification of their performance and collapse potential. A study was conducted to evaluate this vulnerability and is presented in this chapter.

The vulnerability of these frames is recognized by the earthquake engineering community, and this recondition has resulted in substantial changes to the design philosophy and detailing requirements for CBFs, and the advent of the modern SCBF system. However, comprehensive methods to evaluate NCBFs are absent in the literature.

In SCBFs, the connections are designed to withstand the deformations and loads that

result from brace yielding and buckling. In the current AISC Seismic Provisions (AISC 2010a), this design intent is addressed by requiring that the connection strength exceed the expected plastic capacities (both tension and compression) of the brace. Out-of-plane buckling of the brace is accommodated using geometric limits on the gusset plate relative to the end of the brace. Typically, engineers employ a  $2t_p$  linear clearance requirement, as shown in Fig. 2.1. Here, frames designed to meet AISC 2010, including the linear clearance requirement, are referred to as AISC-SCBFs in the model description and analysis results.

Recent research shows that although frames designed to the current code possess ductility, the inelastic deformation capacity of the frame is limited in that the yielding is restricted to a single element, which is the brace (Lehman et al. 2008). Extensive research into the seismic design and behavior of braced frames indicates that when the correct balance between brace yielding/buckling and connection yielding is achieved increased inelastic deformation capacity is possible. This research has resulted in the BDP, as described in Chapter 2, which balances the strength of the brace and capacity of the gusset plate to promote ductility and prevent potential failure modes (Roeder et al. 2011). In addition, the procedure promotes an  $8t_p$  elliptical clearance requirement (Fig. 2.2a), which further enhances constructability of these important systems by reducing the gusset plate area. Models designed to meet the BDP are referred to as BDP-SCBFs.

Prior to the 1988 UBC (ICBO 1988), CBFs were designed using reduced seismic design forces, which were also used to design the braces, beams, columns and connections. There was no consideration of overstrength, its impact on the connection demands or potential failure modes, or requirements for ductile detailing. As a result, these older CBFs are unlikely to exhibit ductile response because of connection failure

and are referred to herein as Pre-1988 NCBFs.

The design requirements for the three CBF systems, AISC-SCBF, BDP-SCBF and Pre-1988 NCBF systems are compared in Table 7.1. Each design requirement, or lack thereof, impacts the system behavior. The more stringent slenderness ( $KL/r$ ) and compactness requirements for SCBF braces reduce post-buckling degradation and provide higher resistance to low-cycle fatigue. Such requirements generally result in larger, less force-efficient brace sections.

Table 7.1 CBF Design Requirements

Component	Pre-1988 NCBFs ( $R_w=8$ )	AISC-SCBF (R = 6): 1997-Current	BDP-SCBF (R = 6)
Sys. Configs.	No limitations	K bracing not allowed, requirements for V & inverted-V	
Braces	$KL/r < 200$ (recommended)	$KL/r < \sim 100$ with exceptions; seismic $b/t$ limit	
Net Section	ASD for service loads	Design for $R_y F_y A_g$ of brace with $\phi$	Design for $R_y F_y A_g$ of brace with $\beta$
Brace Connections	ASD for nominal brace tension or service loads without 33% stress increase	Design for $R_y F_y A_g$ and $1.1R_y P_n$ of brace & permit end rotation of brace with $2t_p$ clearance	Design for $R_y F_y A_g$ and $1.1R_y P_n$ of brace to meet tensile strength of gusset using $W_w$ . Permit end rotation of brace with elliptical $8t_p$ clearance (corner) and linear $6t_p$ clearance (midspan)
Beams	ASD for service loads	V & inverted-V systems design for unbalanced load and amplified seismic load.	
Columns	ASD for service loads	Design for minimum of maximum load of $1.1R_y$ times brace strength or amplified seismic load.	
Column Splices	ASD for service loads	Column design axial load, $0.5M_p$ flexure, plastic shear strength; special PJP weld requirements.	

In comparison Pre-1988 NCBFs have no special detailing requirements, resulting in uncertainty in the strength balance between the brace and the connection, (e.g., some connections will be stronger than the brace and others will be weaker). Finally, NCBF design requirements above do not establish a clear hierarchy of yielding and failure, resulting in uncertain seismic response and high susceptibility to connection failure, frame member damage and soft-story collapse relative to SCBFs.

This study presents research aimed at improving the understanding of NCBF

performance, and the primary content of the chapter was addressed in a journal paper as documented in Appendix G. The research integrated experimental and analytical approaches. First, a pilot experimental study of a single-story NCBF frame was conducted. This test used a similar test setup and specimen configuration as prior tests on SCBFs designed to develop and investigate the BDP (Roeder et al. 2011). The experimental results show the limited deformation capacity and rapid loss of resistance of these prevalent systems.

These test results were used to advance a nonlinear model of NCBF behavior, an extension of a model developed for AISC-SCBF and BDP-SCBF simulation described in Chapters 4 and 5. The model was used to conduct nonlinear response history analyses, to investigate the performance and collapse potential of NCBF systems, and to perform a comparative analysis with SCBF systems. For the investigation, a three-story prototype building was designed using both Pre-1988 NCBF and SCBF requirements. Prior analyses in Chapter 6 and damage in prior earthquakes show that short-story structures are more vulnerable than taller counterparts (e.g., Chen and Mahin 2010, AIJ 1995).

## **7.2 Experimental Results of A NCBF**

A one-story, one-bay NCBF specimen was tested. The test setup was the same as that used for the prior one-story SCBF tests. Figure 7.1 shows the specimen dimensions and experimental setup of the single-story SCBF tests. Example experimental results, including the Specimen HSS5 and HSS12, are shown in Fig. 7.2. Figure 7.2a shows the force-displacement response of a specimen designed to the BDP (Specimen HSS5), and its connection details are shown in Fig. 7.1c. Figure 7.2b shows the response of a



nominally identical specimen, Specimen HSS12, designed to meet the 2005 AISC Seismic Design Provisions (AISC 2005), and Fig. 7.1d shows its connection details. Specimen HSS12 used a CJP weld at the gusset-to-beam and column interface to avoid premature weld fracture sustained by a nominally identical specimen with fillet welds (Lehman et al. 2008). Comparison of the performance of HSS5 and HSS12 demonstrate the ductility of the SCBF and the superior performance of the BDP-SCBF specimen. It is clear that the BDP efficiently controls the yielding and failure hierarchy and maximizes SCBF system ductility before brace fracture.

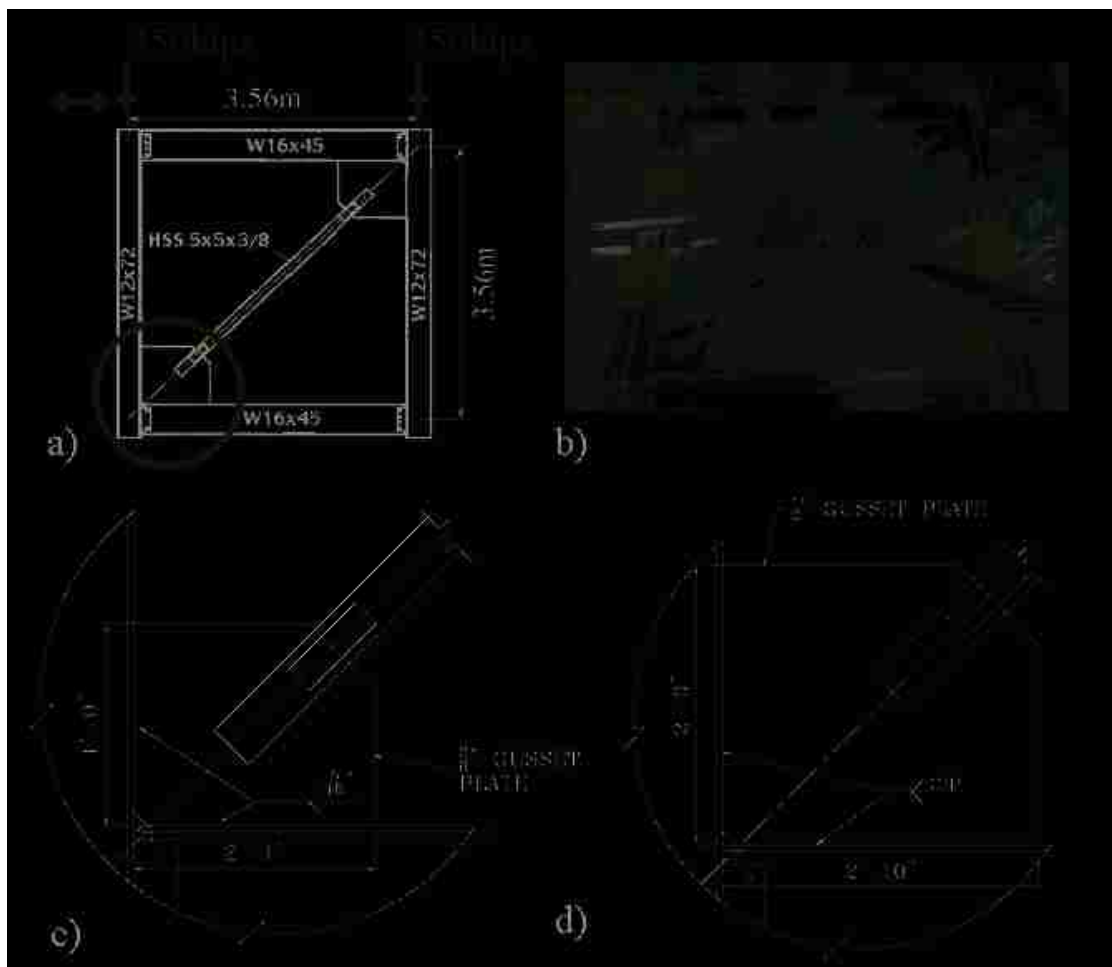


Figure 7.1 Typical (a) Specimen Dimensions and Sizes for SCBF Specimen, (b)

Specimen Photo of Those Single-story Experiments in the Recent SCBF Research, (c) Dimensions of the Gusset Connection of HSS5(BDP) and (d) HSS12(AISC 2005).

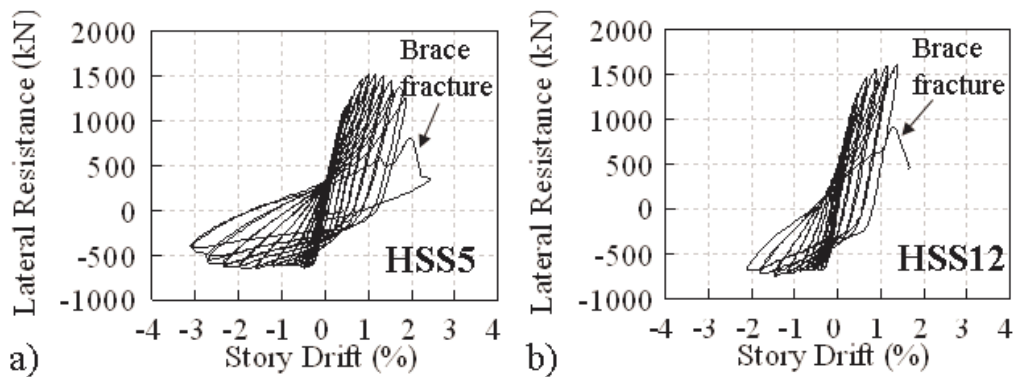


Figure 7.2 Hysteretic Responses of Single-story Frame Specimen (a) HSS5(BDP) and (b) HSS12(AISC 2005)

Using experimental infrastructure built for the prior SCBF study, a pilot NCBF test (Fig. 7.3), designated NCBF32, was conducted. The test consisted of a single-story, single-bay frame with a single HSS6x6x1/4 brace. The test specimen was designed to have a similar force capacity as Specimens HSS 5 and HSS12. However, the brace selected did not meet current width-to-thickness limits for SCBF and the connections were not designed for the expected capacity of the brace. Instead, following design procedure employed prior to 1988, the connections were designed for the design compression strength of the brace using the nominal brace material strength. In the 1988 UBC specification, the connection strength would have been determined from the ELF procedure. In the experiment, the lower bound strength of the brace was used to approximate that force. No special detailing of the gusset plate was carried out. Further, the connection employed a field bolted configuration, where the gusset plate and beam

were bolted to the column by a double angle connection as shown in Fig. 7.3a. The brace and double angles were welded to the gusset plate and beam web. The welds were sized to the compressive design strength of brace. In the test, the welds were AISC demand critical weld rather than less tough welds commonly used in 1988, because of material availability.

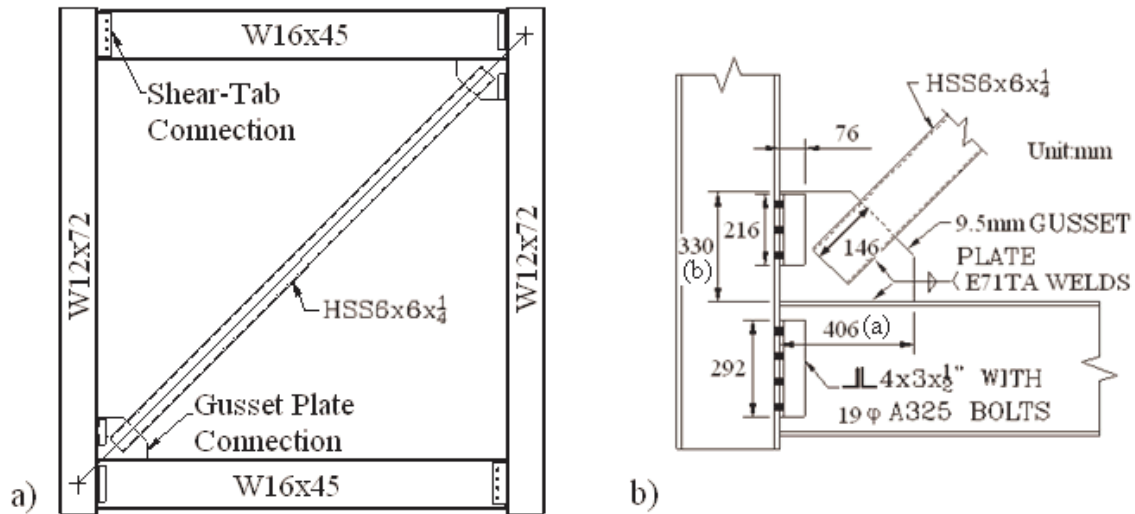


Figure 7.3 Dimensions of (a) Specimen NCBF32 and (b) the Connection Details

Figure 7.4 illustrates the measured lateral force-displacement response and progression of damage for Specimen NCBF32. Limited brace buckling was noted at approximately -0.36% story drift and at a compressive load of approximately 812kN (182 kips). The buckling deformation was very limited as shown in Fig. 7.4a. The calculated  $P_{cr}$  of the brace based upon measured material properties with  $K$  equal to 1.0 and using the actual brace length was 734 kN (165 kips). At 0.44% story drift initial cracking developed in all fillet welds joining the brace to the gusset plate, and the crack length grew longer to approximately 125 mm, during the second cycle to this drift level. At

0.52% story drift, these fillet welds were completely fractured as shown in Fig. 7.4b, and initial tearing was noted at the net section of the brace. It should be noted that the use of tougher E71T8 welds probably provided greater ductility and deformability to this connection prior to complete weld fracture. The fracture of the weld connecting the brace to the gusset resulted in a sharp and dramatic reduction in lateral resistance, as shown in Fig. 7.4. While the fillet welds joining the brace to the gusset fractured at small lateral deformations, the brace was still partially effective in compression at larger negative story drift, because the slotted brace was binding on the gusset plate when the deformation caused the brace slot to close. This behavior caused the modest hump in the compressive resistance seen in Fig. 7.4 at drifts in the range -1.50 to -3.00%. This secondary compressive loading caused substantial deformation of the gusset and increased deformation demands on the beam and gusset connection to the column.

The primary source of lateral resistance at story drift larger than 0.52% is attributed to the beam-to-column connection at the gusset, which retained significant moment resistance. From 0.50% to 2.00% drift the bolted angle connections sustained significant deformation and prying, and the angles fractured at approximately 3.10% story drift (Fig. 7.4c). Gusset-to-beam weld fracture was noted at a similar story drift. The gusset-to-beam weld of the opposing gusset connection failed at similar deformation (Fig. 7.4d).

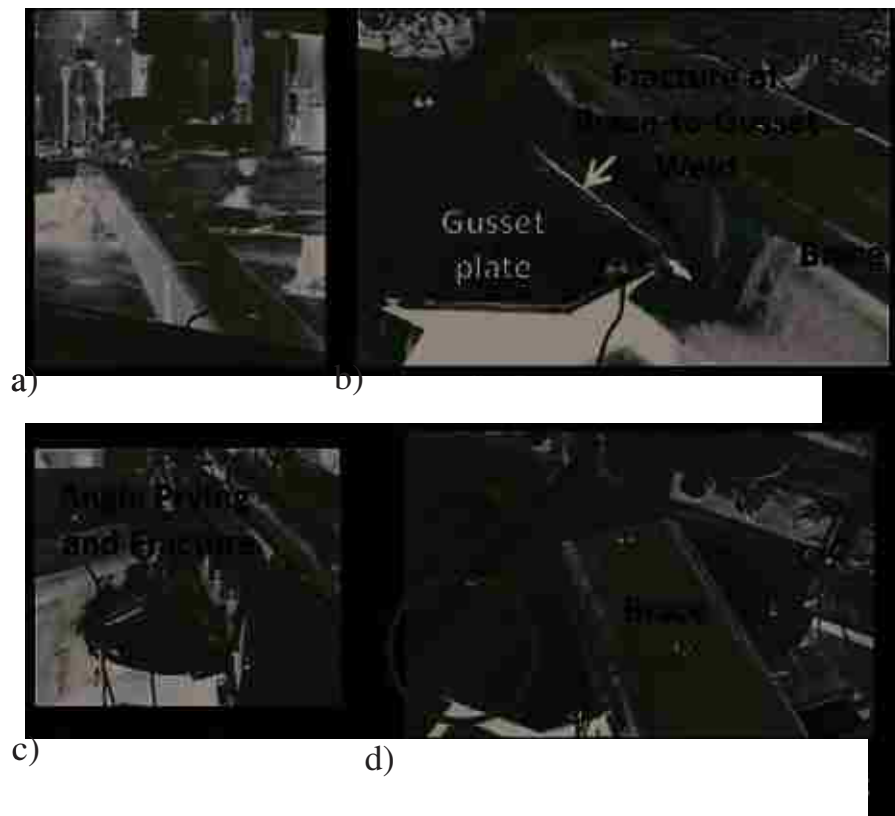
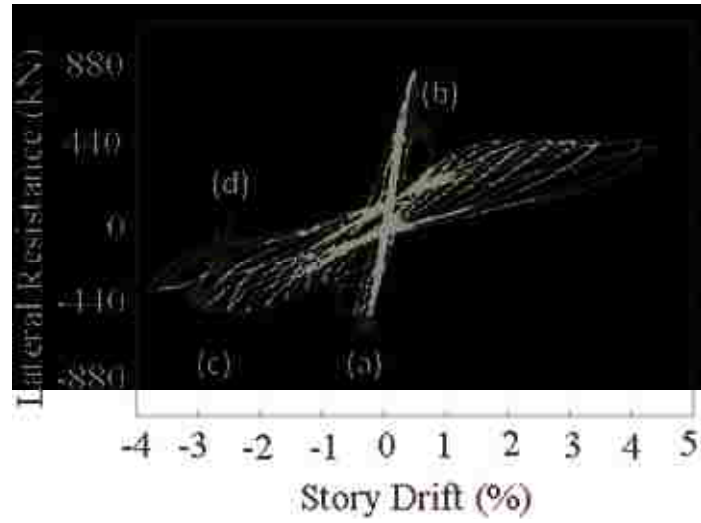


Figure 7.4 Hysteretic Responses of the Pilot NCBF (NCBF32); the Photos of (a) Local Buckling, (b) Connection Fracture, (c) Fracture of Gusset Connecting Angle, and (d) Weld Failure in Opposing Gusset.

The test results for NCBF32 indicated that: (1) the connection substantially impacts

the system response and capacity, (2) inadequate connections can result in a the failure mode that is brittle and therefore difficult to predict analytically, and (3) there is post-damage resistance that may potentially influence the collapse potential of these systems.

### 7.3 Nonlinear Line Element Models for CBF Systems

The nonlinear models developed and described in Chapter 4 and 5 were adapted for a study of the performance of NCBF buildings. The proposed improved models (described in Chapter 4) with the prediction of brace fracture (described in Chapter 5) were used for modeling the AISC-SCBF and BDP-SCBF systems. These models were developed in OpenSees framework (McKenna 1997) and include the occurrence of brace fracture. This model was modified to simulate the NCBF systems, and the experimental results for NCBF32 were used for calibration and validation of the model. The following modifications were made to adapt that approach to NCBFs and to quantify the important variables for the model.

Figure 7.5a illustrates the overall NCBF model and Fig. 7.5b shows the modified concentrated spring element model of the gusset plate and beam-to-column connections. The key differences between the SCBF and NCBF models are:

(1) Inclusion of a zero-length spring in the axial direction of brace. The spring connects the node at end of the brace and the rotational spring. The spring was calibrated to model fracture of the brace-to-gusset connection as observed in the test.

(2) Inclusion of an in-plane rotational spring at the beam-to-column connection. The gusset properties were used to calculate the flexural resistance of the connection,

including the contribution of the gusset plate. The modeling approach used to simulate the shear-tab connections was adopted to simulate the response of the beam-to-column connection modified to include the gusset plate stiffness and strength. The model used the Pinching4 material model, and Fig. 7.6a shows the used model. Initial rotational stiffness and maximum positive ( $M_{\max}^+$ ) and negative moments ( $M_{\max}^-$ ) values in the model were calibrated by the test results of NCBF32. The used  $M_{\max}^+$  and  $M_{\max}^-$  were 880 and -880 kN-m, respectively. The positive ( $M_{\text{res}}^+$ ) and negative residual moment strengths ( $M_{\text{res}}^-$ ) were determined to use plastic moment capacity of the shear-tab cross section to represent the strength of the beam-to-column connection after the bolted angle connections fracture. The used  $M_{\text{res}}^+$  and  $M_{\text{res}}^-$  were 200 and -200 kN-m, respectively. Modeling this connection allowed simulation post brace-connection fracture.

Full performance evaluation of CBFs requires models to simulate fracture. Modeling fracture allows analyses to continue beyond initial fracture of the brace or brace connection to achieve post-fracture performance evaluation. In the SCBFs fracture was initiated in the brace; in the NCBFs fracture occurred in the brace-to-gusset plate connection. In both cases, a practical approach for modeling was used. The brace fracture model proposed in Chapter 5 (Fig. 7.6b) was used for the braces in both of SCBF and NCBF systems in the study. In addition, a new fracture model of the brace connections was developed and added to the model of NCBF systems with the validation of the pilot experimental test (NCBF32).

In the test of NCBF32 fracture occurred at the weld connecting the brace to the gusset plate. It should be noted that this failure mode was specific to this connection design; however, evaluation of other connections indicates that this failure mode is likely in other connection configurations common in NCBFs or that some other failure mode is

likely to make the brace ineffective at a relatively low story drift. There are large variations in existing NCBF connection designs, and therefore response of NCBF connections may vary widely. However, this model clearly simulates some response modes that will occur and will compromise NCBF performance. This study looked at a particular type of connection, but its results are indicative of trends in NCBF performance.

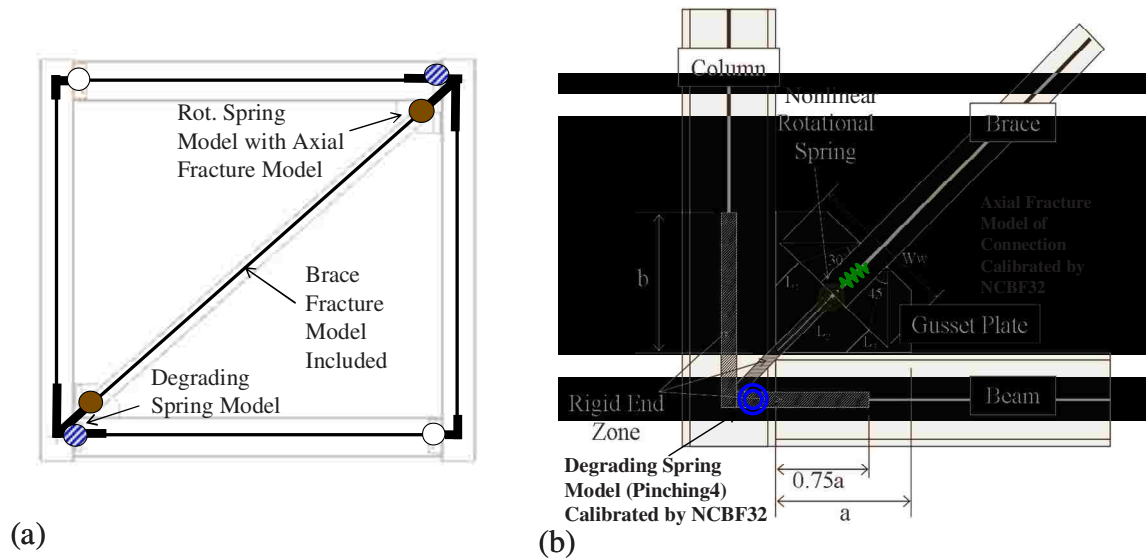


Figure 7.5 Illustrations of the Analytical Models of (a) NCBFs, and (b) Connections of NCBFs.



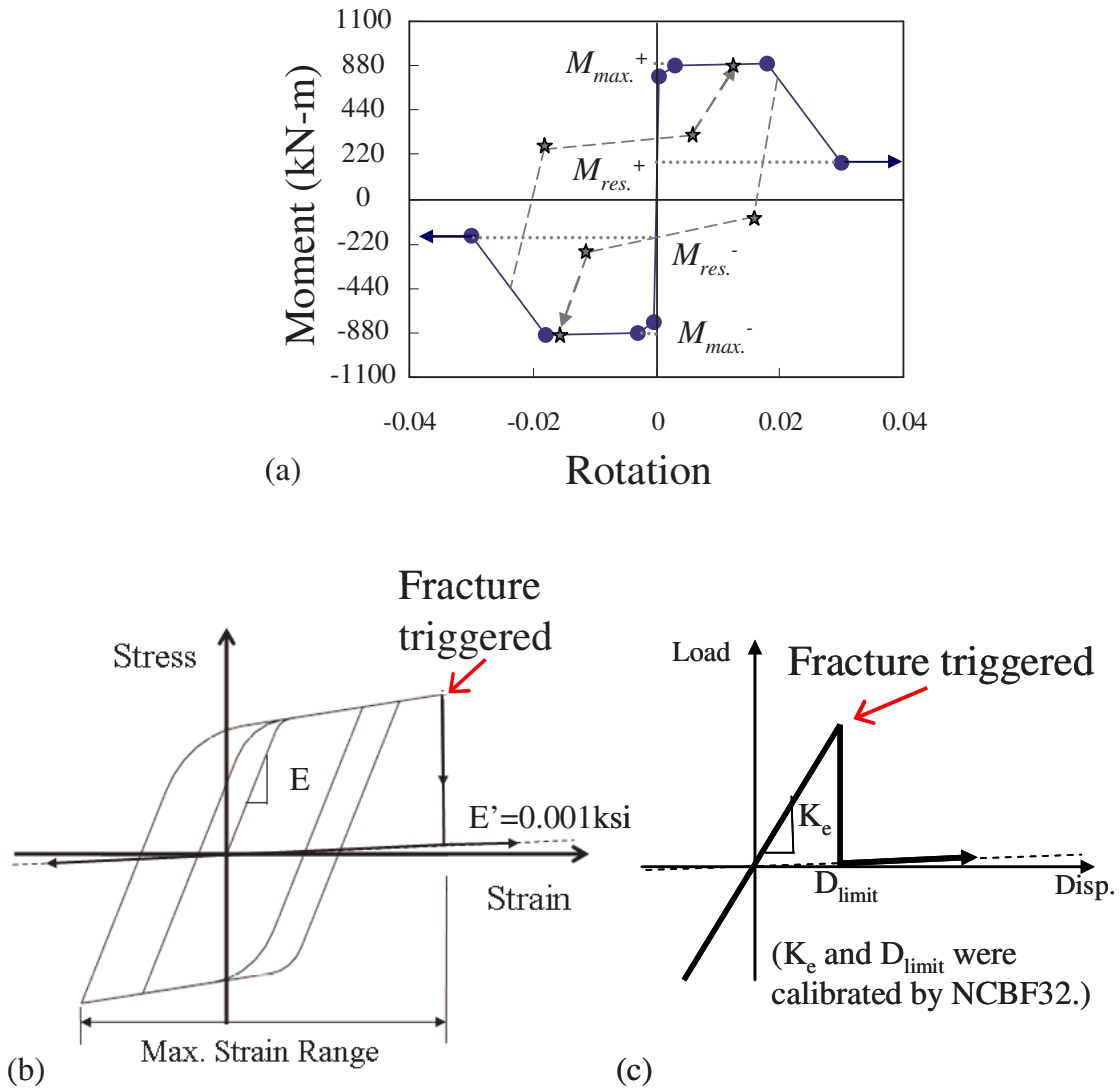


Figure 7.6 Illustrations of Models Representing: (a) Degrading Moment-Rotation Response using the Pinching4 Material Model, (b) Fiber Fracture Applied to the Brace Cross Section, and (c) Brace Connection Fracture.

As shown in Fig. 7.4b, the weld fracture of the test specimen grew rapidly and caused full fracture of the brace-to-gusset weld joint. This fracture behavior was simulated in the OpenSees models of NCBF systems by adding a zero-length spring in the axial direction of the brace at the brace ends. The constitutive model of the spring, as illustrated in Fig. 7.6c, was given an initial stiffness of 5700kN/mm and fracture was

simulated to occur at an axial deformation of 0.14mm. The post fracture response was a flexible elastic material model having a very small stiffness (0.001ksi); a non-zero stiffness value was needed to ensure convergence. After connection fracture, the model simulate the brace as ineffective. These values were calibrated to the test results for NCBF32 and are likely to vary for other NCBF connection configurations. However, in the absence of any additional NCBF test data they are adopted here for the purpose of evaluating system level response.

Figures 7.7a and b compare the experimental and analytical responses for single-story single-bay test specimens designed using the BDP (Specimen HSS5) and the current 2005 AISC Seismic Design Provisions (Specimen HSS12). Figure 7.7c compares the experimental and analytical response for Specimen NCBF32. In all cases, the response is well predicted by the OpenSees models.

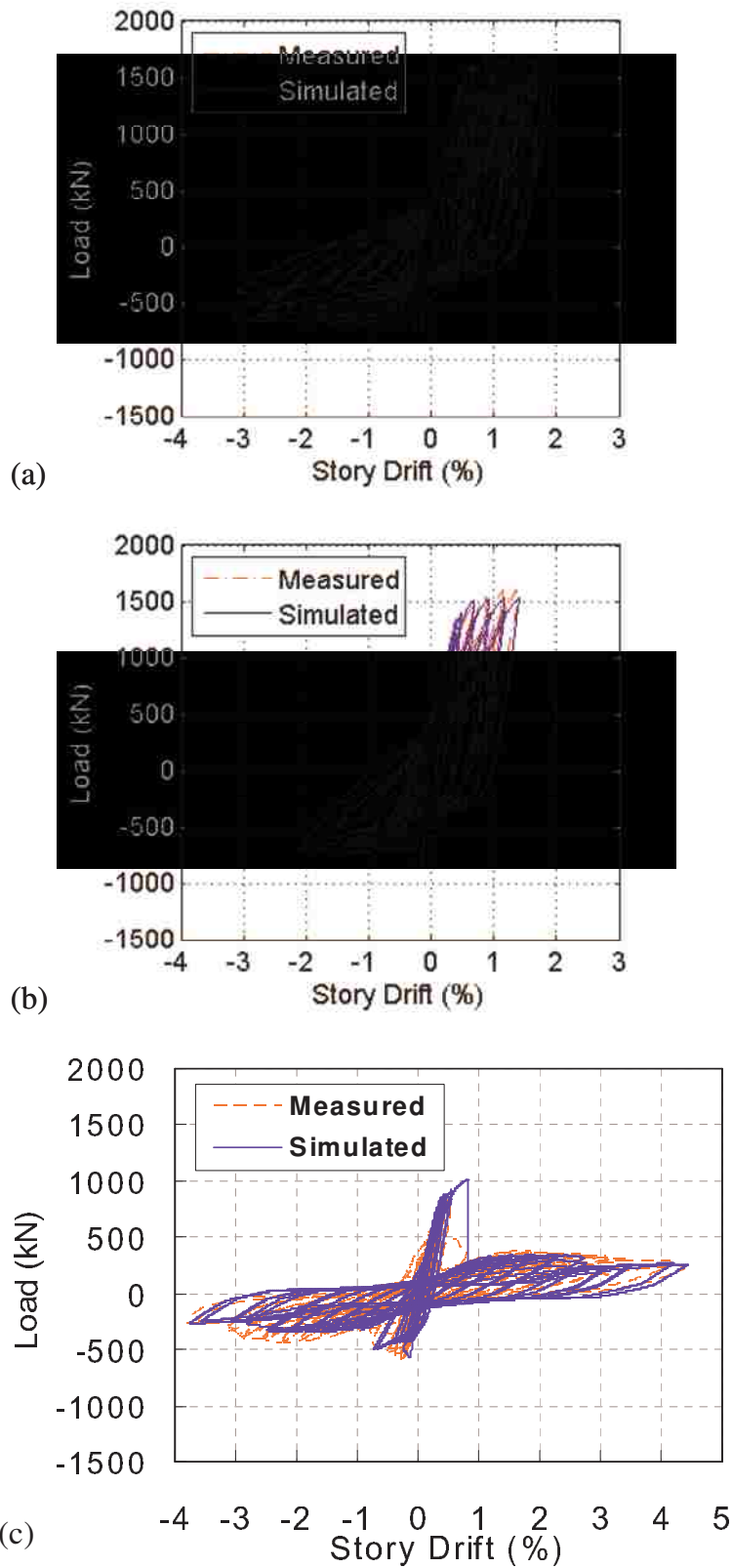


Figure 7.7 Comparison of Analytical and Experimental Responses, Including Fracture.

## 7.4 Nonlinear Dynamic Analysis of SCBF and NCBF Systems

A series of nonlinear dynamic analysis were conducted to evaluate and compare the seismic performance of the SCBF and NCBF systems. An idealized three-story building was the vehicle for this comparison. A three-story building configuration similar to those used in earlier chapters was re-designed.

Three different versions of this prototype braced frame system were designed for performance evaluation. They included: (1) a building with SCBFs designed using current AISC design (AISC-SCBF), (2) a building designed using the proposed balanced design procedure (BDP-SCBF), and (3) an NCBF building designed according to the UBC code used in the seismically active regions of the western US before 1988 (Pre-1988 NCBF).

The SCBF building models were designed to meet the NEHRP design spectrum using the United States Geological Survey's (USGS) mapped spectral acceleration values at 2% in 50 years hazard level for the location of Seattle (updated in 2008), as shown in Fig. 6.7a. The NCBF building model was designed to meet seismic base shear defined the 1988 UBC code for the location of Seattle. The AISC-SCBF and BDP-SCBF buildings were designed using  $R = 6$ , and were identical except the design of the gusset plate connections. The Pre-1988 NCBF building was designed using the system performance factor,  $R_w$ , equal to 8 per the 1988 UBC code.

Table 7.2 shows the resulting member sizes and material yield strengths used in the models, and Table 7.3 provides the dimensions of the gusset plate connections, as illustrated in Fig. 7.5. The braces of SCBFs satisfied the compactness requirement given

by AISC seismic provisions, while the braces of NCBFs did not.

Table 7.2 Member Sizes, Material Strengths and Weights of the Lateral braced Bays of the Three-story CBF Buildings

Building	Story	Beam		Column		Brace		Weight (kN)
		Size	F <sub>y</sub> (MPa)	Size	F <sub>y</sub> (MPa)	Size	F <sub>y</sub> (MPa)	
SCBF (BDP and AISC)	1 <sup>st</sup>	W21x93	400	W14x90	400	HSS 6x6x5/8	455	9379
	2 <sup>nd</sup>	W21x93		W14x90		HSS 6x6x1/2		9379
	3 <sup>rd</sup>	W24x104		W14x90		HSS 5x5x1/2		9011
Pre-1988 NCBF	1 <sup>st</sup>	W18x97	400	W12x58	400	HSS 6x6x3/8	455	8493
	2 <sup>nd</sup>	W18x97		W12x58		HSS 5.5x5.5x3/8		8493
	3 <sup>rd</sup>	W18x97		W12x58		HSS 5x5x3/8		8159

Table 7.3 Dimensions of the Gusset Plates in SCBF Buildings

Building	Story	Location	a (mm)	b (mm)	t <sub>p</sub> (mm)
BDP-SCBF	1 <sup>st</sup>	Bottom	643	711	15.9
		Top (midspan)	648	495	
	2 <sup>nd</sup>	Bottom (midspan)	594	450	
		Top	757	536	
	3 <sup>rd</sup>	Bottom	673	462	
		Top (midspan)	584	404	
AISC-SCBF	1 <sup>st</sup>	Bottom	752	823	15.9
		Top (midspan)	998	823	
	2 <sup>nd</sup>	Bottom (midspan)	919	754	
		Top	980	744	
	3 <sup>rd</sup>	Bottom	663	673	
		Top (midspan)	833	640	
Pre-1988 NCBF	1 <sup>st</sup>	Bottom	587	649	9.5
		Top (midspan)	592	452	
	2 <sup>nd</sup>	Bottom (midspan)	533	404	
		Top	679	481	
	3 <sup>rd</sup>	Bottom	479	329	
		Top (midspan)	416	287	

In all cases, rectangular gusset plates were used. The current AISC design procedures recommend a  $2t_p$  linear clearance, which results in a much larger gusset plate

design relative to the elliptical clearance proposed by the BDP, as shown in Table 7.3. In addition, all of the SCBF beam-to-column connections were welded-flange welded-web connections, while all of those in NCBF frames were shear-tab connections. The SCBF beams and columns were designed to sustain the tensile and compressive capacities of the braces while the NCBF frames were designed using the lateral loads obtained from elastic ELF analyses using a vertical truss model for the braced frame. Thus, the beams and columns were much smaller in the NCBF system.

The second-order effects from gravity loads, also termed P-delta effects, were included in the nonlinear dynamic analysis via a leaning column model. This model represents the properties of the gravity frames tributary to each CBF, as described in Section 6.3. There are two seismic frames in each orthogonal direction of the building, therefore half of the gravity load was applied to the leaning column at each floor level. The base of the leaning column was pinned. The leaning column had a cross-sectional area, moment of inertia and plastic moment capacity equal to the total of the gravity columns for half of the building (11.5 columns total).

#### **7.4.1 Selection and Scaling of Ground Motions**

The SAC Seattle ground motions representative of two different hazard levels with probabilities of exceedance of 2% and 10% in 50 years were used (denoted 2/50 and 10/50 respectively). The scaling process is described in Section 6.5. The SAC ground motions were scaled to match the spectral acceleration values corresponding to the target spectrum for each hazard level. The target spectrum for each hazard level was obtained following the ASCE-7 for New Buildings and Other Structures (ASCE 7 2010) using the

USGS mapped spectral acceleration values (updated in 2008) as a representative of current ground motion intensity at the location of Seattle. Note that when computing the target spectrum values for various hazard levels the 2/3 reduction factor was not used. The site class effect was included and the damped spectra was adjusted to 2% damping by applying  $\beta_S$  and  $\beta_I$  factors of 0.8. Figure 6.7a shows a comparison of the target spectra for the two hazard levels comparing with the design spectra used for the SCBF buildings in the study.

For the NCBF buildings, it was assumed that the brace-to-gusset connections would fracture rapidly through entire story. Therefore, the ground motions for the 2/50 hazard levels were scaled using the fundamental period ( $T_{1,NCBF}$ ) and the periods of the frame losing all of the braces at the critical story ( $T_{2,NCBF}$ ), as shown in Fig. 7.8b.

The following expressions of scaling factor,  $f_{10/50}$  and  $f_{2/50}$ , were used to scale each ground motions for each hazard level.

$$f_{10/50} = \frac{Sa_{1,t}}{Sa_{1,g}} \quad (3a)$$

$$f_{2/50} = \frac{Sa_{1,t}}{Sa_{1,g}} w_1 + \frac{Sa_{2,t}}{Sa_{2,g}} w_2 \quad (3b)$$

In the expression  $Sa_{i,t}$  is the target elastic spectral acceleration value at the  $T_i$  period,  $Sa_{i,g}$  is the elastic spectral acceleration value of the ground motion at the  $T_i$  period,  $w_i$  is the weight for the  $T_i$  period. The weights for the NCBF model were 0.6 for  $T_{1,NCBF}$  and 0.4 for  $T_{2,NCBF}$ . All used scaling factors of the ground motions for different building types are listed in Appendix G.2.

The target and median acceleration spectra for each hazard levels, 10/50 and 2/50, for those BDP-SCBF, AISC-SCBF and Pre-1988N CBF buildings are shown in Figs. 6.8a 7.9a and b, respectively. The periods used in each scaling method are also marked in the

figures. It should be noted that the larger gusset plates in the AISC-SCBF frame led to longer rigid links at the gusset plate connections and overall stiffer frames and smaller first fundamental periods relative to the BDP-SCBF building.

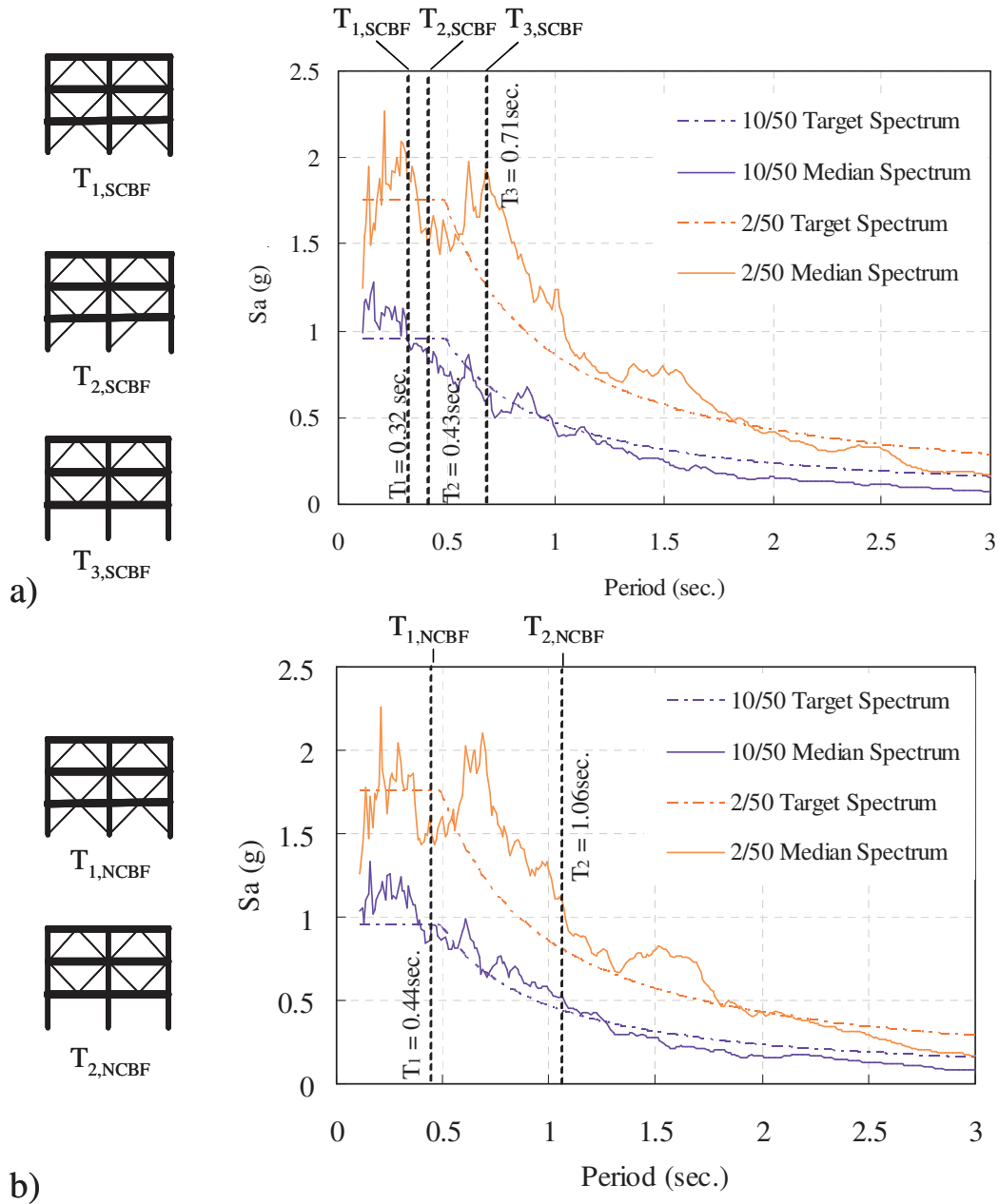


Figure 7.8 Target and Median Spectra of (a) AISC-SCBF and (b) Pre-1988 NCBF



## 7.4.2 Seismic Performance of CBFs

Nonlinear dynamic analyses using a total of forty SAC ground motions were conducted to determine the seismic performance of the three CBF buildings. Three damage states, including brace buckling or yielding, fracture of the brace or connection, and potential collapse were assessed. Yielding and buckling were based on the computed brace response. Fracture of the braces or connections was assessed using the fracture models that were described in earlier chapters.

As described in Section 6.5, collapse assessment cannot be experimentally verified with the available data. A story drift limit of 5% was adopted as the potential collapse criteria, because prior experiments showed that braced frames have considerable inelastic deformation capacity after brace fracture due to the gusset plate connections. Therefore basing collapse solely on brace fracture is unduly conservative.

Figure 7.9 shows the likelihood of each resulting damage state for the BDP-SCBF, AISC-SCBF and Pre-1988 NCBF. The responses for both the 2/50 and 10/50 hazard levels are shown.

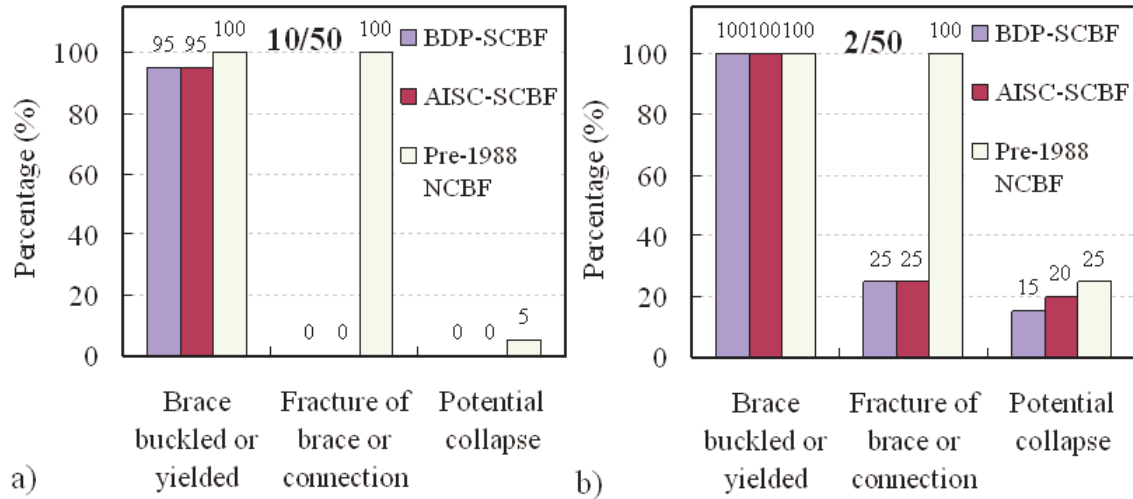


Figure 7.9 Seismic Performance of the Western CBF Buildings at (a) 10/50 and (b) 2/50 Hazard Levels

For the 10/50 hazard level, the analysis indicates a 100% probability of brace connection fracture and 5% probability of collapse potential for the NCBF model. When subjected to the 2/50 ground motions, the NCBF model has a 100% probability of fracture and a 25% probability of collapse potential. The results demonstrate that NCBF systems are susceptible to severe damage and potential collapse.

In contrast, the SCBFs systems have a much lower probability of damage, in particular for the 10/50 event, where no significant damage was predicted. In the 2/50 event, the AISC-SCBF has a 25% probability of brace fracture and 20% probability of collapse potential. The Pre-1988 NCBF sustains severe damage, even in the 10/50 event. This analysis clearly demonstrates the significant vulnerability of these vintage CBF buildings.

At first glance, Figure 7.9 appears to demonstrate minimal improvements afforded by the BDP-SCBF frame. In comparison to the AISC-SCBF models, those systems appear to have similar damage and collapse potential. However, closer scrutiny indicates

a lesser collapse potential for BDP-SCBF. Figure 7.10 presents the maximum story drift range (MSR) through the 20 ground motions at the 2/50 hazard level. The darker bar in the figure, designated as post-fracture, represent the additional frame deformation beyond brace fracture. In both cases, five out of 20 events resulted in brace fracture. However, BDP-SCBF frames achieved larger ductility prior brace to fracture by 32% compared with the AISC-SCBF frame indicating the additional safety of these systems.

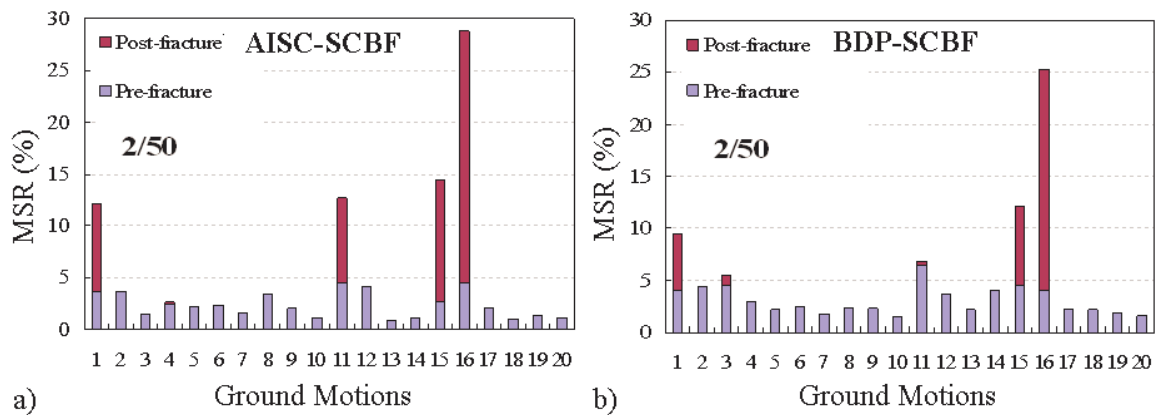


Figure 7.10 Maximum Story Drift Range, MSR, Over 20 Ground Motions at 2/50 Hazard Level For (a) AISC-SCBF and (b) BDP-SCBF Buildings

### 7.4.3 Comparison of P695 Evaluation of SCBF and NCBF Buildings

The 3-story Pre-1988 NCBF model building was evaluated following the FEMA P695 method and compared to the results of the equivalent SCBF model building designed following BDP (BDP-SCBF) as described in Section 6.4.2. Similar with the analyses for SCBF in the previous chapter, the SAC ground motion records for 2%-in-50 year seismic hazard level were adopted for collapse assessment following the IDA procedure. The ground motions were increased until collapse was predicted, and the scaling Method M1 (as described in the previous chapter), which follows the P695

method, was used. A collapse limit state corresponding to 5% story drift was again used. Figure 7.11 shows the results of the IDA process for the NCBF building. The result of  $\hat{S}_{CT}$  upon the IDA procedure was subsequently used to estimate CMR and ACMR and then compared with the acceptable ACMR20% values. Table 7.4 summarized the parameters and results of the evaluation for the NCBF building comparing with the results of the BDP-SCBF building obtained from previous chapter. The results show that this NCBF building “passes” the evaluation criteria following the P695 methodology while the equivalent BDP-SCBF building “fails”. These results are contrary to findings from prior earthquakes and current knowledge that NCBFs are deemed more vulnerable than SCBFs. This again shows the limitation with P695 procedure as described in Section 6.7.

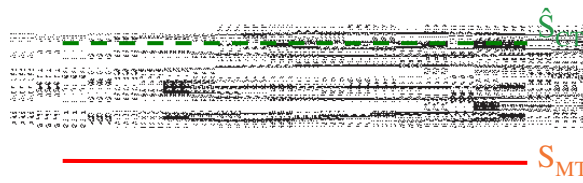


Figure 7.11 IDA Results for the 3-story NCBF Building using M1 Scaling Method with Collapse Story Drift Capacity of 5%.

Table 7.4 Summary of Evaluations of the 3-story SCBF and NCBF Buildings Using  
FEMA P695 IDA Procedure

Frame System	Pre-1988 NCBF	BDP-SCBF
$R$ Factor	8 ( $R_w$ )	6
$S_{MT}$ (g)	1.12	1.76
$\hat{S}_{CT}$ (g)	2.36	1.88
CMR	2.11	1.07
SSF	1.15	1.3
ACMR (CMR $\times$ SSF)	2.75	1.39
Accep. ACMR20%	1.73	1.73
Pass/Fail	<b>Pass</b>	Fail



## **Chapter 8 : Summary, Conclusions and Recommendations**

Concentrically braced frames (CBFs) have been commonly used for seismic design in recent decades. Their large stiffness and resistance led to economical design and easily meet the serviceability limit state of PBS. However, the plastic behavior of these systems is complex and highly nonlinear during large, infrequent earthquakes. CBFs were designed without special detailing requirements prior to 1988. These frames were recognized by the earthquake engineering community as vulnerable, which led to substantial changes to the design philosophy and detailing requirements of CBFs and resulted in the modern special concentrically braced frame (SCBF) system currently used in active seismic regions, on the west coast and in certain areas in the Midwest of the US.

To better understand and improve the seismic performance of the systems, an experimental and analytical research project, titled “NEESR-SG International Hybrid Simulation of Tomorrow’s Braced Frames”, was undertaken. More than 38 tests including single-story to multi-story complete braced frames were conducted. The project emphasizes the design of gusset plate connections, and the BDP was proposed to improve the performance of the gusset plate connections and further extend the system ductility of SCBFs. To extend the results of the experimental studies to explore seismic performance including the collapse potential of the CBFs (older, current and improved SCBFs), the investigation of this dissertation was performed 1) to develop the nonlinear model of SCBFs 2) and brace fracture model, 3) to establish the appropriate evaluation method of

seismic performance of SCBFs, and 4) to compare with the results using FEMA P695 methodology.

The studies in this dissertation are primarily the analytical portion of the braced frame research project which have carried out to 1) evaluate performance and improve the continuum finite element analytical models of SCBFs, 2) develop discrete line element models of SCBFs with brace fracture modeling, and 3) evaluate seismic performance of SCBF systems and the vulnerability of older CBF systems.

## **8.1 Continuum Finite Element Simulations of SCBFs**

A series of 3-story, single-bay SCBF experiments were investigated through a continuum FE analytical study to confirm the overall design of test specimens and to evaluate the designs of midspan and double corner gusset plate connections and in-plane-buckling connections. The FE model was extended from the prior analytical study by Yoo (2006). The fine element mesh and detailed modeling of connections employed by Yoo FE model were extended for this work. Two modifications were included to improve the FE modeling approach of the brace buckling and the composite concrete slabs. With the improvements were developed and evaluated from TCBF1 test data, and the continuum FE ANSYS model accurately simulated the measured and observed responses of the multi-story braced frames at both global and local levels. With the high accuracy of representation, the ANSYS model is a candidate for prediction of any other SCBF systems and a tool for parametric studies of the system.



## 8.2 Development of Discrete Line Element Models of SCBFs

The continuum FE model enabled accurate prediction of the cyclic behavior of braced frames in terms of both global and local responses. However, typical continuum finite element models are too time-consuming and expensive for typical professional practice. Further they are not suitable for completing nonlinear static and dynamic analysis for PBSB of larger braced frame systems. A simplified but relatively accurate nonlinear simulation method was developed for SCBF systems in the study.

Advanced use of SCBF systems requires accurate yet practical computational models. To enable PBSB of steel braced frames, a nonlinear analysis modeling approach was developed and verified. The proposed model was developed with the objective of accurate simulation while minimizing computing cost and time. This type of model enables nonlinear dynamic simulation of these important structures.

The modeling approach used nonlinear fiber based beam-column elements for the beams, columns, and braces. The novel aspect was the gusset plate connection model. This model included nonlinear rotational springs to simulate the nonlinear OOP response of the gusset plate and multiple rigid end zones to simulate stiffener effect of the boundary elements. In addition, an experimentally verified spring was used to simulate the stiffness of the shear-plate connection. The model was verified using a series of experimental specimens. These specimens had different gusset connections, geometries, brace type, and number of stories. The model consistently provided reasonable accuracy for this wide range of tested parameters.

The accuracy of the proposed model was also compared with more conventional approaches, using either pinned or rigid connections at the end of the brace. These

concentrational models provided good but similar variability in accuracy in predicting stiffness and tensile resistance. Relative to the proposed model, the conventional model had significantly reduced accuracy for prediction of the compressive response. The fixed-end brace model significantly overestimated the compressive resistance of the brace and the deterioration of resistance after buckling. The pin-ended brace models significantly underestimated the compressive resistance of the brace. The improved model accurately estimated the distribution of nonlinear deformation among stories of multi-story frames.

There are several key conclusions of the proposed modeling approach. To estimate the buckling capacity and post-buckling response of the frame requires not only an accurate model of the brace but also an accurate model of the connection. This impact is apparent when comparing the proposed model, which uses a more realistic model for the gusset plate connections and a reliable estimate of the compressive response, and the conventional modeling approaches, which use idealized end conditions and fail to accurately simulate this complex response.

### **8.2.1 Fracture Modeling of Braces in SCBFs**

Brace fracture is the primary and desired failure mode of SCBF systems. Therefore a full nonlinear analysis of an SCBF building must include an accurate fracture model, which allows simulating beyond brace fracture to estimate collapse. To achieve this, a material wrapper of the steel model was developed and implemented in the proposed nonlinear line-element model. The model was developed to simulate the behavior of a brace frame prior to and beyond fracture as observed in laboratory testing.

Experimental results show that large local strains in the middle of the brace resulting from out-of-plane movement of the brace cause tearing under tensile loading. These observations formed the basis of the model. The brace was modeled using fiber-based beam column elements, discretized fiber cross sections were used at each integration point. The maximum strain range in the extreme (compression) fiber was used to predict the onset of brace fracture. The model was validated using 44 test results, which had a wide range of brace parameters and system configurations. All of the tests sustained brace fracture. An equation to predict fracture using the fiber-based beam column elements was developed. The fracture limit included the impact of the brace parameters influencing the onset of fracture, including slenderness ratio, yield strength, and width-to-thickness ratio.

Comparison with previous existing fracture models indicates that the proposed model offers improved accuracy over a wide range of parameters with sufficient simplicity to permit implementation in practical nonlinear structural analysis. The fracture model was implemented in the OpenSees framework to permit simulation of SCBF systems. A limited analytical study of a single-bay, single-story braced frame was conducted to evaluate the relationship between story drift and maximum strain range values as a function of the design parameters.

The conclusions of the study were as follows:

- The maximum strain range was found to be the best indicator of brace fracture and was used to estimate the fracture life of the braces.
- Other existing fracture models, based on accumulated axial deformation, end-rotation of the braces and the accumulated strain deformation, were evaluated.

In general, these models underestimated the fracture life of the brace and were not as accurate as the proposed model.

- The new fracture material model used a maximum strain-range limit. The limit is a function of  $KL/r$ ,  $b/t$  and  $E/F_y$ .
- The proposed fracture material model provided accurate simulation of fracture and post-fracture behavior integrated with the proposed nonlinear model. It is capable of prediction seismic demand and capacity of SCBF structures as well as damage prediction as required in PBSO.
- The study of single-bay, single-story frames showed that the maximum strain range varied with  $KL/r$  ratios, larger slenderness and smaller width-to-thickness ratios result in larger inelastic deformation capacities, which lowers their tendency for premature brace fracture.

### 8.3 Evaluation of Seismic Performance of SCBFs

Seismic performance of SCBF systems was investigated by appropriately developed evaluation procedures using the improved models with fracture prediction. The impact of and appropriate values for  $R$  factors of SCBF systems was a primary focus, and the story height (3-, 9- and 20-story) SCBF buildings were studied. All of the buildings were idealized multi-story structures designed for the seismic hazards of Seattle, Washington. Two methods were used to evaluate the appropriate  $R$  factor values as well as their impact on the seismic performance and design parameters for SCBFs. Initially the P695 methodology was used. Finally, an alternate performance-based method was developed.

The ground motions selected for analysis were from two bins and included 2%-in-50 year and 10%-in-50 year Seattle SAC ground motions. Both methods used state-of-the-art line-element modeling which were experimentally validated. The modeling approach was

also used to predict the yielding and buckling behavior of the brace, the post-buckling behavior of the systems, the onset of brace fracture, and the post-fracture behavior of the system.

The research was carried out by first evaluating a pair of 3- and 20-story SCBFs designed with  $R$  factors of 3 and 6. The collapse potential was assessed by using the methodology of FEMA P695 (ATC-63). These results were then compared with the alternative evaluation process, which used an appropriate scaling method for the ground motions to include the impact of the higher mode and performance.

The results were compared with the P695 evaluate results, and were used to evaluate appropriate design parameters for SCBFs, including  $R$ ,  $C_d$ , and  $\Omega_o$ . The conclusions of the modeling requirements, ground motion scaling procedures, effectiveness of the P695 procedure and the proposed procedure follow.

- The contribution of gravity frames to the lateral resistance had considerable impact on and reduces the seismic response for the low-rise buildings (3-story buildings) and should be considered in the performance evaluation. For mid-rise and high-rise buildings (9- and 20-story buildings in the study), the effect of gravity frame is relatively small.
- The evaluation of SCBFs using the FEMA P695 methodology with the IDA procedure to assess collapse potential led to uncertainty of estimating the  $R$  factors. This uncertainty results from the variations of the resulting IDA curves by different scaling approaches of ground motions as well as the difficulty in predicting collapse.
- In the alternate performance evaluation procedure, the proposed scaling method effectively reflects the characteristics of the structural systems to best represent the ground motion intensity at certain hazard levels. For first-mode-governed structures,

such as the low- and mid-rise buildings, the proposed scaling method provided a reasonable fit of the ground motion response spectra to the design response spectra for the variation of structural periods due to brace fracture. While the taller buildings increase the importance of the second mode, the scaling method assures the ground motion response spectra reasonably matching the design response spectra at the first two mode structural periods.

- By using the accurate analytical models including fracture prediction and proper scaling approach of ground motion records, the seismic performance of the SCBFs can be assessed at multiple damage levels for multiple hazard levels. This fulfills the objectives of performance based earthquake engineering and provides a mechanism for a more consistent design among building archetypes. Solely focusing on collapse does not fulfill this objective or provide this consistency.
- The analytical results show that the appropriate  $R$  factors actually varied with number of stories. The results suggest that if consistent safety against collapse is to be achieved, low-rise SCBFs (3-story) require smaller  $R$  value than high-rise buildings. An  $R$  factor of 3 is suggested. The results showed acceptable results for the mid-rise and high-rise SCBF buildings (9- and 20-story) designed with an  $R$ -value of 6.
- The results from all of the dynamic analyses were compiled revealing that both the deflection amplification and overstrength factors varied with the  $R$  factors. The current value of the deflection amplification,  $C_d$ , ( $C_d=5$  for SCBFs) is appropriate for the upper stories of SCBF frames, but the value underestimates the inelastic story drift of the bottom stories for all but the tallest structures. Using the proposed  $R$  factors of 3 (low-rise SCBFs) and 6 (mid-rise SCBFs) an overstrength factor of 2 was deemed appropriate, which agrees with current design code.

- Seismic performance evaluation and particularly collapse entails many variabilities and uncertainties. The alternative evaluation procedure is much better able to address these uncertainties and provide a better picture of SCBF performance than the FEMA P695 method.

#### **8.4 Seismic Vulnerability of Older CBF Systems**

Recent research has resulted in significant improvements in the design and construction of SCBFs. Investigations have resulted in a design method to improve the seismic performance, ductility, and constructability of SCBFs. This design method balances the yield mechanisms and failure modes present in SCBFs, to result in reduced fracture and increased deformability. The resulting design procedure is designated the Balance Design Procedure (BDP) and corresponding analytical simulation models have been developed to simulate its response.

Existing CBFs on the west coast are susceptible to damage. This fact has been acknowledged by the earthquake engineering community, as indicated by the changes to the steel design code. However, methods to assess their vulnerability are absent, since limited research to quantify the seismic vulnerability of these systems has been performed. A research study was undertaken to evaluate the seismic vulnerability of CBFs designed without consideration of ductility. The research used a limited experimental study and adaptation of the improved nonlinear model for CBFs to approximate the seismic vulnerability of NCBFs.

Of interest in this study was the comparison of modern and advanced SCBFs to vintage (pre-1988) CBFs. Primary differences in these systems include: (1) connections

in SCBFs are capacity designed such that the design demand is based on the capacity of the brace, where NCBF connections are designed solely to meet the demands from the prescriptive seismic lateral forces, (2) lack of compactness and slenderness limits for braces used in the NCBFs, and (3) differences in the lateral force demands and reduction factors. The research conducted herein studied the impact of these differences on the seismic performance and collapse potential of these systems. A limited experimental study was conducted. Those experimental results were used to modify a nonlinear analysis model, previously developed for SCBF system, to simulate the impact of the inadequate gusset plate connection and non-seismic brace section on the response. In turn, those results were used to conduct extensive nonlinear dynamic analyses to investigate the seismic damage performance and collapse potential of these systems.

The preliminary investigation undertaken here used experimental and analytical methods to explore the seismic response of NCBFs, and it has shown that:

- Local connection failure limits the resistance and drift capacity of NCBF frames.
- The reserve capacity of the remaining frame is important but depends on the connections remaining intact. Loss of brace-to-gusset connectivity results in a significant loss of strength and stiffness.
- Brace or connection failure for the NCBFs is expected during even moderate earthquakes. This level of damage does not meet modern seismic performance expectations.
- NCBFs in high seismic regions are susceptible to collapse during the MCE (2% in 50 year) event.

The results from this study are important and the first to quantify the vulnerability of this prevalent system. However, the uncertainty goes beyond that found in this study as the



variation in existing NCBF configurations is large. Thus, the progression of yielding and the ultimate failure mode of the majority of NCBF systems remain uncertain. Additional testing is required to develop robust evaluation and rehabilitation methods for these prevalent systems.

## **8.5 Recommendations for Future Research**

The study has resulted in practical yet accurate analytical tools and evaluation procedure for concentrically braced frame structural systems. Advancement of this modeling approach could be achieved by:

- Developing fracture models for different brace sections, such as wide-flange, angle and other built-up cross sections. This advancement would broaden the use of the proposed improved model of CBFs.
- More experimental and analytical investigations of design and performance of in-plane buckling braces and connections are needed to verify their seismic performance.
- Related experimental and analytical works are needed for buckling restrained braced frames (BRBFs).
- Additional research into the seismic performance, evaluation and rehabilitation of NCBFs are needed. The yield mechanisms and failure modes of NCBFs, as well as load redistribution to the gravity frame, need to be investigated. Additional experimental and analytical investigations of NCBFs are needed to develop high-resolution analytical modeling to develop a fundamental data to advance the seismic performance evaluation and rehabilitation of these critical systems.

Steel concentrically braced frame systems have been widely used for both older and new building structures. More comprehensive and precise investigations of the braced frames would lead to further better understanding of the systems which would potentially promote the applications and the design rules of the braced frames.

## **Appendix A: Journal Paper of the FEA Study**

### **A.1 Journal Paper**

Lumpkin, E.J., Hsiao, P.C., Roeder, C.W., Lehman, D.E., Tsai, K.C., Tsai, C.Y., Wei, C.Y., Wu, A.C. (2012) “**Investigation of the Seismic Response of Multi-story Braced Frames.**” *Journal of Constructional Steel Research*; in press. (accepted on Apr, 6th)



## **Appendix B: Journal Paper of the Improved Model of SCBFs**

### **B.1 Journal Paper**

Hsiao, P.C., Lehman, D.E. and Roeder, C.W. (2012) “**Improved Analytical Model for Special Concentrically Braced Frames.**” *Journal of Constructional Steel Research*, Vol.73; pp:80-94.



## Appendix C.: Processing Functions for Model Construction of each component member

### C.1 Bracing Members

This command is used to construct multiple nodes and elements required for the proposed modeling approach of the bracing member, including the brace and its two gusset plate connections at the ends.

***BraceMake*** *\$fromNodeTag \$fromEleTag \$SecID \$RLSecID \$RESecID*  
*\$RigidMatID \$GTID \$startNode \$endNode \$fromX \$fromY*  
*\$toX \$toY \$planeZ \$nfele \$alfa1 \$alfa2 \$RL*  
*\$1MatIDAxialStif \$1MatIDOutRotStif \$1MatIDInRotStif*  
*\$2MatIDAxialStif \$2MatIDOutRotStif \$2MatIDInRotStif.*

<b><i>\$fromNodeTag</i></b>	identifier of the first additional node object to construct the elements of the bracing member.
<b><i>\$fromEleTag</i></b>	identifier of the first element to construct the bracing member.
<b><i>\$SecID</i></b>	identifier for previously-defined section object for the brace.
<b><i>\$RLSecID</i></b>	identifier for previously-defined section object for the brace-to-gusset connection.
<b><i>\$RESecID</i></b>	identifier for previously-defined section object for rigid end zones at the ends of the bracing member.
<b><i>\$RigidMatID</i></b>	identifier for previously-defined rigid material object.
<b><i>\$GTID</i></b>	identifier for previously-defined coordinate-transformation object.
<b><i>\$startNode, \$endNode</i></b>	identifier for previously-defined node objects where the

	bracing member starts and ends.
<i>\$fromX, \$fromY</i>	x, y coordinates of the node object where the bracing member starts.
<i>\$toX, \$toY</i>	x, y coordinates of the node object where the bracing member ends.
<i>\$planeZ</i>	z coordinate of the node objects where the bracing member starts and ends.
<i>\$nfele</i>	number of discrete elements of the brace between the two elements of brace-to-gusset connections.
<i>\$alfa1, \$alfa2</i>	percentages of the rigid end zones at the ends to the workpoint-to-workpoint length of the bracing member. ( <i>\$alfa1</i> is at the started side, and <i>\$alfa2</i> is at the ended side)
<i>\$RL</i>	length of the brace-to-gusset connections. (splice length)
<i>\$1MatIDAxialStif, \$1MatIDOutRotStif, \$1MatIDInRotStif</i>	identifier for previously-defined material objects for the started-side spring element of gusset plate connection at the axial, the out-of-plane rotational and in-plane rotational directions.
<i>\$2MatIDAxialStif, \$2MatIDOutRotStif, \$2MatIDInRotStif</i>	identifier for previously-defined material objects for the ended-side spring element of gusset plate connection at the axial, the out-of-plane rotational and in-plane rotational directions.

EXAMPLE:

```
BraceMake 10 12 12 16 18 55 1 1 23 $X0 $Y0 $X1 $Y1 0.0 10 0.1084 0.1084
24.0 55 2 55 55 3 55
```

## C.2 Beam and Column Members

This command is used to construct multiple nodes and elements required for the proposed modeling approach of the beam or column member.

```
BeamColumnMake $fromNodeTag $fromEleTag $SecID $RESecID $GTID  
$startNode $endNode $fromX $fromY $fromZ $toX $toY  
$toZ $nfele $alfa1 $alfa2
```



<b><i>\$fromNodeTag</i></b>	identifier of the first additional node object to construct the elements of the beam/column member.
<b><i>\$fromEleTag</i></b>	identifier of the first element to construct the beam/column member.
<b><i>\$SecID</i></b>	identifier for previously-defined section object for the beam/column.
<b><i>\$RESecID</i></b>	identifier for previously-defined section object for rigid end zones at the ends of the beam/column member.
<b><i>\$GTID</i></b>	identifier for previously-defined coordinate-transformation object.
<b><i>\$startNode, \$endNode</i></b>	identifier for previously-defined node objects where the beam/column member starts and ends.
<b><i>\$fromX, \$fromY, \$fromZ</i></b>	x, y, z coordinates of the node object where the bracing member starts.
<b><i>\$toX, \$toY, \$toZ</i></b>	x, y, z coordinates of the node object where the bracing member ends.
<b><i>\$nfele</i></b>	number of discrete elements of the beam/column member except the rigid end zones.
<b><i>\$alfa1, \$alfa2</i></b>	percentages of the rigid end zones at the ends to the workpoint-to-workpoint length of the beam/column member. ( <i>\$alfa1</i> is at the started side, and <i>\$alfa2</i> is at the ended side)

EXAMPLE:

```
BeamColumnMake 12 13 402 404 1 2 23 $X0 $Y1 0.0 $X1 $Y1 0.0 1 0.0
0.225
```

### C.3 Source Code of Bracemake( )

*bracemake.tcl* :

---

```
proc BraceMake {fromNodeTag fromEleTag SecID RLSecID RESecID RigidMatID GTID
startNode endNode fromX fromY toX toY planeZ nfele alfa1 alfa2 RL 1MatIDAxialStif
1MatIDOutRotStif 1MatIDInRotStif 2MatIDAxialStif 2MatIDOutRotStif 2MatIDInRotStif } {
    set L [expr sqrt(($toX-$fromX)*($toX-$fromX)+($toY-$fromY)*($toY-$fromY))]
```

---

---

```

set bL [expr $L*(1-$alfa1-$alfa2)]

# set node and fix
set bfromX [expr $fromX+($toX-$fromX)*$alfa1]
set bfromY [expr $fromY+($toY-$fromY)*$alfa1]
set btoX [expr $toX-($toX-$fromX)*$alfa2]
set btoY [expr $toY-($toY-$fromY)*$alfa2]

set DeformZ [expr $bL/500]
set PI [expr 2*asin(1.0)]
set firstNode [expr $fromNodeTag]

# ===== for spring & rigid end zone nodes
for {set M 1} {$M <= 2} {incr M 1} {
  node $fromNodeTag $bfromX $bfromY $planeZ
  fix $fromNodeTag 0 0 0 0 0
  set fromNodeTag [expr $fromNodeTag+1]
}

# ===== for RL end zone nodes
set RLX [expr $bfromX+$RL*($btoX-$bfromX)/$bL]
set RLY [expr $bfromY+$RL*($btoY-$bfromY)/$bL]
set RLZ [expr $planeZ+$DeformZ*sin($PI/$bL*$RL)]

node $fromNodeTag $RLX $RLY $RLZ
fix $fromNodeTag 0 0 0 0 0
set fromNodeTag [expr $fromNodeTag+1]

# ===== for brace nodes
set detaX [expr ($btoX-$bfromX)*(1-2*$RL/$bL)/$nfele]
set detaY [expr ($btoY-$bfromY)*(1-2*$RL/$bL)/$nfele]

for {set I 1} {$I < $nfele} {incr I 1} {
  set coordinateX [expr $RLX+($detaX*$I)]
  set coordinateY [expr $RLY+($detaY*$I)]
  set coordinateZ [expr $planeZ+$DeformZ*sin( $PI/$bL*($RL+($bL-2*$RL)/$nfele*$I) ) ]
  node $fromNodeTag $coordinateX $coordinateY $coordinateZ
  fix $fromNodeTag 0 0 0 0 0
  set fromNodeTag [expr $fromNodeTag+1]
}

# ===== for RL rigid end zone nodes
set coordinateX [expr $btoX-$RL*($btoX-$bfromX)/$bL]
set coordinateY [expr $btoY-$RL*($btoY-$bfromY)/$bL]
set coordinateZ [expr $RLZ]
node $fromNodeTag $coordinateX $coordinateY $coordinateZ
fix $fromNodeTag 0 0 0 0 0
set fromNodeTag [expr $fromNodeTag+1]

# ===== for spring & rigid end zone nodes
for {set N 1} {$N <= 2} {incr N 1} {
  node $fromNodeTag $btoX $btoY $planeZ
  fix $fromNodeTag 0 0 0 0 0
  set fromNodeTag [expr $fromNodeTag+1]
}

# ===== Element Command =====

```

---

---

```

# ===== set brace end spring=====
set x1 [expr $fromX-$toX]
set y1 [expr $fromY-$toY]
set yp1 [expr $fromY-$toY]
set yp2 [expr -($fromX-$toX)]

#===== set rigid zone element=====
element nonlinearBeamColumn $fromEleTag $startNode $firstNode 4 $RESecID $GTID
set fromEleTag [expr $fromEleTag+1]

set bNode [expr $firstNode+1]
element zeroLength $fromEleTag $firstNode $bNode -mat $1MatIDAxialStif $RigidMatID
  $RigidMatID $RigidMatID $1MatIDOutRotStif $1MatIDInRotStif -dir 1 2 3 4 5 6 -orient $x1
  $y1 0 $yp1 $yp2 0
set fromEleTag [expr $fromEleTag+1]

# set rigid zone element=====
set nxNode [expr $bNode+1]
element nonlinearBeamColumn $fromEleTag $bNode $nxNode 4 $RLSecID $GTID
set bNode [expr $bNode+1]
set fromEleTag [expr $fromEleTag+1]

# set brace element=====
for {set J 1} {$J <= $nfele} {incr J 1} {
  set nxNode [expr $bNode+1]
  element nonlinearBeamColumn $fromEleTag $bNode $nxNode 4 $SecID $GTID
  set bNode [expr $bNode+1]
  set fromEleTag [expr $fromEleTag+1]
}

# set rigid zone element=====
set nxNode [expr $bNode+1]
element nonlinearBeamColumn $fromEleTag $bNode $nxNode 4 $RLSecID $GTID
set bNode [expr $bNode+1]
set fromEleTag [expr $fromEleTag+1]

# set rigid zone & spring element=====
set nxNode [expr $bNode+1]
element zeroLength $fromEleTag $bNode $nxNode -mat $2MatIDAxialStif $RigidMatID
  $RigidMatID $RigidMatID $2MatIDOutRotStif $2MatIDInRotStif -dir 1 2 3 4 5 6 -orient $x1
  $y1 0 $yp1 $yp2 0
set fromEleTag [expr $fromEleTag+1]
element nonlinearBeamColumn $fromEleTag $nxNode $endNode 4 $RESecID $GTID

}

```

---

## C.4 Source Code of BeamColumnMake( )

*beammake.tcl* :

---

```

proc BeamColumnMake {fromNodeTag fromEleTag SecID RESecID GTID startNode endNode

```

---

---

```

fromX fromY fromZ toX toY toZ nfele alfa1 alfa2} {

    set L [expr sqrt((($toX-$fromX)*($toX-$fromX)+($toY-$fromY)*($toY-$fromY)+($toZ-$fromZ)
        *($toZ-$fromZ))]
    set REZL1 [expr $L*$alfa1]
    set REZL2 [expr $L*$alfa2]

# set node and fix
    set BCfromX [expr $fromX+($toX-$fromX)*$alfa1]
    set BCfromY [expr $fromY+($toY-$fromY)*$alfa1]
    set BCfromZ [expr $fromZ+($toZ-$fromZ)*$alfa1]
    set BCtoX [expr $toX-($toX-$fromX)*$alfa2]
    set BCtoY [expr $toY-($toY-$fromY)*$alfa2]
    set BCtoZ [expr $toZ-($toZ-$fromZ)*$alfa2]

    set detaX [expr ($BCtoX-$BCfromX)/$nfele]
    set detaY [expr ($BCtoY-$BCfromY)/$nfele]
    set detaZ [expr ($BCtoZ-$BCfromZ)/$nfele]
    set firstNode [expr $fromNodeTag]

# ===== for beam or column nodes
    if {$alfa > 0} {
        node $fromNodeTag $BCfromX $BCfromY $BCfromZ
        fix $fromNodeTag 0 0 0 0 0
        set fromNodeTag [expr $fromNodeTag+1]
    }

    if {$nfele > 1} {
        for {set l 1} {$l < $nfele} {incr l 1} {
            set coordinateX [expr $BCfromX+($detaX*$l)]
            set coordinateY [expr $BCfromY+($detaY*$l)]
            set coordinateZ [expr $BCfromZ+($detaZ*$l)]
            node $fromNodeTag $coordinateX $coordinateY $coordinateZ
            fix $fromNodeTag 0 0 0 0 0
            set fromNodeTag [expr $fromNodeTag+1]
        }
    }

    if {$alfa2 > 0} {
        node $fromNodeTag $BCtoX $BCtoY $BCtoZ
        fix $fromNodeTag 0 0 0 0 0
    }
}

# Element Command =====
# set first rigid end zone element
if {$nfele > 1} {
    if {$alfa > 0} {
        element nonlinearBeamColumn $fromEleTag $startNode $firstNode 4 $RESecID
            $GTID
        set fromEleTag [expr $fromEleTag+1]
        set BCNode [expr $firstNode]
        set nxNode [expr $BCNode+1]
        element nonlinearBeamColumn $fromEleTag $BCNode $nxNode 4 $SecID $GTID
        set BCNode [expr $BCNode+1]
        set fromEleTag [expr $fromEleTag+1]
    }
}

```

---

---

```

    if {$alfa1 == 0} {
        element nonlinearBeamColumn $fromEleTag $startNode $firstNode 4 $SecID
        $GTID
        set BCNode [expr $firstNode]
        set fromEleTag [expr $fromEleTag+1]
    }

# set beam or column seperated elements
for {set J 2} {$J < $nfele} {incr J 1} {
    set nxNode [expr $BCNode+1]
    element nonlinearBeamColumn $fromEleTag $BCNode $nxNode 4 $SecID $GTID
    set BCNode [expr $BCNode+1]
    set fromEleTag [expr $fromEleTag+1]
}
if {$alfa2 > 0} {
    set nxNode [expr $BCNode+1]
    element nonlinearBeamColumn $fromEleTag $BCNode $nxNode 4 $SecID $GTID
    set BCNode [expr $BCNode+1]
    set fromEleTag [expr $fromEleTag+1]
    # set end rigid end zone element
    element nonlinearBeamColumn $fromEleTag $BCNode $endNode 4 $RESecID
    $GTID
}
if {$alfa2 == 0} {
    element nonlinearBeamColumn $fromEleTag $BCNode $endNode 4 $SecID $GTID
}
}
if {$nfele == 1} {
    if {$alfa1 > 0 & $alfa2 > 0} {

        element nonlinearBeamColumn $fromEleTag $startNode $firstNode 4 $RESecID
        $GTID
        set nxNode [expr $firstNode+1]
        set fromEleTag [expr $fromEleTag+1]
        element nonlinearBeamColumn $fromEleTag $firstNode $nxNode 4 $SecID $GTID
        set fromEleTag [expr $fromEleTag+1]
        element nonlinearBeamColumn $fromEleTag $nxNode $endNode 4 $RESecID $GTID
    }
    if {$alfa1 > 0 & $alfa2 == 0} {
        element nonlinearBeamColumn $fromEleTag $startNode $firstNode 4 $RESecID
        $GTID
        set fromEleTag [expr $fromEleTag+1]
        element nonlinearBeamColumn $fromEleTag $firstNode $endNode 4 $SecID $GTID
    }
    if {$alfa1 == 0 & $alfa2 > 0} {
        element nonlinearBeamColumn $fromEleTag $startNode $firstNode 4 $SecID $GTID
        set fromEleTag [expr $fromEleTag+1]
        element nonlinearBeamColumn $fromEleTag $firstNode $endNode 4 $RESecID
        $GTID
    }
    if {$alfa1 == 0 & $alfa2 == 0} {
        element nonlinearBeamColumn $fromEleTag $startNode $endNode 4 $SecID $GTID
    }
}
}
}

```

---



## Appendix D: Journal Paper and Tables of Analytical Results of the Fracture Model

### D.1 Journal Paper

Hsiao, P.C., Lehman, D.E. and Roeder, C.W. (2012) “A Model to Simulate Special Concentrically Braced Frames Beyond Brace Fracture.” *Earthquake Engineering & Structural Dynamics*, DOI: 10.1002/eqe.2202.

### D.2 Tables of Analytical Results

Table D.1. Data of Several Characteristics at Axial Deformation Level

Specimens	Max. Axial Def. Range (%)		Max. Axial Def. (%)		Accumulated Axial Def. (%)		
	Entire history (Tremblay et al. 2003)	For a given cycle	Ten.	Comp.	$\Sigma \Delta_f$ (Lee & Goel 1987)	$\Sigma \Delta_{\text{rain-flow}}$	$\Sigma \Delta$
HSS2	2.05	1.53	-1.28	0.80	95.42	21.81	54.69
HSS3	2.22	1.98	-1.46	0.76	85.43	28.78	50.90
HSS4	2.08	1.98	-1.32	0.76	88.95	26.01	45.76
HSS5	2.60	2.40	-1.63	1.01	103.39	31.49	59.51
HSS6	2.36	2.19	-1.49	0.87	103.81	27.74	53.33
HSS7	2.12	2.12	-1.46	0.69	92.02	23.61	46.46
HSS8	2.40	1.25	-1.28	1.15	104.16	27.92	53.89
HSS9	1.84	1.49	-1.18	0.66	65.22	22.01	38.99
HSS10	2.36	2.08	-1.32	1.04	98.88	26.28	49.44
HSS11	1.35	1.22	-0.80	0.59	47.06	9.51	29.41
HSS12	1.74	1.53	-1.01	0.69	55.34	17.33	31.74
HSS13	2.08	2.08	-1.04	1.04	70.57	18.16	37.64
HSS14	2.01	1.98	-1.01	1.01	79.88	20.35	44.79
HSS15	1.94	1.84	-1.08	0.87	79.75	19.51	38.37
HSS17	2.47	2.12	-1.35	1.08	80.07	23.19	43.47
HSS24	2.19	1.88	-1.22	0.97	69.69	21.91	41.22
HSS25	1.63	1.63	-1.18	0.45	48.00	15.83	27.26

TCBF1-1	4.43	3.90	-2.16	2.27	N.A.	26.16	65.16
TCBF1-3	5.35	2.64	-2.67	2.67	N.A.	39.19	82.90
TCBF2-1	1.91	1.44	-0.96	0.96	N.A.	13.44	28.38
Kavinde-1	2.67	2.58	-1.33	1.33	25.05	13.67	26.00
Kavinde-2	3.92	2.17	-2.92	1.00	6.88	50.25	45.25
Kavinde-4	4.80	3.52	-2.40	2.40	59.44	33.20	71.92
Yang-4	2.66	2.06	-0.60	2.06	24.69	4.72	26.61
Yang-5	2.58	2.32	-1.29	1.29	37.34	14.42	33.05
Patxi-SCBF-1	1.61	1.61	-0.55	1.06	N.A.	5.66	12.25
Broderick-S1-40H	2.30	2.30	-1.33	1.04	53.25	15.19	28.74
Broderick-S4-20H	3.11	3.11	-1.63	1.48	52.35	23.63	45.48
Shaback-1B	1.91	1.91	-1.19	0.70	18.99	13.06	22.28
Shaback-2A	1.81	1.81	-1.09	0.69	12.11	8.27	14.68
Shaback-2B	1.91	1.91	-1.19	0.70	16.14	10.68	18.47
Shaback-3A	1.80	1.80	-1.10	0.70	11.94	8.28	14.68
Shaback-3B	1.89	1.89	-1.19	0.70	22.28	17.88	29.89
Shaback-3C	1.90	1.90	-0.97	0.93	33.84	21.23	44.86
Shaback-4A	1.90	1.90	-1.19	0.71	13.96	10.68	18.49
Shaback-4B	1.89	1.89	-1.16	0.73	17.22	14.75	26.05
Han-S77-28	0.65	0.65	-0.26	0.40	9.70	3.25	6.79
Lee-1	0.89	0.89	-0.59	0.22	5.48	3.19	6.30
Lee-2	0.89	0.67	-0.59	0.22	11.02	3.78	7.63
Lee-4	1.82	0.88	-1.68	0.15	3.61	12.70	15.99
Lee-5	2.72	2.57	-2.50	0.29	8.36	28.68	40.00
Lee-6	1.75	0.80	-1.61	0.15	12.54	12.41	15.99
Lee-7	1.46	1.24	-1.24	0.22	17.82	9.27	16.42
Tremblay-S3A	5.43	5.43	-2.67	2.76	204.60	164.83	332.28

Table D. 2 Data of Fracture Models Based on Fiber Strains

Specimens	Max. Strain		Max. Strain Range		Accum. Strain				
	$\epsilon_{t,max}$	$\epsilon_{c,max}$	Entire history	For a given cycle	$\sum \epsilon_{rain-flo}$ w	$\sum DI_{rain-flo}$ w	$\sum \epsilon$	$\sum \epsilon^2$	$\sum \epsilon^3$
HSS2	0.020	0.025	0.044	0.028	0.612	0.989	1.339	0.0398	0.00130
HSS3	0.023	0.027	0.049	0.037	0.627	1.166	1.346	0.0422	0.00160
HSS4	0.024	0.028	0.052	0.043	0.633	1.121	1.278	0.0431	0.00170
HSS5	0.031	0.029	0.061	0.048	0.723	1.354	1.620	0.0644	0.00300
HSS6	0.024	0.023	0.047	0.040	0.585	0.872	1.347	0.0427	0.00160
HSS7	0.020	0.040	0.061	0.057	0.963	2.352	1.621	0.0615	0.00270
HSS8	0.028	0.023	0.051	0.024	0.601	0.965	1.418	0.0455	0.00170



HSS9	0.020	0.027	0.047	0.047	0.563	1.058	1.116	0.0338	0.00120
HSS10	0.028	0.025	0.053	0.050	0.614	1.151	1.408	0.0459	0.00170
HSS11	0.008	0.036	0.044	0.043	0.464	1.226	0.892	0.0241	0.00080
HSS12	0.021	0.028	0.049	0.048	0.574	1.118	1.092	0.0327	0.00120
HSS13	0.022	0.022	0.044	0.043	0.457	0.656	0.988	0.0284	0.00100
HSS14	0.024	0.021	0.045	0.041	0.507	0.684	1.110	0.0309	0.00100
HSS15	0.022	0.020	0.043	0.041	0.433	0.591	0.927	0.0241	0.00080
HSS17	0.026	0.022	0.049	0.045	0.518	0.845	1.133	0.0313	0.00100
HSS24	0.026	0.025	0.051	0.046	0.446	0.771	1.024	0.0324	0.00120
HSS25	0.012	0.042	0.054	0.052	0.657	1.606	0.985	0.0346	0.00140
TCBF1-1	0.024	0.035	0.059	0.059	0.538	1.115	0.988	0.0409	0.00190
TCBF1-3	0.027	0.022	0.049	0.045	0.398	0.641	0.961	0.0333	0.00130
TCBF2-1	0.026	0.026	0.051	0.041	0.378	0.606	0.842	0.0295	0.00110
Kavinde-1	0.025	0.030	0.055	0.050	0.259	0.468	0.502	0.0175	0.00070
Kavinde-2	0.010	0.051	0.061	0.019	1.078	4.993	0.482	0.0133	0.00060
Kavinde-4	0.040	0.029	0.069	0.050	0.426	0.788	1.119	0.0507	0.00250
Yang-4	0.028	0.033	0.061	0.011	0.274	0.456	0.588	0.0175	0.00060
Yang-5	0.021	0.044	0.065	0.063	0.398	1.110	0.839	0.0385	0.00190
Patxi-SCBF-1	0.012	0.050	0.062	0.058	0.287	0.882	0.470	0.0199	0.00090
Broderick-S1-40 H	0.012	0.057	0.069	0.068	0.553	1.752	0.894	0.0428	0.00230
Broderick-S4-20 H	0.028	0.030	0.058	0.058	0.486	1.003	1.066	0.0448	0.00210
Shaback-1B	0.015	0.033	0.048	0.047	0.342	0.666	0.568	0.0223	0.00090
Shaback-2A	0.014	0.031	0.046	0.045	0.270	0.393	0.374	0.0131	0.00050
Shaback-2B	0.015	0.033	0.048	0.047	0.305	0.530	0.469	0.0177	0.00070
Shaback-3A	0.016	0.023	0.038	0.038	0.203	0.213	0.312	0.0091	0.00030
Shaback-3B	0.017	0.024	0.041	0.040	0.296	0.463	0.624	0.0212	0.00080
Shaback-3C	0.019	0.021	0.040	0.038	0.320	0.511	0.825	0.0276	0.00100
Shaback-4A	0.015	0.025	0.040	0.040	0.240	0.313	0.401	0.0127	0.00040
Shaback-4B	0.017	0.025	0.041	0.040	0.264	0.415	0.533	0.0180	0.00070
Han-S77-28	0.006	0.014	0.020	0.019	0.124	0.086	0.191	0.0026	0.00000
Lee-1	0.003	0.029	0.032	0.021	0.169	0.334	0.183	0.0049	0.00010
Lee-2	0.003	0.032	0.035	0.027	0.214	0.504	0.257	0.0074	0.00020
Lee-4	0.002	0.044	0.045	0.017	0.351	1.056	0.346	0.0090	0.00030
Lee-5	0.006	0.049	0.056	0.052	0.676	2.930	0.671	0.0184	0.00060
Lee-6	0.001	0.068	0.070	0.033	0.531	2.418	0.557	0.0232	0.00100
Lee-7	0.003	0.057	0.059	0.018	0.415	1.793	0.610	0.0242	0.00100
Tremblay-S3A	0.045	0.003	0.048	0.029	0.797	1.336	2.086	0.0458	0.00110



## Appendix E: New Material Model Object for Simulate Brace

### Fracture

#### E.1 New Fracture Material Model

This command is used to construct a uniaxial fracture material object. This stress-strain behavior for this fracture material is initially provided by another material, so-called initial material. If however the strain range ever reach the limiting value based on the developed equation in the study (Chapter 3) or the strain ever falls below or above certain threshold values, the initial material assigned is assumed to have failed. From that point on, the stress-strain behavior of this fracture material is changed to a different material, so-called post material, to represent the behavior beyond the failure.

*uniaxialMaterial FractureMaterial \$matTag, \$matTagInital, \$matTagPost,  
\$intType, \$w\_t, \$KL\_r, \$E\_Fy, \$coeff, \$alfa, \$beta, \$gama,  
\$eMin, \$eMax*

<i>\$matTag</i>	integer tag identifying material
<i>\$matTagInital</i>	tag of the initial material
<i>\$matTagPost</i>	tag of the post material
<i>\$intType</i>	Integer index to determine the type of failure trigger: 0 : to trigger failure using threshold values (min. and max. strains (or deformation)). 1 : to trigger failure based on strain range limit calculated by the concluded equation (Eq.5.10) in the study.
<i>\$w_t</i>	width-to-thickness ratio of the bracing member
<i>\$KL_r</i>	effective slenderness ratio of the bracing member

<b><i>\$E_Fy</i></b>	Ratio of Young's modulus to yield strength of the steel of the bracing member
<b><i>\$coeff</i></b>	Coefficient in the equation of limiting strain range values (=0.1435 according to the results of the study)
<b><i>\$alfa</i></b>	exponent value of the width-to-thickness ratio in the equation. (= -0.4 according to the results of the study)
<b><i>\$beta</i></b>	exponent value of the effective slenderness ratio in the equation. (= -0.3 according to the results of the study)
<b><i>\$gama</i></b>	exponent value of Ratio of Young's modulus to yield strength in the equation. (= 0.2 according to the results of the study)
<b><i>\$eMin</i></b>	Minimum value of strain (or deformation). Optional default = -1.0e16.
<b><i>\$eMax</i></b>	Maximum value of strain (or deformation). Optional default = 1.0e16.

EXAMPLE:

```
uniaxialMaterial FractureMaterial 3 1 2 1 11.3 81.0 396.2 0.1435 -0.4
-0.3 0.2 -1.0e16 1.0e16
```

## E.2 Source Code of the Fracture Material Model

For this new developed material model, here provides the scripts of the head file (FractureMaterial.h) and the main code (FractureMaterial.cpp), written in C++ computer language following the required format for OpenSees framework.

*FractureMaterial.h:*

---

```
#ifndef FractureMaterial_h
#define FractureMaterial_h

#include <UniaxialMaterial.h>
#define MAT_TAG_FractureMaterial 5002

class FractureMaterial : public UniaxialMaterial
```

---

---

```

{
    public:
        FractureMaterial(int tag, UniaxialMaterial &material, UniaxialMaterial &materialpost, int Index,
double w_t, double KL_r, double E_Fy,
            double Cons = 0.1435,
            double Alfa = -0.4,
            double Beta = -0.3,
            double Gama = 0.2,
            double minStrain = -1.0e16,
            double maxStrain = 1.0e16 );

        FractureMaterial();
        ~FractureMaterial();

        const char *getClassType(void) const {return "FractureMaterial";};

        int setTrialStrain(double strain, double strainRate = 0.0);
        double getStrain(void);
        double getStrainRate(void);
        double getStress(void);
        double getTangent(void);
        double getDampTangent(void);
        double getInitialTangent(void) {return theMaterial->getInitialTangent();}

        int commitState(void);

        int revertToLastCommit(void);
        int revertToStart(void);

        UniaxialMaterial *getCopy(void);

        int sendSelf(int commitTag, Channel &theChannel);
        int recvSelf(int commitTag, Channel &theChannel,
            FEM_ObjectBroker &theBroker);

        void Print(OPS_Stream &s, int flag =0);

protected:

private:
        UniaxialMaterial *theMaterial;
        UniaxialMaterial *theMaterialpost;

        int SF;
        //int SFF;

        double w_t;           // w/t Ratio
        double KL_r;         // KL/r slendness Ratio
        double E_Fy;         // E/ Fy

        double Cons;        // Parameters for prediction of the Limit Strain Range
        double Alfa;
        double Beta;
        double Gama;

        double minStrain;

```

---

---

```

double maxStrain;
int Index;

bool Cfailed;
bool Tfailed;
double trialStrain;
double mStress;

// For Recording  maximun of Strain Range
double maxS;
double minS;
double LimitSR;
double MaxSR;
};

#endif

```

---

### *FractureMaterial.cpp:*

---

```

#include <elementAPI.h>
#include <stdlib.h>
#include <MaterialResponse.h>
#include <Information.h>

#include <FractureMaterial.h>
#include <ID.h>
#include <Channel.h>
#include <FEM_ObjectBroker.h>
#include <OPS_Globals.h>
#include <OPS_Stream.h>

#ifdef _USRDLL
#define OPS_Export extern "C" __declspec(dllexport)
#elif _MACOSX
#define OPS_Export extern "C" __attribute__((visibility("default")))
#else
#define OPS_Export extern "C"
#endif

OPS_Export void
localInit()
{
    OPS_Error("FractureMaterial unaxial material - Written by Po-Chien UW Copyright 2010 - \n", 1);
}

OPS_Export void *
OPS_FractureMaterial()
{
    int iData[4];
    double dData[9];
    int numData;

```

---

---

```

numData = 1;
if (OPS_GetIntInput( &numData, iData) != 0) {
    opserr << "WARNING invalid uniaxialMaterial FractureMaterial tag" << endl;
    return 0;
}
numData = 1;
if (OPS_GetIntInput(&numData, &iData[1]) != 0) {
    opserr << "WARNING invalid material tag for FractureMaterial " << endl;
    return 0;
}
numData = 1;
if (OPS_GetIntInput(&numData, &iData[2]) != 0) {
    opserr << "WARNING invalid material tag for FractureMaterial " << endl;
    return 0;
}
numData = 1;
if (OPS_GetIntInput(&numData, &iData[3]) != 0) {
    opserr << "WARNING invalid Index for FractureMaterial " << endl;
    return 0;
}
numData = 9;
if (OPS_GetDoubleInput(&numData, dData) != 0) {
    opserr << "WARNING invalid minStrain & maxStrain \n";
    return 0;
}

int matID = iData[1];
UniaxialMaterial *theMaterial1 = OPS_GetUniaxialMaterial(matID);
if (theMaterial1 == 0) {
    opserr << "WARNING material with tag " << matID << "not found for preFractureMaterial \n"<<
endl;
    return 0;
}

int matID2 = iData[2];
UniaxialMaterial *theMaterial2 = OPS_GetUniaxialMaterial(matID2);
if (theMaterial2 == 0) {
    opserr << "WARNING material with tag " << matID2 << "not found for post FractureMaterial \n"<<
endl;
    return 0;
}

/*(int tag, UniaxialMaterial &material, double w__t , double KL__r, double E__Fy,
    double cons, double alfa, double beta, double gama,
    double epsmin, double epsmax )*/

UniaxialMaterial *theMaterial3 = new FractureMaterial(iData[0], *theMaterial1, *theMaterial2,
iData[3], dData[0], dData[1], dData[2], dData[3], dData[4], dData[5], dData[6], dData[7], dData[8]);
//UniaxialMaterial *theMaterial2 = new FractureMaterial(iData[0], *theMaterial1, dData[0],
dData[1]);
if (theMaterial3 == 0) {
    opserr << "WARNING could not create uniaxialMaterial of type FractureMaterial \n";
    return 0;
}
return theMaterial3;

```

---

---

```

}

FractureMaterial::FractureMaterial(int tag, UniaxialMaterial &material, UniaxialMaterial &materialpost,
int iindex, double w__t, double KL__r, double E__Fy,
double cons, double alfa, double beta, double gama,
double epsmin, double epsmax )
:UniaxialMaterial(tag,MAT_TAG_FractureMaterial), theMaterial(0), theMaterialpost(0),
Index(iindex),
w__t(w__t), KL__r(KL__r), E__Fy(E__Fy),
Cons(cons), Alfa(alfa), Beta(beta), Gama(gama),
minStrain(epsmin), maxStrain(epsmax), Cfailed(false), Tfailed(false), trialStrain(0)
{
SF= 0;
//SFF = 1;

maxS=0.0;
minS=0.0;
LimitSR = Cons*(fabs(pow(w__t,Alfa)))*(fabs(pow(KL__r,Beta)))*(fabs(pow(E__Fy,Gama)));
MaxSR = 0.0;
mStress = 0.0;

theMaterial = material.getCopy();
theMaterialpost = materialpost.getCopy();

if (theMaterial == 0) {
opserr << "FractureMaterial::FractureMaterial -- failed to get copy of material\n";
exit(-1);
}
if (theMaterialpost == 0) {
opserr << "FractureMaterial::FractureMaterial -- failed to get copy of material\n";
exit(-1);
}
}

FractureMaterial::FractureMaterial()
:UniaxialMaterial(0,MAT_TAG_FractureMaterial), theMaterial(0),theMaterialpost(0), Index(0),
w__t(0.0), KL__r(0.0), E__Fy(0.0),
Cons(0.0), Alfa(0.0), Beta(0.0), Gama(0.0),
minStrain(0.0), maxStrain(0.0), Cfailed(false), Tfailed(false), trialStrain(0)
{
SF= 0;
//SFF = 1;

maxS=0.0;
minS=0.0;
LimitSR = 0.0;
MaxSR = 0.0;
mStress = 0.0;
}

FractureMaterial::~FractureMaterial()
{
if (theMaterial)
delete theMaterial;
}

```

---



---

```
int
FractureMaterial::setTrialStrain(double strain, double strainRate)
{
    //if (Cfailed)
        // return 0;
    // trialStrain = strain;

    if( Cfailed )    {
        //Tfailed = true;
        trialStrain = strain;
        return theMaterialpost->setTrialStrain(strain, strainRate);
        //return 0;
    } else {
        Cfailed = false ;
        trialStrain = strain;
        return  theMaterial->setTrialStrain(strain, strainRate);
    }
}

double
FractureMaterial::getStress(void)
{
    if (Cfailed) {
        //double modifier = pow(0.001,SFF);
        return theMaterialpost->getStress();
        //return 0.0;
    } else
        return theMaterial->getStress();
}

double
FractureMaterial::getTangent(void)
{
    if (Cfailed) {
        //double modifier = 1.0e-8 ;
        return theMaterialpost->getTangent() ;
    } else
        return theMaterial->getTangent();
}

double
FractureMaterial::getDampTangent(void)
{
    if (Cfailed)
        return 0.0;
    else
        return theMaterial->getDampTangent();
}

double
FractureMaterial::getStrain(void)
{
    return theMaterial->getStrain();
}
```

---

---

```

}

double
FractureMaterial::getStrainRate(void)
{
    return theMaterial->getStrainRate();
}

int
FractureMaterial::commitState(void)
{
    if (Cfailed) {
        //SFF = SFF +1;
        return 0;
    }
    //Cfailed = Tfailed ;

    //Initialize the fatigue parameters if they have
    // not been initialized yet
    if (SF == 0) {
        SF = 1 ;
        //SFF = 1;
        // Initialize other params if not done so already
        maxS = 0.0;
        minS = 0.0;
        MaxSR = 0.0;
        mStress = 0.0;
    }

    /*//Simple check to see if we reached max strain capacities
    if (trialStrain >= maxStrain || trialStrain <= minStrain) {
        Tfailed = true;
        opserr << "FractureMaterial: material tag " << this->getTag() << " failed from excessive strain\n";

        return 0;
    } */

    // Find the current maximum strain range
    if (trialStrain > maxS) {
        maxS = trialStrain ;
    } else if (trialStrain < minS) {
        minS = trialStrain ;
    }

    MaxSR = fabs( maxS - minS) ;
    //if (Cfailed)
    //      mStress = 10;
    // else
    mStress = theMaterial->getStress();

    if (Index == 0) {
        if ( trialStrain >= maxStrain || trialStrain <= minStrain ) {
            Cfailed =true;
            opserr << "FractureMaterial: material tag " << this->getTag() << " failed \n";
            return 0;
        }
    }
}

```

---

---

```

    } else {
        Cfailed = false;
        return theMaterial->commitState();
    }
} else {
    if ( MaxSR >= LimitSR && mStress >= 0 ) {
        Cfailed =true;
        opserr << "FractureMaterial: material tag " << this->getTag() << " failed \n";
        return 0;
    } else {
        Cfailed = false;
        return theMaterial->commitState();
    }
}
}

int
FractureMaterial::revertToLastCommit(void)
{
    // Check if failed at last step
    if (Cfailed)
        return 0;
    else
        return theMaterial->revertToLastCommit();
}

int
FractureMaterial::revertToStart(void)
{
    Cfailed = false;
    Tfailed = false;
    SF=0;
    maxS=0.0;
    minS=0.0;
    LimitSR = 0.0;
    MaxSR = 0.0;
    w_t = 0.0;
    KL_r = 0.0;
    E_Fy = 0.0;
    Cons = 0.0;
    Alfa = 0.0;
    Beta = 0.0;
    Gama = 0.0;
    Index = 0;
    return theMaterial->revertToStart();
}

UniaxialMaterial *
FractureMaterial::getCopy(void)
{
    FractureMaterial *theCopy =
        new FractureMaterial(this->getTag(), *theMaterial, *theMaterialpost, Index, w_t, KL_r, E_Fy,
        Cons, Alfa, Beta, Gama, minStrain, maxStrain);

    theCopy->Cfailed = Cfailed;
    theCopy->Tfailed = Tfailed;
}

```

---

---

```

    theCopy->trialStrain = trialStrain;
    return theCopy;
}

int
FractureMaterial::sendSelf(int cTag, Channel &theChannel)
{
    int dbTag = this->getDbTag();

    static ID dataID(3);
    dataID(0) = this->getTag();
    dataID(1) = theMaterial->getClassTag();
    int matDbTag = theMaterial->getDbTag();
    if ( matDbTag == 0) {
        matDbTag = theChannelgetDbTag();
        theMaterial->setDbTag(matDbTag);
    }
    dataID(2) = matDbTag;
    if (theChannel.sendID(dbTag, cTag, dataID) < 0) {
        opserr << "FractureMaterial::sendSelf() - failed to send the ID\n";
        return -1;
    }

    static Vector dataVec(11);
    dataVec(0) = w_t;
    dataVec(1) = KL_r;
    dataVec(2) = E_Fy;
    dataVec(3) = Cons;
    dataVec(4) = Alfa;
    dataVec(5) = Beta;
    dataVec(6) = Gama;
    dataVec(7) = minStrain;
    dataVec(8) = maxStrain;
    dataVec(9) = SF;

    if (Cfailed == true)
        dataVec(10) = 1.0;
    else
        dataVec(10) = 0.0;

    if (theChannel.sendVector(dbTag, cTag, dataVec) < 0) {
        opserr << "FractureMaterial::sendSelf() - failed to send the Vector\n";
        return -2;
    }
    if (theMaterial->sendSelf(cTag, theChannel) < 0) {
        opserr << "FractureMaterial::sendSelf() - failed to send the Material\n";
        return -3;
    }
    return 0;
}

int
FractureMaterial::rcvSelf(int cTag, Channel &theChannel,
                          FEM_ObjectBroker &theBroker)
{
    int dbTag = this->getDbTag();

```

---

---

```

static ID dataID(3);
if (theChannel.recvID(dbTag, cTag, dataID) < 0) {
    opserr << "FractureMaterial::recvSelf() - failed to get the ID\n";
    return -1;
}
this->setTag(int(dataID(0)));

// as no way to change material, don't have to check classTag of the material
if (theMaterial == 0) {
    int matClassTag = int(dataID(1));
    theMaterial = theBroker.getNewUniaxialMaterial(matClassTag);
    if (theMaterial == 0) {
        opserr << "FractureMaterial::recvSelf() - failed to create Material with classTag "
            << dataID(0) << endl;
        return -2;
    }
}
theMaterial->setDbTag(dataID(2));

static Vector dataVec(11);
if (theChannel.recvVector(dbTag, cTag, dataVec) < 0) {
    opserr << "FractureMaterial::recvSelf() - failed to get the Vector\n";
    return -3;
}

w_t = dataVec(0);
KL_r = dataVec(1);
E_Fy = dataVec(2);
Cons = dataVec(3);
Alfa = dataVec(4);
Beta = dataVec(5);
Gama = dataVec(6);
minStrain = dataVec(7);
maxStrain = dataVec(8);
SF = dataVec(9);

if (dataVec(10) == 1.0)
    Cfailed = true;
else
    Cfailed = false;
Tfailed = Cfailed;

if (theMaterial->recvSelf(cTag, theChannel, theBroker) < 0) {
    opserr << "FractureMaterial::recvSelf() - failed to get the Material\n";
    return -4;
}
return 0;
}
void
FractureMaterial::Print(OPS_Stream &s, int flag)
{
    s << "FractureMaterial tag: " << this->getTag() << endl;
    s << "\tMaterial: " << theMaterial->getTag() << endl;
    //s << "\tMin strain: " << minStrain << endl;
    //s << "\tMax strain: " << maxStrain << endl;
}

```

---



## Appendix F: Journal Paper and Tables of Analytical Results of the Performance Evaluations of SCBFs

### F.1 Journal Paper

Hsiao, P.C., Lehman, D.E. and Roeder, C.W. (2012) “Evaluation of the Response Modification Coefficient and Collapse Potential of SCBFs.” *Earthquake Engineering & Structural Dynamics*, in- review.

### F.2 Tables of Analytical Results

Table F. 1. Scaling Factors of Ground Motions for the Model Buildings

Ground Motions	10/50			Ground Motions	2/50		
	3-story	9-story	20-story		3-story	9-story	20-story
se01	2.840	1.429	1.316	se21	1.193	0.390	0.645
se02	1.646	2.088	2.532	se22	1.263	0.597	1.314
se03	0.978	0.829	0.867	se23	1.430	0.678	0.867
se04	1.102	0.989	1.124	se24	1.749	1.193	0.664
se05	0.613	1.015	1.014	se25	0.573	0.757	0.781
se06	0.824	1.486	1.113	se26	0.756	1.103	0.907
se07	0.829	0.743	0.629	se27	0.503	0.460	0.435
se08	0.979	0.502	0.889	se28	0.471	0.609	0.407
se09	0.441	1.147	1.352	se29	0.397	0.294	0.503
se10	0.732	0.988	0.581	se30	0.363	0.449	0.440
se11	0.583	0.589	0.563	se31	0.517	0.187	0.367
se12	0.570	0.810	0.494	se32	0.694	0.338	0.729
se13	0.391	1.059	1.050	se33	0.953	0.583	0.551
se14	0.816	1.077	2.065	se34	1.093	0.465	0.446
se15	1.388	0.970	1.156	se35	1.247	0.355	0.804
se16	1.200	0.306	0.739	se36	1.186	0.399	0.325
se17	0.570	0.371	0.619	se37	0.971	0.599	0.634
se18	0.476	0.564	0.539	se38	0.880	0.451	0.709
se19	0.916	0.238	0.475	se39	1.095	0.691	0.529
se20	0.973	0.453	0.864	se40	0.957	0.785	0.528





## Appendix G: Journal Paper and Tables of Analytical Results of the Performance Evaluations of NCBFs

### G.1 Journal Paper

Hsiao, P.C., Lehman, D.E., Berman, J.W., Roeder, C.W. and Powell, J. (2012) “**Seismic Vulnerability of Older Braced Frames.**” *Journal of Performance Constructed Facilities*, ASCE, in-review.

### G.2 Tables of Analytical Results

Table G. 1. Scaling Factors of Ground Motions for the Different Model Building Types

Ground Motions	10/50		Ground Motions	2/50	
	AISC-SCBF	NCBF		AISC-SCBF	NCBF
se01	2.551	2.026	se21	1.365	0.957
se02	1.827	2.190	se22	1.263	1.231
se03	1.079	0.802	se23	1.114	1.283
se04	0.697	0.762	se24	1.674	1.469
se05	0.761	0.728	se25	0.621	0.657
se06	0.899	0.933	se26	0.760	0.800
se07	0.800	0.864	se27	0.480	0.607
se08	0.774	0.813	se28	0.600	0.698
se09	0.639	0.807	se29	0.367	0.331
se10	0.740	0.829	se30	0.323	0.332
se11	0.600	0.717	se31	0.646	0.517
se12	0.779	0.860	se32	0.776	0.591
se13	0.536	0.650	se33	0.472	0.601
se14	0.736	0.771	se34	0.789	1.359
se15	1.420	1.595	se35	1.388	1.024
se16	0.861	0.839	se36	1.278	0.947
se17	0.476	0.433	se37	0.911	0.893
se18	0.405	0.442	se38	0.723	0.828
se19	0.811	0.639	se39	0.937	0.841
se20	1.013	0.659	se40	0.674	0.681



## References

- Aguero A, Izvernari C, and Tremblay R, (2006) "Modeling of the Seismic Response of Concentrically Braced Steel Frames using the OpenSees Analysis Environment," Int. J. of Advanced Steel Construction, 2, 3, 242-274;.
- AISC (1997). "Seismic Provisions for Structural Steel Buildings." American Institute of Steel Construction, Chicago, IL.
- AISC (2005). "Seismic Provisions for Structural Steel Buildings." American Institute of Steel Construction, Chicago, IL.
- AISC (2010a). "Seismic Provisions for Structural Steel Buildings." American Institute of Steel Construction, Chicago, IL.
- AISC (2010b). "Manual of Steel Construction, Load and Resistance Factor Design." 14th Edition, American Institute of Steel Construction, Chicago, IL.
- Archambault M-H. (1995) "Etude du Comportement Seismique Des Contreventements Ductiles en X Avec Profiles Tubulaires en Acier. " Report EPM/GCS-1995-09; Department of Civil Engineering, Ecole Polytechnique, Montreal, Que.
- ASTM. (2003) "ASTM E 1049-85: Standard Practices for Cycle Counting in Fatigue Analysis." West Conshohocken, PA.
- Aslani, F., and Goel, S.C., (1989). "Experimental and Analytical Study of the Inelastic Behavior of Double Angle Bracing Members Under Severe Cyclic Loading," Research Report UMCE 89-5, Department of Civil Engineering, University of Michigan, Ann Arbor, MI.
- Astaneh-Asl, A, Goel, S. C, and Hanson, R.D., (1982) "Cyclic Behavior of Double Angle Bracing Members with End Gusset Plates," Research report UMCE 82R7,

- Department of Civil Engineering, University of Michigan, Ann Arbor, MI
- Astaneh-Asl, A., Goel, S.C., and Hanson, R.D. (1989) "Cyclic behavior of double angle bracing members with end gusset plates," Research Report UMEE 82R7, Department of Civil Engineering, University of Michigan, Ann Arbor, MI.
- ATC-3-06 report. (1978) "Tentative Provisions for the Development of Seismic Regulations for Buildings." ATC.
- ATC-58 (2009) "Fragility Curves for Concentrically Braced Steel Frames with Buckling Braces" Applied Technology Council.
- Baker, J.W. and Cornell, C.A. (2006) "Spectral shape, epsilon and record selection." *Earthquake Engineering. & Structural Dynamics*, 34(10), 1193-1217.
- Black, R.; Wenger, W.; Popov, E., (1980) "Inelastic buckling of steel struts under cyclic load reversals, UCB/EERC-80/40, Berkeley: Earthquake Engineering Research Center, University of California.
- Brown, V. L. S., (1998) "Stability of Gusseted Connections in Steel Structures", Doctorial Dissertation, University of Delaware
- Chen, C-H, and Mahin, S. (2010) "Seismic Collapse Performance of Concentrically Steel Braced Frames" Proceedings of the Structures Congress and 19th Analysis and Computation Specialty Conference, Orlando, Florida.
- Cheng, J. J. R, Yam, M. C. H., and Hu, S. Z., (1994) "Elastic Buckling Strength of Gusset Plate Connections," *Journal of Structural Engineering*, Vol. 120, No. 2, p538-559
- Clark KA, (2009) "Experimental Performance of Multi-Story X-Brace Systems," a thesis submitted in partial fulfillment of the MSCE, University of Washington, Seattle.
- El-Tayem, A. A., and Goel, S. C, (1985) "Cyclic Behavior of Angle X-Bracing with Welded Connections," Research report UMCE 85-4, Department of Civil

- Engineering, University of Michigan, Ann Arbor, MI
- Fell BV, Kanvinde AM, Deierlein GG and Myers AT. (2009) “Experimental Investigation of Inelastic Cyclic Buckling and Fracture of Steel Braces.” *Journal of Structural Engineering*, ASCE.
- FEMA. (1997a). FEMA 273: NEHRP Guidelines for the Seismic Rehabilitation of Buildings, Federal Emergency Management Agency, Washington, DC.
- FEMA. (1997b). FEMA 302: NEHRP Recommended Provisions for regulations for new buildings and other structures, Building Seismic Safety Council, Washington, DC.
- FEMA. (1997c). FEMA 303: Commentary to NEHRP Recommended Provisions for seismic regulations for new buildings and other structures, Building Seismic Safety Council, Washington, DC.
- FEMA. (2000a). FEMA 351: Recommended Seismic Evaluation and Upgrade Criteria for Existing Welded Steel Moment Frame Buildings, Federal Emergency Management Agency, Washington, DC.
- FEMA. (2000b). FEMA 355C: State of the Art Report on Systems Performance of Steel Moment Frames Subject to Earthquake Ground Motion Shaking, H. Krawinkler, ed., Federal Emergency Management Agency, Washington, DC.
- FEMA. (2000c). FEMA 355F: State of the Art Report on Performance Prediction and Evaluation of Steel Moment-Frame Buildings, D. A. Foutch, ed., Federal Emergency Management Agency, Washington, DC.
- FEMA. (2000d). FEMA 356: Prestandard and Commentary for the Seismic Rehabilitation of Building, Federal Emergency Management Agency, Washington, DC.
- FEMA. 450 (2004) “NEHRP Recommended Provisions for Seismic Regulations for New

- Buildings and Other Structures.” FEMA 450-1/2003 Edition, Part 1: Provisions, Federal Emergency Management Agency, Washington, D.C.
- FEMA. P695 (2008) “Quantification of Building Seismic Performance Factors FEMA P695 ATC-63 Project Report.” Federal Emergency Management Agency, Washington, D.C.
- Fisher JW, Kulak GL, Smith IFC. (1997) “A Fatigue Primer for Structural Engineers. Advanced Technologies for Large Structural Systems (ATLSS);” Lehigh University, Bethlehem, PA.
- Foutch, D.A., Goel, S.C. and Roeder, C.W. (1987) “Seismic testing of a full scale steel building - Part I,” Journal of Structural Division, ASCE, No. ST11, Vol. 113, New York, pgs 2111-29.
- Fu, X., Fell, B. V., Kanvinde, A. M., and Myers, A. T. (2007). “Experimental and analytical investigations of net section fracture in brace-gusset plate connections,” Structures Congress
- Goggins J M, Broderick BM, Elghazouli AY. (2006) “Experimental behavior of hollow filled RHS bracing members under earthquake loading. Composite Construction in Steel and Concrete V; ASCE.
- Grondin, G.Y., Nast, T.E., and Cheng, J. J. R., (2000) “Strength and Stability of Corner Gusset Plates under Cyclic Loading,” Proceeding of Annual Technical Session and Meeting, Structural Stability Research Council
- Gross, J. L., and Cheok, G (1988) “Experimental Study of Gusseted Connections for Laterally Braced Steel Buildings,” National Institute of Standards and Technology, NISTIR 88-3849, Gaithersburg, MD
- Gunnarsson IR, (2004) “Numerical performance evaluation of braced frame systems,” a

- thesis submitted in partial fulfillment of the MSCE, University of Washington, Seattle.
- Haddad, M., Tremblay, R. (2006). "Influence of connection design on the inelastic seismic response of HSS steel bracing members," Tubular Structures XI, London.
- Han SW, Kim WT, Foutch DA. (2007) "Seismic behavior of HSS bracing members according to width-thickness ratio under symmetric cyclic loading." *Journal of Structural Engineering*; Vol. 133, No. 2, ASCE.
- Hardash, S.G. and Bjorhovde, R., (1985) "New Design Criteria for Gusset Plate in Tension", AISC, Engineering Journal, Vol. 22, No. 2, p77-94
- Herman D, (2006) "Further improvements on and understanding of SCBF systems," a thesis submitted in partial fulfillment of the MSCE, University of Washington, Seattle.
- Hu, S. Z., and Cheng, J. J. R, (1987) "Compressive Behavior of Gusset Plate Connections," Structural Engineering Report NO 153, University of Alberta
- Huang Y, Mahin SA, (2010) "Simulating the Inelastic Seismic Behavior of Steel Braced Frames Including the Effects of Low-Cycle Fatigue," PEER Report 10/104, Pacific Earthquake Engineering Research Center, University of California, Berkeley, CA.
- ICBO (1994). "Uniform Building Code 1994 (Uniform Building Code Vol. 2: Structural Engineering Design Provisions)." International Conference of Building Officials, Whittier, CA.
- ICBO (1988). "1988 Uniform Building Code" International Conference of Building Officials, Whittier, CA.
- Ikeda, K., and Mahin, S. A. (1986). "Cyclic response of steel braces," *Journal of*

- Structural Engineering, Vol. 112, No. 2
- Jain AK, Hanson RD, Goel SC. (1978) "Inelastic response of restrained steel tubes,"  
Journal Structural Division; 104(6), 897-910.
- Johnson S, (2005) "Improved seismic performance of special concentrically braced frames," a thesis submitted in partial fulfillment of the MSCE, University of Washington, Seattle.
- Kotulka BA, (2007) "Analysis for a design guide on gusset plates used in special concentrically braced frames," a thesis submitted in partial fulfillment of the MSCE, University of Washington, Seattle.
- Kahn, L.F., and Hanson, R.D., (1976) "Inelastic cycles of axially loaded steel members,"  
Journal of Structural Division, ASCE, No. ST5, Vol. 102, pgs 947-59.
- Lee, S., and Goel, S.C., (1987) "Seismic behavior of hollow and concrete filled square tubular bracing members," Research Report UMCE 87-11, Department of Civil Engineering, University of Michigan, Ann Arbor, MI.
- Lehman DE, Roeder CW, (2008) "Improved seismic design of concentrically braced frames and gusset plate connections," ASCE.
- Lehman, D. E., Roeder, C. W., Herman, D., Johnson, S., and Kotulka, B. (2008).  
"Improved seismic performance of gusset plate connections," Journal of Structural Engineering, Vol. 134, No. 6
- Liu Z, Goel SC. (1987) "Investigation of Concrete-filled Steel Tubes under Cyclic Bending and Buckling," Report No. UMCE 87-3; Department of Civil Engineering, University of Michigan, Ann Arbor, MI.
- Liu J, Astaneh-Asl A, (2004) "Moment-Rotation Parameters for Composite Shear Tab Connections," Journal of structural engineering, ASCE, Sep.; Vol.130, No. 9.



- Lumpkin EJ, (2009) “Enhanced seismic performance of multi-Story special concentrically braced frames using a balanced design,” Master thesis, University of Washington, Seattle; December.
- MacRae, G., Roeder, C. W., Gunderson, C., and Kimura, Y. (2004). “Brace-beam-columns for concentrically braced frames with concrete filled tube columns,” *Journal of Structural Engineering*, Vol. 130, No. 2
- McKenna, F. (1997) “Object Oriented Finite Element Programming: Frameworks for Analysis, Algorithms and Parallel Computing,” University of California, Berkeley, Berkeley, CA 94720.
- Powell J, (2009) “Evaluation of special concentrically braced frames for improved seismic performance and constructability,” a thesis submitted in partial fulfillment of the MSCE, University of Washington, Seattle; December.
- Popov, E.P. Takanashi, K., and Roeder, C.W. (1976) “Structural steel bracing systems,” EERC Report 76-17, University of California, Berkeley.
- Rabinovitch, J. S. and Cheng, J. J. R., (1993) “Cyclic Behavior of Steel Gusset Plate Connections,” *Structural Engineering Report No. 191*, University of Alberta.
- Roeder, C. W., (2001) “State of Art Report of Connection Performance,” FEMA 355D, Federal Emergency Management Agency, Washington, D.C.
- Roeder C.W., (2002) “Connection Performance for Seismic Design of Steel Moment Frames,” *ASCE, Journal of Structural Engineering*, p517-525, April,.
- Roeder, C.W., Lehman, D.E., Clark, K, Powell, J., Yoo, J-H, Tsai, K-C, Lin, C-H, and Wei, C-Y (2011a) “Influence of Gusset Plate Connection and Braces on the Seismic Performance of X-Braced Frames.” *Earthquake Engineering and Structural Dynamics*, Vol 40, No. 4, pgs 355-74.

- Roeder, C.W., Lumpkin, E.J., and Lehman, D.E. (2011b) "Balanced Design Procedure for Special Concentrically Braced Frame Connections." Elsevier, Journal of Constructional Steel Research, Vol 67, No. 11, pgs 1760-72.
- Shaback B, Brown T. (2001) "Behavior of square HSS braces with end connections under reserved cyclic axial loading." A thesis submitted in partial fulfillment of the MSCE; Department of Civil Engineering, University of Calgary, Calgary, Canada.
- Shaw SM, Kanvinde AM, Fell BV, (2010) "Earthquake-induced net-section fracture in brace connections - experiments and simulations," Journal of Constructional Steel Research, Elsevier; 66(12), 1492-1501.
- Sheng, N., Yam, M. C. H., and Lu, V.P., (2002) "Analytical Investigation and the Design of the Compressive Strength of Steel Gusset Plate Connections," Journal of Constructional Steel Research, v 58, p 1473-1493
- Somerville, P., Smith, N., Punyamurthula, S., and Sun, J. (1997) "Development of Ground Motion Time Histories for Phase 2 of the FEMA/SAC Steel Project." SAC Background Document, Report No. SAC/BD-97/04.
- Soroushian, P. and Alawa, M. S. (1988). "Efficient formulation of physical theory brace models," Journal of Structural Engineering, Vol. 114, No. 11
- Thornton, W.A., (1984) "Bracing Connections for Heavy Construction", AISC, Engineering Journal, Vol. 21, No 3, p139-148
- Tremblay R, Archambault M-H, Filiatrault A. (2003) "Seismic response of concentrically braced steel frames made with rectangular hollow bracing members." *Journal of Structural Engineering*; ASCE, Vol. 129, No. 12.
- Tremblay R. (2008). "Influence of brace slenderness on the fracture life of rectangular tubular steel bracing members subjected to seismic inelastic loading," Structures

## Congress

- Uriz P, Filippou FC, Mahin SA. (2008) "Model for Cyclic Inelastic Buckling of Steel Braces." J. Struct. Eng., ASCE, 134, 4, 619-628.
- Uriz, P. and Mahin, S, A., (2004) "Seismic performance assessment of concentrically braced steel frames." 13th World Conference on Earthquake Engineering, Vancouver, B.C., Canada <http://www.ce.berkeley.edu/~patxi>
- Uriz P, Filippou FC and Mahin SA, (2008) "Model for Cyclic Inelastic Buckling of Steel Braces," J. Struct. Eng., ASCE, 134, 4, 619-628
- Wakabayashi, M., et al, (1972) "Experiments on the elastic-plastic behavior of bars subjected to cyclic axial loads," AIJ, Proceedings of Annual Meeting, Japan October.
- Walbridge, S. S., Grondin, G. Y., and Cheng, J. J. R, (1998) "An Analysis of the Cyclic Behavior of Steel Gusset Plate Connections" Structural Engineering Report NO 225, University of Alberta
- Whitmore, R.E., (1952) "Experimental Investigation of Stresses in Gusset Plates," Bulletin NO. 16, Engineering experiment station, University of Tennessee
- Workman, G.H. (1969) "The inelastic behavior of multi-story braced frame structures subjected to earthquake excitation," U. of Michigan Research Report, Sept.
- Yang F, Mahin S A. (2005) "Limiting net section failure in slotted HSS braces." Structural Steel Education Council;, Moraga, CA.
- Yoo, J. H. (2006). "Analytical investigation on the seismic performance of special concentrically braced frames," department of civil and environmental engineering, University of Washington, WA, USA.
- Yoo, J. H., Roeder, C. W., and Lehman, D. E. (2008). "Analytical performance simulation

- of special concentrically braced frames,” *Journal of Structural Engineering*, Vol. 134, No. 6.
- Yoo, J. H., Roeder, C. W., and Lehman, D. E. (2009). “Simulated behavior of multi-story X-braced frames,” *Engineering Structures*, Vol. 31, Issue 1, January 2009, Pages 182-197.
- Xu, P. and Goel, S. C., (1990) “Behavior of Double Channel Bracing Members under Large Cyclic Deformations,” Research report UMCE 90-1, Department of Civil Engineering, University of Michigan, Ann Arbor, MI

# Curriculum Vitae

**Po-Chien Hsiao**

## Education

- September  
2007- June  
2012*      ***Doctor of Philosophy, Civil Engineering***  
***University of Washington at Seattle***  
Concentration in Structural Engineering and Mechanics  
Dissertation Title: Seismic Performance Evaluation of  
Concentrically Braced Frames  
Working Project: NEES-SG International Hybrid Simulation of  
Tomorrow's Braced Frame  
Dissertation Advisor: Prof. Charles W. Roeder (PI) and Dawn E.  
Lehman (co-PI)
- September  
2002- June  
2004*      ***Master of Science, Civil Engineering***  
***National Taiwan University***  
Concentration in Structural Engineering and Mechanics  
Thesis Title: Pseudo Dynamic Performance and Analysis of A Full  
Scale CFT/BRB Composite Frame  
Thesis Advisor: Prof. Keh-Chyuan Tsai
- September  
1998- June  
2002*      ***Bachelor of Science, Civil Engineering***  
***National Taiwan University***

## Professional Experience

- 2006- 2007*      Special Research Assistant of Director, National Center on Research  
for Earthquake Engineering (NCREE), Taipei, Taiwan
- 2004- 2005*      ROC Army, Corporal of Military Police, Wugu, Taiwan

## Academic Experience

- 2007- 2012*      ***Analytical Study on the Seismic Performance of Concentrically  
Braced Frames***  
Performed the continuum finite element technique for evaluation  
and prediction of the ongoing braced frame test specimens. Studied  
and developed a reliable and improved line-element modeling  
technique of SCBFs using fiber sections with the assessment of the

brace fracture validated by the prior experimental program. Investigated seismic performances of CBF structural systems, such as the collapse potential and seismic performance factors of the systems. Project work is towards a Dissertation for the degree of Doctor of Philosophy. Working under the supervision of Dr. Charles W. Roeder and Dawn E. Lehman.

2003- 2004

***Experimental and Analytical Study of A Full Scale CFT/BRB Composite Frame***

Designed and conducted the tests of a full scale 3-story 3-bay CFT/BRB composite frame specimen. Modeled and analyzed the nonlinear seismic responses of the tests. Investigated the seismic performance of various types of BRBs and their gusset plate connections. The research also included a study of the unbonding material (asphalt) of BRBs with component tests to improve the brace cyclic performance and reduce the cost of braced manufacture.

Project work resulted in a Thesis for the degree of Master of Science. Worked under the supervision of Dr. Keh-Chyuan Tsai.

**Publications**

Papers in Archival Journal published (full-review):

Hsiao, P.C., Lehman, D.E. and Roeder, C.W. (2012) "Improved Analytical Model for Special Concentrically Braced Frames." *Journal of Constructional Steel Research*, DOI: 10.1016/j.jcsr.2012.01.010.

Hsiao, P.C., Lehman, D.E. and Roeder, C.W. (2012) "A Model to Simulate Special Concentrically Braced Frames Beyond Brace Fracture." *Earthquake Engineering & Structural Dynamics*, in press. (accepted on Apr,12th).

Lumpkin, E.J., Hsiao, P.C., Roeder, C.W., Lehman, D.E., Tsai, K.C., Tsai, C.Y., Wei, C.Y., Wu, A.C. (2012) "Investigation of the Seismic Response of Multi-story Braced Frames." *Journal of Constructional Steel Research*; in press. (accepted on Apr, 6th).

Tsai, K.C., Hsiao, P.C., Wang, K.J., Weng, Y.T., Lin, M.L., Lin, K.C., Chen, C.H., Lai, J.W. and Lin, S.L. (2008) "Pseudo-Dynamic Tests of A Full-Scale CFT/BRBF Frame - Part 1: Specimen Design, Experiment and Analysis." *Earthquake Engineering & Structural Dynamics*, 37:1081-1098.

Tsai, K.C. and Hsiao, P.C. (2008) Pseudo-dynamic test of a full-scale CFT/BRBF frame - Part 2: Seismic Performance of Buckling-Restrained Braces and Connections, *Earthquake Engineering & Structural Dynamics*, 37:1099-1115.

Tsai, K. C., Wang, K. J., Chen, C. H., Hsiao, P. C., Lai, W. C., Lai, J. W., Lin, M. L.,

Weng, Y. T., and Lin, K. C. (2006). "Networked Hybrid Tests of Full-scale Frame Structures in NCREE," *Journal of Hunan University (EI)*, 33(3), pp. 1-9.

Papers in Archival Journal in review::

Hsiao, P.C., Lehman, D.E. and Roeder, C.W. (2012) "Evaluation of the Response Modification Coefficient and Collapse Potential of SCBFs." *Earthquake Engineering & Structural Dynamics*, in- review. (submitted on Feb,14th)

Hsiao, P.C., Lehman, D.E., Berman, J.W., Roeder, C.W. and Powell, J. (2012) "Seismic Vulnerability of Older Braced Frames." *J. Performance Constructed Facilities, ASCE*, in-review. (submitted on Mar,22th)

Reviewed Publications in Conference Proceeding:

Hsiao, P.C., Lehman, D.E. and Roeder, C.W. (2012) "Modeling Fracture Behavior in Simulation of Special Concentrically Braced Frames." *The 9th International Conference on Urban Earthquake Engineering (9CUEE&4ACEE)*, Tokyo, Japan, March 6-8.

Hsiao, P.C., Lehman, D.E. and Roeder, C.W. (2011) "Seismic vulnerability of older braced frames." *SEAOC Convention proceedings*, Las Vegas, NV, September 21-24.

Hsiao, P.C., Lehman, D.E. and Roeder, C.W. (2011) "Computer modeling of special concentrically braced frame structural systems." *The 8th International Conference on Urban Earthquake Engineering (8CUEE)*, Tokyo, Japan, March 7-8.

Hsiao, P.C., Roeder, C.W., Lehman, D.E., and Lumpkin, E. (2009) "Seismic Evaluation and Rehabilitation of Concentrically Braced Frames." *2009 ATC/SEI Conference on Improving the Seismic Performance of Existing Buildings and Other Structures*, San Francisco, CA, December 9-11.

Tsai, K.C., Lin, S.L. and Hsiao, P.C. (2006) "Experiment Tests of Large Scale Buckling Restrained Bracing Components and Systems in Taiwan", 19th KKCNN Symposium on Civil Engineering, Kyoto, Japan, December 10-12.

Tsai, K.C., Hsiao P.C., Lin, S.L., Lin, K.C. (2006) "Overview of the Hybrid Tests of A Full Scale 3-Bay 3-Story CFT/BRB Frame." 4th International Symposium on Steel Structures, Seoul, Korea, November 16-17.

Tsai, K.C., Lai, J.W., Hwang, Y.C., Lin, S.L., Weng, C.H. and Hsiao, P.C. (2005) "Buckling Restrained Braces for Seismic Resistant Structures", 3rd International Symposium on Steel Structures, Seoul, Korea, March 10-11.

Tsai, K.C., Hsiao, P.C., Lai, J.W., Chen, C.H., Lin, M.L. and Weng, Y.T. (2004) "Pseudo Dynamic Tests of a Full Scale CFT/BRB Composite Frame." *The 3rd KU-KAIST-NTU Student Seminar on Civil Engineering Research*, Tuna Height in Awaji, Japan, February 25-28.

Lai, J.W., Tsai, K.C., Hsiao, P.C. and Lin, S.L. (2004) "Test of Large Scale Buckling Restrained Braces for Chinese Cultural University Gymnasium", the 7th National Conference on Structure Engineering, Chung-Li, Taiwan, August 22-24.

Lai, J.W., Tsai, K.C., Lin, S.L. and Hsiao, P.C. (2004) "Large Scale Buckling Restrained Brace Research in Taiwan", 1st ACEE, Manila, Philippine, March 5-6.

Tsai, K.C., Hsiao, P.C., Lai, J.W., Chen, C.H., Lin, M.L. and Weng, Y.T. (2003) "Pseudo Dynamic Tests of a Full Scale CFT/BRB Composite Frame." *The 16th KKCNN Symposium on Civil Engineering*, Korea, December 8-9.

Technical Reports:

Tsai, K.C., Lin, Y.C., Lin, J.L., Lin, S.L., and Hsiao, P.C. (2007) "High Performance Steel Material and Structures for Earthquake Resistant Buildings", Chapter 4 of *High-Performance Construction Materials, Science and Applications*, Caijun Shi and Y.L. Mo, World Scientific (book chapter).

Tsai, K.C., Hsiao, P.C. (2005) "Pseudo Dynamic Performance and Analysis of A Full Scale CFT/BRB Composite Frame" *National Center on Research for Earthquake Engineering*, NCREE-05-001.